



HAL
open science

Cellulose nanocrystals : surface modification and advanced materials

Ning Lin

► **To cite this version:**

Ning Lin. Cellulose nanocrystals : surface modification and advanced materials. Chemical and Process Engineering. Université de Grenoble, 2014. English. NNT : 2014GRENI034 . tel-01296967

HAL Id: tel-01296967

<https://theses.hal.science/tel-01296967v1>

Submitted on 1 Apr 2016

HAL is a multi-disciplinary open access archive for the deposit and dissemination of scientific research documents, whether they are published or not. The documents may come from teaching and research institutions in France or abroad, or from public or private research centers.

L'archive ouverte pluridisciplinaire **HAL**, est destinée au dépôt et à la diffusion de documents scientifiques de niveau recherche, publiés ou non, émanant des établissements d'enseignement et de recherche français ou étrangers, des laboratoires publics ou privés.

THÈSE

Pour obtenir le grade de

DOCTEUR DE L'UNIVERSITÉ DE GRENOBLE

Spécialité : **Matériaux, Mécanique, Génie civil, Electrochimie**

Arrêté ministériel : 7 août 2006

Présentée par

Ning LIN

Thèse dirigée par **Professeur Alain DUFRESNE**

préparée au sein du **Laboratoire du Génie des Procédés Papetiers de l'École Internationale du Papier, de la Communication Imprimée et des Biomatériaux (LGP2-UMR 5518)**

dans l'**École Doctorale Ingénierie – Matériaux, Mécanique, Energétique, Environnement, Procédés de Production**

Cellulose Nanocrystals:

Surface Modification and Advanced Materials

Thèse soutenue publiquement le **24th June 2014**,
devant le jury composé de :

Monsieur Etienne FLEURY

Professeur, INSA de Lyon, France (Président)

Monsieur Christoph WEDER

Professeur, l'Université de Fribourg, Switzerland (Rapporteur)

Monsieur Jean-Marie RAQUEZ

Dr., l'Université de Mons, Belgium (Rapporteur)

Monsieur Jin HUANG

Professeur, Wuhan University of Technology, China (Membre)

Madame Alessandra de ALMEIDA LUCAS

Dr., Federal University of Sao Carlos, Brazil (Membre)

Monsieur Alain DUFRESNE

Professeur, Grenoble INP, France (Membre)



“天行健，君子以自強不息；地勢坤，君子以厚德載物。”

——《周易·乾》

*To my parents who gave and supported my life,
and Yuan for her love and companion*

Acknowledgements

The research presented in this thesis was carried out in the Multiscaled Biobase Materials group at the Department of Grenoble Institute of Technology-Pagora (Institut Polytechnique de Grenoble) in France. Three-year study in Pagora is a long but pleasant journey to explore the research on cellulose nanocrystals.

First and foremost, I am grateful to my PhD supervisor, Professor Alain Dufresne, for his help, support, and patience throughout last three years. He encouraged me to propose any idea during the study, and was always available when I needed his advice. Without his instruction and contribution, this thesis would not have turned out as it is. Alain's never-ending thoughts and enthusiasm for science give me an impression and good example. He has my utmost respect as an excellent scientist, and my deepest gratitude as a good friend.

I am grateful to the dissertation committee, Professor Etienne Fleury, Professor Christoph Weder, Dr. Jean-Marie Raquez, Professor Jin Huang, and Dr. Alessandra de Almeida Lucas, for their interest in my research, taking time to check my thesis, and providing valuable suggestions and insights.

I much appreciate my Master supervisor, Professor Jin Huang from Wuhan University of Technology, China. He led me into the science world, and showed me what cellulose nanocrystal is. Even after my graduation from Master study, we frequently discussed hot research topics on diverse fields of science. His remarks or comments always provided me the promising inspiration on my study.

I would like to thank Professor Jean-Luc Putaux (CERMAV-CNRS), Dr. Gregory Berthome (INPG-SIMaP), and Prof. Yun Chen (School of Basic Medical Sciences-Wuhan University) for their help and discussion on instrument characterizations. Special thanks go to Cécile Sillard and David Dallerac, who provided access and instructions on the laboratory equipment and chemicals reservation.

I am grateful to all the professors and students (and post-doctors) in the team of LGP2 for their kind help and suggestions. Thanks a lot my colleagues and friends, Oussama El Baradai, Ahlem Romdhane, Karima Benhamou, who always cheered me up and encouraged me in difficult periods. Special thanks to Imtiaz Ali, you are my first friend who lent me a helping hand when I arrived at Grenoble. I really feel lucky that during my study in France, all of us can become the good friends.

I dedicate my dissertation to my parent in China, for their unlimited love, support and trust for all my life.

My utmost thanks go to my true love, Yuan Li. She is the kindest and most patient girl I have ever met. Her constant support and encouragement, and her loving care gave me the energy to carry out the experiment and study. Thank God for giving me the best wife of the world and a very happy life.

One day in the September of three years ago, when I walked on the “Rue de la Chimie” of Grenoble, I suddenly realized it was the first time I lived in abroad; an unknown experience for the new life was waiting for me. At that time, I really didn't know this experience would be interesting, exciting or hard or lonely. Now I am about to finish the PhD study. I know there is a long list for the people deserving my gratitude, and I can't write all their names in here. But I will definitely write your names in my heart and remember all of your kind helps!

08th, April 2014 at Grenoble

Table of Contents

— Acknowledgements	I
— Table of Contents	III
— Scientific Publications	V
— General Introduction	1
— Chapter 1. Literature Review	9
1.1 Extraction and Production of Cellulose Nanocrystals	15
1.2 Structure and Properties of Cellulose Nanocrystals	18
1.3 Surface Modification of Cellulose Nanocrystals	34
1.4 Nano-Reinforcement of Cellulose Nanocrystals in Plastic Composites	57
1.5 Advanced Functional Materials based on Cellulose Nanocrystals	69
1.6 Conclusions	90
1.7 References	91
— Chapter 2. Surface Chemistry, Morphological Analysis and Properties of Cellulose Nanocrystals with Graded Sulfation Degrees	111
2.1 Introduction	123
2.2 Experimental Methodology	126
2.3 Spectroscopic Proofs for Gradient Sulfation of Cellulose Nanocrystals	130
2.4 Morphological Observation and Dimensions	134
2.5 Morphological Models and Surface Chemistry of Cellulose Nanocrystals	137
2.6 Effect of Sulfate Groups on the Properties of Cellulose Nanocrystals	142
2.7 Conclusions	148
2.8 References	148
— Chapter 3. Physical and/or Chemical Compatibilization of Extruded Cellulose Nanocrystal Reinforced Polystyrene Nanocomposites	153
3.1 Introduction	165
3.2 Experimental Methodology	167

3.3 Surface Modification and Properties of Cellulose Nanocrystals	175
3.4 Structure and Properties of Extruded Nanocomposites	184
3.5 Conclusions.....	196
3.6 References	197
— Chapter 4. TEMPO-Oxidized Nanocellulose Participating as Crosslinking Aid for Alginate-Based Sponges.....	201
4.1 Introduction.....	213
4.2 Experimental Methodology.....	215
4.3 TEMPO-Mediated Oxidation of Nanocellulose.....	222
4.4 Structure and Properties of Crosslinked Sponges	227
4.5 Roles and Mechanisms of Nanocelluloses in Alginate-Based Sponges	236
4.6 Conclusions.....	238
4.7 References	239
— Chapter 5. Supramolecular Hydrogels from <i>In Situ</i> Host–Guest Inclusion between Chemically Modified Cellulose Nanocrystals and Cyclodextrin	245
5.1 Introduction.....	257
5.2 Experimental Methodology.....	259
5.3 Chemical Modification of Cellulose Nanocrystals	267
5.4 Structure and Properties of Supramolecular Hydrogels.....	271
5.5 Drug Release and Mechanism Study	279
5.6 Conclusions.....	281
5.7 References	282
— Chapter 6. General Conclusions and Perspectives for Future Work.....	287
6.1 General Conclusions	289
6.2 Possible Research Points for Further Study	294
6.3 Perspectives and Challenges in Future	296
— Résumé en Français.....	299
— Appendix and Abbreviations	317

Scientific Publications (2012–2014)

Articles in Scientific Journals

1. **Ning Lin**, Alain Dufresne, “Surface Chemistry, Morphological Analysis and Properties of Cellulose Nanocrystals with Graded Sulfation Degrees”, *Nanoscale*, 2014, 6(10), 5384–5393.
2. **Ning Lin**, Alain Dufresne, “Physical and/or Chemical Compatibilization of Extruded Cellulose Nanocrystal Reinforced Polystyrene Nanocomposites”, *Macromolecules*, 2013, 46(14), 5570–5583.
3. **Ning Lin**, Alain Dufresne, “Supramolecular Hydrogels from in situ Host-Guest Inclusion between Chemically Modified Cellulose Nanocrystals and Cyclodextrin”, *Biomacromolecules*, 2013, 14(3), 871–880.
4. **Ning Lin**, Cécile Bruzzese, Alain Dufresne, “TEMPO-Oxidized Nanocellulose Participating as Crosslinking Aid for Alginate-Based Sponges”, *ACS Applied Materials & Interfaces*, 2012, 4(9), 4948–4959.
5. **Ning Lin**, Jin Huang, Alain Dufresne, “Preparations, Properties and Applications of Polysaccharide Nanocrystals in Advanced Functional nanomaterials: A Review”, *Nanoscale*, 2012, 4(11), 3274–3294.
6. **Ning Lin**, Alain Dufresne, “Nanocellulose in Biomedicine: Current Status and Future Prospect”, *European Polymer Journal*, 2014, in press.

Invited Book Chapters

1. **Ning Lin**, Alain Dufresne: “**Chapter 3.** Surface Modification of Polysaccharide Nanocrystals”;
Ning Lin, Jin Huang, Alain Dufresne: “**Chapter 6.** Polysaccharide Nanocrystals-Based Materials for Advanced Applications”;

Alain Dufresne, **Ning Lin**: “Chapter 7. Characterization of Polysaccharide Nanocrystal-Based Materials”;

*Ed. Jin Huang, Peter R. Chang, **Ning Lin**, Alain Dufresne, “Biobased Polysaccharide Nanocrystals: Chemistry and Applications”, John Wiley & Sons, USA, 2014/12, in press. (Both in English and Chinese)*

2. **Ning Lin**, Alain Dufresne: “Nanocellulose: Biomedical Nanomaterial Applications”, **Entry No. 120050596**; *Ed. Munmaya Mishra, “Encyclopedia of Biomedical Polymers and Polymeric Biomaterials”, CRC Press, USA, 2015/01.*
3. **Ning Lin**, Alain Dufresne, “*In situ* Conjunction of Cellulose Nanocrystals in Supramolecular Hydrogels by the Aid of Host-Guest Inclusion Complexation”, **pp. 123–126**; *Ed. Michael T. Postek, Robert J. Moon, Alan W. Rudie, Michael A. Bilodeau, “Production and Application of Cellulose Nanomaterials”, TAPPI Press, 2013/06.*

Refereed Conference Proceedings

1. **Ning Lin** (2013/12). **Oral Presentation**. “Properties and Electrostatic Interactions from Cellulose Nanocrystals with Gradient Surface Sulfate Groups”. Winter Training School Conference for “Use of Nanopolysaccharides in Packaging”, Grenoble, France.
2. **Ning Lin** (2013/06). **Oral Presentation**. “Structure Properties and Interface in Polystyrene Nanocomposites Based on Cellulose Nanocrystals with Physical and Chemical Modifications from Non-Covalent and Covalent PEG Compatibilization”. 2013 TAPPI International Conference on Nanotechnology for Renewable Materials, Stockholm, Sweden.
3. **Ning Lin**, Alain Dufresne (2013/06). **Poster**. “Supramolecular hydrogels from in situ host-guest inclusion between chemically modified cellulose nanocrystals

and cyclodextrin”. 2013 TAPPI International Conference on Nanotechnology for Renewable Materials, Stockholm, Sweden.

4. **Ning Lin**, Cécile Bruzzese, Alain Dufresne (2013/06). **Poster**. “TEMPO-oxidized nanocellulose participating as crosslinking aid for alginate-based sponges”. 2013 TAPPI International Conference on Nanotechnology for Renewable Materials, Stockholm, Sweden.

Scientific Publications not Included in This Thesis (2009–2011)

1. **Ning Lin**, Jin Huang, Peter R. Chang, Jiwen Feng, Jiahui Yu, “Surface Acetylation of Cellulose Nanocrystal and Its Reinforcing Function for Poly(lactic acid)”, ***Carbohydrate Polymers***, 2011, 83(4), 1834–1842.
2. **Ning Lin**, Jin Huang, Peter R. Chang, Liangdong Feng, Jiahui Yu, “Effect of Polysaccharide Nanocrystals on Structure, Properties and Drug Release Kinetics of Alginate-based Microsphere”, ***Colloids and Surfaces B: Biointerfaces***, 2011, 85(2), 270–279.
3. **Ning Lin**, Jin Huang, Peter R. Chang, Debbie P. Anderson, Jiahui Yu, “Preparation, Modification, and Application of Starch Nanocrystals in Nanomaterials: A Review”, ***Journal of Nanomaterials***, 2011, Article ID: 573687 (13 Pages).
4. **Ning Lin**, Dongkuan Fan, Jiahui Yu, Jinghua Chen, Jin Huang, Peter R. Chang, “Structure and Properties of Poly (Butylene Succinate) Filled with Lignin: A Case of Lignosulphonate”, ***Journal of Applied Polymer Science***, 2011, 121(3), 1717–1724.
5. **Ning Lin**, Jiahui Yu, Peter R. Chang, Junli Li, Jin Huang, “Poly(butylene succinate)-Based Biocomposites Filled with Polysaccharide Nanocrystals: Structure and Properties”, ***Polymer Composites***, 2011, 32(3), 472–482.
6. **Ning Lin**, Guangjun Chen, Jin Huang, Alain Dufresne, Peter R. Chang, “Effects of Polymer-Grafted Natural Nanocrystal on Structure and Mechanical Properties of Poly(lactic acid): A Case of Cellulose Whisker-*graft*-Polycaprolactone”, ***Journal of Applied Polymer Science***, 2009, 113(5), 3417–3425.

General Introduction

Cellulose nanocrystal is the primary structural building block of plant, and can be extracted from wood and plant fibers, or tunicin and bacterial cellulose. The hydrolysis of amorphous regions of native cellulose results in cellulose nanocrystals – rigid, rod-shaped crystalline cellulose domains with 5–20 nm in diameter and tens to hundreds of nanometers in length. The development of scalable technologies for the isolation and application of cellulose nanocrystals has been actively pursued by various groups, notably in USA, Canada, and Europe.¹ As an abundant and renewable nanomaterial, cellulose nanocrystal is expected to be used to manufacture and develop a wide range of high-value products, such as (i) biomedical materials for pharmaceuticals and drug delivery, bone replacement and tooth repair etc.; (ii) advanced reinforced composite materials (high-strength spun fibers and textiles; reinforced polymers and innovative bioplastics; ‘smart’ packaging etc.); (iii) additives for food, cosmetics, coatings, paints, adhesives, pigments and inks; (iv) structural components for papermaking, building, aerospace and transportation; (v) iridescent and optical switchable materials.²

Since the first study on the use of cellulose nanocrystal as a reinforcing phase in nanocomposites about 20 years ago, a huge amount of literature has been devoted to the research on cellulose nanocrystals. Different descriptors of these highly crystalline cellulosic nanoparticles are often referred to in the literature, commonly including ‘cellulose nanocrystals’, ‘nanocrystalline cellulose’, ‘cellulose nanowhiskers’ (or just ‘whiskers’), ‘rod-like cellulose microcrystals’, ‘cellulose crystallites’ and ‘cellulose micelles’ (in early literature). In 2011, some international standards on nanocellulose were proposed by TAPPI’s International Nanotechnology Division, and the nomenclature of “cellulose nanocrystals” was recommended to be used for a general designation.³ Especially during recent ten years, the study on cellulose nanocrystals has become a hot and topical subject all over the world. More and more researchers are dedicated to the study of this wonderful nanomaterial, and every

year many academic conferences are proposed to drive the development of cellulose nanocrystals, such as in the year of 2013, 'TAPPI International Conference on Nanotechnology for Renewable Materials', '245th ACS National Meeting-Divisions of Composites from Natural Resources', 'EPNOE 2013 International Polysaccharide Conference' etc.

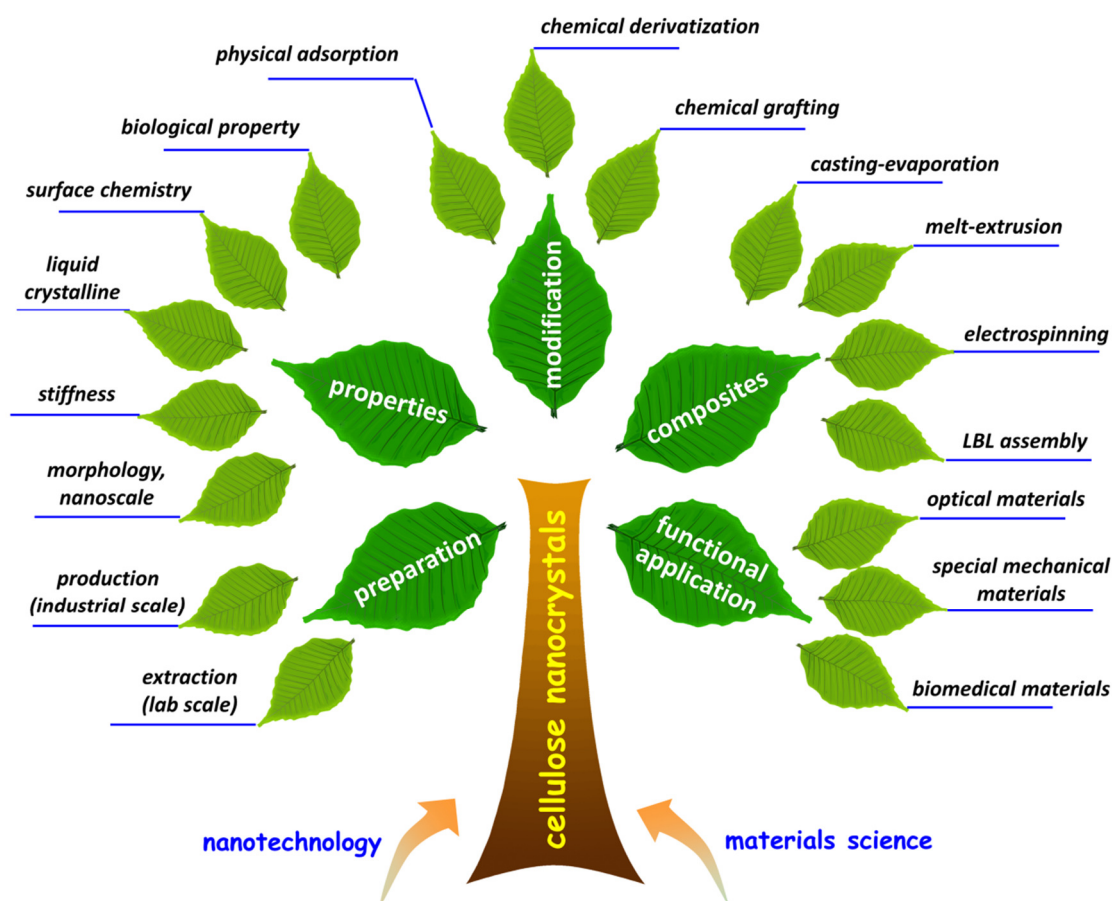


Figure 1. Dendrogram of classification and topics for the research on cellulose nanocrystals.

From the viewpoint of nanotechnology and materials science, the research topics on cellulose nanocrystals can be divided into four areas, viz. preparation, properties, modification, and applications (including composites and functional materials), as shown in Figure 1. For the preparation of cellulose nanocrystals, different approaches to extract cellulose nanocrystals at lab scale are frequently reported. However, perfect technique with 'green', 'simple' and 'low-cost' procedure for large-scale production of cellulose nanocrystals is still in progress. The investigation of cellulose nanocrystal properties includes its physical, surface chemistry and biological properties. The purpose of surface modification on cellulose nanocrystal is the

regulation of surface properties or contribution of novel functional molecules for diverse applications. Regarding traditional nano-reinforcing application of cellulose nanocrystals, four processing approaches are mainly applied to prepare cellulose nanocrystal-based composites, viz. casting-evaporation, melting-compounding, electrospinning, and layer-by-layer assembly. The emergence of functional materials derived from some unique properties of cellulose nanocrystals attracts increasing attentions of researchers especially during recent five years, such as optical-tunable materials, mechanically-adaptive materials, and diverse biomedical materials from cellulose nanocrystals.

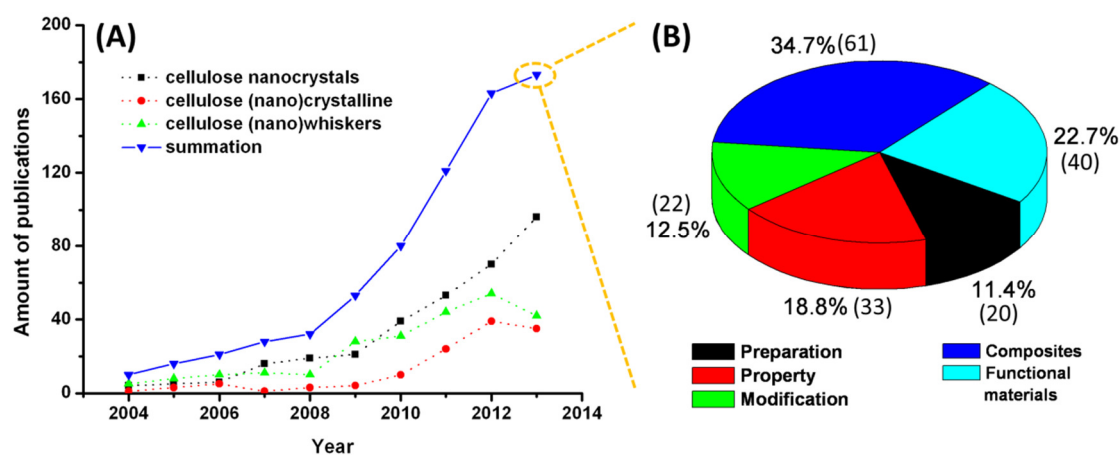


Figure 2. (A) Evolution of the number of research publications on cellulose nanocrystals during last ten years (2004–2013) according to ISI Web of Knowledge system; (B) Proportions of different research topics for the publications in the year of 2013. (In the statistics on the proportions of different topics for the publications in 2013, the review articles are excluded, and some publications may be involved into two research topics.)

Figure 2 (A) shows the number of research publications on cellulose nanocrystals during last ten years according to ISI Web of Knowledge system. Generally, gradient increase of number of publications on cellulose nanocrystals can be found from 2004 to 2013, which induces the sharp change from few articles in 2004 to more than 180 articles in 2013. Specifically, during these years the continuous leap increase of number of articles on the study of cellulose nanocrystals appeared since 2008. Analysis of the research topics in 2013 is more interesting, which indicates the most focused points on the studies of cellulose nanocrystals. As shown in Figure 2 (B), in

2013, applications of cellulose nanocrystals (including both composite and functional materials) is undoubtedly the main research interest, which accounts for about 60% publications. It is found that there is less study on single extraction of cellulose nanocrystals, but more studies on the development of different methods to obtain cellulose nanocrystals with controlled surface properties, such as isolation of thermally stable cellulose nanocrystals by phosphoric acid hydrolysis,⁴ synthesis of ammonium carboxylated cellulose nanocrystals guided by Raman spectroscopy with ammonium persulfate,⁵ shape-controlled cellulose nanocrystals via compositional acid hydrolysis⁶ etc. There is also a decrease in the number of studies on single surface modification of cellulose nanocrystals. In the reports of novel surface modifications, specific purpose for the modification is always involved, especially functional modification for the contribution of additional role or effect to cellulose nanocrystals. This change reflects the rational return of the studies on this topic, which demands more reasonable and useful modifications on cellulose nanocrystals, such as gold/magnetite nanoparticles embedded on cellulose nanocrystal surface for efficient immobilization,⁷ amino-trisulfonate tetraphenylporphyrin conjugated on cellulose nanocrystals for special binding properties and singlet-oxygen production⁸ etc. Interestingly, during the past year, plenty of publications focused on the investigation or discussion of cellulose nanocrystal properties, such as orientational distribution of cellulose nanocrystals by diamagnetic anisotropy,⁹ effects of sulfate groups on the adsorption of cellulase enzymes,¹⁰ prediction of stiffness of cellulose nanocrystals with quantum mechanics model,¹¹ self-assembly behaviors of bacterial and tunicate cellulose nanocrystals¹² etc. Although the mechanisms in some studies should be further verified, fundamental exploration of the properties of cellulose nanocrystal is so important that it significantly promotes its application. Regarding applications of cellulose nanocrystals, investigation on cellulose nanocrystals as nano-reinforcing phase to prepare various composites is still one of the common research topic. However, to meet the requirements of industrial products, many studies process cellulose nanocrystal-based composites with melt-compounding approach. Functional materials from cellulose nanocrystals were an attractive topic

in 2013 (40% in the application studies), because of the innovation of diverse high added-value materials with new or improved properties, such as mechanical gradient nanocomposite from crosslinked cellulose nanocrystals,¹³ recyclable organic solar cells on cellulose nanocrystal substrates,¹⁴ responsive photonic hydrogels based on cellulose nanocrystals,¹⁵ cultivation of skeletal muscle myogenesis on cellulose nanocrystals¹⁶ etc. Despite only initial investigation for some studies or ideas, there is a great potential for this topic in the application of cellulose nanocrystals.



Figure 3. Structure and organization of this dissertation.

Cellulose nanocrystal is both an old and new material. It is a material so ancient since its first extraction in 1947, and it is also so new because of its prominence only during recent 20 years. This dissertation is the summarization of my research during last three years on this ageless bionanomaterial, and the structure of dissertation is shown in Figure 3. Chapter 1 is the literature review on cellulose nanocrystals. In this chapter, four areas of the research on cellulose nanocrystals (preparation, properties, modification, and applications) are introduced in detail through the analysis and comparison of selected publications. Chapter 2 is a research work on the properties

of cellulose nanocrystals. In this chapter, the effect of gradient degrees of sulfate groups on cellulose nanocrystals to surface chemistry, morphology and physical properties are investigated and discussed. Chapters 3, 4 and 5 are research works on some applications of cellulose nanocrystals, which are the preparation of extruded nanocomposites, biocomposite sponges, and supramolecular hydrogels. In chapter 3, a novel strategy involving a double-polymer-layer protection and physical and/or chemical compatibilization of cellulose nanocrystals is proposed to both improve the thermal stability and promote the compatibility of cellulose nanocrystals with non-polar polymeric matrices during the extrusion process. In chapter 4, with the idea of TEMPO-oxidized nanocellulose participating as crosslinking aid for the construction of materials (two types of nanocellulose are used, cellulose nanocrystals and microfibrillated cellulose), alginate-based sponges are developed with improved mechanical stability or structural stability. Supramolecular hydrogels from in situ host-guest inclusion between chemically modified cellulose nanocrystals and cyclodextrin are investigated in chapter 5. In this study, the combination of cellulose nanocrystals and cyclodextrin in hydrogels is realized via a smart design, and the application of prepared hydrogels as drug delivery is further analyzed and discussed. The last chapter (chapter 6) is the conclusions on this dissertation and perspectives for future research on cellulose nanocrystals.

References:

1. Leung, A. C. W.; Lam, E.; Chong, J.; Hrapovic, S.; Luong, J. H. T. Reinforced plastics and aerogels by nanocrystalline cellulose. *J. Nanopart. Res.* **2013**, *15*, 1636 (24 pages).
2. From the introduction of the product of nanocrystalline cellulose in the company of CelluForce. http://celluforce.com/en/product_applications.php
3. TAPPI People Resources Solutions, "Roadmap for the development of international standards for nanocellulose". Published at October 24th, **2011**. <http://www.tappinano.org/pdf/RoadmapforNanocelluloseStandards.pdf>

4. Espinosa, S. C.; Kuhnt, T.; Foster, E. J.; Weder, C. Isolation of thermally stable cellulose nanocrystals by phosphoric acid hydrolysis. *Biomacromolecules* **2013**, *14*, 1223–1230.
5. Lam, E.; Leung, A. C. W.; Liu, Y.; Majid, E.; Hrapovic, S.; Male, K. B.; Luong, J. H. T. Green strategy guided by raman spectroscopy for the synthesis of ammonium carboxylated nanocrystalline cellulose and the recovery of byproducts. *ACS Sustainable Chem. Eng.* **2013**, *1*, 278–283.
6. Baek, C.; Hanif, Z.; Cho, S.-W.; Kim, D.-I.; Um, S. H. Shape control of cellulose nanocrystals via compositional acid hydrolysis. *J. Biomed. Nanotechnol.* **2013**, *9*, 1293–1298.
7. Mahmoud, K. A.; Lam, E.; Hrapovic, S.; Luong, J. H. T. Preparation of well-dispersed gold/magnetite nanoparticles embedded on cellulose nanocrystals for efficient immobilization of papain enzyme. *ACS Appl. Mater. Interfaces* **2013**, *5*, 4978–4985.
8. Chauhan, P.; Hadad, C.; Sartorelli, A.; Zarattini, M.; Herreros-López, A.; Mba, M.; Maggini, M.; Prato, M.; Carofiglio, T. Nanocrystalline cellulose–porphyrin hybrids: synthesis, supramolecular properties, and singlet-oxygen production. *Chem. Commun.* **2013**, *49*, 8525–8527.
9. Song, G.; Kimura, F.; Kimura, T.; Piao, G. Orientational distribution of cellulose nanocrystals in a cellulose whisker as studied by diamagnetic anisotropy. *Macromolecules* **2013**, *46*, 8957–8963.
10. Jiang, F.; Kittle, J. D.; Tan, X.; Esker, A. R.; Roman, M. Effects of sulfate groups on the adsorption and activity of cellulases on cellulose substrates. *Langmuir* **2013**, *29*, 3280–3291.
11. Dri, F. L.; Hector Jr., L. G.; Moon, R. J.; Zavattieri, P. D. Anisotropy of the elastic properties of crystalline cellulose I_β from first principles density functional theory with Van der Waals interactions. *Cellulose* **2013**, *20*, 2703–2718.
12. Khandelwal, M.; Windle, A. H. Self-assembly of bacterial and tunicate cellulose nanowhiskers. *Polymer* **2013**, *54*, 5199–5206.

13. Fox, J. D.; Capadona, J. R.; Marasco, P. D.; Rowan, S. J. Bioinspired water-enhanced mechanical gradient nanocomposite films that mimic the architecture and properties of the squid beak. *J. Am. Chem. Soc.* **2013**, *135*, 5167–5174.
14. Zhou, Y.; Fuentes-Hernandez, C.; Khan, T. M.; Liu, J.-C.; Hsu, J.; Shim, J. W.; Dindar, A.; Youngblood, J. P.; Moon, R. J.; Kippelen, B. Recyclable organic solar cells on cellulose nanocrystal substrates. *Sci. Rep.* **2013**, *3*, 1536 (5 pages).
15. Kelly, J. A.; Shukaliak, A. M.; Cheung, C. C. Y.; Shopsowitz, K. E.; Hamad, W. Y.; MacLachlan, M. J. Responsive photonic hydrogels based on nanocrystalline cellulose. *Angew. Chem. Int. Ed.* **2013**, *52*, 8912–8916.
16. Dugan, J. M.; Collins, R. F.; Gough, J. E.; Eichhorn, S. J. Oriented surfaces of adsorbed cellulose nanowhiskers promote skeletal muscle myogenesis. *Acta Biomaterialia* **2013**, *9*, 4707–4715.

CHAPTER 1.

Literature Review on Cellulose Nanocrystals

Chapter 1. Literature Review

1.1 Extraction and Production of Cellulose Nanocrystals	15
1.1.1 Extraction at Lab Scale.....	15
1.1.2 Pilot and Commercial Production	17
1.2 Structure and Properties of Cellulose Nanocrystals	18
1.2.1 Physical Properties	18
1.2.2 Surface Chemistry	27
1.2.3 Biological Properties	31
1.3 Surface Modification of Cellulose Nanocrystals	34
1.3.1 Approaches and Strategies for Surface Modification.....	34
1.3.2 Adsorption of Anionic, Cationic and Nonionic Surfactants	37
1.3.3 Hydrophobic Groups from Chemical Derivatization	39
1.3.4 Polymeric Chains with Physical Absorption or Chemical Grafting	44
1.3.5 Advanced Functional Groups	53
1.4 Nano-Reinforcement of Cellulose Nanocrystals in Plastic Composites	57
1.4.1 Processing Techniques	57
1.4.2 Pristine Cellulose Nanocrystal Reinforced Plastic Composites	61
1.4.3 Modified Cellulose Nanocrystal Reinforced Plastic Composites	63
1.4.4 Mechanisms for Performance Enhancement	65
1.5 Advanced Functional Materials based on Cellulose Nanocrystals	69
1.5.1 Surface Characteristics Induced Functional Nanomaterials.....	69
1.5.2 Nano-Reinforcing Effects in Functional Nanomaterials	76
1.5.3 Optical Materials Derived from Liquid Crystalline	84
1.5.4 Special Films and Systems Ascribed to Barrier Property	87
1.5.5 Other Functional Applications	90
1.6 Conclusions	90
1.7 References	91

Chapter 1. Literature Review

Cellulose nanocrystals (CNs), produced by acid hydrolysis from wood, cotton or other cellulose-rich sources, constitute a renewable nanoscaled raw material with a broad range of envisaged uses: for example, in composites, coatings, adhesives, construction, pulp and paper, filtration, cosmetics and biomedical devices. Hundreds of scientific articles or patents have been published on the research on cellulose nanocrystals during the last twenty years, even if most of the studies focus on their mechanical properties as reinforcing phase and liquid crystalline self-ordering property. In general, the research topics on cellulose nanocrystals can be divided in four aspects, viz. the preparation, properties, surface modification, and applications. The studies on the preparation of cellulose nanocrystals include the extraction at lab scale and large scale production. Diverse property investigations of cellulose nanocrystals also attract the attentions of researchers, such as dimension and distribution control, elastic modulus measurement, rheological behavior analysis, surface charge conversion, and eco-toxicology evaluation. In order to regulate the surface properties, various surface modifications (physical and chemical approaches) have been performed on cellulose nanocrystals, which promote the applications of cellulose nanocrystals in traditional composites and novel functional materials. This chapter reviews recent studies on cellulose nanocrystals, and gives the introduction and instances on the topics of cellulose nanocrystals with respect to their preparation, properties, modification, and applications.

In this chapter, Section 1.3 is inspired from the book chapter:

Ning Lin, Alain Dufresne, Chapter 3. Surface modification of polysaccharide nanocrystals, in "Biobased polysaccharide nanocrystals: Chemistry and applications", Eds. Jin Huang, Peter R. Chang, Ning Lin, Alain Dufresne, Wiley-VCH Verlag GmbH & Co. KGaA, in press;

Section 1.5 is inspired from the review article:

Ning Lin, Jin Huang, Alain Dufresne, "Preparations, properties and applications of polysaccharide nanocrystals in advanced functional nanomaterials: A review", Nanoscale, 2012, 4(11), 3274–3294;

And the book chapter:

Ning Lin, Jin Huang, Alain Dufresne, Chapter 6. Polysaccharide nanocrystals-based materials for advanced applications, in "Biobased polysaccharide nanocrystals: Chemistry and applications", Eds. Jin Huang, Peter R. Chang, Ning Lin, Alain Dufresne, Wiley-VCH Verlag GmbH & Co. KGaA, in press.

Cellulose was discovered by the French scientist Anselme Payen as early as in 1838,¹ accounting for approximately 1.5×10^{12} tons of natural biomass production each year on earth.² After about twenty years, the existence of anisotropic micelles in native cellulose was defined by Nägeli in 1858 based on optical microscopy observations,³ and the crystalline nature of these micelles was established by X-ray diffraction in the early 1900s.⁴ The first attempt to hydrolyze cellulose fibers with strong acids (HCl/H₂SO₄) appeared in 1947 as reported by Nikerson and Habrle.⁵ In 1949, Rånby and Ribi obtained the first images of isolated cellulose micelles by electron microscopy,^{6,7} now commonly termed cellulose nanocrystals. After ten years, Marchessault et al. first reported the birefringence of colloidal dispersions of cellulose crystallites.⁸ Yet it was not until 1992 that the ability of cellulose nanocrystal suspensions to form colloidal liquid crystalline phases was revealed by Revol et al.⁹ During the last twenty years, research on cellulose nanocrystals was significantly driven by the study of using them as nano-reinforcing additive to prepare composites in 1995,¹⁰ fluorescent modification of cellulose nanocrystals in 2007,¹¹ optical tunable material based on chiral nematic structure of cellulose nanocrystals in 2010,¹² and announcement of official opening of 'world's first commercial-scale producer of cellulose nanocrystals' by CelluForce (Quebec, Canada).¹³ The history of cellulose nanocrystals (important milestones on timeline of cellulose nanocrystal research) is shown in Figure 1.1.

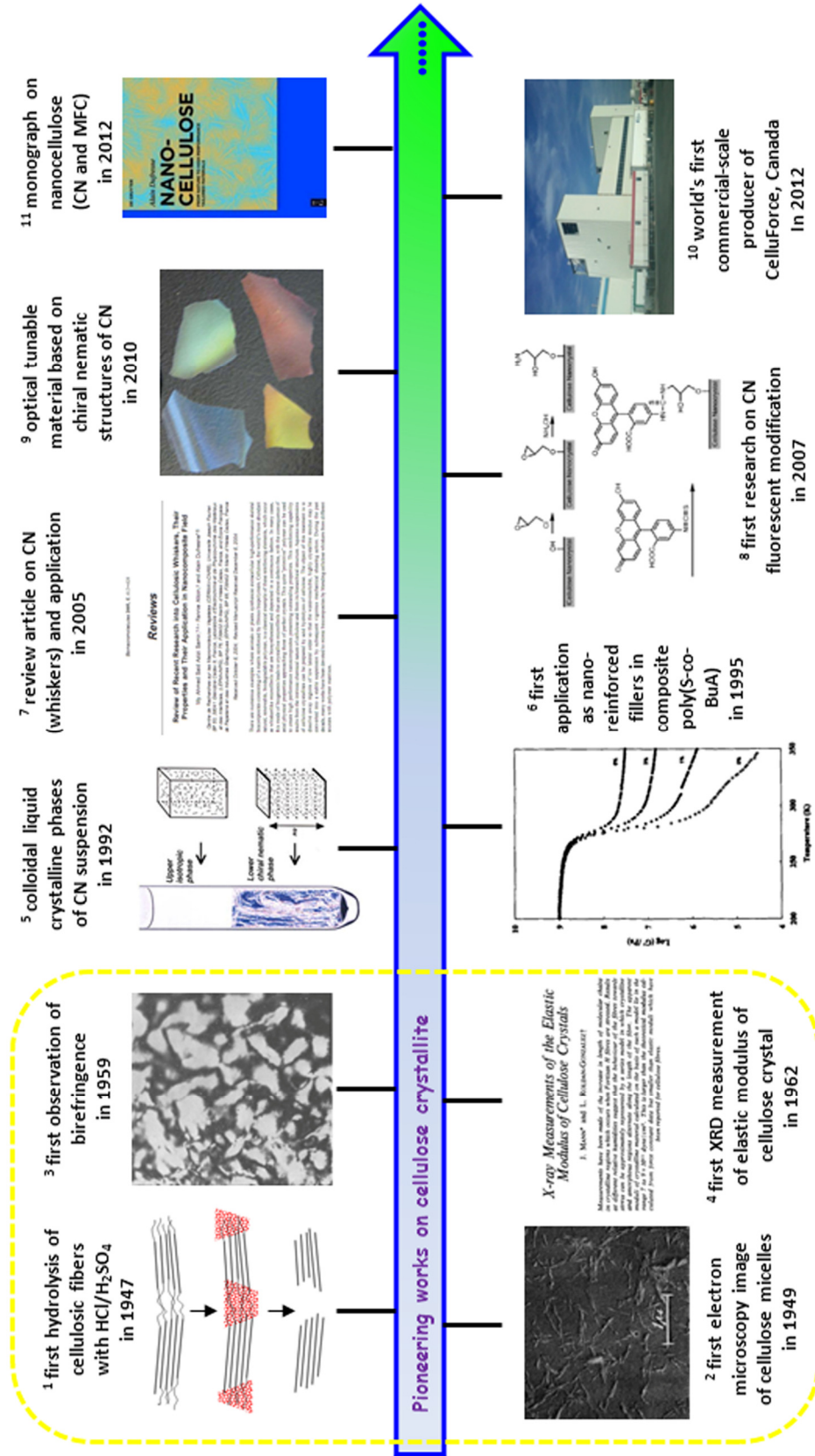


Figure 1.1 Time line of cellulose nanocrystals-based research, involving important milestones throughout the history of cellulose nanocrystals.

1.1 Extraction and Production of Cellulose Nanocrystals

Cellulose microfibrils formed during biosynthesis are 2–20 nm in diameter, depending on the source, and can be several micrometers in length. Each microfibril consists of crystalline domains interspersed with disordered amorphous regions. The preparation of cellulose nanocrystals involves a chemical hydrolysis process to dissolve amorphous chains and release crystalline domains from cellulose fibers.

1.1.1 Extraction at Lab Scale

The extraction of cellulose nanocrystals by chemical hydrolysis is now an established laboratory process and has been applied to a wide variety of raw materials. With diverse hydrolyzing agents, cellulose nanocrystals possessing different surface groups and surface chemistry can be prepared, as shown in Figure 1.2 (A). Hydrolysis with hydrochloric acid preserves the hydroxyl groups of native cellulose but leads to less stable aqueous suspensions.¹⁴ With the combination of TEMPO and hypochlorous sodium, surface hydroxyl groups of cellulose nanocrystals can be selectively transformed into carboxyl groups, which may be useful for subsequent modification.¹⁵ It was reported that ammonium persulfate $[(\text{NH}_4)_2\text{S}_2\text{O}_8]$ can also be used as a low-toxicity oxidant for the isolation of carboxylated cellulose nanocrystals.¹⁶ Moreover, an acid mixture composed of hydrochloric and an organic acid (acetic acid) can be used to hydrolyze cellulose fibers inducing the hydrolysis and modification in one single-step process,¹⁷ which offers the hydrophobic acetyl groups on the surface of cellulose nanocrystals. Recently, some novel systems have been developed for the isolation of cellulose nanocrystals, such as enzymatic hydrolysis,¹⁸ ionic liquid hydrolysis,¹⁹ and gaseous acid hydrolysis.²⁰

For most researches on cellulose nanocrystals, sulfuric acid hydrolysis has been more extensively used for their preparation because of its high efficiency. When sulfuric acid is used as the hydrolyzing agent, disordered or paracrystalline regions of cellulose fibers are preferentially hydrolyzed, whereas crystalline regions that have a higher resistance to acid attack remain intact. The general procedure for the preparation of

sulfuric acid-hydrolyzed cellulose nanocrystals is shown in Figure 1.2 (B). It should be pointed out that during the hydrolysis, sulfuric acid can react with hydroxyl groups of cellulose, which yields charged sulfate esters on the surface of nanocrystals and promotes the dispersion of nanoparticles in water.²¹

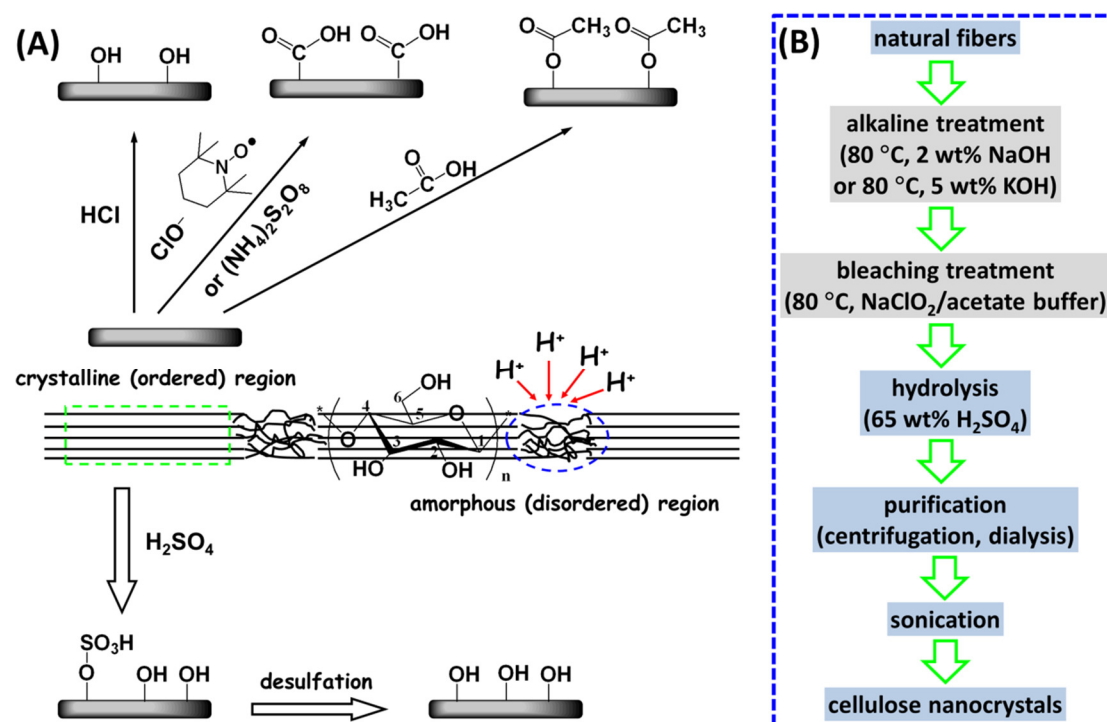


Figure 1.2 (A) The different extraction methods of cellulose nanocrystals providing distinctive surface chemistry: hydrochloric acid treatment provides hydroxyl, acetic acid provides acetyl, TEMPO-mediated hypochlorite treatment provides carboxylic acid, and sulfuric acid treatment provides sulfate esters as well as hydroxyl with desulfation treatment; (B) general procedure for the preparation of cellulose nanocrystals with sulfuric acid hydrolysis.

During the extraction of cellulose nanocrystals with sulfuric acid hydrolysis, Thielemans et al. detected the presence of adsorbed low molecular weight organic compounds on the surface of nanocrystals, which can block the available reactive sites.²² It was reported that a Soxhlet extraction treatment using ethanol was effective in removing adsorbed species, and promoting improved reproducibility of subsequent surface modification reactions.

1.1.2 Pilot and Commercial Production

Scale-up of cellulose nanocrystals for larger production is under way. Several manufacturing facilities (as shown in Table 1.1) have or are being built that will increase production to upwards of multiple tons per year. Alberta Innovates-Technology Futures has constructed the world's first pilot plant to produce cellulose nanocrystals, with the production capacity of 100 kg per week. Domtar Corp. and FPIInnovations have created a joint venture (new organization named CelluForce) to build a commercial-scale plant for the production of cellulose nanocrystals, in a \$40.8 million project. In January 2012, CellForce officially announced to open a plant for the production of cellulose nanocrystals with a target production rate of 1 ton/day.

For the industrial production of cellulose nanocrystals, two issues should be emphasized. One is the standardization for the procedure and conditions of cellulose nanocrystals' production, which is being constituted by TAPPI standard recommendation.²³ Another issue is the further development of practical end-uses for cellulose nanocrystal-based materials, despite the fact that a large and growing body of information on potential applications of cellulose nanocrystals has been identified and demonstrated in the lab. It seems that many companies are interested by the potential of cellulose nanocrystals to improve the quality of their products but face unknowns of cost and sustainability of supply. At the same time, cellulose nanocrystals producers remain mute on production costs and real marketing waiting for the potential uses. It is a vicious circle.

Table 1.1 Industrial production of cellulose nanocrystals (CN) or carboxylated CN.^{24,25}

Producer	Country	Product	Estimated production capacity by 2015
FPIInnovations	Canada	CN	10 kg/week (pilot production)
Alberta Innovates-Technology Futures	Canada	CN	100 kg/week (pilot production)
Bio Vision Technology	Canada	carboxylated CN	4 tons/year (commercial production)
CelluForce/Domtar	Canada	CN	1 tons/day (commercial production)
US Forest Service Forest Products Laboratory	USA	CN, carboxylated CN	35-50 kg/day (pilot production)
Melodea	Israel	CN	unknown
Central Institute for Research on Cotton Technology (CIRCOT)	India	CN, NFC, MFC	unknown

1.2 Structure and Properties of Cellulose Nanocrystals

Cellulose nanocrystal is a special rigid nanoparticle extracted from natural renewable sources, possessing diverse properties, which can be classified mainly as physical properties, surface chemistry and biological properties, as shown in Figure 1.3.

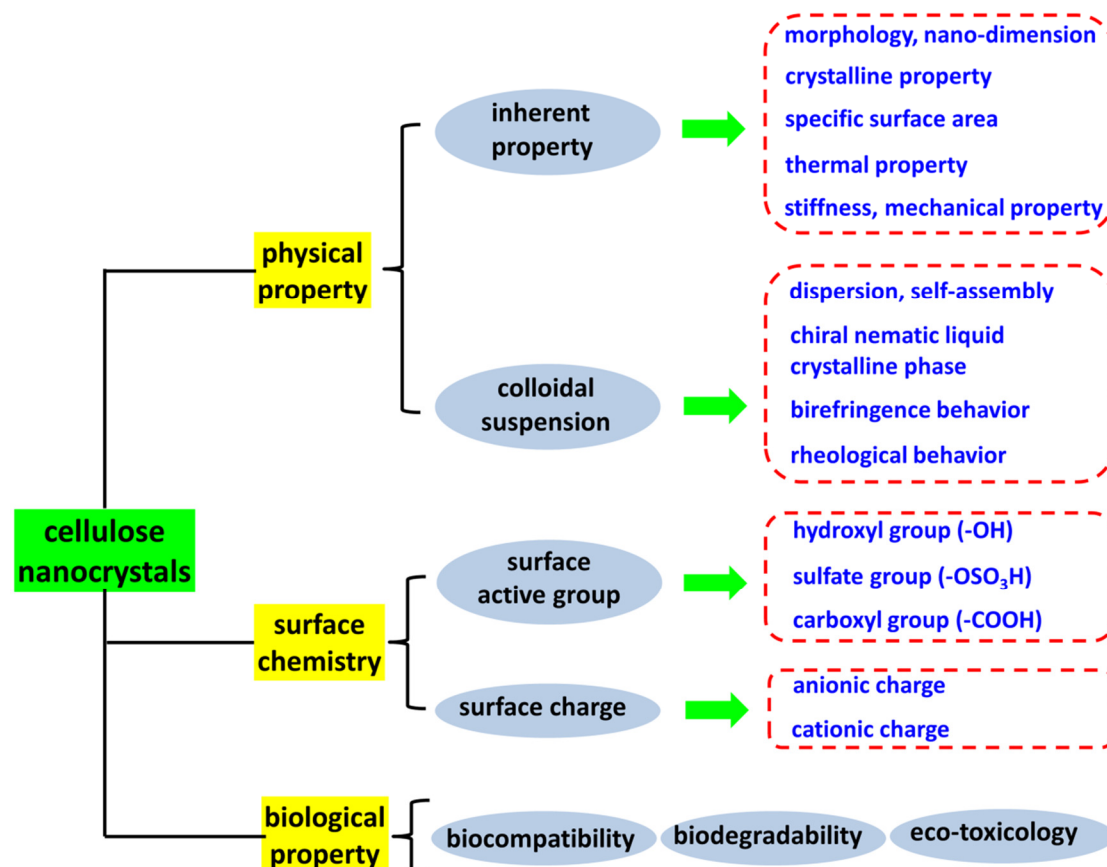


Figure 1.3 Diverse physicochemical and biological properties of cellulose nanocrystals.

1.2.1 Physical Properties

1.2.1.1 Inherent Properties

Morphology and Geometrical Dimensions

The morphology and dimensions of cellulose nanocrystals can be directly accessed by microscopic observations, such as TEM, AFM and FEG-SEM. Numerous evidence from microscopy and light scattering techniques reveal that CNs commonly exhibit more or less elongated rod-like (or needle-like) and cylinder shape, and each rod can therefore be considered as the cellulosic crystal with no apparent defect. However, the

specific nanocrystal cross-section is still in the disputes. According to the early reports, cross-sections of cellulose microfibrils observed by TEM were found to be square or rectangle, whereas their AFM topography showed a round profile.²⁶ Recently, ellipse cross-section for CN observed by AFM was proposed, and the effects of different models of geometrical cross-sections on surface chemistry of cellulose nanocrystals were investigated.^{27,28}

If regarding cellulose nanocrystal as a cylinder with regularly round cross-section, the parameters of CN physical dimension include the length (L), diameter (D) and aspect ratio (L/D). The geometrical dimensions of CN are determined by several factors, including the source of native cellulose and hydrolysis conditions. Nanocrystals extracted from botanical sources (such as cotton, flax, ramie, sisal, etc.) commonly have a length ranging from 100 nm to 700 nm, and a diameter about 5 nm to 30 nm. Nanocrystals from tunicate and bacterial cellulose are several micrometers in length, and 5 nm to 50 nm in diameter due to the highly crystalline property of these sources. TEM images of CNs from four different sources are shown in Figure 1.4.

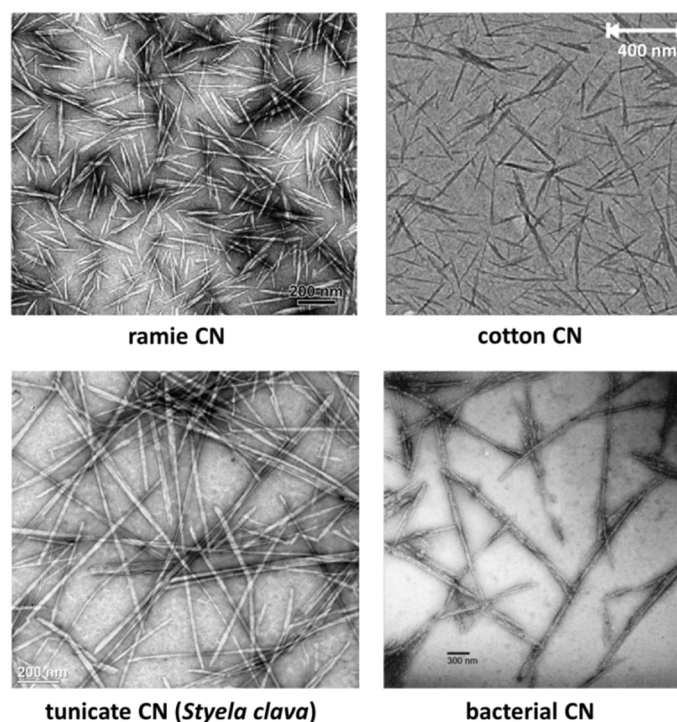


Figure 1.4 TEM images of dilute suspensions of cellulose nanocrystals from (a) ramie;²⁹ (b) cotton;³⁰ (c) tunicate cellulose (*Styela clava*);³¹ (d) bacterial cellulose.³²

Crystalline Properties

The crystalline structure of cellulose nanocrystals depends on the ordered packing of cellulosic chains. During biosynthesis, van der Waals and intermolecular hydrogen bonds between hydroxyl groups and oxygen atoms of adjacent molecules promote parallel stacking of multiple cellulosic chains forming a highly ordered (crystalline) structure. The hydrolysis conditions (acid concentration, temperature and duration) significantly affect the degree of crystallinity (ratio between the mass of crystalline domains and the total mass of nanocrystals) and crystalline dimensions of prepared CN. Theoretically, the degree of crystallinity of CN can be 100%, but incomplete removal of amorphous regions may result in a lower degree of crystallinity. The crystallinity index of CNs is commonly reported as 54–90% depending on the source and hydrolysis conditions.

The crystallinity index of CNs can be analyzed by different techniques including X-ray diffraction (XRD), solid-state ^{13}C NMR, and Raman spectroscopy. XRD height method is the most popular and direct method to calculate the crystallinity index of CN, which generally gives higher values than those of the peak area or peak deconvolution method. The crystallinity index of CN can also be estimated from the spectrum of cellulose samples acquired by solid-state ^{13}C NMR as the peaks at 84 and 89 ppm are assigned to the C4 atom for disordered and ordered cellulose, respectively. The crystallinity index is then calculated as the ratio of the crystalline peak area (87–93 ppm) over the total area assigned to the C4 atom peak (80–93 ppm).³³ Similarly in Raman spectroscopy, the crystallinity index of CN can be estimated as the relative intensity ratio of the Raman lines $I_{1481\text{cm}}$ and $I_{1462\text{cm}}$, reflecting crystalline and amorphous regions of cellulose I.^{34,35}

Specific Surface Area

The specific surface area (A_{sp}) of cellulose nanocrystal affects the determination of surface hydroxyl group amount, which can be estimated from the average geometrical dimensions and cross-section models for crystalline cellulose. Different cross-section models for CN will provide distinct A_{sp} values. For instance, with the square and round

cross-section models, A_{sp} of CN depends only on the width (W) of nanoparticles; whereas with the rectangle and ellipse cross-section models, A_{sp} of CN is determined by both the width (W) and the height (H) of the nanoparticles.

Thermal Properties

Thermal properties of cellulose nanocrystals, especially thermal stability, are of importance for the processing and practical uses. Regardless the source of native cellulose, sulfuric acid-hydrolyzed CNs commonly displays a significant reduction of thermal stability in comparison with raw cellulose. This effect is ascribed to the hydrolysis treatment, and the introduction of sulfate groups resulting from the use of sulfuric acid for the preparation of CNs. Typically, the thermal degradation for sulfated CN can be described as a two-step process, viz. low temperature process with thermal degradation temperature (T_{d1}) between 150 and 300 °C, and high temperature process with thermal degradation temperature (T_{d2}) between 300 and 450 °C. The low temperature process involves the degradation of most accessible amorphous regions which are highly sulfated. The high temperature process involves the degradation of less accessible interior crystalline regions that are comparatively less sulfated. To increase the thermal stability of sulfated CN, desulfation of nanoparticles with diluted alkaline (NaOH) can be performed. A marked increase by 50–100 °C for T_{d1} compared to untreated nanocrystals was reported.^{29,36}

Stiffness, Modulus and Other Mechanical Properties

The elastic modulus of cellulose nanocrystal is an important physical property, especially with respect to the ultimate aim of exploiting its full potential in composite materials. Since 1930s, the elastic modulus of crystalline cellulose has been investigated either by theoretical evaluations or by experimental measurements (wave propagation, XRD, Raman spectroscopy, and AFM). The modulus of cellulose microfibrils is expected to result from a mixing rule between the modulus of the crystalline domains and the amorphous fraction. Therefore, it should be higher for more crystalline cellulose nanocrystals. A broad range of values was reported, as shown in Table 1.2, and it is generally accepted that the Young's modulus of cellulose

nanocrystal should be in the range 100–200 GPa.

Table 1.2 Longitudinal (E_L) and transverse (E_T) moduli of crystalline cellulose.³⁷

Material	Method	E_L (GPa)	E_T (GPa)	Ref.
cellulose I	Calculation	77-121		[38]
		56		[39]
Bleached ramie fibers (cellulose I)	XRD	134		[40]
Fortisan H fibers (cellulose II)	XRD	70 - 90		[41]
Cellulose I	Calculation	172.9*		[42]
		70.8**		
		76	51-57	[43]
Cellulose (two hydrogen bonds -cellulose I)	Calculation	136±6		[44]
Cellulose (one hydrogen bond -cellulose II)		89±4		
Ramie fibers (cellulose I)	XRD	122-135		[45]
Mercerized ramie fibers (cellulose II)		106-112		
Cellulose I	Calculation	167.5	11	[46]
Cellulose II		162.1	50	
Purified ramie fibers (cellulose I)	XRD	138		[47]
Polynosics (cellulose II)		88		
Cellulose III _I		87		
Cellulose III _{II}		58		
Cellulose IV _I		75		
Cellulose I	Calculation	134-135		[48]
Cellulose II		83		
Cellulose II	Calculation	155	24 - 51	[49]
Cellulose I _β	Calculation	127.8		[50]
Cellulose I _β		115.2		
Cellulose I _β	Raman	143		[51]
Cellulose I _β	Calculation	124-155		[52]
Cellulose I _β	Calculation	136-155*		[53]
		114-117**		
Cellulose I _β		116-149*		
		124-127**		
Cellulose II		109-166*		
		101-106**		
Cellulose I _β	Calculation	156 at 300K		[54]
		117 at 500 K		
Cellulose I	Raman	57-105		[55]
Ramie fibers (cellulose I)	Inelastic X-ray scattering	220	15	[56]
TEMPO-oxidized Cellulose I _β	AFM	145		[57]
Acid hydrolyzed Cellulose I _β		150		
Wood	AFM		18-50	[58]
Disaccharide cellulose I _β	Calculation	85.2*/37.6**		[59]
Disaccharide cellulose I _β		99.7*/33.0**		
Extended cellulose I _β chains (10-40 glucoses)		126.0*/63.3**		
Cellulose I _β	Calculation	139.5±3.5	28.8±2.9	[60]
Cellulose I _β	Calculation	206	19	[61]

* with intramolecular hydrogen bondings

** without intramolecular hydrogen bondings

1.2.1.2 Properties of Colloidal Suspensions

Dispersion and Self-assembly in Solvents

The dispersion and self-aggregation states of cellulose nanocrystals in solvents will significantly determine their properties and applications. Due to the high surface area and hydrophilic nature (numerous hydroxyl groups), strong inter-particle hydrogen bonding will inevitably induce the nanocrystals aggregation. This effect can be proved by the weak dispersion and flocculating tendency of unstable HCl-hydrolyzed cellulose nanocrystal aqueous suspensions. Although some solvents were reported to weaken the interchain bonding in cellulose, such as DMF, with N atoms in its structure for the formation of new hydrogen bonds ($O-H\cdots N$) between hydroxyl groups and the N atom,⁶² these solvents (particularly organic solvents) are very limited in terms of practicality. In order to improve the dispersion of cellulose nanocrystals in water or organic solvents, diverse surface treatments or modifications are performed based on the strategy of converting surface properties and weakening interparticle hydrogen bonds. One of the common method for the promotion of cellulose nanocrystals' dispersion in water is the use of sulfuric acid as the hydrolyzing agent, which introduces negatively charged sulfate groups (OSO_3^-/H^+) on the surface of nanocrystals. Attributed to the electrostatic repulsion between sulfate groups, sulfated cellulose nanocrystals can perfectly dispersed in aqueous medium. With similar mechanism, carboxylated cellulose nanocrystals can homogeneously dispersed in water via electrostatic stability of surface carboxyl groups (COO^-/H^+). To facilitate the dispersion of cellulose nanocrystals in organic solvents and enhance the compatibility between nanocrystals and matrices, the surface chemical modification method is generally used. It will be detailedly discussed in Section 1.3 (Surface modification of cellulose nanocrystals) and Section 1.4 (Nano-reinforcing application of cellulose nanocrystals in composites).

Chiral Nematic Liquid Crystalline Phase

It is known that any asymmetric rod-like particle (such as polymer micro-objects, viruses, rod-like alumina, etc.) shows a liquid crystalline behavior and cellulose

nanocrystals are no exception. At low concentrations, suspensions of cellulose nanocrystals are isotropic, that is, the rod-like nanoparticles are randomly oriented. When a critical concentration is exceeded, the nanocrystals in the suspension align and form a colloidal chiral-nematic phase. Over a certain concentration range the isotropic and chiral-nematic phases coexist until finally, upon exceeding an upper critical concentration, only the chiral-nematic phase is present.⁶³ In fact, for sufficiently high concentrations, cellulose crystallites have a helical twist along the main axis, which can induce crystal suspensions to attain a helical twist normal to the main axis of the rod, and thus organize into a chiral nematic phase or cholesteric phase of stacked planes aligned along a perpendicular axis⁶⁴ (as shown in Figure 1.5A). While the helix of cellulose nanocrystals is always left-handed, reflecting the intrinsic chirality of crystalline cellulose, the value of the pitch can vary greatly, from less than 1 to 50 mm and beyond (as shown in Figure 1.5B, C). The pitch depends on the quality and concentration of cellulose nanocrystals, but also temperature, and even ionic strength of the solution.⁶⁵ Many aspects of helix formation are still poorly understood, limiting our ability to control it and to tune the pitch.⁶⁶ It is worth noting that highly sulfonated nanocrystals have different charge behavior than non-sulfonated hydroxyl surface crystals and so can be expected to show different liquid crystalline behavior. For instance, sulfuric acid and phosphoric acid derived nanocrystals give a chiral nematic structure whereas hydrochloric acid derived nanocrystals with post-reaction sulfonation give a birefringent glassy phase that shows a crosshatch pattern.⁶⁷

When ordered colloidal phases of cellulose nanocrystals are dried slowly, the chiral-nematic structure of the suspension can be preserved in solid films.⁶⁸ Chiral-nematic phases have unusual optical properties, such as (a) reflection of light in a Bragg-type manner, generating spectacular iridescent colors (as shown in Figure 1.5D), (b) high optical activity, that is, strong rotation of the plane of linearly polarized light and (c) selective reflection of circularly polarized light of particular handedness without changing the sense of circular polarization. The optical tunable nanomaterials based on the chiral nematic liquid crystalline behavior of cellulose nanocrystals will be

further discussed in Section 1.5 (Advanced functional nanomaterials based on cellulose nanocrystals).

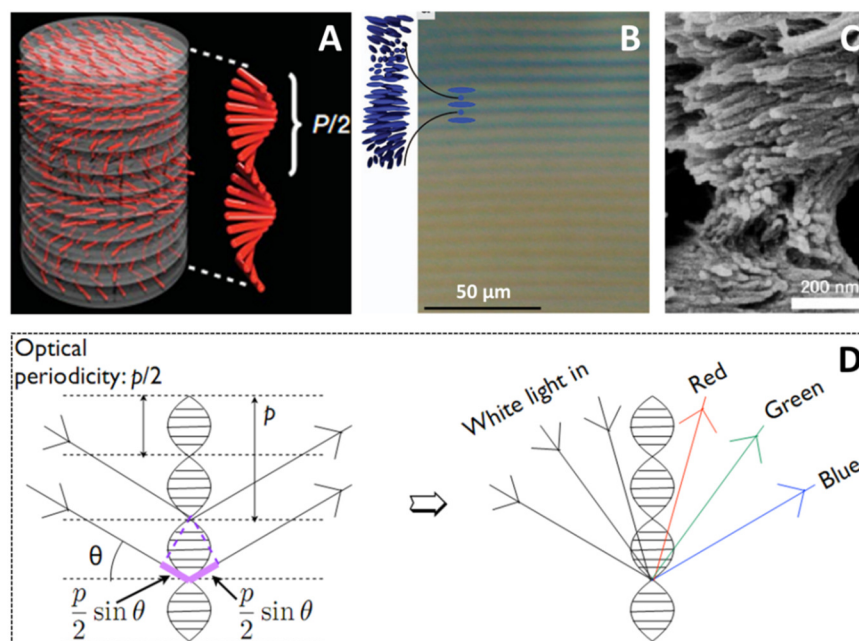


Figure 1.5 (A) Schematic image of chiral nematic ordering present in cellulose nanocrystal suspensions and illustration of half-helical pitch $P/2$;¹² (B) Characteristic regularly spaced helix lines in an aqueous suspension with 5 wt% cellulose nanocrystals derived from sulfuric acid hydrolysis of wood pulp, observed in transmission. The distance between two lines is half-helical pitch ($P/2$), and in this sample $P \approx 13 \mu\text{m}$;⁶⁶ (C) SEM image of helix fracture surface for an actual bulk cellulose nanocrystals film;⁶⁹ (D) Illustration of photonic crystal Bragg reflection from a cholesteric liquid crystal and the angular dependence of the color for the sample.⁶⁶

Birefringence

Theoretically, a beam of unpolarized light entering certain anisotropic materials, such as a crystal, will be divided into two beams, vibrating in different planes perpendicular to each polarized rays. Cellulose nanocrystals display this property with a strong absorption of one of the polarized rays, i.e. they possess two refractive indices. The light emerging from such a material will be plane-polarized light, which is the property of birefringence, or double refraction. The birefringence of cellulose nanocrystal suspension results from two origins: (i) a structural form anisotropy of cellulose ($\Delta n \sim 0.05$) and (ii) a flow anisotropy from alignment of nano-rods under flow operated

before observation. Birefringence of cellulose nanocrystal suspensions can be observed with two linear polarizers crossed at 90° (cross-nicols or crossed-polars). Figure 1.6 shows photographs of birefringence domains for tunicate cellulose nanocrystal suspensions with different concentrations in water (image A), freeze-dried and re-dispersed CNs in water (image B), and dispersed CNs in water and diverse organic solvents (image C). It should be pointed out that the presence of birefringence for cellulose nanocrystal suspensions can be used as the criterion to assess the good or weak dispersability of nanocrystals in solvents.⁷⁰

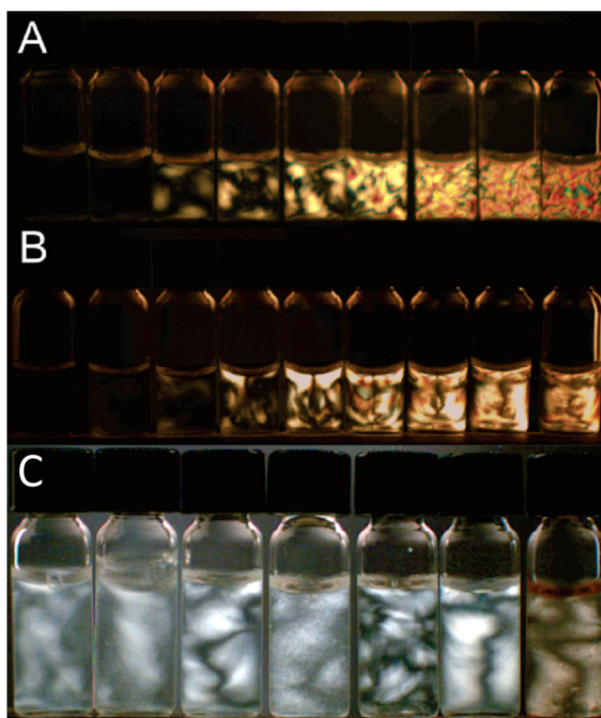


Figure 1.6 Birefringence photographs viewed through crossed polarizers: (A) dispersions of as-prepared H_2SO_4 -hydrolyzed tunicate cellulose nanocrystals in water; (B) freeze-dried CNs re-dispersed in water (concentrations of CNs are 0.1, 0.5, 1.0, 2.0, 3.0, 4.0, 5.0, 6.0, and 7.0 mg/mL from left to right in images A and B); (C) dispersions of 5.0 mg/mL of as-prepared CNs in water, freeze-dried and re-dispersed in water, DMF, DMSO, *N*-methyl pyrrolidone, formic acid, and *m*-cresol from left to right in image C.⁷⁰

Rheological Behavior

The hydrodynamics properties of cellulose nanocrystal suspensions are directly related to the concentration, shear rate, size, length distribution, and temperature. In the dilute

regime, shear thinning behavior of nanocrystal suspensions can be observed, and suspensions exhibit the effect of concentration dependence. At higher concentrations, where cellulose nanocrystal suspensions became lyotropic, a typical behavior of liquid crystalline is generally reported. With regard to the influence of shear rate on the viscosity of nanocrystal suspension, three distinct regions can be observed. At low shear rates, the viscosity of nanocrystal suspension decreases continuously, which is supposed to correspond to a shear thinning behavior where the domains formed by nanocrystals begin to flow. As the shear rate increases, the domains start to break up and a semi-plateau region can be found in the flow curve, where the shear thinning is less pronounced. At a critical rate, a further shear thinning occurred corresponding to the alignment of individual nanocrystals in the flow direction.⁷¹ The aspect ratio is another key parameter in determining the degree of shear-induced order and the relaxation behavior after shear ceased. It was reported that the viscous suspensions derived from long nanocrystals (280 nm) remained aligned for hours and even days after shearing, while suspensions with shorter nanocrystals (180 nm) were found to relax quickly.⁷² An attempt to correlate the intrinsic viscosity of cellulose nanocrystal suspensions to the aspect ratio of constituting nanoparticles was also reported.⁷³ Based on the evaluation of phase behavior using a combination of low-magnification imaging and hot-stage cross-polarized optical microscopy, it was found that both concentration and temperature will significantly affect the microstructure and shear response of cellulose nanocrystal suspensions.⁷⁴ Recently, the effect of surface charges to rheological behavior of cellulose nanocrystal suspensions was reported. Due to the influence of surface charge, the degree of sulfation of cellulose nanocrystals has a significant effect on the critical concentration at which transitions from isotropic to liquid crystal and liquid crystal to gel occur.⁷⁵

1.2.2 Surface Chemistry

1.2.2.1 Surface Active Groups and Reactivity

From a structural point of view, cellulose is a high molecular weight homopolysaccharide composed of β -1,4-anhydro-D-glucopyranose units (Figure 1.7).

These units do not lie exactly in the plane with the structure, but rather they assume a chair conformation with successive glucose residues rotated through an angle of 180° about the molecular axis and hydroxyl groups in an equatorial position.⁷⁶ The ability of these hydroxyl groups to form hydrogen bonds plays a major role in the formation of fibrillar and semicrystalline packing, which governs the important physical properties of these highly cohesive materials.⁷⁷ As indicated with blue dashed lines in Figure 1.7, intramolecular hydrogen bonds occur primarily between the hydrogen borne by the OH group of the C3 carbon and ring oxygen of the adjacent glucose unit (O5). The intermolecular hydrogen bonds occur between the hydrogen of the OH-6 primary hydroxyl and oxygen in position O3 in a cycle of a neighboring unit, as well as the hydrogen of OH-2 and oxygen in position O6.

It is well known that the unidirectional parallel orientation of cellulose chains within the elementary fibrils, occurring during biosynthesis and deposition, induces the formation of crystals having one side face with hydroxyl pendant groups known as the non-reducing end and another front face with reducing end groups bearing hemiacetal functionality. Each cellulose chain possesses directional asymmetry with respect to the termini of its molecular axis: one end has a hemiacetal group (green labeled groups in Figure 1.7), a chemically reducing functionality, and the other has a pendant hydroxyl group, the nominal non-reducing end (pink labeled groups in Figure 1.7).

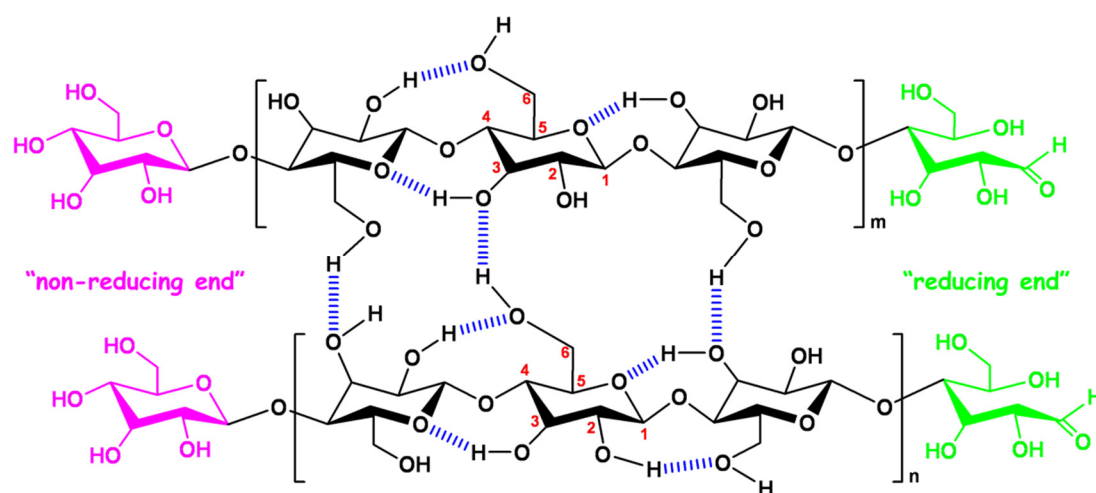


Figure 1.7 Schematic representation of chemical structure and intra-, inter- molecular hydrogen bonds in crystalline cellulose.

One of the most specific characteristics of cellulose is that each of its monomers bears three hydroxyl groups, which endows cellulose nanocrystals a reactive surface covered with numerous active hydroxyl groups. For each anhydroglucose unit, the reactivity of hydroxyl groups on different positions is heterogeneous. The hydroxyl group at the 6 position acts as a primary alcohol whereas the hydroxyl groups in the 2 and 3 positions behave as secondary alcohols. Indeed, the carbon atom which carries the hydroxyl group in the 6 position is only attached to one alkyl group, while the carbons with the hydroxyl groups in the 2 and 3 positions are joined directly to two alkyl groups, which will induce steric effects derived from the supramolecular structure of cellulose and the reacting agent.⁷⁸ It has been reported that on the structure of cellulose, the hydroxyl group at the 6 position can react ten times faster than the other OH groups, while the reactivity of the hydroxyl group on the 2 position was found to be twice that of at the 3 position.⁷⁹ However, regarding the surface reactivity of hydroxyl groups from nanocellulose (such as CNC), the use of reactants or solvents may affect the reactivity of hydroxyl groups from different positions. Recent studies reported the order of reactivity for hydroxyl groups on CNC as nucleophiles with $\text{OH-C6} = \text{OH-C2} > \text{OH-C3}$ by etherification. The reactions between hydroxyl groups and reagents only occur or are controlled on the surface of cellulose nanocrystals. Geometrical considerations obtained from microscopic observations are generally used to determine the content of active hydroxyl groups on the surface of nanocrystals. With the calculation according to the Connely surface methodology, it was reported around 3.8 mmol/g available hydroxyl groups for cotton cellulose nanocrystals with average width $d = 4$ nm and average length $L = 250$ nm.⁶³ Recently, total content of surface hydroxyl groups on cellulose nanocrystals was reported to be affected by the cross-section shapes, such as 0.96 mmol/g for square or round cross-section model, 1.55 mmol/g for ellipse cross-section model, and 2.65 mmol/g for rectangle cross-section model.²⁷ However, even for these surface cellulose chains, not all hydroxyl groups are accessible, since some are oriented toward the inner of the nanoparticle. Indeed, due to different orientation of some hydroxyl groups and high crystallinity of nanocrystals, as well as large difference in reactivity of hydroxyl groups, it was assumed that the fraction of

hydroxyl groups available on the surface for the chemical modification was only 1/3 for nanocrystals.⁸⁰

The surface chemistry of cellulose nanocrystals, especially surface groups, is mainly governed by the hydrolysis procedure for the extraction of nanocrystals. As discussed previously (Figure 1.2A), besides hydroxyl groups ($-OH$), diverse surface groups can also be introduced on cellulose nanocrystals during different hydrolysis process, including sulfate groups ($-OSO_3^-/H^+$), carboxyl groups ($-COO^-/H^+$), and acetyl groups ($-COCH_3$). Recently, it is reported that with some mild reactions, surface hydroxyl groups on cellulose nanocrystals can be simply converted as other active groups, such as amino groups ($-NH_2$),⁸¹ thiol group ($-SH$).⁸²

1.2.2.2 Surface charges

The dispersion stability of cellulose nanocrystals is dependent on the electrostatic repulsion caused by surface charged groups. The surface hydroxyl groups remain intact during hydrochloric acid hydrolysis, resulting in essentially no introduction of charged groups. The amount of surface charge on cellulose nanocrystals prepared by hydrochloric acid hydrolysis is therefore zero, which can be called as “charge-free” nanocrystals (although traces of carboxyl groups up to 1.8×10^{-5} mol/g of cellulose may be detected for nanocrystals from bleached wood pulp, as a result of oxidative bleaching of the starting material).⁸³ In contrast, surface sulfate groups are introduced on cellulose nanocrystals during sulfuric acid hydrolysis via condensation esterification (sulfation) between surface hydroxyls and an H_2SO_4 molecule, using another H_2SO_4 molecule as a condensation agent. The H_2SO_4 -hydrolyzed nanocrystals, therefore, are highly negatively charged, and form a well-dispersed aqueous colloidal suspension. Surface charge amounts from sulfate groups of cellulose nanocrystals can be controlled through the duration and temperature of H_2SO_4 hydrolysis. Phosphate group with negative charges was also reported to be introduced on the surface of cellulose nanocrystals, using a urea-phosphoric acid mixture for surface phosphorylation reaction.⁸⁴ Another negatively charged group, carboxyl group, can also be introduced on the surface of cellulose nanocrystals with the acid hydrolysis and subsequent

TEMPO oxidation.

Besides the anionic surface charged groups, viz. negatively charged nanocrystals, the preparation of positively charged cellulose nanocrystals by post-surface treatments was also reported. Epoxypropyltrimethylammonium chloride,^{85,86} and quaternary ammonium salts^{87,88} were generally used as cationization agents for the preparation of cationic cellulose nanocrystals. The type and amount of surface charged groups, ζ -potential value, and dimensions of electrostatically stabilized cellulose nanocrystals are summarized in Table 1.3.

Table 1.3 Surface charge amount and type, ζ -potentials, and dimensions for various electrically stabilized cellulose nanocrystals. (Adapted from Ref. 89)

Types of charged group	Source of CNs	Amount of surface charge		ζ -potential (mV)	Dimensions of CN (nm)		Ref.	
		In mol per g of CN	In e (nm ⁻²)		Width	Length		
sulfate	wood	8.4×10 ⁻⁵	—	—	3.5	180±75	[83,90]	
		^a 4.7×10 ⁻⁵	—	-32	6±1.5	145±25	[91]	
		—	—	-51.5±0.8	8±1	90±10	[92]	
	cotton	—	0.16	—	—	7	115	[67,93]
		9.38–	—	—	—	7	177–390	[21]
		21.2×10 ⁻⁵	—	—	—	—	—	—
		—	0.41±0.05	-39±3	5–10	100–350	[94]	
	tunicin ^b BC	8.5×10 ⁻⁵	—	—	—	20	2200	[95]
		5.0×10 ⁻⁶	2.0×10 ⁻²	—	—	10–50	1000–	[96]
		—	—	—	—	2000	—	—
—	—	1.53×10 ⁻⁵	5.1×10 ⁻²	—	40±20	800±250	[97]	
		6±3×10 ⁻⁶	—	—	7±17	855	[98]	
—	ramie	—	0.6	—	10.8±4.5	134±59	[99]	
carboxyl	cotton	7.6×10 ⁻⁴	—	—	23±7	250±91	[100]	
	cotton	~1.14×10 ⁻³	—	—	5–10	100–200	[101]	
trance carboxyl	wood	1.8×10 ⁻⁵	—	—	3.5	180±75	[84]	
phosphate	wood	3.0×10 ⁻⁵	—	—	3.5	180±75	[84]	
^c HTAP	cotton	1.12×10 ⁻⁴	0.26	+30±5	11±2	174±18	[85]	
	wood	0.02–	—	+63	—	—	[86]	
	fiber	2.05×10 ⁻³	—	—	—	—	—	

^a The value is the sum of total anionic groups, including sulfate and carboxyl groups. ^b BC: bacterial cellulose. ^c HTAP: 2-hydroxy-3-trimethyl-ammoniopropyl

1.2.3 Biological Properties

1.2.3.1 Eco-toxicology

Most studies reported non-toxicity of cellulose nanocrystals or toxicity similar to

microcrystalline cellulose and table salt. Kovacs et al. initially studied the inherent eco-toxicology of cellulose nanocrystals with aquatic organisms.¹⁰² Rainbow trout hepatocytes were selected as the model cells, and the toxicity monitoring program as well as the in-depth toxicity assessment component was included in the toxicity testing strategy. With the eco-toxicological characterization, cellulose nanocrystal was found to have low toxicity potential and environmental risk, but showed no harm to aquatic organisms at concentrations that could occur in receiving waters. In another report, the cytotoxicity of cellulose nanocrystals against nine different cell lines was determined by MTT and LDH assay, and no cytotoxic effects of cellulose nanocrystals against any of these cell lines in the concentration range and exposure time studied (0~50 µg/mL and 48 h)¹⁰³ were reported. Similarly, cellulose nanocrystal was also found to have non-toxic effect towards micro-organisms necessary for oxygen take-up.¹⁰⁴ However, recently it was reported that cellulose nanocrystals may induce some slight dose-responsive cytotoxic and inflammatory effects on human lung cells, especially the risk with inhalatory exposure under high concentrations of released cellulose nanocrystal powders.^{105,106}

It is well known that human body can only clear out impurity with the scale in micrometer or above, while nanoparticles will penetrate into cells and eventually remain in the system. Therefore, although studies conducted so far on cellulose nanocrystals seem to indicate absence of toxicity, the research and systematic assessment of eco-toxicology of cellulose nanocrystals are still incomplete and need deeper investigation, especially for the effect of nanoparticle aggregation in body and long-term *in vivo* data.

1.2.3.2 Biocompatibility

Biocompatibility is referred to as the capability of a prosthesis implanted in the body to exist in harmony with tissue without causing deleterious changes, which is an essential requirement for biomedical materials. It is a pity that direct study on the biocompatibility of cellulose nanocrystals is rare. Even for the evaluation of the biocompatibility of cellulose, the different studies are difficult to compare due to the

range of methodologies and sample preparations. According to the early reports,^{107,108} cellulose can be generally considered to be broadly biocompatible, invoking only moderate (if any) foreign body responses *in vivo*. More recently, cellulose nanocrystals or its composites were also reported to be used as bioscaffolds for cell cultivation (which will be further introduced in Section 1.5.1.3). However, regardless the type of cellulosic material (native cellulose, nanofibrillar cellulose, or cellulose nanocrystals), it is sensible to judge the biocompatibility of such materials on a case-by-case basis.¹⁰⁹

1.2.3.3 Biodegradability

In terms of degradation, cellulose may be considered as non-biodegradable *in vivo* or, at best, slowly degradable, due to the lack of cellulase enzymes in animals. However, the form (i.e., crystallinity, hydration and swelling) of cellulose may affect the degree of degradation, absorption and immune response observed. Nonenzymatic, spontaneous biodegradability of cellulose chains may perhaps account for slow breakdown of unaltered cellulose within the human body, though this is admittedly conjecture and has not been adequately studied.¹¹⁰ In an early *in vivo* study, Miyamoto et al. found that the degradation of cellulose and cellulose derivatives in canine specimens depended significantly on the cellulose crystalline form and chemical derivatization.¹⁰⁷ Regenerated cellulose prepared by deacetylation of cellulose acetate (presumably the highly crystalline cellulose II polymorph) did not measurably degrade over the course of the 6-week experiment. Contrarily, however, up to 75% (w/w) of equivalent samples of amorphous regenerated cellulose were degraded and absorbed over the same experimental period.¹⁰⁷ Another study reported that cellulose nanocrystals were actually more biodegradable than their macroscopic counterparts in aqueous environments.¹⁰⁴ Recently, oxidized cellulose was rendered more vulnerable to hydrolysis and therefore potentially degradable by the human body. Based on this proposal, researchers attempted to enhance the biodegradability of cellulose through oxidation, such as the report of improving bacterial cellulose degradability *in vitro* (in water, phosphate buffered saline, and simulated body fluid) through periodate oxidation.¹¹¹ However, no *in vivo* result on the improvement of bacterial cellulose

biodegradability through oxidation treatment was reported, which needed further investigation.

1.3 Surface Modification of Cellulose Nanocrystals

1.3.1 Approaches and Strategies for Surface Modification

1.3.1.1 Purpose and Challenge

Efficiency of nanofiller dispersion in a continuous matrix and adequacy of nanofiller-matrix interfacial interactions are widely known to critically affect material physical and mechanical properties. Hydroxyl groups present on cellulose and sulfate ester units introduced during hydrolysis with sulfuric acid both contribute to the hydrophilic character of cellulose nanocrystals. However, owing to the electrostatic character and high ionic strength of CN, it is difficult to achieve a good dispersion level of the nanoparticles in most common non-water organic solvents or non-polar polymeric matrices. The reasons stem primarily from the inefficient electrostatic repulsion and establishment of strong hydrogen bonds between nanocrystals, which induce the rapid aggregation or flocculation of the colloidal suspension in highly hydrophobic media.⁸

To prevent self-aggregation and promote efficient dispersion in non-aqueous media, the surface of CN can be modified with hydrophobic compounds using covalent or non-covalent coupling approaches. The purpose of the modification of CN consists in reducing the surface energy and improving the degree of dispersion by transforming the polar hydroxyl groups sitting at the surface of nanocrystals into moieties capable of enhancing the interactions with non-polar polymers. In most cases the surface modification of CNs can be conducted to (1) introduce stable negative or positive electrostatic charges on the surface of nanocrystals to obtain better dispersion; (2) tune the surface energy characteristics of nanocrystals to improve compatibility, especially when used in conjunction with non-polar or hydrophobic matrices in nanocomposites; and (3) tailor the nanoparticles to impart specific functional groups on nanocrystals for advanced functional nanomaterials. The main challenge for surface modification of CN

is to choose a reagent and reaction medium that enable modification in such a way that it only changes the surface of nanocrystals, while preserving the original morphology to avoid any undesired bulk changes,¹¹² polymorphic conversion and to maintain the integrity of the crystal.⁷⁶

1.3.1.2 Comparison of Approaches and Strategies

Surface modification of CN can be achieved by attaching small molecules or polymers via covalent bonds or physical interactions. A wide variety of surface modification techniques can be performed on the surface of CN, including physical absorption of surfactant, chemical derivatization of coupling hydrophobic small molecules, or chemical grafting of polymeric chains and advanced functional molecules (as shown in Figure 1.8). These modification methods generally rely on the surface functionality such as hydroxyl groups in native cellulose or on functionality derived from synthesis of the nanoparticles as a “handle” for modification.¹¹³ Among these methods, a convenient operation and procedure, i.e. physical absorption of surfactant or polymer coating, is the simplest treatment in comparison with chemical modification. However, this method was developed for improving dispersibility of CN in organic solvents and is not expected to be effective in composite applications because of the lack of covalent bonding between the hydroxyl groups from CNs and the groups from surfactants. In the field of chemical modification, derivatization is the most effective approach to change the surface properties of CNs, involving the hydrophilicity, surface charge and density,

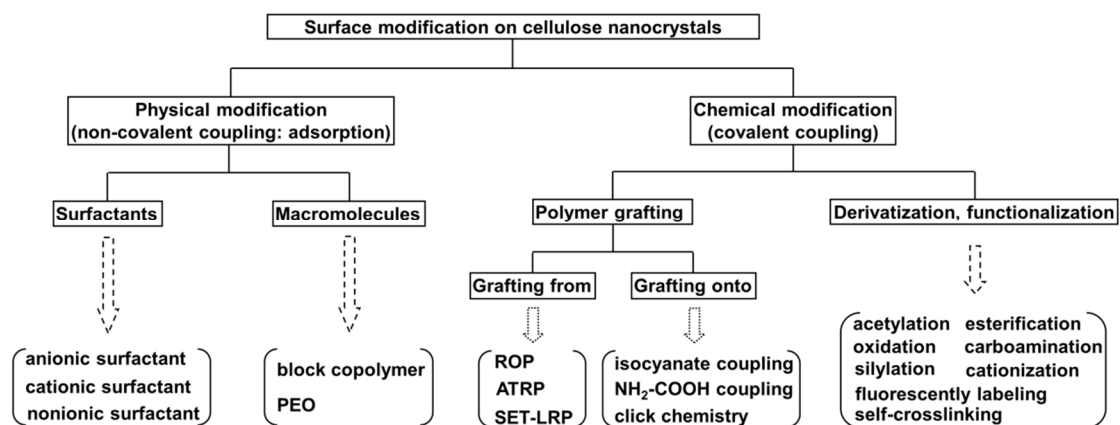


Figure 1.8 Diverse surface modifications on cellulose nanocrystals.

which can be carried out with the covalent conjunction between nanocrystals and hydrophobic small molecules. In spite of easy achievement, it should be paid more attention to the degree of derivatization on CNs to avoid the destruction of the substrate if the reaction is pushed too far. Modification consisting of introducing functional molecules on CN is a rather new field largely depending on its unique properties. Some novel techniques such as “click chemistry” have been used in the functional modification on CNs, which endows nanocrystals with advanced functions, such as fluorescent labeling, gene delivery or photobactericidal effect.

Another chemical modification method, polymer grafting, can be realized with two strategies, namely ‘grafting onto’ and ‘grafting from’. The ‘grafting onto’ approach involves attachment of pre-synthesized polymer chains, carrying reactive end groups, to the surface of CNs, whereas the ‘grafting from’ approach consists in mixing nanocrystals with a monomer and an initiator agent to induce the polymerization of the monomer from the nanoparticle surface. The schematic representation of diverse approaches of modification of CNs is shown in Figure 1.9. For the first approach, traditional ‘carboxylation–amidation reaction’ consisting in creating a covalent amide bond between a primary amine-terminated polymer and carboxylated CNs by COOH–NH₂ coupling and ‘isocyanate-mediated reaction’ depending on the different reactivity of isocyanate groups are widely used to graft polymeric chains onto the surface of nanocrystals. The grafted polymers can be fully characterized before grafting on the surface, offering the possibility of controlling the properties of the prepared material. However, one can’t expect high grafting densities because of steric hindrance and blocking of reactive sites by the already grafted polymer chains using the ‘grafting onto’ method. ‘Grafting from’ has been proved to be a very effective approach to create high grafting densities and well-controlled polymer structures on different kinds of surfaces. Surface-initiated ring opening polymerization (ROP) and living radical polymerization (LRP) are two methods that can be used for the strategy of ‘grafting from’. In ROP, the hydroxyl groups on the surface of CNs act as initiator and the ratio of monomer (such as ϵ -caprolactone or L-lactide) to initiating groups determines the DP

of the grafted polymer chains. For LRP modification, such as atom transfer radical polymerization (ATRP) and single electron transfer-living radical polymerization (SET-LRP), two steps are involved, which are the initial formation of initiating sites for LRP with the immobilized initiator on CNs, and the reaction of the initiator-modified nanoparticles with a monomer to induce the polymerization. Because of the lower viscosity of the medium and limitation of steric hindrance, this strategy has been proved to be an effective way to create high grafting densities on the surface. However, the drawback of this approach is the difficulty to precisely determine and characterize the molecular weight of grafted polymers. To solve this problem, some studies recently reported methods of cleaving the polymeric chains from the cellulose backbone, such as dissolving PS-grafted CNs¹¹⁴ or PDMAEMA-grafted CNs¹¹⁵ in acidic condition with acid hydrolysis or saponification treatment to cleave grafted PNiPAAm polymeric chains from the surface of grafted CNs.¹¹⁶

Recently, some new strategies for the surface modification on CNs have been proposed, such as grafting amine compounds or drug molecules on nanocrystals through the change of glucose structure with periodate oxidation, while keeping the crystalline integrity of nanocrystals.^{117,118}

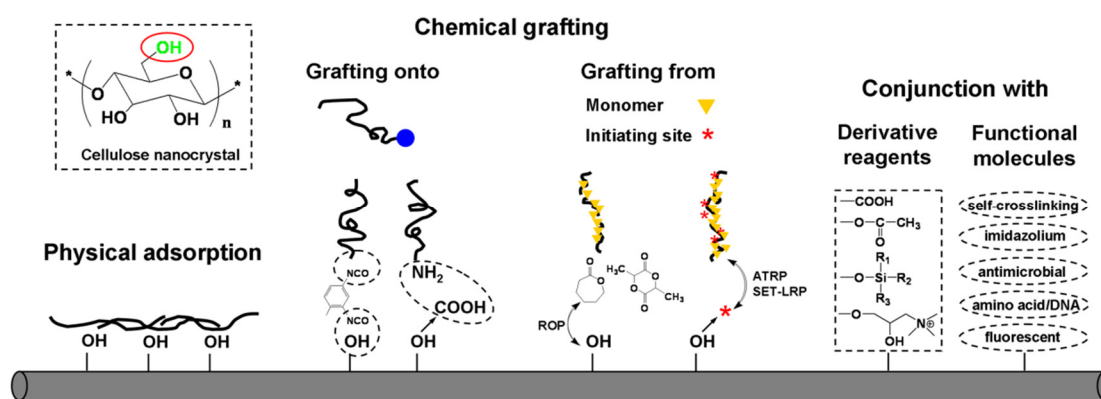


Figure 1.9 Comparison of different modifications of cellulose nanocrystals.

1.3.2 Adsorption of Anionic, Cationic and Nonionic Surfactants

In order to obtain non-flocculated dispersion of CNs in non-polar solvents, the easiest approach is to coat the surface of nanocrystals with surfactants having polar heads and long hydrophobic tails. With the simple mixing in solvent, non-covalent physical

absorption of surfactant on CNs will be a much more controllable and easy-operated process than delicate chemical modification. Surfactants are usually amphiphilic organic compounds, containing both water-insoluble (oil soluble) component for hydrophobic groups (so-called tails) and water-soluble component for hydrophilic groups (so-called heads). The hydrophilic end of the surfactant molecule may adhere on the surface of CNs whereas the hydrophobic end may extend out providing a non-polar surface and lowering the surface tension of the nanoparticles. With this process, the ensuing surfactant-coated nanoparticles display reduced surface energy and improved dispersibility or compatibility with non-polar organic media.

Since surfactant Beycostat NA (BNA) was applied as stabilizing agent to prepare stable suspensions of CNs in nonpolar solvents,¹¹⁹ there were more studies focusing on the influence and property of BNA-modified CNs. BNA is a commercial anionic surfactant, and its chemical structure involves a phosphoric ester of polyoxyethylene nonylphenyl ether. It was shown that the mixing ratio of surfactant and CNs should be cautiously controlled. A low amount of surfactant is not sufficient to obtain a good dispersion in organic solvents, whereas a too high amount of surfactant may induce self-aggregation of nanoparticles during the mixing process. Meanwhile, using small angle neutron scattering, it was observed that a surfactant layer 15 Å thick coated the surface of CNs, which indicated the effective adsorption of BNA and folded conformation of the surfactant molecule on the surface of nanocrystals.¹²⁰ In further studies, the properties of BNA-adsorbed CNs, such as morphology, self-assembling and chiral nematic property, were investigated with various techniques including AFM, TEM, and FESEM.¹²¹ Particularly, the chiral nematic ordering of BNA-adsorbed CNs suspensions in cyclohexane with different concentrations was observed and discussed.¹²² When using these surfactant-modified CNs as nanofillers to reinforce polymeric matrix (such as PLA or PP), the presence of the surfactant on the surface of nanocrystals was found to facilitate the dispersion of the nanofiller in the matrix and improve the nucleation effect of the matrix for ensuing materials.^{123–125}

Different from the hydrophilic-hydrophobic mechanism for the absorption of common

surfactants, cationic surfactant (such as DODA-Br) can be adsorbed on the surface of CNs through strong electrostatic interactions between the negative charge of sulfate groups on H₂SO₄-hydrolyzed nanocrystals and cationic charge of the surfactant. DODA is a cationic surfactant that has been widely used in Langmuir films to investigate adsorption and binding processes involving anionic polyelectrolytes at the air/water interface. Rojas et al. applied cationic surfactant DODA to modify the surface of CNs, and used this surfactant as the carrier to crosslink cellulose nanoparticles.¹²⁶ With Langmuir-Schaeffer (LS) technique, the precursor CNs-DODA complexes were subsequently used to prepare monolayer films.

A nonionic surfactant, such as sorbitan monostearate, was also used to improve the dispersion of CNs in organic solvents and to prevent their self-aggregation.¹²⁷ From the results of turbidity experiment performed on 0.3 and 0.6 wt% nanocrystals suspension in THF, it was reported that the surfactant concentration determined the stability of modified CNs in solvent. For high surfactant concentrations, the surfactant molecules self-aggregate and probably do not adhere to the surface of nanocrystals, which probably caused the weak stress transfer effect when using CNs as reinforcing filler. The same surfactant was used to improve the dispersion of CNs in a polystyrene (PS) matrix and to produce bead-free electrospun composite webs.¹²⁸ In another study, as a small surfactant molecule, *tert*-butanol, was used to modify the surface of CNs.¹²⁹ It was reported that *tert*-butanol was able to limit the aggregation of nanocrystals during freeze-drying process, and promote more loose condition and homogeneous dispersion in poly(lactic acid) (PLA) matrix.

1.3.3 Hydrophobic Groups from Chemical Derivatization

Because of their high surface area and hydrophilic nature, CNs tend to seriously aggregate through hydrogen bonding, and can't be easily dispersed in apolar solvents and are poorly compatible with hydrophobic matrices. The inefficient reinforcement results from poor dispersion induced by poor interfacial interaction between pristine CNs and non-polar polymer matrices. Derivatization is one of the simplest and immediate approach considering diverse chemical modifications. The chemical

derivatization is mainly divided into five categories, which are acetylation (or esterification), oxidation, carboamination, silylation and cationization.

1.3.3.1 Acetyl and Ester Groups with Acetylation and Esterification

Surface esterification is the most common way for the chemical derivatization of CNs. It is a reaction that introduces an ester functional group COO on the surface of nanocrystals by condensation of a carboxylic acid group COOH and alcohol group OH. As one of the simplest method of esterification, acetylation that introduces an acetyl group COCH₃ on the surface of CNs, has been well studied generally using acid anhydrides as acetylating agent.

1.3.3.2 Carboxyl Groups from TEMPO-Mediated Oxidation

In general, there are three targets for the utilization of TEMPO-mediated oxidation of cellulose. The first one aims the change of surface properties of CNs. The second one is the transformation of surface hydroxyl groups to carboxyl groups, which can be used for subsequent introduction of functional molecules or grafting polymeric chains with carboxylation–amidation reaction. The third target consists in using TEMPO-mediated oxidation coupled with low speed mechanical treatment for the conversion of native cellulose to micro- or nanofibers and preparation of nanocellulose.

TEMPO and its analogues are water-soluble, commercially-available and stable nitroxyl radicals. With the TEMPO catalytic oxidation, the C6 primary hydroxyls of cellulose are expected to be oxidized to C6 carboxylate groups by TEMPO/NaBr/NaClO or TEMPO/NaClO/NaClO₂ oxidation systems in water at pH 10–11.^{130,131} The oxidation process can be monitored from the pattern of aqueous NaOH consumption, which is continuously added to the reaction mixture to maintain the pH at 10 during oxidation. The oxidized products have almost homogeneous chemical structures of sodium (1→4)-β-D-poly-glucuronate or sodium salt of cellouronic acid consisting of D-glucuronosyl units alone. Hence, the C6 primary hydroxyls of cellulose can be entirely and selectively converted to C6 sodium carboxyl groups by TEMPO-mediated oxidation.¹³² Araki et al. first applied TEMPO-mediated

oxidation to introduce carboxyl groups and then graft PEG chains onto the surface of CNs. It was a pity that this study only focused on the effect of grafting polymers, and changes of dispersion state and fingerprint texture of oxidized CNs.¹⁰¹ Montanari et al. systematically investigated the degree and size influence of the TEMPO-mediated oxidation of cotton linter CNs.¹³³ The degree of oxidation (DO) was determined by conductometric titration as 0.24. During TEMPO-mediated oxidation, a decrease of the crystal size occurred, and the introduction of negative charges on the surface of the crystalline domains induced a better individualization and dispersion of the crystallites,¹³³ as shown in Figure 1.10a and a'. In another study, the maximum degree of oxidation (DO_{max}) for CNs with TEMPO treatment was calculated as 0.095 (roughly 0.1) with a simplified rectangle model. With the change of NaClO/anydroglucose unit ratio, the degree of oxidation of CNs varied from partial oxidation ($DO=0.029$) to nearly complete oxidation ($DO=0.097$).¹³⁶

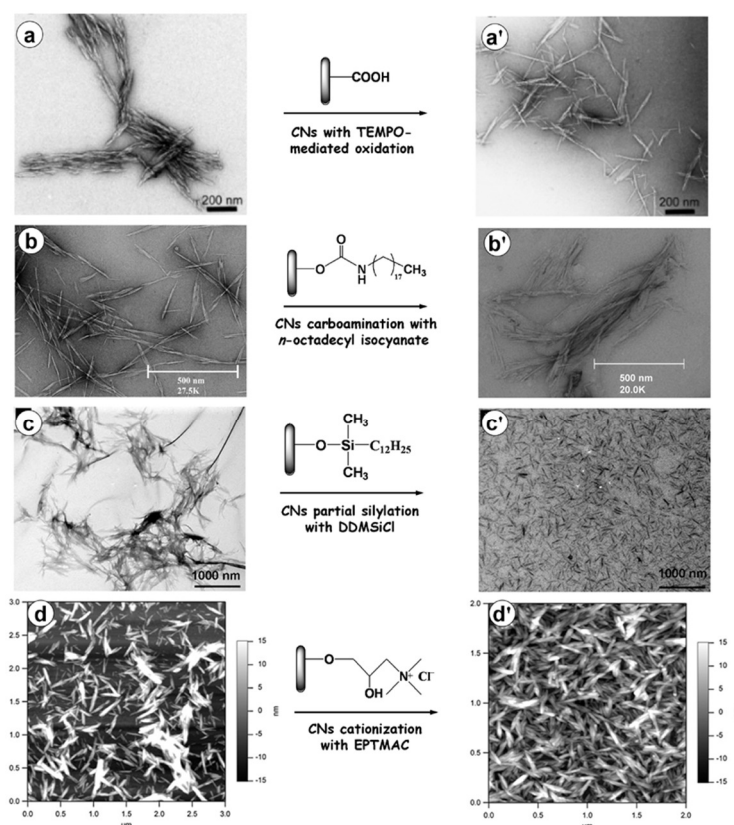


Figure 1.10 (a and a') TEM images of cotton CNs and TEMPO-oxidized CNs;¹³³ (b and b') TEM images of sisal CNs and carboaminated CNs;¹³⁴ (c and c') TEM images of cotton CNs and silylated CNs dispersed in THF;¹³⁵ (d and d') AFM height images of cotton CNs cationic modified CNs.⁸⁵

1.3.3.3 Derivatization with Isocyanate Carboamination

Through the reaction between isocyanate group and hydroxyl group, isocyanate possessing a single isocyanate group can be coupled onto the surface of CNs. The chemical modification with isocyanate as coupling agent presents some advantages such as (i) relatively high reaction rate; (ii) absence of secondary products, and (iii) chemical stability of urethane moiety.¹³⁷ Isocyanates used for the derivatization modification of CNs were mainly phenyl isocyanate (PI), dimethylbenzyl isocyanate (TMI) and *n*-octadecyl isocyanate (C₁₈H₃₇NCO). The former reagents (PI and TMI) are isocyanates bearing a rigid phenyl in their chemical structure. The reactivity of isocyanate with OH group is higher than that of anhydride and, on the other hand, aromatic NCO group is more reactive than aliphatic one. It was reported that the modification on CNs using long-chain *n*-octadecyl isocyanate with a degree of substitution DS of 0.07 improved the dispersion of CNs in dichloromethane, as shown in Figure 1.10b and b').^{80,134} Recently, a new isocyanate agent, UPy-NCO, was used for the surface modification of CNs, which can provide active UPy motifs for further reactions.¹³⁸

1.3.3.4 Silyl Groups from Silylation

Silylation consists in the introduction of substituted silyl groups on the surface of cellulose nanocrystals. The chemical structure of organosilanes (R₁R₂R₃SiX) presents two kinds of functional groups, namely hydrophobic aliphatic groups with different lengths of carbon chains (R₁R₂R₃) and functional groups (X) for the coupling with hydroxyl groups of CNs. In the structure of most silylating agents used for the derivatization of CNs, R₁ and R₃ are generally methoxy, and R₂ varies from one carbon chains to twelve carbon chains (CH₃, *i*-C₃H₇, *n*-C₄H₉, *n*-C₈H₁₇, *n*-C₁₂H₂₅). X is a hydrolyzable group able to react with active hydroxyl groups from CNs, typically alkoxy, acyloxy, amine, or more commonly chlorine.

Trimethylsilylation was first applied for the silylation modification of CNs.³² The topochemically trimethylsilylated derivatization of CNs reduced their hydrophilicity and improved their dispersion in acetone. However, the degree and mechanism of

silylation of CNs were not investigated. Goussé et al. studied the process of silylation modification of CNs and proposed a mechanism model to describe the influence of silylation on CNs structure. Four alkyltrimethylchlorosilane silylating agents (IPDMSiCl, BDMSiCl, ODMSiCl, and DDMSiCl), with alkyl moieties ranging from isopropyl to *n*-butyl, *n*-octyl and *n*-dodecyl, were used to prepare more stable silylated CNs.¹³⁹ It was shown that under low degree of silylation, just a few silyl groups are distributed randomly on the surface of CNs, which provided them the structural integrity but unchanged hydrophilic property. If too much silylating agent is used or too long reaction duration is performed, excessive silylation breaks up the cellulose chains and cause the solubilization of CNs in the reaction medium. Therefore, silylated derivatization of CNs should be controlled in the moderate degree range to provide a sufficient number of silyl groups, and confer a change to hydrophobic surface but not induce the destruction of the original structure of CNs. With the silylating agent DDMSiCl, Pei et al. conducted partial silylation of cotton CNs in toluene (as shown in Figure 1.10c and c'), and used the modified CNs to reinforce PLA.¹³⁵ The effect of methacryloxypropyltrimethoxysilane (MPS) as silylating agent for the surface modification of CNs was also investigated.¹⁴⁰ Recently, A-174 as new silane coupling agent for the surface silylation of CNs was reported. This special silylating agent can provide vinyl groups on the surface of CNs acting as the initiator for successive free radical polymerization.¹⁴¹

1.3.3.5 Cationic Groups from Cationization

A few studies were conducted on the surface cationic modification of CNs, to convert surface anionic charges to cationic charges. Surface cationization of CNs with 2,3-epoxypropyltrimethylammonium chloride (EPTMAC) proceeds through the nucleophilic addition of the alkali-activated cellulose hydroxyl groups to the epoxy moiety of EPTMAC.⁸⁵ The cationization process reversed the surface charge from -39 ± 3 mV before to $+30 \pm 5$ mV after treatment with EPTMAC, and led to a reduction of the total surface charge density from $0.41 e \text{ nm}^{-2}$ to $0.26 e \text{ nm}^{-2}$. The modification also promoted the formation of stable dispersions and cationized CNs were more

spreadable than pristine CNs on flat mica surfaces, as shown from AFM images in Figure 1.10d and d'. Glycidyltrimethylammonium chloride (GTMAC) and quaternary ammonium salts were also used as cationic agents for surface cationization of CNs.^{86,87} Different from the common electrostatic adsorption method, a chemical grafting method was proposed to introduce cationic poly(ethylene imine) (PEI) polymers on the surface of CNs. The synthesis of PEI-grafted CNs included three steps, which were surface modification of CNs using tosyl chloride, then cationic ring opening grafting polymerization of 2-ethyl-2-oxazoline monomer with tosylated CNs as macroinitiators, and finally production of cationic PEI-modified CNs with the hydrolysis treatment in acidic condition.¹⁴²

1.3.4 Polymeric Chains with Physical Adsorption or Chemical Grafting

The practical application of CNs faced many obstacles mainly related to poor dispersibility in common nonpolar solvents and interfacial incompatibility between the hydrophobic components and hydrophilic CNs. To prevent the aggregation and improve the compatibility of CNs in diverse matrices, polymer chain grafting seems to be of interest because the grafted polymer chains can act as compatibilizer, particularly when they are of the same nature as the matrix, which can further improve the interfacial adhesion and maximize the compatibility between both components. On the other hand, grafting special polymers on CNs may endow these natural nanoparticles advanced functional application. Polymer grafting can be accomplished by utilizing different approaches such as “grafting onto” or “grafting from” strategies. Polymer adsorption can also promote interfacial interactions with a polymeric matrix.

1.3.4.1 Hydrophilic Polymer–PEG and PEO

Cellulose nanocrystals are hydrophilic and therefore have limited ability to disperse in hydrophobic solvents and polymer matrices.¹⁴³ To restrain the coagulation of nanoparticles in apolar solvents, the method of grafting or adsorption of hydrophilic polymers on the surface of CNs was proposed. This modification involves the steric colloidal stabilization of CN suspension, which results from the hindrance of direct contact between nanoparticles and therefore inhibition of suspension coagulation. A

promising candidate is poly(ethylene glycol) (PEG), a water-soluble polymer consisting of hydrophilic and flexible long chains. Four synthetic routes were proposed to introduce PEG (or PEO) on the surface of CNs, which were mainly based on the strategy of “grafting onto” and physical interaction, as shown in Figure 1.11. However, one of the drawbacks of the “grafting onto” approach is the increase of the viscosity of the reaction medium especially for polymeric chains with high molecular weight (M_n). Therefore, the M_n s of grafted PEG onto CNs in these systems were lower than 2500 g/mol. In 2001, Araki et al. first reported the steric stabilization of CN suspensions by PEG grafting using a carboxylation–amidation procedure.¹⁰¹ By grafting PEG in a ratio of 0.2–0.3 g/g of cellulose on CNs, the modified CNs showed drastically enhanced dispersion stability and ability to redisperse into either water or chloroform from the freeze-dried state. However, due to uncompleted reaction between surface carboxyl groups and amino groups (only 20–30% carboxyl consumption in the amidation step), the improved stability effect induced by the modification could not exactly be proved. For these reasons, Kloser and Gray proposed an alkaline epoxide ring-opening method for the surface grafting of PEG onto CNs.¹⁴⁴ Desulfation of sulfuric acid-prepared

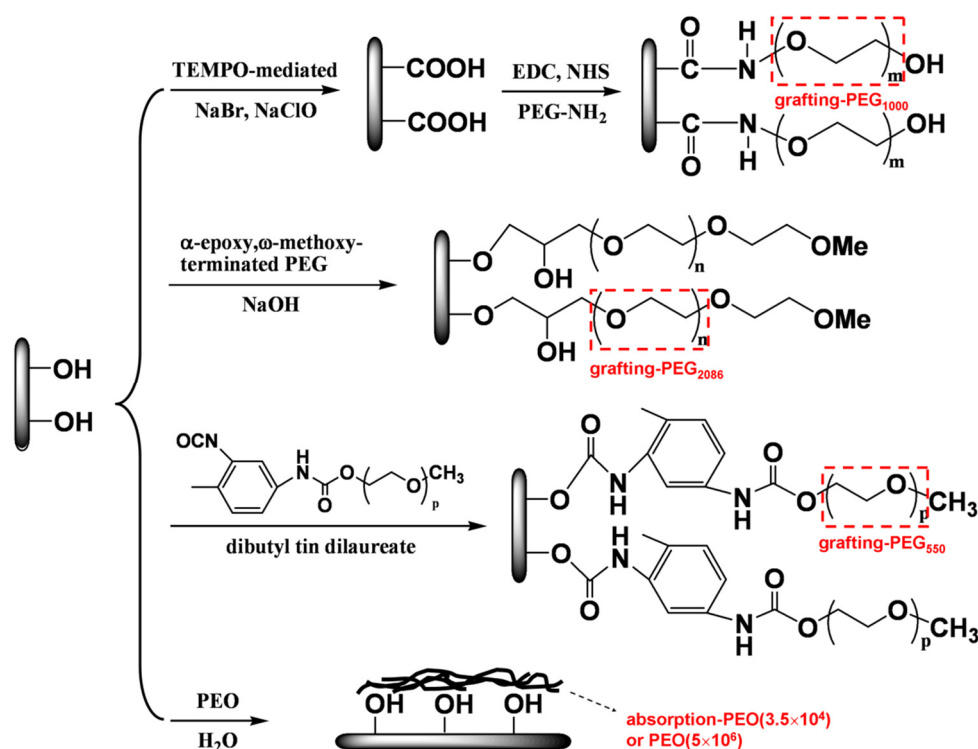


Figure 1.11 Different methods of introducing PEG chains on the surface of cellulose nanocrystals.

nanocrystals were carried out and the nanoparticles were modified with α -epoxy, ω -methoxy-terminated PEG under alkaline conditions. Aqueous dispersions of PEG-grafted CNs were stable over time and exhibited similar phase behavior as the initial electrostatically stabilized CN suspensions, with the onset of chiral nematic phase separation occurring at 5 wt%.

Physical interaction of PEG with cellulose in water was performed to introduce high molecular weight PEG (polyoxyethylene-PEO) on the surface of CNs. Different from grafting PEG of low molecular weight, adsorbed long PEO chains wrapped the nanoparticles and promoted the interactions between CNs and apolar matrix, which improved the dispersibility and thermal stability of CNs.¹⁴⁵

1.3.4.2 Polyester–PCL and PLA

Aliphatic polyesters constitute the most versatile group of degradable polymers, which are often biocompatible and hydrophobic with low glass transition temperature. In the family of polyester, poly(caprolactone) (PCL) and poly (lactic acid) (PLA) are the most common materials, which can be traditionally synthesized by ring-opening polymerization (ROP) of cyclic ϵ -caprolactone and L-lactide monomers, respectively. Therefore, grafting of PCL and PLA polymeric chains (especially PCL) on the surface of CNs was widely investigated.

In the initial stage, several studies mainly focused on grafting PCL chains onto CNs with isocyanate-mediated reaction. This chemical modification is based on the different reactivity of the two isocyanate groups from 2,4-TDI, the isocyanate at the 4-position being 7 times more reactive than the isocyanate at the 2-position.¹⁴⁶ Grafting PCL onto the surface of CNs involves a three-step process. The first step requires the reaction of PCL on isocyanate group of phenylisocyanate. The second step involves the reaction of PCL, now protected, with 4-position isocyanate group of 2,4-TDI. During the third step, unreacted 2-position isocyanate group of 2,4-TDI is then reacted with the surface hydroxyl groups of CNs to graft PCL chains onto the nanoparticles. PCL chains with various molecular weights (such as 10000, 42500, 80000 and 2000 g/mol) were grafted onto CNs for the reinforcement of co-continuous nanocomposites or electrospun

nanofibers.^{147,148} It was shown that the grafting efficiency decreased with the length of polymeric chains, and there was stronger reinforcing effect for long chains PCL-modified CNs to nanocomposites resulting from presence of chain entanglements and co-crystallization.

Because of the high achievable grafting density, and possibility of chain length control, the “grafting from” strategy is generally privileged aiming in grafting PCL chains on the surface of CNs in recent studies. Regarding this modification, the hydroxyl groups on the surface of nanocrystals act as initiator to induce the polymerization of cyclic ϵ -caprolactone (CL) monomer and the ratio of monomer to initiating groups determines the DP of the grafted polymer chains. The grafting reaction was performed under predetermined conditions and stopped by adding a few drops of dilute hydrochloric acid solution. The non-grafted PCL homopolymer can be removed by solubilization–centrifugation or Soxhlet extraction. Surface grafting of hydrophobic PCL moieties on CNs can facilitate the dispersibility of nanoparticles in hydrophobic systems. Habibi et al. and Goffin et al. applied Sn(Oct)₂-catalyzed ROP grafting of PCL on CNs to reinforce a PCL matrix using casting–evaporation²⁹ and extrusion.¹⁴⁹ In another study, Lin et al. performed microwave irradiation to assist PCL surface ROP on CNs, and prepared filaceous PCL-grafted CNs¹⁵⁰ that were used to reinforce PLA matrix. Reaction conditions and grafting efficiency reported in the literature for the preparation of PCL-grafted CNs are summarized in Table 1.4. Citric acid was also used as a benign alternative to metal catalyst in surface-initiated ROP for grafting PCL on CNs. With “green” citric acid as catalyst, grafting efficiency of PCL on the surface of CNs was up to 58 wt %, about 4 times higher than for earlier reported PCL-grafted CNs using common catalyst of Sn(Oct)₂.¹⁵¹ Carlsson et al. reported the monitoring of CN surface grafting with PCL by Quartz Crystal Microbalance, which provided a tool to regulate the polymerization reaction.¹⁵²

Recently, two studies investigated the reproducibility and interfacial molecular modeling of the PCL grafting on the surface of CNs. It was reported that the process of Soxhlet extraction using ethanol before modification can effectively remove the

adsorbed low molecular weight organic compounds produced during the hydrolysis, which may block the reactive sites of CNs and cause the variable surface composition.²² Molecular dynamics simulation was used to estimate the adhesion based on surface energies with different amounts of grafted caprolactone. The modifications on nanocrystals lead to an increased work of adhesion between the surface and its surrounding medium. Hydrogen bonds were formed extensively between the grafted caprolactone and the surrounding medium.¹⁵³

Table 1.4 Reactive conditions and grafting efficiency for the preparation of poly(caprolactone) (PCL)-grafted CNs (*L*= length, *W*= width, *T*= thick, *D*= diameter; *GE*%: Grafting efficiency).

Source of cellulose	Dimensions of CNs (nm)	Method	Catalyst/coupling agent	Solvent	Condition	<i>GE</i> %	Ref.
ramie	<i>L</i> =150-250 <i>D</i> =6-8	grafting onto	2,4-TDI	toluene	70-80 °C, 7 days	—	[147]
ramie	<i>L</i> =100-250 <i>D</i> =3-10	grafting onto	2,4-TDI	toluene	75 °C, 24 h	30%	[148]
ramie	<i>L</i> =150-250 <i>D</i> =6-8	grafting from	Sn(Oct) ₂	toluene	95 °C, 24 h	85%	[29, 149]
cotton linter	<i>L</i> =200-300 <i>D</i> =10-20	microwave -grafting from	Sn(Oct) ₂	—	several minutes	85%	[150]
cotton wool	—	grafting from	citric acid	—	120 °C, 24 h	58%	[22, 151]

Another biodegradable polyester, namely PLA, was chemically grafted on the surface of CNs using the “grafting from” strategy with Sn(Oct)₂-catalyzed ROP of L-lactide initiated from the hydroxyl groups available on the CNs surface.¹⁵⁴ The grafting reaction was performed in toluene at 80 °C for 24 h, and grafting efficiency of PLA chains was determined by gravimetry as 83%. The effect of covalent bounding of PLA chains on CNs was investigated by dispersion experiment in organic solvent (chloroform) in comparison with ungrafted CNs and CNs with physically adsorbed PLA chains. It was shown that hydrophobic PLA chains grafted on CN surface were highly solvated maintaining the nanoparticles in more stable and homogeneous suspension in the apolar solvent. Another study investigated the “grafting from” strategy for high molecular weight PLA chains with partial pre-acetylation of surface hydroxyl groups to control the grafting density, while maintaining sufficient interparticle contact for efficient stress transfer within a percolating network.¹⁵⁵

1.3.4.3 Polymethacrylates

Originating from the attributes of “livingness”, control, and robustness from living radical polymerization (LRP), the techniques of surface-initiated ATRP (SI-ATRP) and SET-LRP (SI-SET-LRP) were developed to “graft from” polymer chains or brushes on the surface of CNs. It was proved to be a versatile technique to synthesize well-defined polymers with high surface grafting density and low polydispersity on the surface of CNs. Copper-mediated LRP is generally chosen for its versatility with respect to monomer choice and ease of synthesis. Generally, two steps are involved in the chemical modification of grafting polymeric chains on CNs with LRP techniques, as shown in Figure 1.12. The first step is the initial formation of initiating sites for LRP, in which an initiator is immobilized on the nanoparticles, and macromolecular initiator (commonly used as CNs-Br) can be obtained. It should be pointed out that 2-bromoisobutyryl bromide (BriB) is always chosen for the esterification of nanocrystals, and provides the initiating sites. To prevent the destruction of the crystalline structure of CNs, this reaction should be performed at low temperature (sometimes with ice bath), which can dissipate superfluous heat. The second step involves the reaction of the initiator-modified nanoparticles with monomers (C=C alkene molecules) to induce the polymerization.

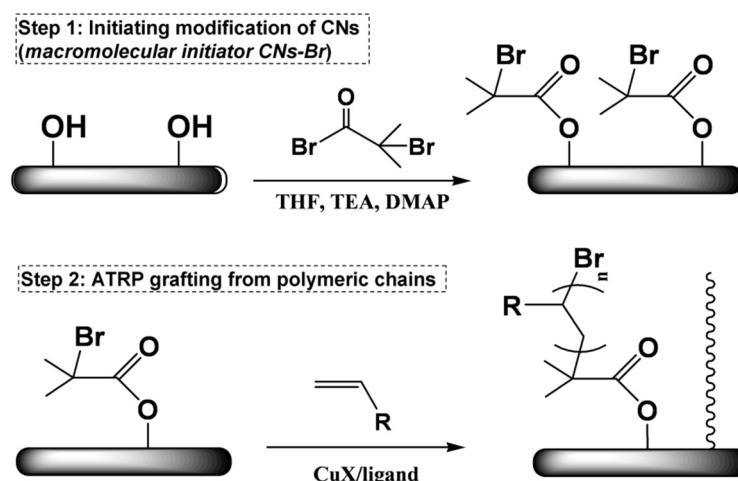


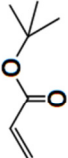
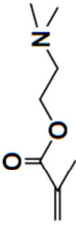
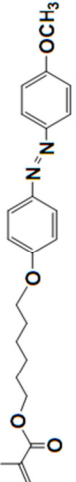
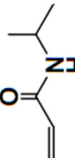
Figure 1.12 Synthetic routes of grafting polyolefin chains on CNs with the technique of ATRP.

Early reports on using SI-ATRP to graft polyolefin polymeric chains on CNs surface were published by Zhang et al. concerning polystyrene (PS),¹¹⁴ poly [2-(*N,N*-dimethyl

amino) ethyl methacrylate] (PDMAEMA),¹¹⁵ and poly{6-[4-(4-methoxyphenylazo) phenoxy] hexyl methacrylate} (PMMAZO).¹⁵⁶ All modifications were performed on the investigation of CNs extracted from filter paper, and the focus of these studies emphasized on liquid crystal phase behavior and fingerprint texture of modified CNs. It was a pity that the amount of bromine in the initiator-modified CNs was very low (only 0.6 wt%) in these studies, which restricted the subsequent grafting reaction. On the other hand, the issue of grafting polymeric chains with different lengths, which implied the controllable feature of ATRP, was not investigated. By altering the extent of initiator surface modification through polymerization control, Morandi et al. produced PS-grafted CNs with varying grafting densities and different polymer brush lengths.¹⁵⁷ Various grafting densities of PS on the surface of CNs were realized by controlling the final content of initiating sites under different conditions (duration and temperature of BriB/CNs reactions). They further reported a method of grafting a photosensitive moiety bearing initiating sites onto the surface of CNs, followed by grafting PS chains with ATRP. This new pathway for the synthesis of PS-grafted CNs provided a possibility to degraft the PS chains using UV-irradiation, and exactly investigated the grafted polymer brush length and molecular weights.¹⁵⁸ Walther et al. reported an effective method of chemical vapor deposition (CVD) and continued esterification to improve the initiator density on CN surface.¹⁵⁹ The simple CVD pretreatment of BriB for CNs was conducted for 24 h at room temperature (5 wt% bromine content), which promoted the subsequent esterification to obtain more initiating sites (15 wt% bromine content). Whereafter, poly(acrylic acid) (PAA) polyelectrolyte chains were grafted from CNs via Cu-mediated surface initiated-ATRP of tert-butyl acrylate (tBA) and subsequent hydrolysis. Via SI-SET-LRP technique at room temperature,¹¹⁶ CNs derived from ramie fiber can be grafted with thermoresponsive poly(*N*-isopropylacrylamide) (PNiPAAm) brushes. In their further study, based on these grafted copolymers, an ultrathin and temperature-responsive material was prepared without the need of anchoring polymeric matrix.¹⁶⁰

With the method of HCl hydrolysis or saponification, grafted polyolefin chains can be

Table 1.5 Reactive conditions and properties of various grafted polyolefin chains on CNs with the technique of ATRP and SET-LRP.

Monomer	Polymeric chain	Catalyst/ ligand	Solvent	Condition	^a Grafting efficiency	Grafted polymer (M_n)	^b PDI	Ref.
	PS	Cu(I)Br/ HMTETA	—	110 °C 12 h	68%	74700	1.21	[114]
		Cu(I)Br/ PMDETA	anisole	30 °C or 70 °C 16 h or 24 h	24%-40%	2800-17800	1.09 -1.13	[157]
	PtBA (PAA)	Cu(I)Br/ PMDETA	DMF	75 °C	—	6200-36300	1.10	[159]
	PDMAEMA	Cu(I)Br/ HMTETA	CH ₃ OH	55 °C 12 h	53%	10,200	1.38	[115]
	PMMAZO	Cu(I)Br/ HMTETA	chlorobenzene	90 °C 24 h	74.6%	—	—	[156]
	P(NiPAAm)	Cu(I)Br/ PMDETA	H ₂ O:MeOH	25 °C 24 h	—	10630-42860	1.20	[116]

^a The grafting efficiency listed here is determined according to the weight percent of grafted polymer in the modified-CN.

^b PDI is polydispersity index, which represents the uniform degree of M_n from grafted polymers on CNs.

cleaved from the surface of CNs, and the properties of grafted polymers, such as molecular weight (M_n) and polydispersity, can be carefully investigated by gel permeation chromatography (GPC) or size exclusion chromatography (SEC). As shown in Table 1.5, diverse monomers, reactive conditions and properties of grafted polyolefin chains on CNs are summarized.

Despite the advantages of controllability and high grafting density of surface-initiated LRP, there are some shortcomings for this technique, which are the inconvenience of experimental operation (with three freeze-pump-thaw or vacuum-nitrogen cycles) and rigorous reactive conditions of anaerobic circumstance. Some studies exploited other approaches to graft polyolefin on the surface of CNs. Harrisson et al. grafted PS and poly(*t*-butyl acrylate) (PtBA) chains on CNs via the carbodiimide-mediated amidation reaction between the terminal amine groups from polyolefin polymers and carboxylic acid groups on the surface of oxidized CNs.¹⁰⁰ PS or PtBA polymers were first synthesized on a chemical of *N*-(2-(2-Bromoisobutyryl) ethoxy) ethyl phthalimide, which provided the terminal amine groups through subsequent deprotection reaction. Whereafter, the hydrophobic polymer was grafted onto the surface of oxidized CNs with the amidation reaction. The polymer-grafted nanocrystals can be readily dispersed in nonpolar solvents such as acetone.

1.3.4.4 Block Copolymer

Besides the introduction of hydrophilic polymers (such as PEG) and hydrophobic polymers (such as polyolefin), block copolymers including both hydrophilic and hydrophobic segments can be used to modify the surface of CNs. A kind of saccharide-based amphiphilic triblock copolymer, xyloglucan oligosaccharide-poly(ethylene glycol)-polystyrene (XGO-*co*-PEG-*co*-PS), was used for the surface modification of CNs.¹⁶¹ The triblock copolymer was pre-synthesized and physically adsorbed on CNs in the DMF/H₂O (1:100 v/v) solvent. The weight fraction of adsorbed copolymer on CNs was determined as 45% by TGA. The modified CNs with adsorbed triblock copolymer were easily redispersed in organic solvent (toluene), and chiral nematic self-ordering of modified CNs was observed in nonpolar solvent. In another

study, Azzam et al. introduced PPG-*co*-PEG copolymers on the surface of CNs using the “grafting onto” approach.¹⁶² The coupling reaction was performed between the carboxyl groups from oxidized CNs and amine-terminated groups from Jeffamine copolymers either in water or in DMF. It was shown that in DMF, the low molecular weight copolymer can be grafted onto CNs with a high grafting density ($DS=0.1049$). Individual nanocrystal was decorated by a shell of polymer chains, which induced the steric stabilization, surface-active, and thermoreversible aggregation of modified nanoparticles. However, due to the limitation of “grafting onto” strategy, only copolymers of low M_n (1000 or 2070 g/mol) can be used in this chemical modification.

1.3.4.5 Other Hydrophobic Polymer

Polypropylene (PP) is a common hydrophobic polymer, which is classically used as the representative apolar matrix. The comparison of the reinforcing effect of CN grafted with maleated PP and CN dispersed with the surfactant Beycostat NA (BNA) into atactic PP as the matrix was reported.¹⁶³ It was shown that the PP-grafted CNs tended to aggregate in the matrix, and reduced the ductility of ensuing nanocomposites, whereas surfactant-coated CNs showed good dispersion in the matrix (transparent films), and improved ductility. Via the carboxylation–amidation procedure, polypropylene glycol (PPG, $M_n=600$) hydrophobic chains can also be grafted onto the surface of CNs with the covalent reaction between carboxylated CNs and amine-terminated PPG.¹⁶⁴ The approach involving direct ‘grafting onto’ modification for the introduction of hydrophobic polymers on CNs seems to be inefficient, which may be attributed to the weak interaction resulting from the compulsive conjunction between hydrophilic nanocrystals and hydrophobic long chains.

1.3.5 Advanced Functional Groups

Recently, more and more studies have led to the emergence of diverse potential special applications of CNs as advanced functional nanomaterials, which are closely associated with their modification using common derivatization or polymer grafting through the introduction of advanced functional groups.⁶³ The properties and applications of these functional nanomaterials based on CNs will be systematically discussed in Section 1.5,

and this section will just focus on the modification reaction and process.

1.3.5.1 Fluorescent and Dye Molecules

Through covalent conjunction with nanoparticles, fluorophores can be used to label these nanoparticles not only for fluorescence bioassay and bioimaging applications but also for the investigation of bioeffects and safety of nanoparticles inside cells or human being. For the first time, Dong and Roman introduced a fluorescent molecule (FITC) on the surface of CNs via a three-step approach.¹¹ First, the surface of the nanocrystal was decorated with epoxy functional groups via the reaction with epichlorohydrin. Then, the epoxy ring was opened with ammonium hydroxide to introduce primary amino groups on CNs. Finally, the primary amino group was reacted with the isothiocyanate group of FITC, in which covalent association between CNs and FITC was realized via the formed thiourea groups. It was shown that unlabeled suspension was colorless and slightly opaque, whereas FITC-labeled CNs suspension appeared clear and yellow. Meanwhile, according to the results of UV/vis spectroscopy, FITC-labeled nanocrystals showed absorption maxima of both the dianionic (490 nm) and the anionic (453 and 472 nm) form of FITC, whereas unlabeled CNs did not show any absorption peaks in the wavelength range 200 to 600 nm. In another study, with similar method, two fluorescent molecules (FITC and RBITC), were introduced on the surface of CNs, which was used to investigate the effects of cellular uptake and cytotoxicity for different fluorescent CNs.¹⁶⁵ The grafting of fluorescent terpyridine molecules^{166,167} and pyrene molecules¹⁶⁸ on the surface of CNs was also reported.

Ryley and Thielemans developed two synthetic approaches to introduce two fluorescent or dye molecules on CNs for the preparation of dual fluorescent labeled CNs.¹⁶⁹ The dual fluorescent labeled CNs (FITC and RBITC labeled CNs) and two dual dyes labeled CNs (FAM-SE and TAMRA-SE labeled CNs as well as OG-SE and TAMRA-SE labeled CNs) both exhibited pH sensing in McIlvaine buffers with varying pH conditions.

1.3.5.2 Amino Acid and DNA

As natural rigid nanocrystals, CNs are expected to be good candidates for the construction of biocompatible and biologically active nanomaterials, such as drug carrier and gene delivery. The anchoring of amino acid or DNA molecules on the surface of CNs allows the creation of a binding site to which drugs or targeting molecules can be attached. The chemical modification of L-leucine on CNs was performed through a two-step process involving the reaction between Fmoc-protected L-leucine and thereafter the removal of Fmoc-protecting group. The first step consisted in the reaction between CNs and Fmoc-L-leucine using DMAP as the catalyst and EDC·HCl as the coupling agent. The removal of the protecting Fmoc group was performed by stirring Fmoc-L-leucine CNs in piperidine/DMF solution.¹⁷⁰ Mangalam et al. developed the synthetic route of grafting different single-stranded oligonucleotides with an amino modifier on CNs, and subsequent duplexing complementary oligonucleotides formed with individual modified CNs via the molecular recognition ability of the oligomeric base pairs.¹⁷¹ The grafting reaction of amino-modified ssDNA on CNs was realized using the carboxylation–amidation procedure. Two kinds of oligonucleotide-modified CNs, both strand A and strand B modified CNs, were mixed together in water for the preparation of duplexed DNA-modified CNs. It was shown that complementary strands of DNA bonded to separate populations of CNs hybridized under suitable conditions to form bonded structures.

1.3.5.3 Photobactericidal Porphyrin Molecule

With the benefits of biocompatibility and biodegradability of CNs, these kind of natural nanoparticles have been more studied for biomedical material applications. Feese et al. developed surface-modified CNs with cationic porphyrin via the Cu(I)-catalyzed Huisgen–Meldal–Sharpless 1,3-dipolar cycloaddition “click reaction” occurring between azide groups on the cellulosic surface and porphyrinic alkynes.^{172,173} During the reaction, about 50% of all azide groups on the surface of modified CNs were substituted by porphyrin molecules. Covalent attachment of porphyrin molecule to the

surface of CNs will potentially contribute to the longer lasting or permanent antimicrobial property, minimizing the leaching of the biocidal agent into the surrounding environment.

1.3.5.4 Self-Crosslinking of Nanocrystals

Contrarily to the traditional application of CNs as the reinforcing filler, some studies apply CNs themselves to be the matrix for the construction of self-crosslinked materials. Goetz et al. first developed the self-crosslinking of CNs extracted from MCC with poly(methyl vinyl ether comaleic acid) (PMVEMA) and PEG as the crosslinking agents by reacting varying amounts of CNs (0–100%).^{174,175} The crosslinking of CNs with PMVEMA and PEG was anticipated to occur via an esterification reaction among the hydroxyl groups of cellulose, terminal hydroxyl groups of PEG and the carboxylic acid groups of PMVEMA. The crosslinking between three components trapped the nanocrystals in the crosslinked network, preventing aggregation and subsequently producing CNs self-crosslinked nanomaterials through intramolecular and interchain reactions.

In another study, a three-step route of click chemistry was utilized for the synthesis and formation of cellulose nanoplatelet gels with the regular self-crosslinking of CNs.¹⁷⁶ Initially the primary hydroxyl groups on the surface of CNs were selectively activated by converting them to carboxylic acids using TEMPO-mediated oxidation. Further reactions were carried out via carbodiimide-mediated formation of an amide linkage between precursors carrying the amine groups and the carboxylic acid groups on the surface of oxidized CNs. Finally, with two kinds of modified CNs containing the azide derivative or alkyne derivative on their surface, the click chemistry reaction of Cu(I)-catalyzed Huisgen 1,3-dipolar cycloaddition between the azide and the alkyne was performed on CNs, bringing together the nanocrystalline materials in a unique regularly packed arrangement demonstrating a degree of molecular control for creating self-crosslinked CNs nanomaterials.

Inspired by the water-enhanced mechanical gradient character of the squid beak, Fox et al. recently reported a mechanical gradient nanocomposite made from modified

tunicate CNs by nanocrystals–nanocrystals crosslinking in PVA matrix. CNs were first modified by the introduction of allyl moieties on the surface. With the addition of small molecule tetra-thiol cross-linker and radical photoinitiator, modified CNs self-crosslinked under exposure to UV irradiation via photoinduced thiol–ene chemistry reaction. With the control of UV exposure duration, the degree of crosslinking of the nanocrystals can be regulated, and fabricated mechanical gradient nanocomposites.¹⁷⁷

1.4 Nano-Reinforcement of Cellulose Nanocrystals in Plastic Composites

The use of cellulose nanocrystals as reinforcing additive (or named as nanofiller) is their most widely studied application. They have the potential to significantly enhance the mechanical performance of plastic composites. As shown in Table 1.6, more than half of recent review publications on cellulose nanocrystals during past three years focused on or mentioned their application in composites. Various instances will be only summarized but not repeatedly expounded in this section and the emphasis will be put on the discussion of enhancing effect and mechanism.

1.4.1 Processing Techniques

Four common strategies, viz. casting-evaporation, melt-compounding, electrospinning, and layer-by-layer assembly, have been reported in the literature to homogeneously mix cellulose nanocrystals with a polymeric matrix, as shown in Figure 1.13. The earliest study on the effect of processing approach to properties of cellulose nanocrystals-based composites was reported by Hajji et al.¹⁹³ Composites prepared by casting-evaporation method showed higher mechanical performance than melt-compounding method, which was probably attributed to less structural damage and preservation of nanocrystals' orientation in matrix during casting-evaporation.

Because of the good dispersion level of sulfated cellulose nanocrystals (H_2SO_4 hydrolysis) in water, it is simple to process nanocomposites by casting and water evaporation using either water-soluble polymers or polymer aqueous dispersions

Table 1.6 Review publications on cellulose nanocrystals during past three years (2012–2014).

Title	Journal	Year	Ref.
Processing of polymer nanocomposites reinforced with cellulose nanocrystals: a challenge	Int. Polym. Proc.	2012	[178]
Green composites from sustainable cellulose nanofibrils: a review	Carbohydr. Polym.	2012	[179]
Cellulose nanocrystals and microfibrillated cellulose as building blocks for the design of hierarchical functional materials	J. Mater. Chem.	2012	[180]
Preparation, properties and applications of polysaccharide nanocrystals in advanced functional nanomaterials: a review	Nanoscale	2012	[63]
Review of cellulose nanocrystals patents: preparation, composites and general applications	Recent Pat. Nanotechnol.	2012	[181]
Applications of functionalized and nanoparticle-modified nanocrystalline cellulose	Trends Biotechnol.	2012	[182]
Production of nanocrystalline cellulose from lignocellulosic biomass: Technology and applications	Carbohydr. Polym.	2013	[183]
Cellulose reinforced polymer composites and nanocomposites: a critical review	Cellulose	2013	[184]
Reinforced plastics and aerogels by nanocrystalline cellulose	J. Nanopart. Res.	2013	[185]
State of the art manufacturing and engineering of nanocellulose: a review of available data and industrial applications	J. Biomater. Nanobiotechnol.	2013	[186]
Assessing nanocellulose developments using science and technology indicators	Mater. Res.	2013	[187]
Nanocellulose: a new ageless bionanomaterial	Mater. Today	2013	[188]
Bacterial cellulose scaffolds and cellulose nanowhiskers for tissue engineering	Nanomedicine	2013	[109]
Strength and barrier enhancements of composites and packaging boards by nanocelluloses – a literature review	Nord. Pulp Pap. Res. J.	2013	[189]
Nanocellulose patents trends: a comprehensive review on patents on cellulose nanocrystals, microfibrillated and bacterial cellulose	Recent Pat. Nanotechnol.	2013	[190]
Electrostatic or steric? – preparations and characterizations of well-dispersed systems containing rod-like nanowhiskers of crystalline polysaccharides	Soft Matter	2013	[89]
Sustainable nanomaterials derived from polysaccharides and amphiphilic compounds	Soft Matter	2013	[191]
Key advances in the chemical modification of nanocelluloses	Chem. Soc. Rev.	2014	[192]
Cellulose nanocrystal-based materials: from liquid crystal self-assembly and glass formation to multifunctional thin films	NPG Asia Mater.	2014	[66]

(latex) as matrix. For the processing from water-insoluble polymers, the casting-evaporation approach can be performed by involving a solvent exchange procedure, in which the aqueous suspension of cellulose nanocrystals is solvent exchanged in the proper liquid medium for the dissolution of the polymer by several successive centrifugation and redispersion operations, using sonication after each solvent exchange step to avoid aggregation.¹⁷⁸ This mode of casting-evaporation processing allows the preservation of the individualization state of the nanocrystals resulting from their colloidal dispersion in solvents, and therefore keeps the maximum nanoreinforcing effect for the composites. Indeed, during liquid evaporation, strong interactions between nanoparticles can settle and promote the formation of a rigid percolating network (which will be discussed in the following section). During slow solvent evaporation, because of Brownian motions in the suspension or solution (whose viscosity remains low, up to the end of the process when the latex particle or polymer concentration becomes very high), the rearrangement of the nanoparticles is possible. There is enough time for the interaction and connection among cellulose nanocrystals to form a percolating network, which is the basis of their reinforcing effect for composites.^{194,195}

The wet processing approach, such as casting-evaporation, has been extensively used in various reports for the preparation of cellulose nanocrystal-based composites. However, this technique is both non-industrial and non-economic, and also limits the number of polymer matrices that can be used in association with cellulose nanocrystals. In view of the realization of large-scale production of cellulose nanocrystals (as discussed in Section 1.1.2), more industrial composite processing techniques should be introduced for the preparation of cellulose nanocrystal-based composites, e.g. melt-compounding techniques, such as extrusion or injection molding. The processing through the melt-compounding technique is commonly regarded as a “green” (solvent-free), and industrially and economically viable procedure. However, due to the issues of inherent incompatibility and thermal stability, this processing method is infrequently employed for the preparation of cellulose nanocrystal-based composites.

In fact, the hydrophilic nature of cellulose causes irreversible agglomeration of the nanoparticles during drying and aggregation in non-polar matrices, and the sulfate groups resulting from H_2SO_4 hydrolysis seriously induce the reduction of the thermal stability of nanocrystals.¹⁸⁸

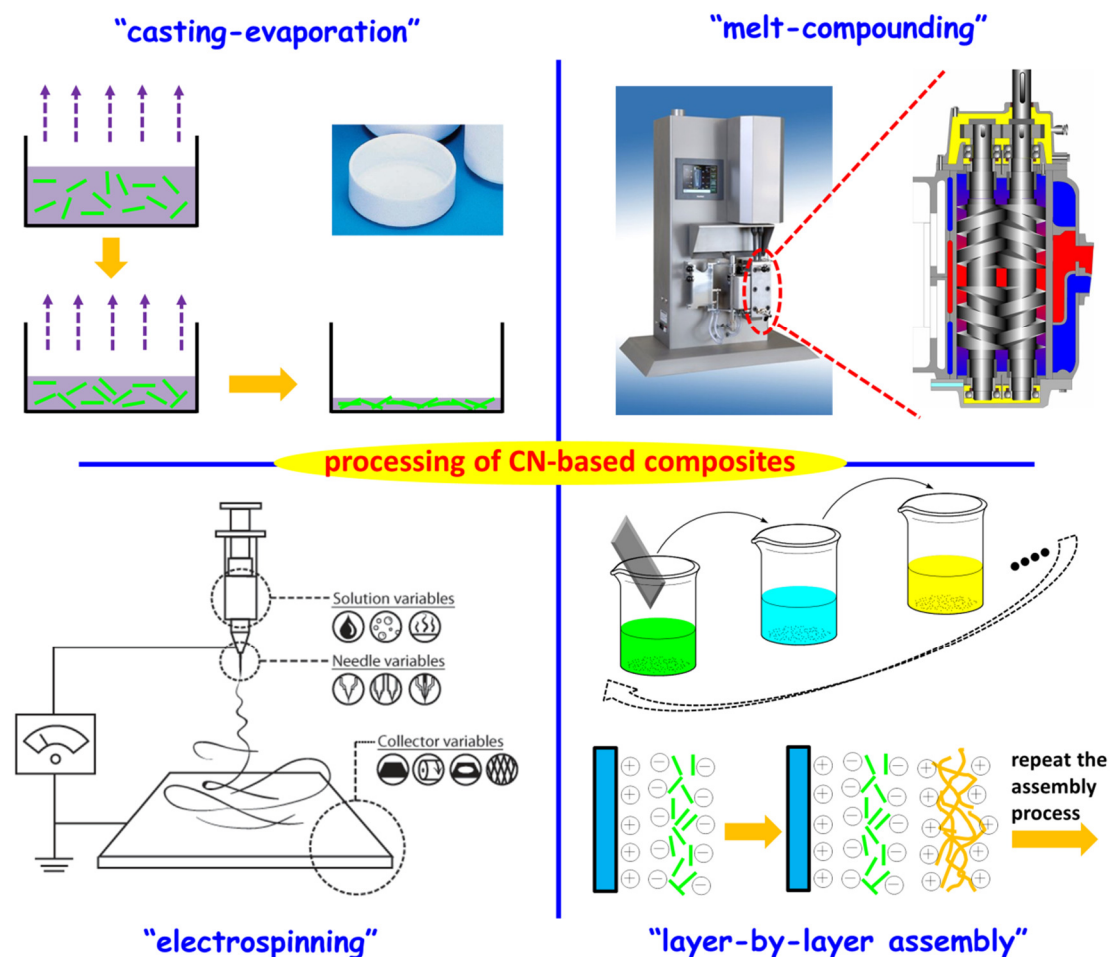


Figure 1.13 Four common processing techniques for the preparation of cellulose nanocrystal (CN)-based composites.

Electrospinning is another alternative processing approach to mix cellulose nanocrystals and polymer matrix, which can be used to prepare composite fibers with diameters ranging from several microns down to 100 nm. In this process, a polymer solution is positively charged to high voltage to produce the submicron scale fibers from an orifice to a collector. Therefore, to find suitable solvents to dissolve cellulose and to process it in the melt state are the key points for this processing technique.¹⁹⁶ Unfortunately, only a few studies reported the preparation of cellulose

nanocrystal-based electrospinning composite fibers, which shows the remaining challenge of this processing approach.

Layer-by-layer assembly (LBL) is a technique by which thin films or nanoparticles of oppositely charged layers are deposited. In a common procedure of LBL assembly, positive or negative charged species are sequentially adsorbed by alternatively dipping into the solutions. The excess solution after each adsorption step is rinsed with solvent and thus a thin layer of charged species on the surface ready for the next adsorption step is obtained. There are many obvious advantages of LBL technique, such as simple manipulation, controllable thickness, and high concentration of cellulose nanocrystals in multilayer films. However, the matrix materials used in this approach must be polycation or polyanion with positive or negative charges (corresponding to anionic sulfated CNs, or cationic modified CNs), as few reported for chitosan, PDDA, PHA, PEI, DODA,⁶³ which limits the wide application of LBL technique.

1.4.2 Pristine Cellulose Nanocrystal Reinforced Plastic Composites

Cellulose nanocrystal-based composites have been studied extensively because of the promising reinforcing effect of these nanoparticles for numerous polymeric matrices. A spectacular improvement of the shear modulus by more than two orders of magnitude was observed in cellulose nanocrystal-reinforced poly(styrene-co-butyl acrylate) latex nanocomposites.¹⁰ Since then, this rod-like nanoparticle was attempted to be incorporated into various polymers, as shown in Figure 1.14. Broadly, the polymeric matrices used for the preparation of cellulose nanocrystal-reinforced plastic composites can be divided into two parts, biodegradable polymers and non-biodegradable polymers. Natural polymers (including cellulose derivatives, starch, natural rubber (NR) etc.) and various biopolymers (such as PHA, PLA, PCL etc.) are commonly used as biodegradable polymeric matrices to prepare cellulose nanocrystals-reinforced “bionanocomposites”. In the family of non-degradable polymers, polymers derived from petrochemical sources are used as matrix for cellulose nanocrystal-reinforced nanocomposites, such as PP, PS, PE etc.

Considering the most used processing approach “casting-evaporation”, aqueous and

organic-solvent systems are two divisions for the preparation of cellulose nanocrystal-based plastic composites. The incorporation of cellulose nanocrystals into aqueous polymer system is relatively straight forward because of the good dispersion of nanocrystals in water. Casting and drying to remove the water result in successful incorporation of cellulose nanocrystals into the polymer matrices. The use of water over organic solvents promotes the use of cellulose nanocrystals in greener production process. However, as discussed before, proper dispersion of cellulose nanocrystals in polymer systems using organic solvents is difficult due to the tendency of nanocrystals to aggregate in these solvents. Despite several reports on the use of DMF, it is still a trouble to find suitable organic solvents for both dispersing cellulose nanocrystals and solubilizing most of hydrophobic polymers. Therefore, in many organic-solvent systems, solvent-exchange procedure is performed to convert the well dispersed cellulose nanocrystals from water to organic solvent (such as ethanol or acetone), and then introduce the suspension into the desired organic polymer solution to prepare composites. The resulting mixture of polymer and cellulose nanocrystals in the organic solvent can be processed in a manner similar to regular polymer solutions, including solution casting and evaporative drying to form thin films, or melting extrusion.¹⁸⁵

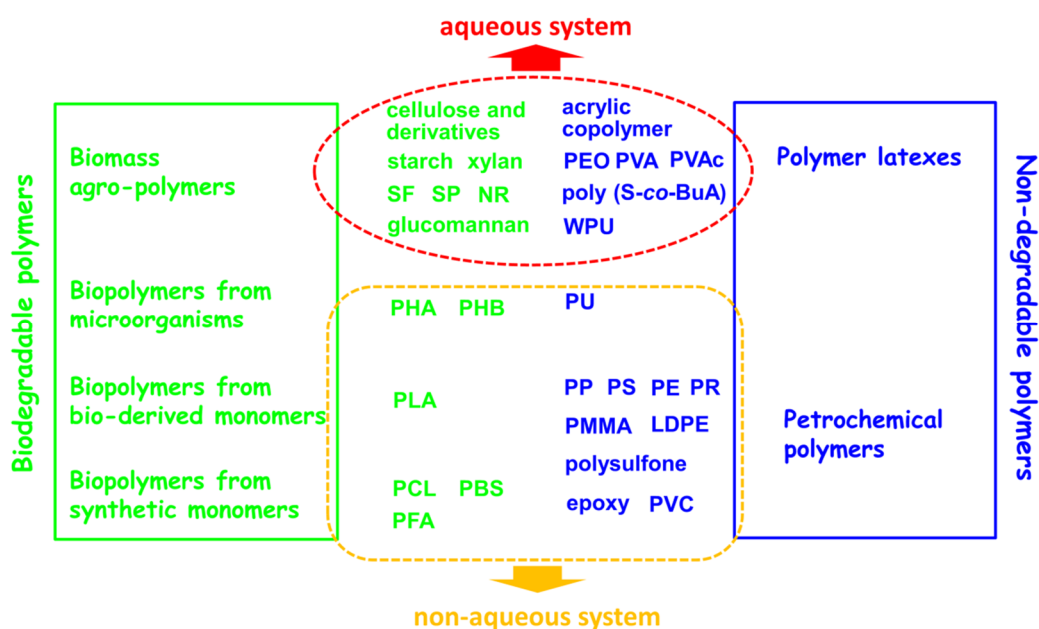


Figure 1.14 Various polymeric matrices used for the preparation of cellulose nanocrystal-reinforcing plastic composites. (SF: silk fibroin; SP: soy protein; NR: natural rubber; PHA: poly(hydroxy alkanoate); PHB: poly(hydroxyl butyrate); PLA: poly(lactic acid); PCL:

polycaprolactone; PBS: poly(butylene succinate); PFA: poly(furfuryl alcohol); PEO: polyoxyethylene; PVA: poly(vinyl alcohol); PVAc: poly(vinyl acetate); WPU: waterborne polyurethane; PU: polyurethane; PP: polypropylene; PS: polystyrene; PR: phenolic resin; PMMA: poly(methyl methacrylate); PVC: poly(vinyl chloride); LDPE: low-density polyethylene)

Generally, when using pristine cellulose nanocrystals in composites, most studies report similar tendency of improved mechanical stiffness, corresponding to the increase of strength and elastic modulus (especially for elastic modulus), but at the cost of elasticity. Mechanical reinforced mechanism will be discussed in the following section.

1.4.3 Modified Cellulose Nanocrystal Reinforced Plastic Composites

In order to promote their dispersion and improve the compatibility of cellulose nanocrystals in non-polar or hydrophobic matrices, the surface characteristics of cellulose nanoparticles can be tuned by surface chemical modification (such as derivatization and grafting) or physical modification (such as coating with surfactant and macromolecules). Various strategies and instances of surface modification of cellulose nanocrystals have been introduced before, so emphasis of this section will be paid on the effects of surface modification to the performance of prepared composites. Table 1.7 summarizes diverse systems of modified cellulose nanocrystal reinforced polymeric matrices for plastic composites.

Surface chemical modification of cellulose nanocrystals has a dual effect on the mechanical properties of ensuing composites. The decoration of nanoparticles with grafted moieties obviously restricts the possibility of inter-particle interactions and then the establishment of a percolating network within the continuous medium. Therefore, the outstanding properties resulting from this phenomenon are definitely lost. However, depending on the matrix and processing conditions, it can allow a better dispersion and then promote the compatibility of the filler with the matrix, which will induce higher mechanical performance to be reached compared to the aggregated state of nanoparticles. Specifically, the approach of chemical derivatization can be easily performed by covalently introducing hydrophobic small molecules or groups, such as acetylation, esterification, silylation etc. Derivatization is the most effective mean to

change the surface properties of cellulose nanocrystals, such as hydrophilicity, surface energy, surface charge and density, which can significantly improve the dispersion of nanocrystals in organic solvents and hydrophobic polymers. Another approach, polymer grafting, is specially beneficial to the enhancement of compatibility between cellulose nanocrystals and matrix, which derives from interfacial interactions between grafted polymer chains and polymeric matrix.

Table 1.7 Modified cellulose nanocrystals reinforcing various matrices for plastic composites.

	Modification	Matrix	Filler content	Processing	Ref.
Physical modification	surfactant coating (sorbitan monostearate)	PS	0–6 wt%	casting-evaporation	[127]
	surfactant coating (BeycostatA B09)	PLA	0–5 wt%	melt-extrusion	[124]
	surfactant coating (BeycostatA B09)	PLA	0–5 wt%	casting-evaporation	[197]
	surfactant coating (BNA)	PP	0–6 wt%	casting-evaporation	[125]
	surfactant coating (sorbitan monostearate)	PS	0–9 wt%	electrospinning	[128]
	polyaniline coating	PU	0–15 wt%	casting-evaporation	[198]
	PEO adsorption	LDPE	0–9 wt%	melt-extrusion	[145]
	polyamide 6 coating	PA	0–3 wt%	melt-extrusion	[199]
Chemical modification	silylation	CAB	0–10 wt%	casting-evaporation	[32]
	silylation	PLA	0–2 wt%	casting-evaporation	[135]
	silylation	PLA	0–3 wt%	melt-extrusion	[140]
	acetylation	PLA	0–10 wt%	casting-evaporation	[200]
	acetylation	CAB	0–7 wt%	casting-evaporation	[201]
	acetylation	PU	0–25 wt%	casting-evaporation	[202]
	carbamation	PCL	0–12 wt%	casting-evaporation	[80, 203]
	carboxylation	protein	0–5 wt%	electrospinning	[204]
	oxidation	fibrin	0–50 wt%	casting-evaporation	[205]
	esterification	PHB	0–7 wt%	casting-evaporation	[206]
	esterification	CAB	0–0.9 wt%	casting-evaporation	[207]
	grafting onto aliphatic chain	LDPE	0–15 wt%	melt-extrusion	[99]
	grafting onto aliphatic chain	PLA	0–15 wt%	melt-extrusion	[208]
	grafting onto PCL	PCL	0–50 wt%	casting-evaporation	[147]
	grafting onto PCL	PCL	0–7.5 wt%	electrospinning	[148]
	grafting onto maleated-PP	PP	0–6 wt%	casting-evaporation	[125]
	grafting onto PHBV	PHBV	0–30 wt%	casting-evaporation	[209]
	in situ grafting onto PU	PU	0–5 wt%	casting-evaporation	[210]
	in situ grafting onto chitosan	chitosan	0–1.9 wt%	casting-evaporation	[211]
	grafting from PCL	PCL	0–8 wt%	melt-extrusion	[149]
grafting from PCL	PCL	0–40 wt%	casting-evaporation	[29]	
grafting from PCL	PLA	0–12 wt%	casting-evaporation	[150]	
grafting from PLA	PLA	0–8 wt%	melt-extrusion	[154]	
carbamation; or grafting from PLA	PLA/NR	0–5 wt%	melt-extrusion; or casting-evaporation	[212, 213]	
grafting onto PEG and adsorbing PEO	LDPE	0–20 wt%	melt-extrusion	[214]	

Non-covalent modification, viz. physical interactions or adsorption of molecules onto the surface of cellulose nanocrystals, is a simpler approach than chemical modification to regulate the properties of cellulose nanocrystals. As introduced before, agents for physical modification of cellulose nanocrystals include diverse surfactants and high molecular weight polymers or copolymers. It is a pity that in order to tune the surface property, the amount of surfactant or macromolecules required to cover cellulose nanocrystals' surface is high, which may undermine the properties of prepared composites. In addition, specific physical interaction and mechanism between cellulose nanocrystals and different adsorbed agents need to be further investigated, especially adsorbing concentration and strength.

Although there have been intensive studies on surface modification of cellulose nanocrystals to reinforce all kinds of polymeric matrices (as shown in Table 1.7), no available industrial modification for the conversion of surface property of cellulose nanocrystals to adapt their practical application in composites is reported. Regardless of physical or chemical modification, each modification method has its limitations. In future, for the purpose of developing cellulose nanocrystal-based composites to replace petrochemical plastics, novel surface modification is required, with simple treatment or procedure, high-efficiency property regulation, optimized performance of composites and industrial production.

1.4.4 Mechanisms for Performance Enhancement

1.4.4.1 Mechanical Properties Enhancement

Besides the processing approaches discussed before, another two factors are also expected to determine the reinforcing capability of cellulose nanocrystals, which are compatibility between nanocrystals and matrix (interfacial mechanism), and dimensions of cellulose nanocrystals (percolating mechanism). Interfacial mechanism refers to the interactions between nanoparticles and matrix, while percolating mechanism only depends on the hydrogen bonds among nanoparticles. The filler/matrix interactions can be tuned by appropriate surface modification treatment of the nanoparticles. This strategy is classically used in composite science to

compatibilize the reinforcing phase with the matrix for optimal performance. The challenge consists therefore in promoting the homogeneous dispersion of cellulose nanocrystals and avoiding agglomeration during processing, thus requiring eventually favorable filler/matrix interactions, and at the same time promoting filler/filler interactions to allow the beneficial formation of a percolating network of nanoparticles. These two requirements are simply conflicting and no suitable strategy has been proposed so far.

Cellulose Nanocrystal/Matrix Interfacial Interactions

Strong interfacial interactions are often associated with the existence of an interphase. By definition, the interphase exists from some points in the fillers where the local properties begin to change from the filler bulk properties, through the actual interface into the matrix where the local properties again equal the bulk properties. The usual question is to quantify the magnitude of the interactions between filler and polymer chains and the distance away from the surface where the force field may be still in effect. If significant specific interactions between polymer and filler exist, this will tend to immobilize a layer of polymer around each solid particle. This immobilized polymer layer contributes to the effective filler volume fraction in the compound.²¹⁵

The filler/matrix interaction can be altered by different means. It obviously depends on the chemical structure of the matrix. Polar matrices tend to strongly interact with the cellulosic surface whereas apolar matrices weakly interact. The polarity of nanoparticles can be tuned by a surface chemical modification allowing favorable interactions with a non-polar matrix. The microstructure of the interfacial zone in the vicinity of the reinforcing phase can also be locally altered by the presence of the filler and affects the mechanical performance of the material.²¹⁵

Rigid Percolating Network

The use of the percolation model to describe and predict the mechanical behavior of cellulose nanocrystal-based composites suggests the formation of a rigid network of nanocrystals, which should be responsible for the unusual reinforcing effect observed at

high temperature. Above the percolation threshold, cellulose nanoparticles can connect and form a continuous pathway through the nanocomposite film. The formation of this cellulose nanocrystal network is supposed to result from strong interaction (hydrogen bonds) among nanocrystals. Generally, percolation modeling consists of three main steps: (1) calculation of the percolation threshold; (2) estimation of the modulus of the percolating network; and (3) model construction.²¹⁶

For cylindrical shape particles, the volume fraction of percolation threshold (v_{Rc}) can be determined with the following equation (1.1):²¹⁷

$$v_{Rc} = \frac{0.7}{L/d} \quad (1.1)$$

where L/d corresponds to the aspect ratio of the rod.

In this percolation approach, the percolating filler network is set in parallel with a series part composed of the matrix and the non-percolating filler phase. The elastic tensile modulus (E_c) of the composite can be calculated by the following equation (1.2), which has been reported to fit adequately the experimental data.

$$E_c = \frac{(1 - 2\psi + \psi v_R)E_S E_R + (1 - v_R)\psi E_R^2}{(1 - v_R)E_R + (v_R - \psi)E_S} \quad (1.2)$$

The subscripts S and R refer to the soft (polymer matrix) and rigid (cellulose nanocrystal) phase, respectively. The adjustable parameter, ψ , involved in the series-parallel model corresponds in the adapted prediction to the volume fraction of the percolating rigid phase. With b being the critical percolation exponent, ψ can be written as:

$$\begin{aligned} \psi &= 0 && \text{for } v_R < v_{Rc} \\ \psi &= v_R \left(\frac{v_R - v_{Rc}}{1 - v_{Rc}} \right)^b && \text{for } v_R > v_{Rc} \end{aligned}$$

where $b = 0.4$ for a three-dimensional network.²¹⁸

At higher temperatures when the polymeric matrix could be assumed to have zero stiffness ($E_S \sim 0$), the calculated stiffness of the composites is simply the product of that of the percolating filler network by the volume fraction of percolating filler phase,

which can be calculated according to the following equation (1.3):

$$E_c = \psi E_R \quad (1.3)$$

1.4.4.2 Thermal Properties Improvement

For most nanocomposite systems reinforced with cellulose nanocrystals, the addition of the nanoparticles did not affect appreciably the glass transition temperature (T_g) and melting/crystallization temperature (T_m) of the host polymer. This observation is quite surprising considering the highly reactive nature and high specific area of polysaccharide nanocrystals. Nevertheless, it can be well understood for hydrophobic polymers because of the poor filler/matrix adhesion. The effect of cellulose nanocrystals on the thermal stability (T_d) of nanocomposites depends obviously on the initial thermal stability of the neat polymer. Improved thermal stability of the composites results from favorable interactions with the cellulosic filler and the confinement effect of the filler to the polymeric matrix.²¹⁹

1.4.4.3 Barrier Properties Enhancement

Most studies of cellulose nanocrystal-based composites focus on their mechanical properties. However, there is an increasing interest in their barrier properties due to increased tortuosity provided by nanoparticles (as shown in Figure 1.15). Indeed, because of their small size, the surface-to-volume ratio of the nanoparticles is significantly greater than that of microparticles. Moreover, the low permeability of cellulose can be enhanced by the highly crystalline nature of cellulose nanocrystals and ability to form a dense percolating network (Figure 1.15). Provided that strong

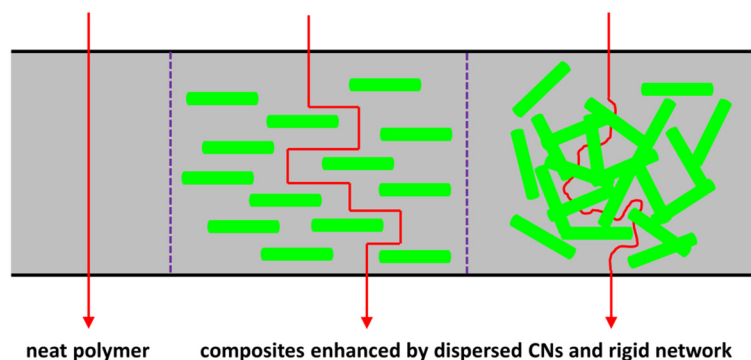


Figure 1.15 Barrier effects of cellulose nanocrystals in plastic composites.

particle-polymer molecular interactions exist, the smaller particles have a greater ability to bond to the surrounding polymer material, thereby reducing the chain segmental mobility and thus the penetrant diffusivity.²²⁰

1.5 Advanced Functional Materials Based on Cellulose Nanocrystals

Based on the special properties and construction strategies of CNs in functional materials, this section will comprehensively discuss the emerging applications on four sections, including surface properties-induced functional materials; unique nano-reinforcing effects in functional materials; optical materials derived from chiral nematic ordering; and special films and systems ascribed to barrier properties.

1.5.1 Surface Characteristics Induced Functional Materials

Even the most rigorous researcher will be attracted by diverse and interesting surface characteristics of cellulose nanocrystals. First of all, cellulose nanocrystals possess a reactive surface covered with numerous active hydroxyl groups ($-OH$), which provide the possibility of modification via a chemical reaction strategy. Designing the chemical grafting routes, various functional molecules or polymeric chains (such as fluorescent molecules, DNA, peptide etc.) can be introduced on the surface of nanocrystals, with the target of tailoring physicochemical properties and contributing novel functions. In addition, surface hydroxyl groups of cellulose nanocrystals can be used as anchoring and stabilizing sites, which provides a preferential template or scaffold for these natural nanocrystals during the synthesis of various inorganic nanoparticles. On the other hand, negatively charged surface (sulfated groups $-OSO_3H$) of CNs resulting from H_2SO_4 -hydrolysis induces the electrostatic stabilization of the nanoparticles in aqueous medium, and also provides the feasibility to perform electrostatic adsorption or grafting. From the reactions by surface charges, CNs can be constructed as high-efficiency adsorbing materials and emulsion nano-stabilizer. Finally, as nanoscaled particles, CNs exhibited promising bioactivity and biocompatibility in cellular cultivation and high surface area for application in water decontamination.

1.5.1.1 Active Groups

Importing Functional Groups or Molecules

Since the first report on the fluorescently labeling of CNs with FITC molecule,¹¹ more and more researchers investigated the fluorescent modification on the surface of CNs. Modification on CNs with fluorescently labeling enables potential use of nanocrystals in the field of biomedical applications, such as optical bioimaging, biosensor, bio-probe, photodynamic therapy (PDT), together with diverse fluorescence techniques, such as spectrofluorometry, fluorescence microscopy, and flow cytometry. Besides the most common FITC reagent, many fluorescent molecules have been attempted to covalently attach on the surface of CNs, such as RBITC,¹⁶⁵ pyrene dyes,¹⁶⁸ terpyridine and its derivatives,^{167,221} tryptophan-based peptides,²²² PSE,²²³ FAM-SE, TAMRA-SE, OG-SE,²²⁴ and PEI-chlorin *p6* derivatives.²²⁵ However, most studies focused on the pathway of introducing fluorescent molecules on CNs, but rarely covered the *in vivo* or even clinic research. Consequently, there is a long way for the practical application of fluorescent cellulose nanocrystals in biomedical materials.

Available hydroxyl groups and negative charges on the surface of CNs provide the possibility of enzyme/protein immobilization on the basis of chemical conjunction and electrostatic adsorption. Regarding the chemical conjunction approach, some studies directly immobilized enzyme/protein on CNs with chemical grafting, such as immobilization of lysozyme on amino-glycine-CNs with carbodiimide-activation coupling reaction;²²⁶ and peroxidase on CNs with the activation of cyanogen bromide treatment.²²⁷ Another approach consists in functionalizing with smaller nanoparticles (generally gold nanoparticles Au), and then realizing the immobilization of enzyme/protein on CNs with the aid of inorganic nanoparticles. Luong et al. investigated Au/CNs as a catalytic platform for enzyme immobilization, which exhibited significant biocatalytic activity and preservation of original activity. The recovered specific activities were ~70% and 95% for CGTase and alcohol oxidase enzymes, respectively.²²⁸ More complicated carrier based on CNs/PEI/Au was developed to immobilize glucose oxidase enzyme.²²⁹ Mahmoud et al. developed a

special nanocomposite consisting of magnetite nanoparticles (Fe_3O_4) and Au nanoparticles embedded on CNs used as a magnetic support for the covalent conjugation of papain and facilitated recovery of this immobilized enzyme.²³⁰ The conjugated material retained high enzyme activity and good stability and reusability. Based on the similar strategy of enzyme/protein immobilization, labeled DNA or enzyme was immobilized on CNs as a probe, and this material can be used for the identification or recognition of target DNA sequence, enzyme molecules, and as a platform for immunoassays and diagnostics.^{231,232} Edwards et al. reported a colorimetric approach to the detection of human neutrophil elastase (HNE) using peptide conjugated cotton CNs.²³³

As mentioned in Section 1.3.5, some reports recently focus on the functional modification of CNs for potential biological application, such as surface grafting of amino acid molecules to offer biologically active building blocks on CNs,¹⁷⁰ surface grafting duplexing complementary DNA oligonucleotides to produce DNA-based biocompatible materials;¹⁷¹ ferrocene-decorated CNs potentially to be used in biosensors and bioelectrochemical assemblies;²³⁴ surface grafting imidazolium salt ([MPIM][Br]) for ion exchange systems or catalysts;¹⁶⁹ and introduced cationic porphyrin groups for the development of photobactericidal materials.^{172,173}

Template for Synthesizing Inorganic Nanoparticles

The strategy of natural nanocrystals as templates for synthesizing inorganic nanoparticles breaks new ground to make optimum use of inorganic materials, such as rare noble metal resources, in association with the most abundant and renewable bioresources. As a promising template in the synthesis of inorganic nanoparticles, cellulose nanocrystals always play the role of reducing agent, structure-directing agent and stabilizer during the reactions. Using rod-like CN suspensions as the template, diverse inorganic nanoparticles have been prepared, such as mesoporous silica (Si, SiO_2 , SiC) nanoparticles;^{235–239} calcium carbonate (CaCO_3) nanoparticles;²⁴⁰ silver (Ag) nanoparticles;^{231,241,242} gold (Au) nanoparticles;^{243,244} nickel (Ni) nanocrystals;²⁴⁵ platinum (Pt) nanoparticles;^{246,247} selenium (Se) nanoparticles;²⁴⁸ palladium (Pd)

nanoparticles;²⁴⁹ Titania (Ti) core-shell and hollow nanoparticles;²⁵⁰ TiO₂ nanocubes cadmium sulfide (CdS), zinc sulfide (ZnS), lead sulfide (PbS);²⁵¹ Au–Ag alloy nanoparticles;²⁵² and Ag–Pd alloy nanoparticles.²⁵³ Figure 1.16 shows the different morphologies and dimensions of various inorganic nanoparticles templated synthesis with CNs.

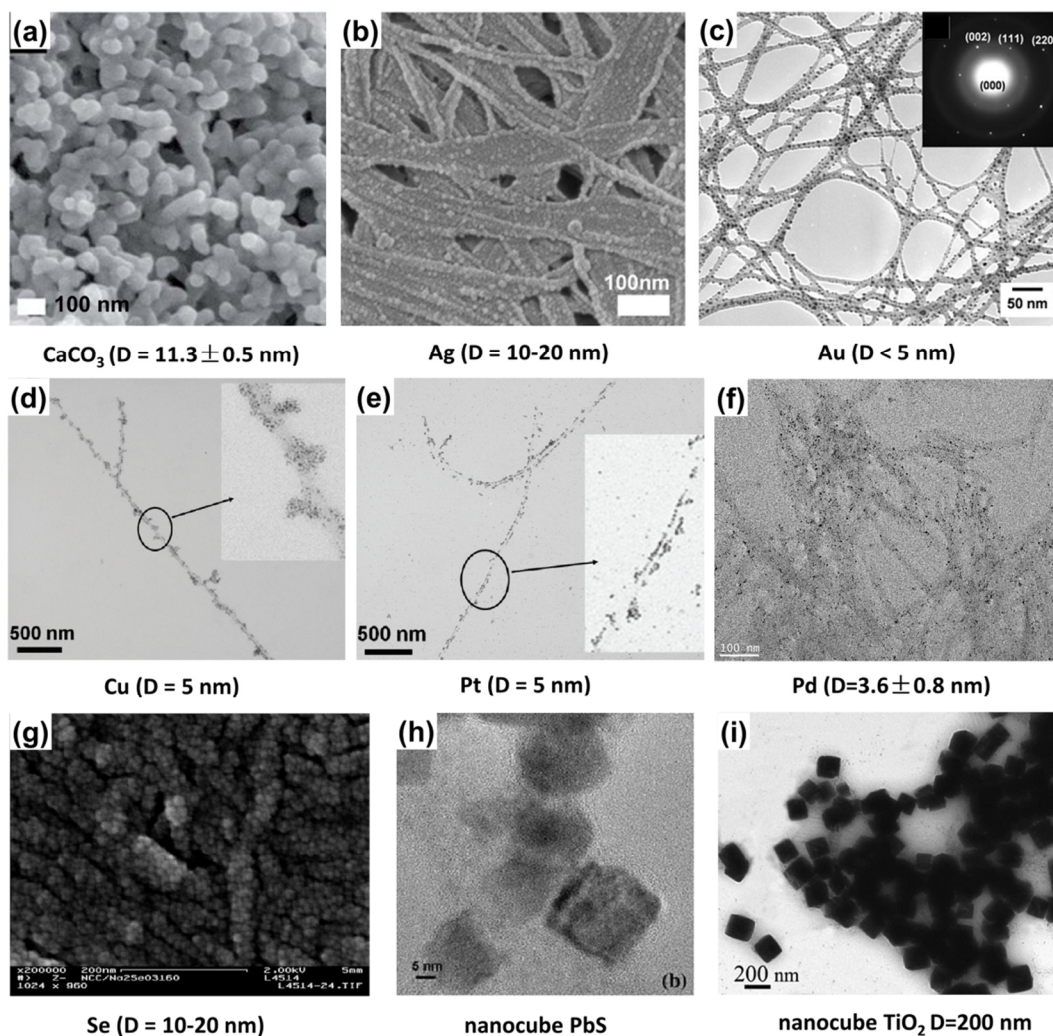


Figure 1.16 Morphologies and dimensions of inorganic nanoparticle templated synthesis with cellulose nanocrystals. (a) CaCO₃ nanoparticles;²⁴⁰ (b) Ag nanoparticles;²⁴² (c) Au nanoparticles;²⁴³ (d) Cu nanoparticles;²⁵⁴ (e) Pt nanoparticles;²⁵⁴ (f) Pd nanoparticles;²⁴⁹ (g) Se nanoparticles;²⁴⁸ (h) PbS nanoparticles;²⁵¹ (i) TiO₂ nanocubes.²⁵⁵

It is worth noting that some studies on the synthesis of inorganic nanoparticles using CNs as templates reported some interesting results. In comparison with different roles of three natural biotemplates (lignin, amorphous bleached cellulose, and CNs) during the synthesis of SiC nanoparticles, only the CN template can produce clean and

uniform SiC nanowires (70 nm in diameter, > 100 μm in length) without the camelback structure.²³⁹ Padalkar et al. reported the effects of the concentration of surfactant, salt solution, reaction time, and pH of the salt solution to the average size of synthesized inorganic nanoparticles (Ag, Cu, Au, and Pt) and coverage of CNs.²⁵⁴ Monodisperse palladium (Pd) nanoparticle synthesized from colloidal CNs showed excellent active catalyst effect on the Heck coupling of styrene and iodobenzene, which proved the possibility of using CNs as an efficient support for catalysis.²⁴⁹ The introduction of CNs that acted as a morphology-inducer and coordinating agent results in acceleration of the crystal growth of TiO_2 particles and promotes the formation of nanocube morphology.²⁵⁵ The synthesis of porous TiO_2 nanoclusters with different shapes,²⁴⁸ flower-like TiO_2 nanocrystals²⁵⁶ using CNs as templates, and investigation of photocatalytic activity of TiO_2/CNs ²⁵⁷ were also reported.

Based on the template synthesis of inorganic nanoparticles with CNs, some organic/inorganic hybrid nanomaterials were reported. Especially for the combination of Ag nanoparticles and CNs, ensuing materials exhibited the antimicrobial property from nano-Ag, and enhanced mechanical performance from CNs.^{258,259}

1.5.1.2 Surface Charges and Hydrophilicity

Cellulose nanocrystals are generally prepared by sulfuric acid hydrolysis inducing the formation of sulfate ester groups ($-\text{OSO}_3^-/\text{H}^+$) on the surface of the nanoparticles via an esterification process. These charged moieties, which density increases with the severity (acid concentration, time, temperature) of the treatment, cause the formation of a negative electrostatic layer covering the nanocrystals and promote the high stability of the H_2SO_4 -prepared nanocrystal aqueous suspensions. Meanwhile, surface negative charge provides the accessibility to electrostatic adsorption and conjunction with cationic groups or molecules. With the negative charges on the surface of CNs, some structural materials (such as layer-by-layer (LBL) assembling nanomaterials) and functional materials (such as emulsion nano-stabilizer and adsorbed or permselective materials) can be developed.

High-Efficiency Adsorption and Permselective Membrane

Owing to the negatively charged surface of CNs, direct application should be the adsorption against positively charged molecules. Based on this strategy, Hsiao and co-workers developed some efficient adsorbing membranes from cellulose nanofibers and nanocrystals.^{260,261} Generally, CNs were anchored on the matrix surface, forming a crosslinked nanostructured mesh with very high surface-to-volume ratio and a negatively charged surface. The mean pore size and pore size distribution of this system could be adjusted by the loading of CNs, where the resulting membrane not only possessed good mechanical properties but also high surface charge density. Prepared CN-based membrane exhibited 16 times higher adsorption capacity against a positively charged dye over a commercial nitrocellulose-based membrane.²⁶²

The negatively charged sulfate groups on the surface of CNs can also be used to develop permselective membranes, which are attributed to the inhibition of negatively charged species but admission of positively charged species. A suspension of cotton CNs (1.5 wt%) was used to form membranes at glassy carbon electrodes via the interparticle hydrogen bonding between negatively charged nanocrystals with the simple drop-coating procedure. This nanostructured membrane possesses the permselective function to substances with different charge properties. It was shown that positively charged ruthenium hexamine $[\text{Ru}(\text{NH}_3)_6^{3+}]$ was significantly adsorbed by the membrane, with a large permeability (P) value of 216%, whereas the negatively charged potassium hexachloroiridate $[\text{IrCl}_6^{3-}]$ was almost excluded by the membrane, with a P value of only 33.9%.²⁶³

Emulsion Nano-stabilizer

Research effort on the development of sustainable, biodegradable, and nontoxic solid particle emulsion stabilizers has not stopped since several decades. Capron and co-workers firstly introduced CNs in emulsion and investigated their effects to stabilize the emulsion. Cellulose nanocrystal was observed to promote monodispersed oil (hexadecane) droplets around 4 μm in diameter in water stable for several months, which proved the promising ability of CNs to stabilize the hexadecane–water

interface.²⁶⁴ Subsequent study indicated that neutral CNs dispersed in water can stabilize oil/water interfaces and produce Pickering emulsions with outstanding stability, whereas sulfated nanocrystals did not show this interfacial property.²⁶⁵ Surface charge density of CNs can be modulated by various postsulfation/desulfation treatments. Regardless the crystalline origin, electrostatic interaction played the major role in the control of the interface between oil and water. Cellulose nanocrystals with a surface charge density above 0.03 e/nm^2 were not able to efficiently stabilize at the oil/water interface, whereas a decreasing surface charge density led to stable emulsions. Recently, Capron and Cathala investigated the formation of a gel structure from oil-in-water high internal phase emulsions by colloidal network of CNs. They found that high internal phase emulsions are only possible when a Pickering emulsion is formed, suggesting that a reorganization of CNs at the oil/water interface occurs as the volume of the internal phase and the interfacial area increases.²⁶⁶ Zoppe et al. compared different nano-stabilized effects of CNs before and after polymer brushes grafting. Water-continuous Pickering emulsions produced by thermo-responsive PNIPAAm brushes grafted onto CNs can be stable during the time of observation for 4 months, whereas unmodified nanocrystals were unable to stabilize heptane-in-water emulsions.²⁶⁷

1.5.1.3 Nanoscale and High Surface Area

Because of the properties of porosity, biocompatibility and right mechanical properties similar to natural tissue, CN-based biomaterials can provide a cell-friendly environment to encourage cells attachment and proliferation as a special tissue bioscaffold. Furthermore, derived from the nanoscale dimensions, cellulose nanocrystals have high surface area (several hundred m^2/g), which is useful and efficient to adsorb organic molecules and other nanoparticles for water purification.

Surface Cell Cultivation

Regarding CN-based media for the cultivation of cells, most of the studies applied conventional suspensions of unmodified or fluorescent-modified nanocrystals as the environment for cells. From insect cells Sf9 and Hamster lung fibroblast V79, to human

foreskin fibroblasts and human embryonic kidney cells HEK-293, no significant cytotoxicity to various cell models was found, and promising cellular uptake and proliferation were reported in these studies.^{165,268,269} Recently, using a spin-coating method, Dugan et al. prepared submonolayer film with oriented surfaces of adsorbed CNs. Due to the shape and nanoscale dimensions of CNs, murine myoblasts cells C2C12 adopted increasingly oriented morphologies in response to more densely adsorbed and oriented nanocrystals surface (Figure 1.17). With a mean feature height of only 5–6 nm, CN surface presented the smallest features ever reported to induce contact guidance in skeletal muscle myoblasts.^{270,271}

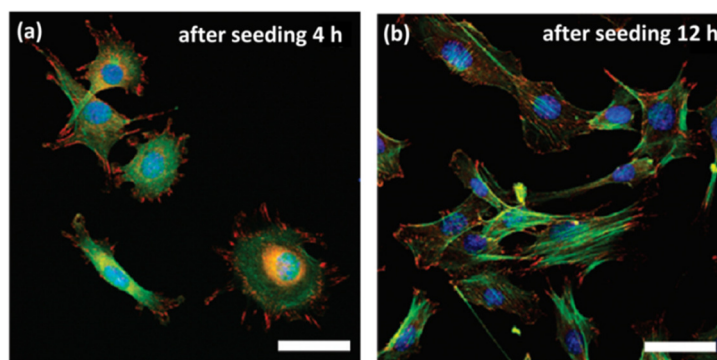


Figure 1.17 Myoblasts cells C2C12 were cultivated on the surface of oriented CNs.²⁷⁰ Cell was stained for vinculin (red), F-actin (green), and nuclei (blue), scale bar = 50 μm .

Water Decontamination

A double layer consisting of polyacrylonitrile electrospun membrane reinforced with TEMPO-oxidized CNs was prepared, which showed efficient filtrating capacity for 7–40 nm nanoparticles and oil/water separation (with rejection of over 99%).²⁷²

1.5.2 Nano-Reinforcing Effects in Functional Materials

The most important attributes of CNs are their mechanical properties, in particular their unusual ability to provide high mechanical strength and high strength-to-weight ratio. For example, the Young's modulus of CNs with a density for crystalline cellulose around 1.5–1.6 g/cm^3 is much higher than the one of glass fibers, around 70 GPa with a density around 2.6 g/cm^3 , which are classically used in composite applications. It is similar to Kevlar (60–125 GPa, density around 1.45 g/cm^3) and potentially stronger than steel (200–220 GPa, density around 8 g/cm^3).¹⁸⁸ These impressive mechanical

properties make cellulose nanocrystals ideal candidates for the processing of reinforced nanocomposites (as discussed in Section 1.4) and development of functionally mechanical materials.

1.5.2.1 Soft Matter

Hydrogels and Gels

Hydrogels are defined as three-dimensional polymer networks swollen by trapping large amounts of solvent (usually water), and widely used in the fields of food, biomaterials, agriculture etc. Hydrogels from rod-like CNs are usually divided in two types. One consists in the direct preparation from CN suspension; another consists in composite hydrogels prepared from CN reinforced matrices. Cellulose nanocrystals can form gels by themselves under some conditions resulting from the strong hydrogen bonding interactions between nanoparticles. Aqueous suspensions with 0.4 wt% CNs extracted from softwood flour can form a transparent hydrogel with unique rigid and uniform morphology, and the elastic solid-like behavior of hydrogel was dependent on the mechanical agitation.²⁷³ In addition, by involving a solvent exchange process, CNs were proved to be able to form stable macroscopic organogels in glycerol,²⁷⁴ ethanol²⁷⁵ or acetone.²⁷⁶ More recently, Way et al. reported the different gelation behaviors of surface modified CNs with either carboxylic acid ($-\text{COOH}$) or amine ($-\text{NH}_2$). At low pH, amine-modified nanocrystals formed flocculent suspension because of the electrostatic repulsions of the ammonium moieties inhibiting aggregation of the nanoparticles. However, a transition to hydrogels was observed at higher pH where the amine-modified nanocrystals are neutral and the attractive forces based on hydrogen bonding dominate. The opposite behavior was observed for carboxylated CNs, which were dispersible in water at high pH and form stable hydrogels in an acidic environment.⁸¹

On the basis of the crosslinking method, composite hydrogels can be divided into chemical gels and physical gels. Physical gels are formed by molecular self-assembly through ionic or hydrogen bonds, while chemical gels are formed by covalent bonds. The introduction of rigid CNs in polymeric matrices to prepare physical hydrogel

nanomaterials generally improves the structural stability and enhances the elastic modulus. To date, it was reported that CNs have been used in various synthetic polymeric matrices for the preparation of gel nanomaterials, such as PEG,²⁷⁷ PVA,^{278,279} PHEMA,^{280,281} poly(NIPAM-*co*-BMA),²⁸² starch-*g*-poly(sodium acrylate),²⁸³ PAM,^{141,284} as well as natural polymeric matrices, for instance regenerated cellulose,²⁸⁵ agarose,^{286–288} and cyclodextrin.^{289,290}

On the other hand, cellulose nanocrystal-based hydrogels can also be obtained by chemical crosslinking method, such as *in situ* crosslinking between CNs and poly(MVE-*co*-MA)-PEG,^{174,175} gelation,²⁹¹ PAA,²⁹² and PNiPAAm²⁹³ as matrices.

Sponge, Foam, Aerogel and Tissue-Engineering Nanoscaffold

Sponge is a material full of pores and channels allowing water or other molecules to circulate through them. With a similar structure, foam is a substance that is formed by trapping pockets of gas in a liquid or solid. Aerogel is a synthetic porous ultralight material derived from the gel, in which the liquid component of the gel has been replaced by gas. As nanomaterials with high porosity and specific surface area as well as low density, sponge, foam and aerogel materials generally can be produced by extracting the liquid component using freeze-drying or supercritical CO₂ drying. These treatments allow the liquid to be slowly dried off without causing the solid matrix to collapse through capillary action, as happen with conventional evaporation. Table 1.8 shows diverse CN-based sponge, foam and aerogel materials prepared with different techniques.

Table 1.8 Diverse cellulose nanocrystals-based sponge, foam, aerogel and nanoscaffold materials.

Sources	Matrices	Materials	Techniques	Ref.
cotton	alginate	sponge	ionic crosslinking/freeze-casting	[294]
cotton	starch/PVA	sponge	freezing/thawing cycles	[295]
—	polyurethane	foam	evaporation under high vacuum	[296]
MCC	xylans	foam	freeze-casting	[297]
softwood pulp	PVA	foam	freeze-casting	[298]
ramie fiber	arabinoxylan	aerogel	freeze-casting	[299]
cotton wool	—	aerogel	supercritical CO ₂ drying	[300]
tunicate	clay/PVA	aerogel	freeze-casting	[301]
cotton	MAH- <i>g</i> -PLA	scaffold	electrospinning	[302]

Tissue-engineered porous nanoscaffold is a kind of novel biomedical nanomaterial providing the necessary template and physical support to guide the differentiation and proliferation of cells into targeted functional tissues or organs. Blaker et al. developed a technique of combining the ice-microsphere template with thermally induced phase separation lining the pore walls with bacterial CNs to produce *in situ* porous PLA/CN scaffolds. The resultant nanoscaffolds showed porous morphology with controlled porosities up to 97% of spherical interconnected pore walls lined by CNs, which can be more suitable for the expansion and direct interaction with cells in three-dimensional culture.³⁰³ Electrospun fibrous nanoscaffolds reinforced with CNs in MAH-grafted-PLA matrix with improved interfacial adhesion were also reported.³⁰²

1.5.2.2 Special Mechanical Materials

Special mechanical materials based on CNs are mainly referred as mechanically switchable, stimuli-responsive materials, such as mechanically adaptive materials and mechanically gradient materials. As inspired by biological creatures such as sea cucumbers, which have the ability to reversibly change the stiffness of their dermis, three-dimensional percolating networks based on rigid CNs were introduced in various polymeric matrices, such as poly(EO-EPI) copolymer (1:1), PVA and poly(butylmethacrylate) (PBMA). The first generation of percolating CN materials was based on poly(EO-EPI) and PVA matrix.³⁰⁴ In the rubbery zone, the tensile storage moduli (E'_c) of the dry matrix materials at 25 °C increased by over two orders of magnitude from 3.7 MPa (neat matrix) to about 800 MPa for a nanocrystal content of 19% (v/v). However, upon exposure to water, these CN/matrix nanomaterials exhibit a pronounced and reversible modulus reduction (40-fold), from 800 to 20 MPa, for the materials with the same nanocrystal content of 19% (v/v) at room temperature. The second generation of mechanically adaptive nanomaterials was on the basis of PVA or PBMA matrices, which are dynamically sensitive to the change of thermal transition [ambient (ca. 23 °C) to physiological (37 °C)].^{305–307} For instance, below the glass-transition temperature (T_g), the tensile storage moduli of dry nanomaterials increased only 2–2.5 fold when adding 16.5% (v/v) nanocrystals, while E' increased

1000 fold above T_g . At the same time, when being exposed to physiological conditions (immersion in artificial cerebrospinal fluid, 37 °C) these nanomaterials displayed a significant decrease of E' from several GPa to several MPa. Recently, introduction of cotton CNs in rubbery polyurethane matrix was also reported, to produce mechanically adaptive nanocomposites, which can change their mechanical properties upon exposure to water and displayed a water-activated shape-memory effect.³⁰⁸

The theoretical model for the mechanically adaptive nanomaterial mechanism has been proposed, as shown in Figure 1.18.⁶³ The mechanical properties of these chemoresponsive materials can selectively and reversibly be controlled through the formation and decoupling of a three-dimensional network of well-individualized rigid nanocrystals in response to specific chemical triggers. In the “on” state, strong hydrogen bonds between rigid, percolating nanocrystals maximize stress transfer and induce the reinforcement of the nanomaterials. In contrast, with the environmental stimuli, such as exposure to water or the increase of temperature, the hydrogen bonding interactions among nanocrystals are disrupted and dissociated from each other, which are switched “off” by the introduction of the chemical regulators.

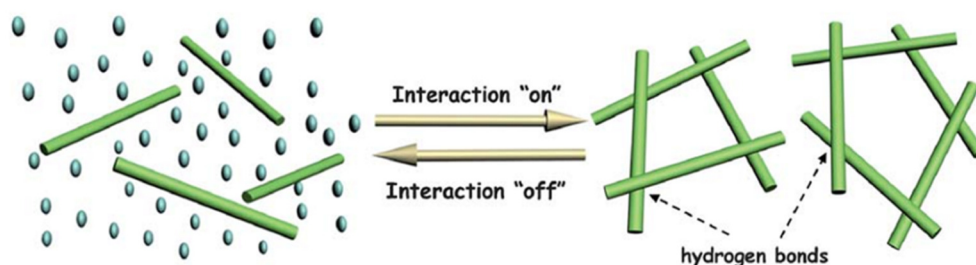


Figure 1.18 Schematic representation of the architecture and switching mechanism in the mechanically adaptive nanomaterials.⁶³

Recently, inspired by the water-enhanced mechanical gradient character of the squid beak, Fox et al. reported mechanically gradient nanocomposites made from CNs where the degree of crosslinking can be controlled along the length of the materials. With the reaction between modified CNs and photoinitiator, different crosslinking degrees of nanocrystals were controlled by UV irradiation. Under varied states (dry or wet) and temperatures, different lengths and regions of the film exhibited different mechanical

properties, with an increase in irradiation time consistent with the increased crosslinking. A dramatic increase in the mechanical contrast was observed for the wet film ($E'_{\text{stiff}}/E'_{\text{soft}} > 5$) over the dry film either below or above T_g ($E'_{\text{stiff}}/E'_{\text{soft}}$ of ca. 1.1 and 1.5, respectively).¹⁷⁷

1.5.2.3 Self-Healable and Shape-Memory Materials

Named as “self-healable materials” and “shape-memory materials”, these two kinds of materials are repairable or revertible after being damaged or changed in shape, which are attractive for many applications because the features can improve the reliability, functionality, and lifetime of a broad range of products. The self-healable ability of materials is generally realized with the division and re-conjunction of supramolecular structure in materials under an external stimulus, such as ultraviolet radiation or heating energy. Biyani et al. reported light-healable nanocomposites based on a telechelic poly(ethylene-*co*-butylene) that was functionalized with hydrogen-bonding ureidopyrimidone (UPy) and CNs decorated with the same binding motif.¹³⁸ When these materials were exposed to ultraviolet radiation, the UPy motifs were excited and the absorbed energy was converted into heat, which caused the conjunction of the hydrogen-bonding motifs and restoration of the material. As a result, deliberately introduced defects can be healed quickly and efficiently and exhibited high strength and stiffness from the reinforcement provided by CNs. As shown in Figure 1.19, the nanocomposite samples containing 10 wt% CNs were found to heal considerably faster, requiring less than 20 s of UV exposure (image a). In another study, a supramolecular polymer blend, formed via π - π interactions between a π -electron rich pyrenyl end-capped oligomer and a chain-folding oligomer containing pairs of π -electron poor naphthalene-diimide units, has been reinforced with CNs (from 1.25 to 20.0 wt%) to afford a healable nanocomposite material. All the nanocomposites can reheal upon exposure to elevated temperatures. The best combination of healing efficiency and mechanical properties was obtained with the 7.5 wt% CNs nanocomposite which exhibited a tensile modulus enhanced by as much as a factor of 20 over the matrix material alone and could be fully rehealed at 85 °C within 30 min.³¹

With the regulation of reversible formation and disruption of CN percolation network, elastomeric polyurethane nanocomposites containing CNs (from 1.1 to 29.6 wt%) can be prepared, which are rapidly switchable shape-memory materials activated by water. The CN percolation network reformed after drying to provide a fixing force for the temporary shape. The entropy elasticity of polyurethane matrix then enabled rapid shape recovery when percolation network was disrupted again during wetting.^{309,310}

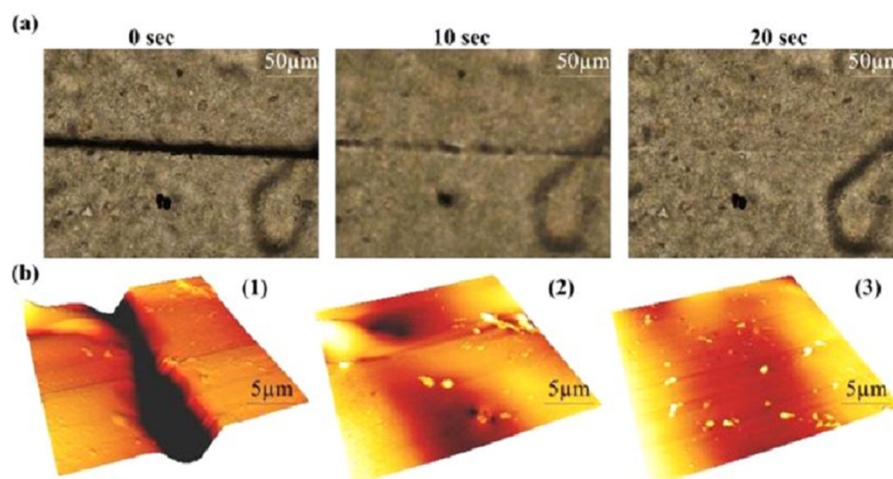


Figure 1.19 (a) Optical microscope images of deliberately damaged ureidopyrimidone-CN materials (with 10 wt% nanocrystal content) before, during, and after exposure to UV light (320–390 nm, 350 mW/cm², 20 s). (b) Atomic force micrographs of ureidopyrimidone-CN materials (with 10 wt% nanocrystal content) in the deliberately damaged (1), partially healed (2), and completely healed (3) state (color range; black = 7 μm, white = 0 μm).¹³⁸

1.5.2.4 Polymeric Electrolytes and Batteries

The incorporation of CNs into ion-conducting solid polymer electrolytes allows combination of both mechanical reinforcement of a separator and high ionic conductivity medium. Dufresne et al. have investigated a series of PEO-based polymer electrolytes reinforced with CNs, which displayed high ionic conductivity as well as electro-chemical, thermal, and mechanical stability. Solid polymer electrolytes with CNs were generally prepared in two steps: the first step consisting in the preparation of a polymeric matrix–nanocrystal mixture; and the second step involving the introduction of the lithium salt, such as [lithium trifluoromethyl sulfonyl imide (LiTFSI) or LiClO₄] into the swelled nanocrystal-reinforced polymer nanomaterial in a concentrated acetonitrile salt solution.^{311–313} Recently, electrospinning and hot-pressing technique

without solvent was also reported to prepare composite polymer electrolytes reinforced with CNs.³¹⁴

Generally, the addition of rigid CNs in polymer electrolytes leads to high mechanical performance with a high increase in the storage modulus at higher temperatures, and a slight decrease of ionic conductivity. For instance, by adding 10 wt% tunicin nanocrystals in PEO composite materials, the gain in storage modulus exceeded by far a factor of 100 with respect to the unfilled polymer electrolyte; while the values of ionic conductivity still remained higher than 10^{-4} S/cm above 60 °C (melting point of PEO).^{313,315} To further enhance the performance of polymer electrolytes, different solvents (water or organic medium) for the dispersion of nanocrystals, crosslinking agent,³¹⁶ plasticizer,³¹⁷ or different polymeric matrices^{318,319} were chosen to develop and investigate the effects in the solid polymer electrolyte system.

Recently, cellulose nanocrystal was reported to be used as optically transparent substrate for the preparation of recyclable organic solar cells. The solar cells fabricated on CNs substrates displayed good rectification in the dark and reached a power conversion efficiency of 2.7%. Meanwhile, this solar cell can be easily separated and recycled into its major components using low-energy processes at room temperature.³²⁰

1.5.2.5 Semi-Conducting Material

Based on the combination of anionic surface charged CNs and positively charged π -conjugated polymers, functional semi-conducting material can be prepared. Stable suspension of CNs and PANI-PPE derivative mixture can be used to produce the semi-conducting film by solution-casting treatment. Further investigations on electrical conductivity, photoluminescence, and mechanical properties revealed that this semi-conducting material synergistically combined the electronic characteristics from the conjugated polymers with the outstanding mechanical reinforcement from CNs.³²¹ In another study, the introduction of CNs in PEDOT/PSS-based PS conductive polymer matrix extremely reduced the electrical percolation threshold 5-fold of ensuing nanocomposites. It was reported that the percolation threshold of PEDOT:PSS in PEDOT:PSS/PS blends, being 2.2 wt%, was lowered to 0.4 wt% by adding 0.8 wt% of

nonconducting CNs. Such a low percolation threshold of PEDOT:PSS was attributed to the templating effect of CNs, which adsorbed the conductive polymers on the surface and covered the electrical percolation with the network formed by CNs.³²²

1.5.3 Optical Materials Derived From Liquid Crystalline

Owing to their anisotropic rod-like morphology, cellulose nanoparticles have a lyotropic liquid crystalline behavior in suspensions, which is a phase transition from an isotropic liquid to an ordered liquid crystal when changing the concentration.⁶⁹ Indeed, above a critical concentration, a chiral nematic phase forms. Under certain conditions, the suspension may be slowly evaporated to obtain semi-translucent films that maintain the chiral nematic liquid crystal order formed in the suspension. These films exhibit iridescence reflecting polarized light in a narrow wavelength range determined by the chiral nematic pitch and the refractive index of the film. Derived from the liquid crystalline property, tunable optical nanomaterials can be prepared based on rod-like CNs with two strategies. The first strategy is the simple slow evaporation for CN suspension to preserve the chiral nematic ordering phase. Another strategy is the combination of liquid crystalline CNs and inorganic matrix to produce optical materials.

Ultrasound treatment was found to increase the chiral nematic pitch in suspension and red-shift the reflection wavelength of CN films as the applied energy increased.³²³ Figure 1.20 shows solid films cast from aliquots of 2.8 wt% CN suspensions prepared from bleached softwood kraft pulp and sonicated with increasing (left to right) energy inputs. The energy was measured in J/g of CNs. The films exhibit reflected iridescence with colors ranging from blue-violet to red. By combining sonication and electrolyte addition the reflective properties of the film can be predictably tuned. The effects of sonicating a CNs suspension were shown to be cumulative and permanent. Moreover, suspensions sonicated with different energy inputs can be mixed to prepare films having a reflection band intermediate between those obtained from the individual suspensions. Recently, differential heating rates of aqueous CNs suspension during film casting were investigated.⁶⁵ Placing materials of different temperatures beneath an

evaporating CNs suspension resulted in watermark-like patterns of different reflection wavelength incorporated within the final film structure. The patterned areas are of different thickness and different chiral nematic pitch than the surrounding film; heating results in thicker areas of longer pitch. Thermal pattern creation in CNs films is proposed to be caused by differences in evaporation rates and thermal motion in the areas of the suspension. These CN-based optical materials with tunable iridescence were proposed to have the potential for covert encryption as an anti-counterfeiting measure and an intrinsic level of covert encryption since the reflection left-circularly polarized light.³²⁴

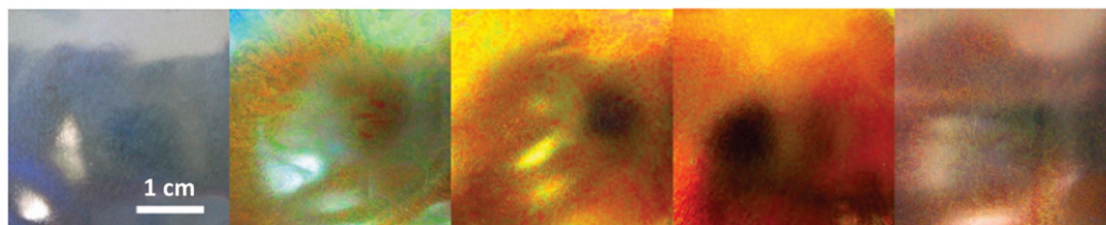


Figure 1.20 Cellulose nanocrystal films produced from suspensions treated with increasing applied ultrasonic energy (0, 250, 700, 1800, and 7200 J/g of nanocrystals) from left to right. Viewing is normal to the film surface under diffuse lighting. Samples of CNs suspension were sonicated using a Sonics vibra-cell 130 W 20 kHz ultrasonic processor with a 6 mm diameter probe: typically, 15 mL of a 2–3 wt% CNs suspension was placed in a 50 mL plastic tube and sonicated at 60% of the maximum power.³²³

MacLachlan M. J. and his team developed a series of photonic, mesoporous, inorganic (silica) optical materials which were a cast of a chiral nematic liquid crystal formed from CNs. Inspired by the brilliant iridescent colors of beetle exoskeletons, their first study consisted in preparing the free-standing mesoporous silica films with tunable chiral nematic structures from CNs.^{12,325} As shown in Figure 1.21a, the peak reflected wavelength of the biomimetic optical nanomaterials can be varied across the entire visible spectrum and into the near-infrared through simple changes under synthetic conditions. Figure 1.21b shows photographs of the different colors of mesoporous silica nanomaterials. With increasing CN contents from samples S1 to S4, the mesoporous films exhibited blue, green, yellow and red color, respectively. The colors in these films can be attributed to the chiral nematic pore structure arising from CNs

present in the materials. Moreover, the addition of a drop of water will cause the wet part of the film to become completely transparent, as shown in Figure 1.21d. With the elimination of water (or other common solvents) upon drying, these optical nanomaterials can fully regain their iridescence, which results in a reversible decrease of the circular dichroism signal to 30 millidegrees (Figure 1.21c). Furthermore, some mesoporous silica and carbon films decorated with CNs and metal nanoparticles through calcination and carbonization were developed.^{326–328} Recently, the preparation of responsive photonic hydrogels from self-assembly of CNs and hydrogel precursors was reported. Because of the long-range chiral nematic order from CN component, this kind of hydrogel showed iridescence and rapidly response to various stimuli.³²⁹

Although the mechanism of CN optical materials is commonly recognized as the chiral nematic liquid crystal ordering from nanocrystal suspension, another explanation is also proposed. Picard et al. observed a solid multilamellar structure for CN suspension after evaporation, with each lamella made of roughly parallel rows of bundles. Consequently, they explained the iridescence of CN optical films as a multilamellar structure inducing light interference, not a helical cholesteric liquid crystal.³³⁰

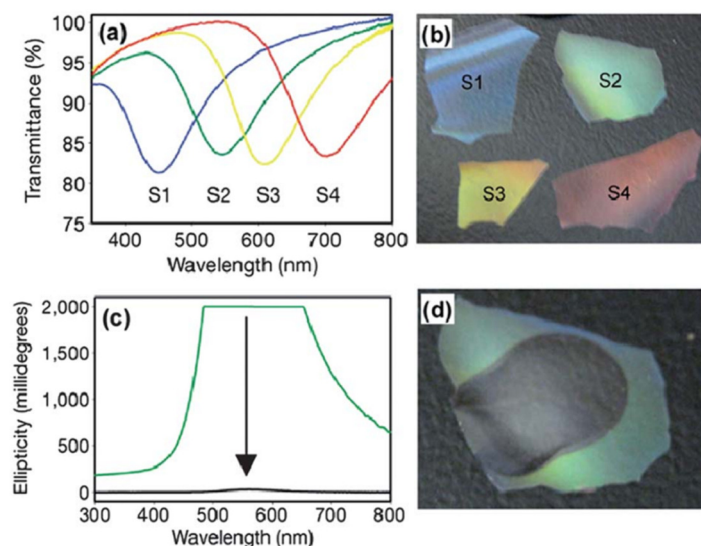


Figure 1.21 Optical characterization of CNs/silica composite films. (a) Transmission spectra; (b) photographs showing the different colors of mesoporous films S1 to S4 with gradual increase of nanocrystal contents; (c) circular dichroism spectra of a green mesoporous film before (green curve) and after (black curve) infiltration with water; and (d) photograph of the transparent green film after the addition of a drop of water.¹²

1.5.4 Special Films and Systems Ascribed to Barrier Properties

1.5.4.1 Drug Delivery—Barrier for Drug Molecules

Despite an extended history of use in tableting, there is still considerable continuing research into the use of cellulose with other types (nanocellulose) in advanced drug-loaded systems whereby the rate of tablet disintegration as special excipients, or prolonged drug release as novel drug carriers. As a drug delivery excipient, Burt et al. investigated the capability of pure cellulose nanocrystals to bind the water soluble antibiotics (tetracycline and doxorubicin), and the potential of cationic-CNs to bind nonionized hydrophobic anticancer agents (docetaxel, paclitaxel, and etoposide).³³¹ Besides direct use as excipient, CNs can also be used as co-stabilizer to improve the physicochemical and flow properties of polymeric excipients. Acrylic beads prepared via emulsion polymerization using CNs as co-stabilizer were proved to be a suitable excipient. The presence of CNs affected positively the size and size distribution of the bead excipient, which formed the stable structure together with low flow time and reduced cotangent of angle.³³²

The biomaterial application of cellulose nanocrystals in drug delivery can be mainly divided into two aspects, viz. microspheres (or microparticles),³³³ and hydrogels (or gels).^{289,290,334} Table 1.9 summarizes various drug carrier systems based on CNs. It was reported that solid carriers formed from CNs and different matrices spatially trapped drug molecules, and imparted the regulation of drug release. Lin et al. developed a pH-sensitive CN/sodium alginate microsphere-based controlled release system for drug delivery. The presence of CNs in alginate-based microspheres showed more consistent swelling patterns, higher encapsulation efficiency, and promising sustained release profiles of the drug.³³³ With similar strategy, another work developed a polyelectrolyte macroion complex via the conjunction between cationic chitosan and anionic CNs, which has the potential as the multiparticulate oral drug delivery, but unfortunately without drug loading or drug release results.²⁸⁵

Recently, some researchers attempted to directly attach drug molecules on CNs, which were performed using covalent coupling between modified CNs and drug molecules.

Table 1.9 Drug carrier systems based on cellulose nanocrystals.

Source	Matrix	Carrier	Model drug	Release time and medium	Mechanism model	Ref.
cotton	sodium alginate	microsphere	theophylline	16 h in pH=7.4 PBS solution	Ritger-Peppas equation	[333]
cotton	cyclodextrin/Pluronic	hydrogel	DOX	6.5 d in water	Ritger-Peppas equation	[290]
cotton	cyclodextrin/Pluronic	hydrogel	BSA	20 h in pH=7.4 PBS solution	—	[289]
MCC	PLA	fiber	<i>Columbia Blue</i>	48 h in water	Higuchi equation	[337]
cotton pulp	regenerated cellulose	gel	BSA	48 h in simulated body fluid	Fickian diffusion law	[334]
eucalyptus	EA; MMA; BMA	bead	propranolol	12 h in pH=6.8 PBS solution	—	[332]
wood pulp			hydrochloride			
commercial	CTAB	suspension	DOX; TET; etoposide;	1-4 d in PBS solution	—	[331]
softwood			paclitaxel; docetaxel			

With a series of oxidation, reductive-amination and esterification reactions in aqueous media, a novel CN-based delivery system attached to the syringyl alcohol linker through a γ -aminobutyric acid spacer molecule can be produced, on which small model amine drugs (e.g. phenylpropanolamine) can be covalently connected.¹¹⁸ Similarly, with the binding of bi-functional fusion protein on CNs, hydrophobic solid drug nanoparticles can be adsorbed by the packed protein film on nanocrystals, and improve the long-term stability of drugs under physiological condition.³³⁵

1.5.4.2 Barrier Nanocomposites—Barrier for Water and Oxygen

Cellulose is a hydrophilic polymer and it obviously absorbs water when immersed in liquid water or conditioned in moist atmosphere. However, the water vapor permeability is decreased when the cellulose fibers are disintegrated to the nanoscale level, such as cellulose nanocrystals.³³⁶ Moreover, the sensitivity to moisture of the nanoparticles can be tuned via pre-treatment before homogenization or post-treatment (polymer impregnation, or chemical grafting).²¹⁴ The gas permeability is also reduced in dry atmospheres when decreasing the size of the cellulosic particles because of the crystalline and dense structure of the nanoparticle film. Whatever the treatment or the experimental conditions used to produce nanocellulose (including CNs and MFC), it is seen as a new biomaterial for the creation of a good barrier for extending food shelf-life, and also improves food quality for antioxidants and antimicrobials.

1.5.5 Other Functional Applications

Cellulose nanocrystal (1, 2, 3 wt%) was used to improve the performance of PVA as a wood adhesive. With the measurement of block shear tests, wood failure value increased from 59% (pure PVA) to 84% for adhesive with 1 wt% CNs and finally to 97% for adhesive with 3 wt% CNs. Fluctuations in properties of PVA as a wood adhesive and a polymer at different CN loadings can be attributed to the effect of homogeneous dispersion of nanocrystals to the change of PVA structure.³³⁸

1.6 Conclusions

The study of cellulose nanocrystals is a fascinating research field that has attracted significant interest during last twenty years, largely attributed to the potential of cellulose nanocrystals to be used as a renewable and rigid nanomaterial. In light of this review chapter, specific research topics on cellulose nanocrystals generally can be classified as four parts, including ‘evolution of preparation’, ‘exploration of property’, ‘revolution of modification’, and ‘development of application’.

In spite of the fact that there has been industrial production of cellulose nanocrystals in some companies, more high-efficiency and ‘green’ technique is demanded; and standardization for the procedure and control for the properties of produced cellulose nanocrystals are absolutely necessary. Investigation on special properties of cellulose nanocrystals is the prerequisite and fundament for their potential applications. The discovery of new property and exploration of further mechanism will extend the research on cellulose nanocrystals. The presence of a large number of chemical functionalities within their structure provides a unique platform for significant surface modification on cellulose nanocrystals. Through surface modification, researchers can voluntarily transform the surface properties of cellulose nanocrystals, or impart functional molecules on cellulose nanocrystals for novel properties and applications. Further attention, focusing on the development of innovative modification approach, will be put on the simplicity, cost reduction, and potential functions for the growth of this topic. Many institutes all over the world are dedicated to the application of cellulose nanocrystals, especially on the plastic composites and functional materials. However, due to various reasons, only the statement of “on the edge of breakthrough” for practical application of cellulose nanocrystals can be given until now.

Undoubtedly, the production of cellulose nanocrystals and their nanomaterials is an emerging area of nanotechnology and materials science. However, it is also clear that there are still many challenges to overcome for diverse areas of cellulose nanocrystals research and the development of a practical product.

1.7 References

1. Payen, A. Mémoire sur la composition du tissu propre des plantes et du ligneux. *C. R. Hebd. Seances Acad. Sci.* **1838**, 7, 1052–1056.
2. Wertz, J.-L.; Bédué, O.; Mercier, J. P. Cellulose science and technology. EPFL Press, Lausanne, Switzerland, **2010**.
3. Nägeli, C. Die Stärkekörner. In pflanzenphysiologische untersuchungen, Nägeli, C.; Cramer, C. Eds. Friedrich Schulthess, Zürich, Switzerland, **1858**.
4. Hull, A. W. A new method of X-ray crystal analysis. *Phys. Rev.* **1917**, 10, 661–696.
5. Nikerson, R. F.; Habrle, J.-A. Cellulose intercrystalline structure study by hydrolytic methods. *Ind. Eng. Chem.* **1947**, 39, 1507–1512.
6. Ranby, B. G. Aqueous colloidal solutions of cellulose micelles. *Acta Chemica Scandinavica* **1949**, 3, 649–650.
7. Ranby, B. G.; Ribi, E. Ueber den feinaufbau der zellulose. *Experientia* **1950**, 6, 12–14.
8. Marchessault, R. H.; Morehead, F. F.; Walter, N. M. Liquid crystal systems from fibrillar polysaccharides. *Nature* **1959**, 184, 632–633.
9. Revol, J. F.; Bradford, H.; Giasson, J.; Marchessault, R. H.; Gray, D. G. Helicoidal self-ordering of cellulose microfibrils in aqueous suspension. *Int. J. Biol. Macromol.* **1992**, 14, 170–172.
10. Favier, V.; Canova, G. R.; Cavallé, J. Y.; Chanzy, H.; Dufresne, A.; Gauthier, C. Nanocomposite materials from latex and cellulose whiskers. *Polym. Adv. Technol.* **1995**, 6, 351–355.
11. Dong, S.; Roman, M. Fluorescently labeled cellulose nanocrystals for bioimaging applications. *J. Am. Chem. Soc.* **2007**, 129, 13810–13811.
12. Shopsowitz, K. E.; Qi, H.; Hamad, W. Y.; MacLachlan, M. J. Free-standing mesoporous silica films with tunable chiral nematic structures. *Nature* **2010**, 468, 422–426.
13. <http://www.nrcan.gc.ca/media-room/news-release/2012/1915>
14. Beck-Candanedo, S.; Roman, M.; Gray, D. G. Effect of reaction conditions on the properties and behavior of wood cellulose nanocrystal suspensions. *Biomacromolecules* **2005**, 6, 1048–1054.
15. Hirota, M.; Tamura, N.; Saito, T.; Isogai, A. Water dispersion of cellulose II nanocrystals prepared by TEMPO-mediated oxidation of mercerized cellulose at pH 4.8. *Cellulose* **2010**, 17, 279–288.
16. Leung, A. C. W.; Hrapovic, S.; Lam, E.; Liu, Y.; Male, K. B.; Mahmoud, K. A.; Luong, J. H. T. Characteristics and properties of carboxylated cellulose nanocrystals prepared from a novel one-step procedure. *Small* **2011**, 7, 302–305.
17. Braun, B.; Dorgan, J. R. Single-step method for the isolation and surface functionalization of cellulosic nanowhiskers. *Biomacromolecules* **2009**, 10, 334–341.
18. Filson, P. B.; Dawson-Andoha, B. E.; Schwegler-Berry, D. Enzymatic-mediated production of cellulose nanocrystals from recycled pulp. *Green Chem.* **2009**, 11, 1808–1814.
19. Man, Z.; Muhammad, N.; Bustam, A. S. M. A.; Kumar, M. V.; Rafiq, S. Preparation of cellulose nanocrystals using an ionic liquid. *J. Polym. Environ.* **2011**, 19, 726–731.
20. Kontturi, E.; Meriluoto, A.; Nuopponen, M. Processing for preparing micro- and nanocrystalline cellulose. **2011**, Patent WO2011/114005.

21. Dong, X. M.; Revol, J.-F.; Gray, D. G. Effect of microcrystallite preparation conditions on the formation of colloid crystals of cellulose. *Cellulose* **1998**, *5*, 19–32.
22. Labet, M.; Thielemans, W. Improving the reproducibility of chemical reactions on the surface of cellulose nanocrystals: ROP of ϵ -caprolactone as a case study. *Cellulose* **2011**, *18*, 607–617.
23. TAPPI, Workshop on international standards for nanocellulose. Arlington, USA, June 9th, **2011**.
24. The global market for nanocellulose to 2017; Futures Markets Inc., Edinburgh, Lothian EH74NA, United Kingdom, **2012**, pp. 1–66.
25. Dufresne, A.; Thomas, S.; Pothan, L. A. Biopolymer nanocomposites: Processing, properties and applications. John Wiley & Sons, Inc., **2013**, USA, pp. 461–508.
26. Hanley, S. J.; Giasson, J.; Revol, J.-F.; Gray, D. G. Atomic force microscopy of cellulose microfibrils: comparison with transmission electron microscopy. *Polymer* **1992**, *33*, 4639–4642.
27. Lin, N.; Dufresne, A. Surface Chemistry, Morphological Analysis and Properties of Cellulose Nanocrystals with Graded Sulfation Degrees. *Nanoscale* **2014**, *6*, 5384–5393.
28. Frascini, C.; Chauve, G.; Le Berre, J.-F.; Ellis, S.; Méthot, M.; O'Connor, B.; Bouchard, J. Critical discussion of light scattering and microscopy techniques for CNC particle sizing. *Nord. Pulp Pap. Res. J.* **2014**, *29*, 31–40.
29. Habibi, Y.; Goffin, A.-L.; Schiltz, N.; Duquesne, E.; Dubois, P. Bionanocomposites based on poly(ϵ -caprolactone)-grafted cellulose nanocrystals by ring-opening polymerization. *J. Mater. Chem.* **2008**, *18*, 5002–5010.
30. Fleming, K.; Gray, D.; Prasannan, S.; Matthews, S. Cellulose crystallites: a new and robust liquid crystalline medium for the measurement of residual dipolar couplings. *J. Am. Chem. Soc.* **2000**, *122*, 5224–5225.
31. Fox, J.; Wie, J. J.; Greenland, B. W.; Burattini, S.; Hayes, W.; Colquhoun, H. M.; Mackay, M. E.; Rowan, S. J. High-strength, healable, supramolecular polymer nanocomposites. *J. Am. Chem. Soc.* **2012**, *134*, 5362–5368.
32. Grunert, M.; Winter, W. T. Nanocomposites of cellulose acetate butyrate reinforced with cellulose nanocrystals. *J. Polym. Environ.* **2002**, *10*, 27–30.
33. Newman, R. H. Homogeneity in cellulose crystallinity between samples of *Pinus radiata* wood. *Holzforschung* **2004**, *58*, 91–96.
34. Schenzel, K.; Fischer, S.; Brendler, E. New method for determining the degree of cellulose I crystallinity by means of FT Raman spectroscopy. *Cellulose* **2005**, *12*, 223–231.
35. Chunilall, V.; Bush, T. Application of FT-Raman spectroscopy to study changes in cellulose I crystallinity through the dissolving pulp process. Proceedings of the 16th International symposium on Wood, Fibre and Pulp Chemistry, 8th–10th June **2011**, pp. 472–477.
36. Roman, M.; Winter, W. T. Effect of sulfate groups from sulfuric acid hydrolysis on the thermal degradation behavior of bacterial cellulose. *Biomacromolecules* **2004**, *5*, 1671–1677.
37. Dufresne, A. Nanocellulose. From nature to high performance tailored materials. Walter de Gruyter GmbH, Berlin/Boston, **2012**, pp. 30–31.
38. Meyer, K.; Lotmar, W. Sur l'élasticité de la cellulose. *Helv. Chim. Acta* **1936**, *19*, 68–86.
39. Treloar, L. R. G. Calculations of elastic moduli of polymer crystals: III. Cellulose. *Polymer* **1960**, *1*, 290–303.

40. Sakurada, I.; Nukushina, Y.; Ito, T. Experimental determination of the elastic modulus of crystalline regions oriented polymers. *J. Polym. Sci.* **1962**, *57*, 651–660.
41. Mann, J.; Roldan-Gonzales, L. X-ray measurements of the elastic modulus of cellulose crystals. *Polymer* **1962**, *3*, 549–553.
42. Tashiro, K.; Kobayashi, M. Calculation of crystallite modulus of native cellulose. *Polym. Bull.* **1985**, *14*, 213–218.
43. Jaswon, M. A.; Gillis, P. P.; Mark, R. E. The elastic constants of crystalline native cellulose. *Proc. Roy. Soc.* **1968**, *306*, 389–412.
44. Kroon-batenburg, L. M. J.; Kroon, J.; Northolt, M. G. Chain modulus and intermolecular hydrogen bonding in native and regenerated cellulose fibers. *Polym. Commun.* **1986**, *27*, 290–292.
45. Matsuo, M.; Sawatari, C.; Iwai, Y.; Ozaki, F. Effect of orientation distribution and crystallinity on the measurement by X-ray diffraction of the crystal lattice moduli of cellulose I and II. *Macromolecules* **1990**, *23*, 3266–3275.
46. Tashiro, K.; Kobayashi, M. Theoretical evaluation of three-dimensional elastic constants of native and regenerated celluloses: role of hydrogen bonds. *Polymer* **1991**, *32*, 1516–1526.
47. Nishino, T.; Takano, K.; Nakamae, K. Elastic modulus of the crystalline regions of cellulose polymorphs. *J. Polym. Sci. B: Polym. Phys.* **1995**, *33*, 1647–1651.
48. Reiling, S.; Brickmann, J. Theoretical investigations on the structure and physical properties of cellulose. *Macromol. Theory Simul.* **1995**, *4*, 725–743.
49. Ganster, J.; Blackwell, J. NpH-MD-simulations of the elastic moduli of cellulose II at room temperature. *J. Mol. Model.* **1996**, *2*, 278–285.
50. Neyertz, S.; Pizzi, A.; Merlin, A.; Maigret, B.; Borwn, D.; Deglise, X. A new all-atom force field for crystalline cellulose I. *J. Appl. Polym. Sci.* **2000**, *78*, 1939–1946.
51. Šturcova, A.; Davies, G. R.; Eichhorn, S. J. Elastic modulus and stress-transfer properties of tunicate cellulose whiskers. *Biomacromolecules* **2005**, *6*, 1055–1061.
52. Tanaka, F.; Iwata, T. Estimation of the elastic modulus of cellulose crystal by molecular mechanics simulation. *Cellulose* **2006**, *13*, 509–517.
53. Eichhorn, S. J.; Davies, G. R. Modelling the crystalline deformation of native and regenerated cellulose. *Cellulose* **2006**, *13*, 291–307.
54. Bergensträhle, M.; Berglund, L. A.; Mazeau, K. Thermal response in crystalline I cellulose: A molecular dynamics study. *J. Phys. Chem. B* **2007**, *111*, 9138–9145.
55. Rusli, R.; Eichhorn, S. J. Determination of the stiffness of cellulose nanowhiskers and the fiber-matrix interface in a nanocomposite using Raman spectroscopy. *Appl. Phys. Lett.* **2008**, *93*, 033111.
56. Diddens, I.; Murphy, B.; Krisch, M.; Müller, M. Anisotropic elastic properties of cellulose measured using inelastic X-ray scattering. *Macromolecules* **2008**, *41*, 9755–9759.
57. Iwamoto, S.; Kai, W.; Isogai, A.; Iwata, T. Elastic modulus of single cellulose microfibrils from tunicate measured by atomic force microscopy. *Biomacromolecules* **2009**, *10*, 2571–2576.
58. Lahiji, R. R.; Xu, X.; Reifenberger, R.; Raman, A.; Rudie, A.; Moon, R. J. Atomic force microscopy characterization of cellulose nanocrystals. *Langmuir* **2010**, *26*, 4480–4488.
59. Cintrón, M. S.; Johnson, G. P.; French, A. D. Young's modulus calculations for cellulose I_β by MM3 and quantum mechanics. *Cellulose* **2011**, *18*, 505–516.

60. Wu, X.; Moon, R. J.; Martini, A. Crystalline cellulose elastic modulus predicted by atomistic models of uniform deformation and nanoscale indentation. *Cellulose* **2013**, *20*, 43–55.
61. Dri, F. L.; Hector Jr., L. G.; Moon, R. J.; Zavattieri, P. D. Anisotropy of the elastic properties of crystalline cellulose I_β from first principles density functional theory with Van der Waals interactions. *Cellulose* **2013**, *20*, 2703–2718.
62. Wu, Q.; Henriksson, M.; Liu, X.; Berglund, L. A. A high strength nanocomposite based on microcrystalline cellulose and polyurethane. *Biomacromolecules* **2007**, *8*, 3687–3692.
63. Lin, N.; Huang, J.; Dufresne, A. Preparation, properties and applications of polysaccharide nanocrystals in advanced functional nanomaterials: a review. *Nanoscale* **2012**, *4*, 3274–3294.
64. Shopsowitz, K. E.; Qi, H.; Hamad, W. Y.; MacLachlan, M. J. Free-standing mesoporous silica films with tunable chiral nematic structures. *Nature* **2010**, *468*, 422–426.
65. Beck, S.; Bouchard, J.; Chauve, G.; Berry, R. Controlled production of patterns in iridescent solid films of cellulose nanocrystals. *Cellulose* **2013**, *20*, 1401–1411.
66. Lagerwall, J. P. F.; Schütz, C.; Salajkova, M.; Noh, J.; Park, J. H.; Scalia, G.; Bergström, L. Cellulose nanocrystal-based materials: from liquid crystal self-assembly and glass formation to multifunctional thin films. *NPG Asia Mater.* **2014**, *6*, e80.
67. Fleming, K.; Gray, D. G.; Matthews, S. Cellulose crystallites. *Chem.–Eur. J.* **2001**, *7*, 1831–1835.
68. Roman, M.; Gray, D. G. Parabolic focal conics in self-assembled solid films of cellulose nanocrystals. *Langmuir* **2005**, *21*, 5555–5561.
69. Majoinen, J.; Kontturi, E.; Ikkala, O.; Gray, D. G. SEM imaging of chiral nematic films cast from cellulose nanocrystal suspensions. *Cellulose* **2012**, *19*, 1599–1605.
70. van den Berg, O.; Capadona, J. R.; Weder, C. Preparation of homogeneous dispersions of tunicate cellulose whiskers in organic solvents. *Biomacromolecules* **2007**, *8*, 1353–1357.
71. Bercea, M.; Navard, P. Shear dynamics of aqueous suspensions of cellulose whiskers. *Macromolecules* **2000**, *33*, 6011–6016.
72. Orts, W. J.; Godbout, L.; Marchessault, R. H.; Revol, J.-F. Enhanced ordering of liquid crystalline suspensions of cellulose microfibrils: a small angle neutron scattering study. *Macromolecules* **1998**, *31*, 5717–5725.
73. Boluk, Y.; Lahiji, R.; Zhaod, L.; McDermott, M. T. Suspension viscosities and shape parameter of cellulose nanocrystals (CNC). *Colloid. Surface A.* **2011**, *377*, 297–303.
74. Ureña-Benavides, E. E.; Ao, G.; Davis, V. A.; Kitchens, C. L. Rheology and phase behavior of lyotropic cellulose nanocrystal suspensions. *Macromolecules* **2011**, *44*, 8990–8998.
75. Shafiei-Sabet, S.; Hamad, W. Y.; Hatzikiriakos, S. G. Influence of degree of sulfation on the rheology of cellulose nanocrystal suspensions. *Rheol. Acta.* **2013**, *52*, 741–751.
76. Habibi, Y.; Lucia, L. A.; Rojas, O. J. Cellulose nanocrystals: chemistry, self-assembly, and applications. *Chem. Rev.* **2010**, *110*, 3479–3500.
77. French, A. D.; Bertoniere, N. R.; Brown, R. M.; Chanzy, H.; Gray, D.; Hattori, K.; Kirk-Othmer G. W. Encyclopedia of chemical technology. ed. Seidel, A. John Wiley & Sons, Inc., 5th edn, **2004**, *5*, pp. 360–394.
78. Wakelyn, P. J. Handbook of fiber chemistry. ed. Levin, M.; Pearce, E. M. Marcel Dekker, New York, **1998**, pp. 642–654.
79. Hebeish, A.; Guthrie, J. T. The chemistry and technology of cellulosic copolymers. Springer-Verlag, Berlin, **1981**.

80. Siqueira, G.; Bras, J.; Dufresne, A. Cellulose whiskers versus microfibrils: Influence of the nature of the nanoparticle and its surface functionalization on the thermal and mechanical properties of nanocomposites. *Biomacromolecules* **2009**, *10*, 425–432.
81. Way, A. E.; Hsu, L.; Shanmuganathan, K.; Weder, C.; Rowan, S. J. pH-Responsive cellulose nanocrystal gels and nanocomposites. *ACS Macro Lett.* **2012**, *1*, 1001–1006.
82. Lokanathan, A. R.; Nykänen, A.; Seitsonen, J.; Johansson, L.-S.; Campbell, J.; Rojas, O. J.; Ikkala, O.; Laine, J. Cilia-mimetic hairy surfaces based on end-immobilized nanocellulose colloidal rods. *Biomacromolecules* **2013**, *14*, 2807–2813.
83. Araki, J.; Wada, M.; Kuga, S.; Okano, T. Flow properties of microcrystalline cellulose suspension prepared by acid treatment of native cellulose. *Colloid. Surface A.* **1998**, *142*, 75–82.
84. Araki, J.; Wada, M.; Kuga, S.; Okano, T. Hydrocolloids: physical chemistry and industrial application of gels, polysaccharides, and proteins, ed. Nishinari, K. Elsevier, Amsterdam, **2000**, *1*, pp. 283–288.
85. Hasani, M.; Cranston, E. D.; Westman, G.; Gray, D. G. Cationic surface functionalization of cellulose nanocrystals. *Soft Matter* **2008**, *4*, 2238–2244.
86. Zaman, M.; Xiao, H.; Chibante, F.; Ni, Y. Synthesis and characterization of cationically modified nanocrystalline cellulose. *Carbohydr. Polym.* **2012**, *89*, 163–170.
87. Salajková, M.; Berglund, L. A.; Zhou, Q. Hydrophobic cellulose nanocrystals modified with quaternary ammonium salts. *J. Mater. Chem.* **2012**, *22*, 19798–19805.
88. Cao, X.; Wang, X.; Ding, B.; Yu, J.; Sun, G. Novel spider-web-like nanoporous networks based on jute cellulose nanowhiskers. *Carbohydr. Polym.* **2013**, *92*, 2041–2047.
89. Araki, J. Electrostatic or steric? – preparations and characterizations of well-dispersed systems containing rod-like nanowhiskers of crystalline polysaccharides. *Soft Matter* **2013**, *9*, 4125–4141.
90. Araki, J.; Wada, M.; Kuga, S.; Okano, T. Influence of surface charge on viscosity behavior of cellulose microcrystal suspension. *J. Wood Sci.* **1999**, *45*, 258–261.
91. de Mesquita, J. P.; Donnici, C. L.; Pereira, F. V. Biobased nanocomposites from layer-by-layer assembly of cellulose nanowhiskers with chitosan. *Biomacromolecules* **2010**, *11*, 473–480.
92. Boluk, Y.; Zhao, L.; Incani, V. Dispersions of nanocrystalline cellulose in aqueous polymer solutions: structure formation of colloidal rods. *Langmuir* **2012**, *28*, 6114–6123.
93. Dong, X. M.; Kimura, T.; Revol, J.-F.; Gray, D. G. Effects of ionic strength on the isotropic–chiral nematic phase transition of suspensions of cellulose crystallites. *Langmuir* **1996**, *12*, 2076–2082.
94. Cranston, E. D.; Gray, D. G.; Rutland, M. W. Direct surface force measurements of polyelectrolyte multilayer films containing nanocrystalline cellulose. *Langmuir* **2010**, *26*, 17190–17197.
95. Rusli, R.; Shanmuganathan, K.; Rowan, S. J.; Weder, C.; Eichhorn, S. J. Stress transfer in cellulose nanowhisiker composites—influence of whisker aspect ratio and surface charge. *Biomacromolecules* **2011**, *12*, 1363–1369.
96. Araki, J.; Kuga, S. Effect of trace electrolyte on liquid crystal type of cellulose microcrystals. *Langmuir* **2001**, *17*, 4493–4496.

97. Hirai, A.; Inui, O.; Horii, F.; Tsuji, M. Phase separation behavior in aqueous suspensions of bacterial cellulose nanocrystals prepared by sulfuric acid treatment. *Langmuir* **2009**, *25*, 497–502.
98. Winter, H. T.; Cerclier, C.; Delorme, N.; Bizot, H.; Quemener, B.; Cathala, B. Improved colloidal stability of bacterial cellulose nanocrystal suspensions for the elaboration of spin-coated cellulose-based model surfaces. *Biomacromolecules* **2010**, *11*, 3144–3151.
99. de Menezes, A. J.; Siqueira, G.; Curvelo, A. A. S.; Dufresne, A. Extrusion and characterization of functionalized cellulose whiskers reinforced polyethylene nanocomposites. *Polymer* **2009**, *50*, 4552–4563.
100. Harrisson, S.; Drisko, G. L.; Malmström, E.; Hult, A.; Wooley, K. L. Hybrid rigid/soft and biologic/synthetic materials: polymers grafted onto cellulose microcrystals. *Biomacromolecules* **2011**, *12*, 1214–1223.
101. Araki, J.; Wada, M.; Kuga, S. Steric stabilization of a cellulose microcrystal suspension by poly(ethylene glycol) grafting. *Langmuir* **2001**, *17*, 21–27.
102. Kovacs, T.; Naish, V.; O'Connor, B.; Blaise, C.; Gagné, F.; Hall, L.; Trudeau, V.; Martel, P. An ecotoxicological characterization of nanocrystalline cellulose (NCC). *Nanotoxicology* **2010**, *4*, 255–270.
103. Dong, S.; Hiran, A. A.; Colacino, K. R.; Lee, Y. W.; Roman, M. Cytotoxicity and cellular uptake of cellulose nanocrystals. *Nano Life* **2012**, *2*, 1241006 (11 pages).
104. Kümmerer, K.; Menz, J.; Schubert, T.; Thielemans, W. Biodegradability of organic nanoparticles in the aqueous environment. *Chemosphere* **2011**, *82*, 1387–1392.
105. Clift, M. J. D.; Foster, E. J.; Vanhecke, D.; Studer, D.; Wick, P.; Gehr, P.; Rothen-Rutishauser, B.; Weder, C. Investigating the interaction of cellulose nanofibers derived from cotton with a sophisticated 3D human lung cell coculture. *Biomacromolecules* **2011**, *12*, 3666–3673.
106. Endes, C.; Müller, S.; Schmid, O.; Vanhecke, D.; Foster, E. J.; Petri-Fink, A.; Rothen-Rutishauser, B.; Weder, C.; Clift, M. J. D. Risk assessment of released cellulose nanocrystals – mimicking inhalatory exposure. *J. Physics: Conference Series* **2013**, *429*, 012008 (10 Pages).
107. Miyamoto, T.; Takahashi, S.; Ito, H.; Inagaki, H.; Noishiki, Y. Tissue biocompatibility of cellulose and its derivatives. *J. Biomed. Mater. Res.* **1989**, *23*, 125–133.
108. Mårtson, M.; Viljanto, J.; Hurme, T.; Laippala, P.; Saukko, P. Is cellulose sponge degradable or stable as implantation material? An *in vivo* subcutaneous study in the rat. *Biomaterials* **1999**, *20*, 1989–1995.
109. Dugan, J. M.; Gough, J. E.; Eichhorn, S. J. Bacterial cellulose scaffolds and cellulose nanowhiskers for tissue engineering. *Nanomedicine* **2013**, *8*, 287–298.
110. Czaja, W. K.; Young, D. J.; Kaweck, M.; Brown, R. M. The future prospects of microbial cellulose in biomedical applications. *Biomacromolecules* **2007**, *8*, 1–12.
111. Li, J.; Wan, Y. Z.; Li, L. F.; Liang, H.; Wang, J. H. Preparation and characterization of 2,3-dialdehyde bacterial cellulose for potential biodegradable tissue engineering scaffolds. *Mater. Sci. Eng. C* **2009**, *29*, 1635–1642.
112. Klemm, D.; Kramer, F.; Moritz, S.; Lindström, T.; Ankerfors, M.; Gray, D.; Dorris, A. Nanocelluloses: a new family of nature-based materials. *Angew. Chem. Int. Ed.* **2011**, *50*, 5438–5466.

113. Moon, R. J.; Martini, A.; Nairn, J.; Simonsen, J.; Youngblood, J. Cellulose nanomaterials review: structure, properties and nanocomposites. *Chem. Soc. Rev.* **2011**, *40*, 3941–3994.
114. Yi, J.; Xu, Q.; Zhang, X.; Zhang, H. Chiral-nematic self-ordering of rodlike cellulose nanocrystals grafted with poly(styrene) in both thermotropic and lyotropic states. *Polymer* **2008**, *49*, 4406–4412.
115. Yi, J.; Xu, Q.; Zhang, X.; Zhang, H. Temperature-induced chiral nematic phase changes of suspensions of poly(*N,N*-dimethylaminoethyl methacrylate)-grafted cellulose nanocrystals. *Cellulose* **2009**, *16*, 989–997.
116. Zoppe, J. O.; Habibi, Y.; Rojas, O. J.; Venditti, R. A.; Johansson, L.-S.; Efimenko, K.; Österberg, M.; Laine, J. Poly(*N*-isopropylacrylamide) brushes grafted from cellulose nanocrystals via surface-initiated single-electron transfer living radical polymerization. *Biomacromolecules* **2010**, *11*, 2683–2691.
117. Dash, R.; Elder, T.; Ragauskas, A. J. Grafting of model primary amine compounds to cellulose nanowhiskers through periodate oxidation. *Cellulose* **2012**, *19*, 2069–2079.
118. Dash, R.; Ragauskas, A. J. Synthesis of a novel cellulose nanowhisiker-based drug delivery system. *RSC Adv.* **2012**, *2*, 3403–3409.
119. Heux, L.; Chauve, G.; Bonini, C. Nonflocculating and chiral-nematic self-ordering of cellulose microcrystals suspensions in nonpolar solvents. *Langmuir* **2000**, *16*, 8210–8212.
120. Bonini, C.; Heux, L.; Cavallé, J.-Y.; Lindner, P.; Dewhurst, C.; Terech, P. Rodlike cellulose whiskers coated with surfactant: a small-angle neutron scattering characterization. *Langmuir* **2002**, *18*, 3311–3314.
121. Kvien, I.; Tanem, B. S.; Oksman, K. Characterization of cellulose whiskers and their nanocomposites by atomic force and electron microscopy. *Biomacromolecules* **2005**, *6*, 3160–3165.
122. Elazzouzi-Hafraoui, S.; Putaux, J.-L.; Heux, L. Self-assembling and chiral nematic properties of organophilic cellulose nanocrystals. *J. Phys. Chem. B* **2009**, *113*, 11069–11075.
123. Bondeson, D.; Oksman, K. Dispersion and characteristics of surfactant modified cellulose whiskers nanocomposites. *Compos. Interfaces* **2007**, *14*, 617–630.
124. Fortunati, E.; Armentano, I.; Zhou, Q.; Iannoni, A.; Saino, E.; Visai, L.; Berglund, L. A.; Kenny, J. M. Multifunctional bionanocomposite films of poly(lactic acid), cellulose nanocrystals and silver nanoparticles. *Carbohydr. Polym.* **2012**, *87*, 1596–1605.
125. Ljungberg, N.; Cavallé, J.-Y.; Heux, L. Nanocomposites of isotactic polypropylene reinforced with rod-like cellulose whiskers. *Polymer* **2006**, *47*, 6285–6292.
126. Habibi, Y.; Hoeger, I.; Kelley, S. S.; Rojas, O. J. Development of Langmuir-Schaeffer cellulose nanocrystal monolayers and their interfacial behaviors. *Langmuir* **2010**, *26*, 990–1001.
127. Kim, J.; Montero, G.; Habibi, Y.; Hinestroza, J. P.; Genzer, J.; Argyropoulos, D. S.; Rojas, O. J. Dispersion of cellulose crystallites by nonionic surfactants in a hydrophobic polymer matrix. *Polym. Eng. Sci.* **2009**, *49*, 2054–2061.
128. Rojas, O. J.; Montero, G. A.; Habibi, Y. Electrospun nanocomposites from polystyrene loaded with cellulose nanowhiskers. *J. Appl. Polym. Sci.* **2009**, *113*, 927–935.
129. Petersson, L.; Kvien, I.; Oksman, K. Structure and thermal properties of poly(lactic acid)/cellulose whiskers nanocomposite materials. *Compos. Sci. Technol.* **2007**, *67*, 2535–2544.

130. Hirota, M.; Tamura, N.; Saito, T.; Isogai, A. Oxidation of regenerated cellulose with NaClO₂ catalyzed by TEMPO and NaClO under acid-neutral conditions. *Carbohydr. Polym.* **2009**, *78*, 330–335.
131. Fujisawa, S.; Isogai T.; Isogai, A. Temperature and pH stability of cellouronic acid. *Cellulose* **2010**, *17*, 607–615.
132. Isogai, A.; Saito, T.; Fukuzumi, H. TEMPO-oxidized cellulose nanofibers. *Nanoscale* **2011**, *3*, 71–85.
133. Montanari, S.; Roumani, M.; Heux, L.; Vignon, M. R. Topochemistry of carboxylated cellulose nanocrystals resulting from TEMPO-mediated oxidation. *Macromolecules* **2005**, *38*, 1665–1671.
134. Siqueira, G.; Bras, J.; Dufresne, A. New process of chemical grafting of cellulose nanoparticles with a long chain isocyanate. *Langmuir* **2010**, *26*, 402–411.
135. Pei, A.; Zhou, Q.; Berglund, L. A. Functionalized cellulose nanocrystals as biobased nucleation agents in poly(L-lactide) (PLLA)–Crystallization and mechanical property effects. *Compos. Sci. Technol.* **2010**, *70*, 815–821.
136. Habibi, Y.; Chanzy, H.; Vignon, M. R. TEMPO-mediated surface oxidation of cellulose whiskers. *Cellulose* **2006**, *13*, 679–687.
137. Gandini, A.; Belgacem, M. N. Chemical modification of wood. In monomers, polymers and composites from renewable resources, 1st ed.; Elsevier: Great Britain, **2008**, 419–432.
138. Biyani, M. V.; Foster, E. J.; Weder, C. Light-healable supramolecular nanocomposites based on modified cellulose nanocrystals. *ACS Macro Lett.* **2013**, *2*, 236–240.
139. Goussé, C.; Chanzy, H.; Excoffier, G.; Soubeyrand, L.; Fleury, E. Stable suspensions of partially silylated cellulose whiskers dispersed in organic solvents. *Polymer* **2002**, *43*, 2645–2651.
140. Raquez, J.-M.; Murena, Y.; Goffin, A.-L.; Habibi, Y.; Ruelle, B.; DeBuyl, F.; Dubois, P. Surface-modification of cellulose nanowhiskers and their use as nanoreinforcers into polylactide: A sustainably-integrated approach. *Compos. Sci. Technol.* **2012**, *72*, 544–549.
141. Yang, J.; Han, C.-R.; Duan, J.-F.; Ma, M.-G.; Zhang, X.-M.; Xu, F.; Sun, R.-C. Synthesis and characterization of mechanically flexible and tough cellulose nanocrystals–polyacrylamide nanocomposite hydrogels. *Cellulose* **2013**, *20*, 227–237.
142. Tehrani, A. D.; Neysi, E. Surface modification of cellulose nanowhisker throughout graft polymerization of 2-ethyl-2-oxazoline. *Carbohydr. Polym.* **2013**, *97*, 98–104.
143. de Souza Lima, M. M.; Borsali, R. Rodlike cellulose microcrystals: structure, properties, and applications. *Macromol. Rapid Commun.* **2004**, *25*, 771–787.
144. Kloser, E.; Gray, D. G. Surface grafting of cellulose nanocrystals with poly(ethylene oxide) in aqueous media. *Langmuir* **2010**, *26*, 13450–13456.
145. Azouz, K. B.; Ramires, E. C.; den Fonteyne, W. V.; El Kissi, N.; Dufresne, A. Simple method for the melt extrusion of a cellulose nanocrystal reinforced hydrophobic polymer. *ACS Macro Lett.* **2012**, *1*, 236–240.
146. Belgacem, M. N.; Quillerou, J.; Gandini, A. Urethanes and polyurethanes bearing furan moieties—3. Synthesis, characterization and comparative kinetics of the formation of diurethanes. *Eur. Polym. J.* **1993**, *29*, 1217–1224.
147. Habibi, Y.; Dufresne, A. Highly filled bionanocomposites from functionalized polysaccharide nanocrystals. *Biomacromolecules* **2008**, *9*, 1974–1980.

148. Zoppe, J. O.; Peresin, M. S.; Habibi, Y.; Venditti, R. A.; Rojas, O. J. Reinforcing poly(ϵ -caprolactone) nanofibers with cellulose nanocrystals. *ACS Appl. Mater. Interfaces* **2009**, *9*, 1996–2004.
149. Goffin, A.-L.; Raquez, J.-M.; Duquesne, E.; Siqueira, G.; Habibi, Y.; Dufresne, A.; Dubois, P. Poly(ϵ -caprolactone) based nanocomposites reinforced by surface-grafted cellulose nanowhiskers via extrusion processing: Morphology, rheology, and thermo-mechanical properties. *Polymer* **2011**, *52*, 1532–1538.
150. Lin, N.; Chen, G.; Huang, J.; Dufresne, A.; Chang, P. R. Effects of polymer-grafted natural nanocrystals on the structure and mechanical properties of poly(lactic acid): A case of cellulose whisker-graft-polycaprolactone. *J. Appl. Polym. Sci.* **2009**, *113*, 3417–3425.
151. Labet, M.; Thielemans, W. Citric acid as a benign alternative to metal catalysts for the production of cellulose-grafted-polycaprolactone copolymers. *Polym. Chem.* **2012**, *3*, 679–684.
152. Carlsson, L.; Utsel, S.; Wågberg, L.; Malmström, E.; Carlmark, A. Surface-initiated ring-opening polymerization from cellulose model surfaces monitored by a Quartz Crystal Microbalance. *Soft Matter* **2012**, *8*, 512–517.
153. Bergenstråhle, M.; Mazeau, K.; Berglund, L. A. Molecular modeling of interfaces between cellulose crystals and surrounding molecules: Effects of caprolactone surface grafting. *Eur. Polym. J.* **2008**, *44*, 3662–3669.
154. Goffin, A.-L.; Raquez, J.-M.; Duquesne, E.; Siqueira, G.; Habibi, Y.; Dufresne, A.; Dubois, P. From interfacial ring-opening polymerization to melt processing of cellulose nanowhiskey-filled polylactide-based nanocomposites. *Biomacromolecules* **2011**, *12*, 2456–2465.
155. Braun, B.; Dorgan, J. R.; Hollingsworth, L. O. Supra-molecular ecobionanocomposites based on polylactide and cellulosic nanowhiskers: synthesis and properties. *Biomacromolecules* **2012**, *13*, 2013–2019.
156. Xu, Q.; Yi, J.; Zhang, X.; Zhang, H. A novel amphotropic polymer based on cellulose nanocrystals grafted with azo polymers. *Eur. Polym. J.* **2008**, *44*, 2830–2837.
157. Morandi, G.; Heath, L.; Thielemans, W. Cellulose nanocrystals grafted with polystyrene chains through surface-initiated atom transfer radical polymerization (SI-ATRP). *Langmuir* **2009**, *25*, 8280–8286.
158. Morandi, G.; Thielemans, W. Synthesis of cellulose nanocrystals bearing photocleavable grafts by ATRP. *Polym. Chem.* **2012**, *3*, 1402–1407.
159. Majoinen, J.; Walther, A.; McKee, J. R.; Kontturi, E.; Aseyev, V.; Malho, J. M.; Ruokolainen, J.; Ikkala, O. Polyelectrolyte brushes grafted from cellulose nanocrystals using Cu-mediated surface-initiated controlled radical polymerization. *Biomacromolecules* **2011**, *12*, 2997–3006.
160. Zoppe, J. O.; Österberg, M.; Venditti, R. A.; Laine, J.; Rojas, O. J. Surface interaction forces of cellulose nanocrystals grafted with thermoresponsive polymer brushes. *Biomacromolecules* **2011**, *12*, 2788–2796.
161. Zhou, Q.; Brumer, H.; Teeri, T. T. Self-organization of cellulose nanocrystals adsorbed with xyloglucan oligosaccharide-poly(ethylene glycol)-polystyrene triblock copolymer. *Macromolecules* **2009**, *42*, 5430–5432.

162. Azzam, F.; Heux, L.; Putaux, J.-L.; Jean, B. Preparation by grafting onto, characterization, and properties of thermally responsive polymer-decorated cellulose nanocrystals. *Biomacromolecules* **2010**, *11*, 3652–3659.
163. Ljungberg, N.; Bonini, C.; Bortolussi, F.; Boisson, C.; Heux, L.; Cavallé J. Y. New nanocomposite materials reinforced with cellulose whiskers in atactic polypropylene: Effect of surface and dispersion characteristics. *Biomacromolecules* **2005**, *6*, 2732–2739.
164. Peng, B.; Han, X.; Liu, H.; Berry, R. C.; Tam, K. C. Interactions between surfactants and polymer-grafted nanocrystalline cellulose. *Colloid. Surface. A* **2013**, *421*, 142–149.
165. Mahmoud, K. A.; Mena, J. A.; Male, K. B.; Hrapovic, S.; Kamen, A.; Luong, J. H. T. Effect of surface charge on the cellular uptake and cytotoxicity of fluorescent labeled cellulose nanocrystals. *ACS Appl. Mater. Interfaces* **2010**, *2*, 2924–2932.
166. Hassan, M. L.; Moorefield, C. M.; Elbatal, H. S.; Newkome, G. R. New metallo-supramolecular terpyridine-modified cellulose functional nanomaterials. *J. Macromol. Sci. A* **2012**, *49*, 298–305.
167. Hassan, M. L.; Moorefield, C. M.; Elbatal, H. S.; Newkome, G. R.; Modarelli, D. A.; Romano, N. C. Fluorescent cellulose nanocrystals via supramolecular assembly of terpyridine-modified cellulose nanocrystals and terpyridine-modified perylene. *Mater. Sci. Eng. B* **2012**, *177*, 350–358.
168. Zhang, L.; Li, Q.; Zhou, J.; Zhang, L. Synthesis and photophysical behavior of pyrene-bearing cellulose nanocrystals for Fe³⁺ sensing. *Macromol. Chem. Phys.* **2012**, *213*, 1612–1617.
169. Eyley, S.; Thielemans, W. Imidazolium grafted cellulose nanocrystals for ion exchange applications. *Chem. Commun.* **2011**, *47*, 4177–4179.
170. Cateto, C. A.; Ragauskas, A. Amino acid modified cellulose whiskers. *RSC Adv.* **2011**, *1*, 1695–1697.
171. Mangalam, A. P.; Simonsen, J.; Benight, A. S. Cellulose/DNA hybrid nanomaterials. *Biomacromolecules* **2009**, *10*, 497–504.
172. Feese, E.; Sadeghifar, H.; Gracz, H. S.; Argyropoulos, D. S.; Ghiladi, R. A. Photobactericidal porphyrin-cellulose nanocrystals: synthesis, characterization, and antimicrobial properties. *Biomacromolecules* **2011**, *12*, 3528–3539.
173. Carpenter, B. L.; Feese, E.; Sadeghifar, H.; Argyropoulos, D. S.; Ghiladi, R. A. Porphyrin-cellulose nanocrystals: A photobactericidal material that exhibits broad spectrum antimicrobial activity. *J. Photochem. Photobiol.* **2012**, *88*, 527–536.
174. Goetz, L.; Mathew, A.; Oksman, K.; Gatenholm, P.; Ragauskas, A. J. A novel nanocomposite film prepared from crosslinked cellulosic whiskers. *Carbohydr. Polym.* **2009**, *75*, 85–89.
175. Goetz, L.; Foston, M.; Mathew, A. P.; Oksman, K.; Ragauskas, A. J. Poly(methyl vinyl ether-co-maleic acid)-polyethylene glycol nanocomposites cross-linked in situ with cellulose nanowhiskers. *Biomacromolecules* **2010**, *11*, 2660–2666.
176. Filpponen, I.; Argyropoulos, D. S. Regular linking of cellulose nanocrystals via click chemistry: synthesis and formation of cellulose nanoplatelet gels. *Biomacromolecules* **2010**, *11*, 1060–1066.
177. Fox, J. D.; Capadona, J. R.; Marasco, P. D.; Rowan, S. J. Bioinspired water-enhanced mechanical gradient nanocomposite films that mimic the architecture and properties of the squid beak. *J. Am. Chem. Soc.* **2013**, *135*, 5167–5174.

178. Dufresne, A. Processing of polymer nanocomposites reinforced with cellulose nanocrystals: a challenge. *Int. Polym. Proc.* **2012**, *27*, 557–564.
179. Abdul Khalil, H. P. S.; Bhat, A. H.; Ireana Yusra, A. F. Green composites from sustainable cellulose nanofibrils: a review. *Carbohydr. Polym.* **2012**, *87*, 963–979.
180. Tingaut, P.; Zimmermann, T.; Sèbe, G. Cellulose nanocrystals and microfibrillated cellulose as building blocks for the design of hierarchical functional materials. *J. Mater. Chem.* **2012**, *22*, 20105–20111.
181. Durán, N.; Lemes, A. P.; Seabra, A. B. Review of cellulose nanocrystals patents: preparation, composites and general applications. *Recent Pat. Nanotech.* **2012**, *6*, 16–28.
182. Lam, E.; Male, K. B.; Chong, J. H.; Leung, A. C. W.; Luong, J. H. T. Applications of functionalized and nanoparticle-modified nanocrystalline cellulose. *Trends Biotechnol.* **2012**, *30*, 283–290.
183. Brinchi, L.; Cotana, F.; Fortunati, E.; Kenny, J. M. Production of nanocrystalline cellulose from lignocellulosic biomass: Technology and applications. *Carbohydr. Polym.* **2013**, *94*, 154–169.
184. Miao, C.; Hamad, W. Y. Cellulose reinforced polymer composites and nanocomposites: a critical review. *Cellulose* **2013**, *20*, 2221–2262.
185. Leung, A. C. W.; Lam, E.; Chong, J.; Hrapovic, S.; Luong, J. H. T. Reinforced plastics and aerogels by nanocrystalline cellulose. *J. Nanopart. Res.* **2013**, *15*, 1636. (24 pages)
186. Rebouillat, S.; Pla, F. State of the art manufacturing and engineering of nanocellulose: a review of available data and industrial applications. *J. Biomater. Nanobiotechnol.* **2013**, *4*, 165–188.
187. Milanez, D. H.; do Amaral, R. M.; de Faria, L. I. L.; Gregolin, J. A. R. Assessing nanocellulose developments using science and technology indicators. *Mater. Res.* **2013**, *16*, 635–641.
188. Dufresne, A. Nanocellulose: a new ageless bionanomaterial. *Mater. Today* **2013**, *16*, 220–227.
189. Paunonen, S. Strength and barrier enhancements of composites and packaging boards by nanocelluloses – a literature review. *Nord. Pulp Pap. Res. J.* **2013**, *28*, 165–181.
190. Charreau, H.; Foresti, M. L.; Vázquez, A. Nanocellulose patents trends: a comprehensive review on patents on cellulose nanocrystals, microfibrillated and bacterial cellulose. *Recent Pat. Nanotechnol.* **2013**, *7*, 56–80.
191. Akhlaghi, S. P.; Peng, B.; Yao, Z.; Tam, K. C. Sustainable nanomaterials derived from polysaccharides and amphiphilic compounds. *Soft Matter* **2013**, *9*, 7905–7918.
192. Habibi, Y. Key advances in the chemical modification of nanocelluloses. *Chem. Soc. Rev.* **2014**, *43*, 1519–1542.
193. Hajji, P.; Cavaille, J. Y.; Favier, V.; Gauthier, C.; Vigier, G. Tensile behavior of nanocomposites from latex and cellulose whiskers. *Polym. Compos.* **1996**, *17*, 612–619.
194. Dufresne, A. Comparing the mechanical properties of high performances polymer nanocomposites from biological sources. *J Nanosci. Nanotechnol.* **2006**, *6*, 322–330.
195. Dufresne, A. Polysaccharide nanocrystal reinforced nanocomposites. *Can. J. Chem.* **2008**, *86*, 484–494.
196. Dufresne, A. Nanocellulose. From nature to high performance tailored materials. Walter de Gruyter GmbH, Berlin/Boston, **2012**, pp. 261–262.

197. Fortunati, E.; Peltzer, M.; Armentano, I.; Torre, L.; Jiménez, A.; Kenny, J. M. Effects of modified cellulose nanocrystals on the barrier and migration properties of PLA nano-biocomposites. *Carbohydr. Polym.* **2012**, *90*, 948–956.
198. Auad, M. L.; Richardson, T.; Orts, W. J.; SMedeiros, E.; Mattoso, L. H. C.; Mosiewicki, M. A.; Marcovich, N. E.; Aranguren, M. I. Polyaniline-modified cellulose nanofibrils as reinforcement of a smart polyurethane. *Polym. Int.* **2011**, *60*, 743–750.
199. Corrêa, A. C.; de Moraes Teixeira, E.; Carmona, V. B.; Teodoro, K. B. R.; Ribeiro, C.; Mattoso, L. H. C.; Marconcini, J. M. Obtaining nanocomposites of polyamide 6 and cellulose whiskers via extrusion and injection molding. *Cellulose* **2014**, *21*, 311–322.
200. Lin, N.; Huang, J.; Chang, P. R.; Feng, J.; Yu, J. Surface acetylation of cellulose nanocrystal and its reinforcing function in poly(lactic acid). *Carbohydr. Polym.* **2011**, *83*, 1834–1842.
201. Yang, Z.-Y.; Wang, W.-J.; Shao, Z.-Q.; Zhu, H.-D.; Li, Y.-H.; Wang, F.-J. The transparency and mechanical properties of cellulose acetate nanocomposites using cellulose nanowhiskers as fillers. *Cellulose* **2013**, *20*, 159–168.
202. Lin, S.; Huang, J.; Chang, P. R.; Wei, S.; Xu, Y.; Zhang, Q. Structure and mechanical properties of new biomass-based nanocomposite: Castor oil-based polyurethane reinforced with acetylated cellulose nanocrystal. *Carbohydr. Polym.* **2013**, *95*, 91–99.
203. Follain, N.; Belbekhouche, S.; Bras, J.; Siqueira, G.; Marais, S.; Dufresne, A. Water transport properties of bio-nanocomposites reinforced by *Luffa cylindrica* cellulose nanocrystals. *J. Membrane Sci.* **2013**, *427*, 218–229.
204. Wang, Y.; Chen, L. Cellulose nanowhiskers and fiber alignment greatly improve mechanical properties of electrospun prolamin protein fibers. *ACS Appl. Mater. Interfaces* **2014**, *6*, 1709–1718.
205. Brown, E. E.; Hu, D.; Lail, N. A.; Zhang, X. Potential of nanocrystalline cellulose–fibrin nanocomposites for artificial vascular graft applications. *Biomacromolecules* **2013**, *14*, 1063–1071.
206. Zhang, R.; Zhu, C.; Shan, X.; Xia, J.; Zhu, Q.; Hu, Y. Study on the poly(3-hydroxybutyrate-co-4-hydroxybutyrate)-based nanocomposites reinforced by surface modified nanocrystalline cellulose. *J. Appl. Polym. Sci.* **2013**, *130*, 2015–2022.
207. Blachechen, L. S.; de Mesquita, J. P.; de Paula, E. L.; Pereira, F. V.; Petri, D. F. S. Interplay of colloidal stability of cellulose nanocrystals and their dispersibility in cellulose acetate butyrate matrix. *Cellulose* **2013**, *20*, 1329–1342.
208. Espino-Pérez, E.; Bras, J.; Ducruet, V.; Guinault, A.; Dufresne, A.; Domenek, S. Influence of chemical surface modification of cellulose nanowhiskers on thermal, mechanical, and barrier properties of poly(lactide) based bionanocomposites. *Eur. Polym. J.* **2013**, *49*, 3144–3154.
209. Yu, H.-Y.; Qin, Z.-Y.; Yan, C.-F.; Yao, J.-M. Green nanocomposites based on functionalized cellulose nanocrystals: a study on the relationship between interfacial interaction and property enhancement. *ACS Sustainable Chem. Eng.* DOI: 10.1021/sc400499g
210. Park, S. H.; Oh, K. W.; Kim, S. H. Reinforcement effect of cellulose nanowhisiker on bio-based polyurethane. *Compos. Sci. Technol.* **2013**, *86*, 82–88.
211. de Mesquita, J. P.; Donnici, C. L.; Teixeira, I. F.; Pereira, F. V. Bio-based nanocomposites obtained through covalent linkage between chitosan and cellulose nanocrystals. *Carbohydr. Polym.* **2012**, *90*, 210–217.

212. Bitinis, N.; Verdejo, R.; Bras, J.; Fortunati, E.; Kenny, J. M.; Torre, L.; López-Manchado, M. A. Poly(lactic acid)/natural rubber/cellulose nanocrystal bionanocomposites Part I. Processing and morphology. *Carbohydr. Polym.* **2013**, *96*, 611–620.
213. Bitinis, N.; Fortunati, E.; Verdejo, R.; Bras, J.; Kenny, J. M.; Torre, L.; López-Manchado, M. A. Poly(lactic acid)/natural rubber/cellulose nanocrystal bionanocomposites. Part II: Properties evaluation. *Carbohydr. Polym.* **2013**, *96*, 621–627.
214. Lin, N.; Dufresne, A. Physical and/or chemical compatibilization of extruded cellulose nanocrystal reinforced polystyrene nanocomposites. *Macromolecules* **2013**, *46*, 5570–5583.
215. Dufresne, A. Nanocellulose: From nature to high performance tailored materials. Walter de Gruyter GmbH, Berlin/Boston, **2012**, pp. 339–340.
216. Dufresne, A. Nanocellulose: From nature to high performance tailored materials. Walter de Gruyter GmbH, Berlin/Boston, **2012**, pp. 327–333.
217. Favier, V.; Dendievel, R.; Canova, G.; Cavallé, J. Y.; Gilormini, P. Simulation and modeling of three-dimensional percolating structures: case of a latex matrix reinforced by a network of cellulose fibers. *Acta Mater.* **1997**, *45*, 1557–1565.
218. Stauffer, D. Introduction to Percolation Theory (Taylor and Francis, London and Philadelphia), **1985**.
219. Dufresne, A. Nanocellulose: From nature to high performance tailored materials. Walter de Gruyter GmbH, Berlin/Boston, **2012**, pp. 277–320.
220. Dufresne, A. Nanocellulose: From nature to high performance tailored materials. Walter de Gruyter GmbH, Berlin/Boston, **2012**, pp. 373–409.
221. Hassan, M. L.; Moorefield, C. M.; Elbatal, H. S.; Newkomeb, G. R. New metallo-supramolecular terpyridine-modified cellulose functional nanomaterials. *J. Macromol. Sci. A* **2012**, *49*, 298–305.
222. Barazzouk, S.; Daneault, C. Tryptophan-based peptides grafted onto oxidized nanocellulose. *Cellulose* **2012**, *19*, 481–493.
223. Yang, Q.; Pan, X. A facile approach for fabricating fluorescent cellulose. *J. Appl. Polym. Sci.* **2010**, *117*, 3639–3644.
224. Nielsen, L. J.; Eyley, S.; Thielemans, W.; Aylott, J. W. Dual fluorescent labelling of cellulose nanocrystals for pH sensing. *Chem. Commun.* **2010**, *46*, 8929–8931.
225. Drogat, N.; Granet, R.; Morvan, C. L.; Bégau-Grimaud, G.; Krausz, P.; Sol, V. Chlorin-PEI-labeled cellulose nanocrystals: synthesis, characterization and potential application in PDT. *Bioorg. Med. Chem. Lett.* **2012**, *22*, 3648–3652.
226. Edwards, J. V.; Prevost, N.; Condon, B.; French, A.; Wu, Q. Immobilization of lysozyme-cellulose amide-linked conjugates on cellulose I and II cotton nanocrystalline preparations. *Cellulose* **2012**, *19*, 495–506.
227. Yang, R.; Tan, H.; Wei, F.; Wang, S. Peroxidase conjugate of cellulose nanocrystals for the removal of chlorinated phenolic compounds in aqueous solution. *Biotechnology* **2008**, *7*, 233–241.
228. Mahmoud, K. A.; Male, K. B.; Hrapovic, S.; Luong, J. H. T. Cellulose nanocrystal/gold nanoparticle composite as a matrix for enzyme immobilization. *ACS Appl. Mater. Interfaces* **2009**, *1*, 1383–1386.
229. Incani, V.; Danumah, C.; Boluk, Y. Nanocomposites of nanocrystalline cellulose for enzyme immobilization. *Cellulose* **2013**, *20*, 191–200.

230. Mahmoud, K. A.; Lam, E.; Hrapovic, S.; Luong, J. H. T. Preparation of well-dispersed gold/magnetite nanoparticles embedded on cellulose nanocrystals for efficient immobilization of papain enzyme. *ACS Appl. Mater. Interfaces* **2013**, *5*, 4978–4985.
231. Liu, H.; Wang, D.; Shang, S.; Song, Z. Preparation of silver nanoparticles on cellulose nanocrystals and the application in electrochemical detection of DNA hybridization. *Cellulose* **2011**, *18*, 67–74.
232. Cerclier, C.; Guyomard-Lack, A.; Moreau, C.; Cousin, F.; Beury, N.; Bonnin, E.; Jean, B.; Cathala, B. Coloured semi-reflective thin films for biomass-hydrolyzing enzyme detection. *Adv. Mater.* **2011**, *23*, 3791–3795.
233. Edwards, J. V.; Prevost, N.; Sethumadhavan, K.; Ullah, A.; Condon, B. Peptide conjugated cellulose nanocrystals with sensitive human neutrophil elastase sensor activity. *Cellulose* **2013**, *20*, 1223–1235.
234. Eyley, S.; Shariki, S.; Dale, S. E. C.; Bending, S.; Marken, F.; Thielemans, W. Ferrocene-decorated nanocrystalline cellulose with charge carrier mobility. *Langmuir* **2012**, *28*, 6514–6519.
235. Dujardin, E.; Blaseby M.; Mann, S. Synthesis of mesoporous silica by sol-gel mineralisation of cellulose nanorod nematic suspensions. *J. Mater. Chem.* **2003**, *13*, 696–699.
236. Scheel, H.; Zollfrank, C.; Greil, P. Luminescent silica nanotubes and nanowires: Preparation from cellulose whisker templates and investigation of irradiation-induced luminescence. *J. Mater. Res.* **2009**, *24*, 1709–1715.
237. Gruber, S.; Gottschlich, A.; Scheel, H.; Aresipathi, C.; Bannat, I.; Zollfrank, C.; Wark, M. Molecular and supramolecular templating of silica-based nanotubes and introduction of metal nanowires. *Phys. Status Solidi B* **2010**, *247*, 2401–2411.
238. Gruber, S.; Taylor, R. N. K.; Scheel, H.; Greil P.; Zollfrank, C. Cellulose-biotemplated silica nanowires coated with a dense gold nanoparticle layer. *Mater. Chem. Phys.* **2011**, *129*, 19–22.
239. Shin, Y.; Exarhos, G. J. Conversion of cellulose materials into nanostructured ceramics by biomineralization. *Cellulose* **2007**, *14*, 269–279.
240. Gebauer, D.; Oliynyk, V.; Salajkova, M.; Sort, J.; Zhou, Q.; Bergström, L.; Salazar-Alvarez, G. A transparent hybrid of nanocrystalline cellulose and amorphous calcium carbonate nanoparticles. *Nanoscale* **2011**, *3*, 3563–3566.
241. Drogat, N.; Granet, R.; Sol, V.; Memmi, A.; Saad, N.; Koerkamp, C. K.; Bressollier, P.; Krausz, P. Antimicrobial silver nanoparticles generated on cellulose nanocrystals. *J. Nanopart. Res.* **2011**, *13*, 1557–1562.
242. Ifuku, S.; Tsuji, M.; Morimoto, M.; Saimoto, H.; Yano, H. Synthesis of silver nanoparticles templated by TEMPO-mediated oxidized bacterial cellulose nanofibers. *Biomacromolecules* **2009**, *10*, 2714–2717.
243. Koga, H.; Tokunaga, E.; Hidaka, M.; Umemura, Y.; Saito, T.; Isogai, A.; Kitaoka, T. Topochemical synthesis and catalysis of metal nanoparticles exposed on crystalline cellulose nanofibers. *Chem. Commun.* **2010**, *46*, 8567–8569.
244. Lam, E.; Hrapovic, S.; Majid, E.; Chong, J. H.; Luong, J. H. T. Catalysis using gold nanoparticles decorated on nanocrystalline cellulose. *Nanoscale* **2012**, *4*, 997–1002.
245. Shin, Y.; Bae, I.-T.; Arey, B. W.; Exarhos, G. J. Simple preparation and stabilization of nickel nanocrystals on cellulose nanocrystal. *Mater. Lett.* **2007**, *61*, 3215–3217.

246. Benaissi, K.; Johnson, L.; Walsh, D. A.; Thielemans, W. Synthesis of platinum nanoparticles using cellulosic reducing agents. *Green Chem.* **2010**, *12*, 220–222.
247. Johnson, L.; Thielemans, W.; Walsh, D. A. Synthesis of carbon-supported Pt nanoparticle electrocatalysts using nanocrystalline cellulose as reducing agent. *Green Chem.* **2011**, *13*, 1686–1693.
248. Shin, Y.; Blackwood, J. M.; Bae, I.-T.; Arey, B. W.; Exarhos, G. J. Synthesis and stabilization of selenium nanoparticles on cellulose nanocrystal. *Mater. Lett.* **2007**, *61*, 4297–4300.
249. Cirtiu, C. M.; Dunlop-Brière, A. F.; Moores, A. Cellulose nanocrystallites as an efficient support for nanoparticles of palladium: application for catalytic hydrogenation and Heck coupling under mild conditions. *Green Chem.* **2011**, *13*, 288–291.
250. Nelson, K.; Deng, Y. The shape dependence of core–shell and hollow titania nanoparticles on coating thickness during layer-by-layer and sol–gel synthesis. *Nanotechnology* **2006**, *17*, 3219–3225.
251. Padalkar, S.; Capadona, J. R.; Rowan, S. J.; Weder, C.; Moon, R. J.; Stanciu, L. A. Self-assembly and alignment of semiconductor nanoparticles on cellulose nanocrystals. *J. Mater. Sci.* **2011**, *46*, 5672–5679.
252. Shin, Y.; Bae, I.-T.; Arey, B. W.; Exarhos, G. J. Facile stabilization of gold-silver alloy nanoparticles on cellulose nanocrystal. *J. Phys. Chem. C* **2008**, *112*, 4844–4848.
253. Liu, H.; Wang, D.; Shang, S.; Song, Z. Synthesis and characterization of Ag–Pd alloy nanoparticles/carboxylated cellulose nanocrystals nanocomposites. *Carbohydr. Polym.* **2011**, *83*, 38–43.
254. Padalkar, S.; Capadona, J. R.; Rowan, S. J.; Weder, C.; Won, Y.-H.; Stanciu, L. A.; Moon, R. J. Natural biopolymers: novel templates for the synthesis of nanostructures. *Langmuir* **2010**, *26*, 8497–8502.
255. Zhou, Y.; Ding, E.-Y.; Li, W.-D. Synthesis of TiO₂ nanocubes induced by cellulose nanocrystal (CNC) at low temperature. *Mater. Lett.* **2007**, *61*, 5050–5052.
256. Peng, X.; Ding, E. Low-temperature synthesis of flower-like TiO₂ nanocrystals. *Micro Nano Lett.* **2011**, *6*, 998–1001.
257. Liu, S.; Tao, D.; Bai, H.; Liu, X. Cellulose-nanowhisker-templated synthesis of titanium dioxide/cellulose nanomaterials with promising photocatalytic abilities. *J. Appl. Polym. Sci.* **2012**, *126*, E281–E289.
258. Xiong, R.; Lu, C.; Zhang, W.; Zhou, Z.; Zhang, X. Facile synthesis of tunable silver nanostructures for antibacterial application using cellulose nanocrystals. *Carbohydr. Polym.* **2013**, *95*, 214–219.
259. Liu, H.; Song, J.; Shang, S.; Song, Z.; Wang, D. Cellulose nanocrystal/silver nanoparticle composites as bifunctional nanofillers within waterborne polyurethane. *ACS Appl. Mater. Interfaces* **2012**, *4*, 2413–2419.
260. Ma, H.; Burger, C.; Hsiao, B. S.; Chu, B. Ultrafine polysaccharide nanofibrous membranes for water purification. *Biomacromolecules* **2011**, *12*, 970–976.
261. Ma, H.; Hsiao, B. S.; Chu, B. Ultrafine cellulose nanofibers as efficient adsorbents for removal of UO₂²⁺ in water. *ACS Macro Lett.* **2012**, *1*, 213–216.
262. Ma, H.; Burger, C.; Hsiao, B. S.; Chu, B. Nanofibrous microfiltration membrane based on cellulose nanowhiskers. *Biomacromolecules* **2012**, *13*, 180–186.

263. Thielemans, W.; Warbey, C. R.; Walsh, D. A. Permselective nanostructured membranes based on cellulose nanowhiskers. *Green Chem.* **2009**, *11*, 531–537.
264. Kalashnikova, I.; Bizot, H.; Cathala, B.; Capron I. New pickering emulsions stabilized by bacterial cellulose nanocrystals. *Langmuir* **2011**, *27*, 7471–7479.
265. Kalashnikova, I.; Bizot, H.; Cathala, B.; Capron I. Modulation of cellulose nanocrystals amphiphilic properties to stabilize oil/water interface. *Biomacromolecules* **2012**, *13*, 267–275.
266. Capron, I.; Cathala, B. Surfactant-free high internal phase emulsions stabilized by cellulose nanocrystals. *Biomacromolecules* **2013**, *14*, 291–296.
267. Zoppe, J. O.; Venditti, R. A.; Rojas, O. J. Pickering emulsions stabilized by cellulose nanocrystals grafted with thermo-responsive polymer brushes. *J. Colloid Interface Sci.* **2012**, *369*, 202–209.
268. Liebert, T.; Kostag, M.; Wotschadlo, J.; Heinze, T. Stable cellulose nanospheres for cellular uptake. *Macromol. Biosci.* **2011**, *11*, 1387–1392.
269. Male, K. B.; Leung, A. C. W.; Montes, J.; Kamen, A.; Luong, J. H. T. Probing inhibitory effects of nanocrystalline cellulose: inhibition *versus* surface charge. *Nanoscale* **2012**, *4*, 1373–1379.
270. Dugan, J. M.; Gough, J. E.; Eichhorn, S. J. Directing the morphology and differentiation of skeletal muscle cells using oriented cellulose nanowhiskers. *Biomacromolecules* **2010**, *11*, 2498–2504.
271. Dugan, J. M.; Collins, R. F.; Gough, J. E.; Eichhorn, S. J. Oriented surfaces of adsorbed cellulose nanowhiskers promote skeletal muscle myogenesis. *Acta Biomaterialia* **2013**, *9*, 4707–4715.
272. Cao, X.; Huang, M.; Ding, B.; Yu, J.; Sun, G. Robust polyacrylonitrile nanofibrous membrane reinforced with jute cellulose nanowhiskers for water purification. *Desalination* **2013**, *316*, 120–126.
273. Gong, G.; Mathew, A. P.; Oksman, K. Strong aqueous gels of cellulose nanofibers and nanowhiskers isolated from softwood flour. *Tappi J.* **2011**, *2*, 7–14.
274. Dorris, A.; Gray, D. G. Gelation of cellulose nanocrystal suspensions in glycerol. *Cellulose* **2012**, *19*, 687–694.
275. Siqueira, G.; Mathew, A. P.; Oksman, K. Processing of cellulose nanowhiskers/ cellulose acetate butyrate nanocomposites using sol–gel process to facilitate dispersion. *Compos. Sci. Technol.* **2011**, *71*, 1886–1892.
276. Capadona, J. R.; Shanmuganathan, K.; Triftschuh, S.; Seidel, S.; Rowan, S. J.; Weder, C. Polymer nanocomposites with nanowhiskers isolated from microcrystalline cellulose. *Biomacromolecules* **2009**, *10*, 712–716.
277. Yang, J.; Han, C.-R.; Duan, J.-F.; Xu, F.; Sun, R.-C. Mechanical and viscoelastic properties of cellulose nanocrystals reinforced poly(ethylene glycol) nanocomposite hydrogels. *ACS Appl. Mater. Interfaces* **2013**, *5*, 3199–3207.
278. Abitbol, T.; Johnstone, T.; Quinn, T. M.; Gray, D. G. Reinforcement with cellulose nanocrystals of poly(vinyl alcohol) hydrogels prepared by cyclic freezing and thawing. *Soft Matter* **2011**, *7*, 2373–2379.
279. Mihranyan, A. Viscoelastic properties of cross-linked polyvinyl alcohol and surface- oxidized cellulose whisker hydrogels. *Cellulose* **2013**, *20*, 1369–1376.

280. Zhou, C.; Wu, Q.; Yue, Y.; Zhang, Q. Application of rod-shaped cellulose nanocrystals in polyacrylamide hydrogels. *J. Colloid Interface Sci.* **2011**, *353*, 116–123.
281. Zhou, C.; Wu, Q.; Zhang, Q. Dynamic rheology studies of in situ polymerization process of polyacrylamide–cellulose nanocrystal composite hydrogels. *Colloid Polym. Sci.* **2011**, *289*, 247–255.
282. Wu, L.; Zhou, H.; Sun, H.-J.; Zhao, Y.; Yang, X.; Cheng, S. Z. D.; Yang, G. Thermoresponsive bacterial cellulose whisker/poly(NIPAM-co-BMA) nanogel complexes: synthesis, characterization, and biological evaluation. *Biomacromolecules* **2013**, *14*, 1078–1084.
283. Spagnol, C.; Rodrigues, F. H. A.; Pereira, A. G. B.; Fajardo, A. R.; Rubira, A. F.; Muniz, E. C. Superabsorbent hydrogel nanocomposites based on starch-g-poly(sodium acrylate) matrix filled with cellulose nanowhiskers. *Cellulose* **2012**, *19*, 1225–1237.
284. Karaaslan, M. A.; Tshabalala, M. A.; Yelle, D. J.; Buschle-Diller, G. Nanoreinforced biocompatible hydrogels from wood hemicelluloses and cellulose whiskers. *Carbohydr. Polym.* **2011**, *86*, 192–201.
285. Wang, H.; Roman, M. Formation and properties of chitosan/cellulose nanocrystal polyelectrolyte macroion complexes for drug delivery applications. *Biomacromolecules* **2011**, *12*, 1585–1593.
286. Bica, C. I. D.; Borsali, R.; Geissler, E.; Rochas, C. Dynamics of cellulose whiskers in agarose gels. 1. polarized dynamic light scattering. *Macromolecules* **2001**, *34*, 5275–5279.
287. Bica, C. I. D.; Borsali, R.; Rochas, C.; Geissler, E. Dynamics of cellulose whiskers spatially trapped in agarose hydrogels. *Macromolecules* **2006**, *39*, 3622–3627.
288. Osorio-Madrado, A.; Eder, M.; Rueggeberg, M.; Pandey, J. K.; Harrington, M. J.; Nishiyama, Y.; Putaux, J.-L.; Rochas, C.; Burgert, I. Reorientation of cellulose nanowhiskers in agarose hydrogels under tensile loading. *Biomacromolecules* **2012**, *13*, 850–856.
289. Zhang, X.; Huang, J.; Chang, P. R.; Li, J.; Chen, Y.; Wang, D.; Yu, J.; Chen, J. Structure and properties of polysaccharide nanocrystal-doped supramolecular hydrogels based on Cyclodextrin inclusion. *Polymer* **2010**, *51*, 4398–4407.
290. Lin, N.; Dufresne, A. Supramolecular hydrogels from in situ host–guest inclusion between chemically modified cellulose nanocrystals and cyclodextrin. *Biomacromolecules* **2013**, *14*, 871–880.
291. Dash, R.; Foston, M.; Ragauskas, A. J. Improving the mechanical and thermal properties of gelatin hydrogels cross-linked by cellulose nanowhiskers. *Carbohydr. Polym.* **2013**, *91*, 638–645.
292. Yang, J.; Han, C.-R.; Duan, J.-F.; Ma, M.-G.; Zhang, X.-M.; Xu, F.; Sun, R.-C.; Xie, X.-M. Studies on the properties and formation mechanism of flexible nanocomposite hydrogels from cellulose nanocrystals and poly(acrylic acid). *J. Mater. Chem.* **2012**, *22*, 22467–22480.
293. Cha, R.; He, Z.; Ni, Yong. Preparation and characterization of thermal/pH-sensitive hydrogel from carboxylated nanocrystalline cellulose. *Carbohydr. Polym.* **2012**, *88*, 713–718.
294. Lin, N.; Bruzzese, C.; Dufresne, A. TEMPO-oxidized nanocellulose participating as crosslinking aid for alginate-based sponges. *ACS Appl. Mater. Interfaces* **2012**, *4*, 4948–4959.
295. Wang, Y.; Chang, C.; Zhang, L. Effects of freezing/thawing cycles and cellulose nanowhiskers on structure and properties of biocompatible starch/PVA sponges. *Macromol. Mater. Eng.* **2010**, *295*, 137–145.

296. Li, Y.; Ragauskas, A. J. Ethanol organosolv lignin-based rigid polyurethane foam reinforced with cellulose nanowhiskers. *RSC Adv.* **2012**, *2*, 3347–3351.
297. Köhnke, T.; Lin, A.; Elder, T.; Theliander, H.; Ragauskas, A. J. Nanoreinforced xylan–cellulose composite foams by freeze-casting. *Green Chem.* **2012**, *14*, 1864–1869.
298. Dash, R.; Li, Y.; Ragauskas, A. J. Cellulose nanowhisker foams by freeze casting. *Carbohydr. Polym.* **2012**, *88*, 789–792.
299. Paës, G.; Chabbert, B. Characterization of arabinoxylan/cellulose nanocrystals gels to investigate fluorescent probes mobility in bioinspired models of plant secondary cell wall. *Biomacromolecules* **2012**, *13*, 206–214.
300. Heath, L.; Thielemans, W. Cellulose nanowhisker aerogels. *Green Chem.* **2010**, *12*, 1448–1453.
301. Gawryla, M. D.; van den Berg, O.; Weder, C.; Schiraldi, D. A. Clay aerogel/cellulose whisker nanocomposites: a nanoscale wattle and daub. *J. Mater. Chem.* **2009**, *19*, 2118–2124.
302. Zhou, C.; Shi, Q.; Guo, W.; Terrell, L.; Qureshi, A. T.; Hayes, D. J.; Wu, Q. Electrospun bio-nanocomposite scaffolds for bone tissue engineering by cellulose nanocrystals reinforcing maleic anhydride grafted PLA. *ACS Appl. Mater. Interfaces* **2013**, *5*, 3847–3854.
303. Blaker, J. J.; Lee, K.-Y.; Mantalaris, A.; Bismarck, A. Ice-microsphere templating to produce highly porous nanocomposite PLA matrix scaffolds with pores selectively lined by bacterial cellulose nano-whiskers. *Compos. Sci. Technol.* **2010**, *70*, 1879–1888.
304. Capadona, J. R.; Shanmuganathan, K.; Tyler, D. J.; Rowan, S. J.; Weder, C. Stimuli-responsive polymer nanocomposites inspired by the sea cucumber dermis. *Science* **2008**, *319*, 1370–1374.
305. Shanmuganathan, K.; Capadona, J. R.; Rowan, S. J.; Weder, C. Bio-inspired mechanically-adaptive nanocomposites derived from cotton cellulose whiskers. *J. Mater. Chem.* **2010**, *20*, 180–186.
306. Shanmuganathan, K.; Capadona, J. R.; Rowan, S. J.; Weder, C. Stimuli-responsive mechanically adaptive polymer nanocomposites. *ACS Appl. Mater. Interfaces* **2010**, *2*, 165–174.
307. Rusli, R.; Shanmuganathan, K.; Rowan, S. J.; Weder, C.; Eichhorn, S. J. Stress-transfer in anisotropic and environmentally adaptive cellulose whisker nanocomposites. *Biomacromolecules* **2010**, *11*, 762–768.
308. Mendez, J.; Annamalai, P. K.; Eichhorn, S. J.; Rusli, R.; Rowan, S. J.; Foster, E. J.; Weder, C. Bioinspired mechanically adaptive polymer nanocomposites with water-activated shape-memory effect. *Macromolecules* **2011**, *44*, 6827–6835.
309. Luo, H.; Hu, J.; Zhu, Y. Path-dependent and selective multi-shape recovery of a polyurethane/cellulose-whisker nanocomposite. *Mater. Lett.* **2012**, *89*, 172–175.
310. Zhu, Y.; Hu, J.; Luo, H.; Young, R. J.; Deng, L.; Zhang, S.; Fan, Y.; Ye, G. Rapidly switchable water-sensitive shape-memory cellulose/elastomer nano-composites. *Soft Matter* **2012**, *8*, 2509–2517.
311. Alloin, F.; Azizi Samir, M. A. S.; Cavailié, J.-Y.; Dufresne, A.; Paillet, M.; Sanchez, J.-Y. French patent FR0207746, **2002**.
312. Alloin, F.; D'Apréa, A.; Kissi, N. E.; Dufresne, A.; Bossard, F. Nanocomposite polymer electrolyte based on whisker or microfibrils polyoxyethylene nanocomposites. *Electrochim. Acta* **2010**, *55*, 5186–5194.

313. Azizi Samir, M. A. S.; Alloin, F.; Gorecki, W.; Sanchez, J.-Y.; Dufresne, A. Nanocomposite polymer electrolytes based on poly(oxyethylene) and cellulose nanocrystals. *J. Phys. Chem. B* **2004**, *108*, 10845–10852.
314. Lalia, B. S.; Samad, Y. A.; Hashaiekh, R. Nanocrystalline cellulose-reinforced composite mats for lithium-ion batteries: electrochemical and thermomechanical performance. *J. Solid State Electrochem.* **2013**, *17*, 575–581.
315. Azizi Samir, M. A. S.; Chazeau, L.; Alloin, F.; Cavaillé, J.-Y.; Dufresne, A.; Sanchez, J.-Y. POE-based nanocomposite polymer electrolytes reinforced with cellulose whiskers. *Electrochim. Acta* **2005**, *50*, 3897–3903.
316. Azizi Samir, M. A. S.; Alloin, F.; Sanchez, J.-Y.; Dufresne, A. Cross-linked nanocomposite polymer electrolytes reinforced with cellulose whiskers. *Macromolecules* **2004**, *37*, 4839–4844.
317. Azizi Samir, M. A. S.; Mateos, A. M.; Alloin, F.; Sanchez, J.-Y.; Dufresne, A. Plasticized nanocomposite polymer electrolytes based on poly(oxyethylene) and cellulose whiskers. *Electrochim. Acta* **2004**, *49*, 4667–4677.
318. Schroers, M.; Kokil, A.; Weder, C. Solid polymer electrolytes based on nanocomposites of ethylene oxide–epichlorohydrin copolymers and cellulose whiskers. *J. Appl. Polym. Sci.* **2004**, *93*, 2883–2888.
319. Angulakshmi, N.; Thomas, S.; Nahm, K. S.; Stephan, A. M.; Elizabeth, R. N. Electrochemical and mechanical properties of nanochitin-incorporated PVDF-HFP-based polymer electrolytes for lithium batteries. *Ionics* **2011**, *17*, 407–414.
320. Zhou, Y.; Fuentes-Hernandez, C.; Khan, T. M.; Liu, J.-C.; Hsu, J.; Shim, J. W.; Dindar, A.; Youngblood, J. P.; Moon, R. J.; Kippelen, B. Recyclable organic solar cells on cellulose nanocrystal substrates. *Sci. Rep.* **2013**, *3*, 1536 (5 pages).
321. van den Berg, O.; Schroeter, M.; Capadona, J. R.; Weder, C. Nanocomposites based on cellulose whiskers and (semi)conducting conjugated polymers. *J. Mater. Chem.* **2007**, *17*, 2746–2753.
322. Tkalya, E.; Ghislandi, M.; Thielemans, W.; van der Schoot, P.; de With, G.; Koning, C. Cellulose nanowhiskers templating in conductive polymer nanocomposites reduces electrical percolation threshold 5-fold. *ACS Macro Lett.* **2013**, *2*, 157–163.
323. Beck, S.; Bouchard, J.; Berry R. Controlling the reflection wavelength of iridescent solid films of nanocrystalline cellulose. *Biomacromolecules* **2011**, *12*, 167–172.
324. Zhang, Y. P.; Chodavarapu, V. P.; Kirk, A. G.; Andrews, M. P. Nanocrystalline cellulose for covert optical encryption. *J. Nanophotonics* **2012**, *6*, 063516.
325. Shopsowitz, K. E.; Hamad, W. Y.; MacLachlan, M. J. Flexible and iridescent chiral nematic mesoporous organosilica films. *J. Am. Chem. Soc.* **2012**, *134*, 867–870.
326. Shopsowitz, K. E.; Hamad, W. Y.; MacLachlan, M. J. Chiral nematic mesoporous carbon derived from nanocrystalline cellulose. *Angew. Chem. Int. Ed.* **2011**, *50*, 10991–10995.
327. Shopsowitz, K. E.; Kelly, J. A.; Hamad, W. Y.; MacLachlan, M. J. Biopolymer templated glass with a twist: controlling the chirality, porosity, and photonic properties of silica with cellulose nanocrystals. *Adv. Funct. Mater.* **2014**, *24*, 327–338.
328. Kelly, J. A.; Shopsowitz, K. E.; Ahn, J. M.; Hamad, W. Y.; MacLachlan, M. J. Chiral nematic stained glass: controlling the optical properties of nanocrystalline cellulose-templated materials. *Langmuir* **2012**, *28*, 17256–17262.

329. Kelly, J. A.; Shukaliak, A. M.; Cheung, C. C. Y.; Shopsowitz, K. E.; Hamad, W. Y.; MacLachlan, M. J. Responsive photonic hydrogels based on nanocrystalline cellulose. *Angew. Chem. Int. Ed.* **2013**, *52*, 8912–8916.
330. Picard, G.; Simon, D.; Kadiri, Y.; LeBreux, J. D.; Ghozayel, F. Cellulose nanocrystal iridescence: a new model. *Langmuir* **2012**, *28*, 14799–14807.
331. Jackson, J. K.; Letchford, K.; Wasserman, B. Z.; Ye, L.; hamad, W. Y.; Burt, H. M. The use of nanocrystalline cellulose for the binding and controlled release of drugs. *Int. J. Nanomed.* **2011**, *6*, 321–330.
332. Villanova, J. C. O.; Ayres, E.; Carvalho, S. M.; Patrício, P. S.; Pereira, F. V.; Oréface, R. L. Pharmaceutical acrylic beads obtained by suspension polymerization containing cellulose nanowhiskers as excipient for drug delivery. *Eur. J. Pharm. Sci.* **2011**, *42*, 406–415.
333. Lin, N.; Huang, J.; Chang, P. R.; Feng, L.; Yu, J. Effect of polysaccharide nanocrystals on structure, properties, and drug release kinetics of alginate-based microspheres. *Colloid. Surface. B* **2011**, *85*, 270–279.
334. Wang, Y.; Chen, L. Impacts of nanowhisiker on formation kinetics and properties of all-cellulose composite gels. *Carbohydr. Polym.* **2011**, *83*, 1937–1946.
335. Varjonen, S.; Laaksonen, P.; Paananen, A.; Valo, H.; Hähl, H.; Laaksonen, T.; Linder, M. B. Self-assembly of cellulose nanofibrils by genetically engineered fusion proteins. *Soft Matter* **2011**, *7*, 2402–2411.
336. Minellia, M.; Baschettia, M. G.; Doghiera, F.; Ankerforsb, M.; Lindströmb, T.; Siróc, I.; Plackett, D. Investigation of mass transport properties of microfibrillated cellulose (MFC) films. *J. Membrane Sci.* **2010**, *358*, 67–75.
337. Xiang, C.; Taylor, A. G.; Hinestroza, J. P.; Frey, M. W. Controlled release of nonionic compounds from poly(lactic acid)/cellulose nanocrystal nanocomposite fibers. *J. Appl. Polym. Sci.* **2013**, *127*, 79–86.
338. Kaboorani, A.; Riedl, B.; Blanchet, P.; Fellin, M.; Hosseinaei, O.; Wang, S. Nanocrystalline cellulose (NCC): A renewable nano-material for polyvinyl acetate (PVA) adhesive. *Eur. Polym. J.* **2012**, *48*, 1829–1837.

CHAPTER 2.

Property of Cellulose Nanocrystals: Surface Sulfate Groups

“Surface Chemistry, Morphological Analysis and Properties of Cellulose Nanocrystals with Graded Sulfation Degrees”

Chapter 2. Surface Chemistry, Morphological Analysis and Properties of Cellulose Nanocrystals with Graded Sulfation Degrees

ENGLISH ABSTRACT	114
RESUME FRANÇAIS	117
2.1 Introduction	123
2.2 Experimental Methodology	126
2.2.1 Materials.....	126
2.2.2 Extraction of Cellulose Nanocrystals via Sulfuric Acid Hydrolysis	126
2.2.3 Surface Postsulfation of H ₂ SO ₄ -hydrolyzed Cellulose Nanocrystals.....	126
2.2.4 Surface Desulfation of H ₂ SO ₄ -hydrolyzed Cellulose Nanocrystals.....	127
2.2.5 Characterization and Analyses	127
2.3 Spectroscopic Proofs for Gradient Sulfation of Cellulose Nanocrystals	130
2.3.1 Fourier Transform Infrared Spectroscopy (FTIR).....	130
2.3.2 X-ray photoelectron spectroscopy (XPS).....	132
2.4 Morphological Observation and Dimensions	134
2.5 Morphological Models and Surface Chemistry of Cellulose Nanocrystals	137
2.6 Effect of Sulfate Groups on the Properties of Cellulose Nanocrystals	142
2.6.1 Crystalline Structure and Crystalline Dimensions	143
2.6.2 ζ -potential of Aqueous Suspensions	145
2.6.3 Thermal Stability.....	145
2.6.4 Birefringence of Aqueous Suspensions	147
2.7 Conclusions	148
2.8 References	148

ENGLISH ABSTRACT

Typical procedure currently employed for the extraction of cellulose nanocrystals consists of subjecting pure cellulosic material to strong acid hydrolysis under strictly controlled conditions of temperature, agitation, and duration. The nature of the acid is extremely important for the surface properties of prepared cellulose nanocrystals. Sulfuric acid is the most extensively used acid for the production of cellulose nanocrystals; and in most commonly reported protocol, the hydrolyzing conditions include ca. 65 wt% H₂SO₄–concentration with ratios of acid to cellulose of 8.75–17.5 mL/g as well as temperature of 45 °C for 30–90 min. When sulfuric acid is used as hydrolyzing agent, sulfation of cellulose nanocrystals occurs during the course of H₂SO₄–catalyzed hydrolysis through the esterification reaction between surface hydroxyl groups borne by cellulose nanoparticles and H₂SO₄ molecules. This process provides charged surfaces bearing sulfate esters ($-OSO_3^-$) and releases sulfated cellulose nanocrystals.

It is commonly regarded that the esterification level of cellulose nanocrystals, viz. sulfate group contents, depends highly on several factors, such as hydrolysis duration, temperature, and H₂SO₄ concentration. Therefore, sulfate group contents on cellulose nanocrystals should increase with acid concentration, acid-to-cellulose ratio, and hydrolysis duration,¹ because of the durative aspect of the esterification reaction. However, there is also report on the minor effect of H₂SO₄–hydrolysis conditions to the surface charge and sulfur content of cellulose nanocrystal, which gave the contrary conclusion of “sulfur content of the cellulose may be controlled by factors other than hydrolysis conditions.”² Inconsistent results from different studies indicate that it is not so easy to precisely control or determine the amount of sulfate groups on cellulose nanocrystals. For the prepared cellulose nanocrystals, regardless the surface sulfate group content, removal or addition of sulfate groups can be achieved by different post-treatment methods, such as desulfation and postsulfation. For the former treatment, solvolytic desulfation (with pyridine),³ acid desulfation (with HCl)⁴ and alkaline desulfation (with NaOH)⁵ have been reported to remove (or “wash”)

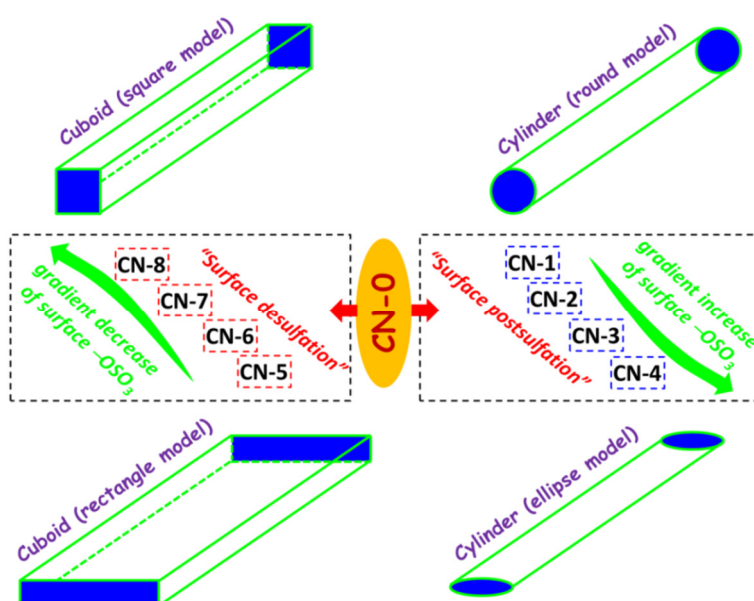
most of sulfate groups from the surface of cellulose nanocrystals. To introduce additional sulfate esters, postsulfation with H_2SO_4 solution of cellulose nanocrystals is commonly performed,⁶ but the degree of postsulfation of the nanocrystals should be carefully controlled (no destruction of the crystalline structure).

The presence of sulfate groups on the surface of cellulose nanocrystals is expected to significantly affect various properties of nanocrystals. The most promising influence of sulfate groups to cellulose nanocrystals is the promotion of nanoparticle dispersion in water derived from the electrostatic repulsion, which induces the desired formation of stable colloidal suspensions of cellulose nanocrystals. Meanwhile, the introduction of charged sulfate esters makes the formation of negative layer covering nanocrystals, which can be used for electrostatic adsorption or layer-by-layer assembly. It is widely reported that sulfate groups cause a sharp decrease in degradation temperature for cellulose nanocrystals even at low levels.¹ However, a recent study reported a slight increase of the degradation temperature for higher levels of sulfated cellulose nanocrystals.⁷ Another influence of sulfate groups is the transformation of rheological properties of cellulose nanocrystal suspensions, including the change of viscosity,⁸ and transitions from isotropic to liquid crystal and liquid crystal to gel.⁹ Recently, a study further revealed an interesting effect of surface sulfate groups on cellulose nanocrystals to material adhesion. It was reported that cellulose nanocrystals bearing sulfate groups yielded adhesion strength to PDMA gel materials, whereas HCl-hydrolyzed cellulose nanocrystals bearing only hydroxyl groups were useless as a glue.¹⁰

In fact, direct influence of sulfate groups to cellulose nanocrystals is the change of surface chemistry, viz. the reduction of available hydroxyl groups. Especially for studies intending to subsequent chemical modification, the issue of accurate content of hydroxyl and sulfate groups (surface degree of substitution of available or total hydroxyl groups to sulfate groups) is necessary and important. It should be pointed out that the determination of the surface $-\text{OSO}_3^-$ degree of substitution is on the basis of dimension measurement and specific surface area analysis of cellulose

nanocrystals. Different characterization techniques can offer distinct results for the dimensions of cellulose nanocrystals (such as AFM and TEM). Moreover, with different methods and experiments for the calculation, the data for specific surface area of cellulose nanocrystals are dramatically varied, such as reported values of 22.9 m²/g,¹¹ 170 m²/g,¹² and 533 m²/g.¹³ Despite the fact that several studies attempted to calculate the proportion of sulfate and hydroxyl groups on the surface of cellulose nanocrystals after H₂SO₄ hydrolysis, inconsistent conclusions were provided due to the reasons mentioned before.^{11,14} The study introduced in this chapter is a new attempt to analyze the effect of sulfate groups to surface chemistry, and physical properties of cellulose nanocrystals according to theoretical calculations. As shown in the schematic diagram, two series of cellulose nanocrystal samples (postsulfated and desulfated nanocrystals) behaving gradient degrees of sulfate groups were prepared through the regulation of reactant ratios and reactive conditions. Through the comparison of four cross-section models (square, round, rectangle, ellipse), different effects of sulfate groups to surface chemistry and physical properties (crystallinity, zeta-potential, thermal stability, and birefringence behavior) of cellulose nanocrystals were further discussed and validated.

Schematic diagram for the preparation of cellulose nanocrystals with gradient sulfation degrees, and surface chemistry affected by different cross-section models.



RESUME FRANÇAIS

La méthode classique actuellement employée pour l'extraction de nanocristaux de cellulose consiste à soumettre un matériau cellulosique pur à une hydrolyse acide forte dans des conditions strictement contrôlées de température, d'agitation et de durée. La nature de l'acide est extrêmement importante pour les propriétés de surface des nanocristaux de cellulose ainsi préparés. L'acide sulfurique est l'acide le plus largement utilisé pour la production de nanocristaux de cellulose; et le protocole le plus fréquemment mentionné implique les conditions d'hydrolyse suivantes : environ 65% en poids de H_2SO_4 , avec des rapports acide/cellulose de 8,75 à 17,5 ml/g, ainsi qu'une température de 45 °C et une durée d'hydrolyse de 30 à 90 min. Lorsque l'acide sulfurique est utilisé comme agent d'hydrolyse, une sulfatation des nanocristaux de cellulose se produit au cours du traitement d'hydrolyse catalysé par H_2SO_4 à travers une réaction d'estérification entre les groupements hydroxyles de surface portés par les nanoparticules de cellulose et les molécules de H_2SO_4 . Ce processus produit des surfaces chargées portant des esters de sulfate ($-OSO_3^-$) et la libération de nanocristaux de cellulose sulfatés.

On considère généralement que le degré d'estérification des nanocristaux de cellulose, à savoir le taux de groupements sulfate, est fortement lié à plusieurs facteurs, tels que la durée d'hydrolyse, la température et la concentration en H_2SO_4 . Par conséquent, le taux de groupements sulfate sur les nanocristaux de cellulose devrait augmenter avec la concentration de l'acide, le rapport acide/cellulose et la durée de l'hydrolyse,¹ en raison de l'aspect duratif de la réaction d'estérification. Cependant, certaines études montrent l'effet limité des conditions d'hydrolyse avec H_2SO_4 sur la charge de surface et la teneur en soufre des nanocristaux de cellulose, ce qui conduit à la conclusion contraire que "la teneur en soufre de la cellulose peut être contrôlée par des facteurs autres que les conditions d'hydrolyse".² Ces résultats contradictoires émanant de différentes études indiquent qu'il n'est pas si facile de contrôler avec précision ou de déterminer la quantité de groupements sulfates des nanocristaux de cellulose. Pour les nanocristaux de cellulose ainsi préparés, quelle

que soit la teneur en groupements sulfates de surface, la suppression ou l'addition de groupements sulfates peuvent être obtenus par différentes méthodes de post-traitement, telles que la désulfatation et la postsulfation. Pour le premier traitement, il a été montré que la désulfatation solvolytique (avec de la pyridine),³ la désulfatation acide (HCl)⁴ et la désulfatation alcaline (avec NaOH)⁵ permettait d'éliminer (ou de "laver") la plupart des groupements sulfates de la surface des nanocristaux de cellulose. Pour introduire des sulfates d'ester supplémentaires, la postsulfation avec une solution de H₂SO₄ des nanocristaux de cellulose est couramment réalisée,⁶ mais le degré de postsulfation des nanocristaux doit être contrôlé avec soin (pour éviter la destruction de la structure cristalline).

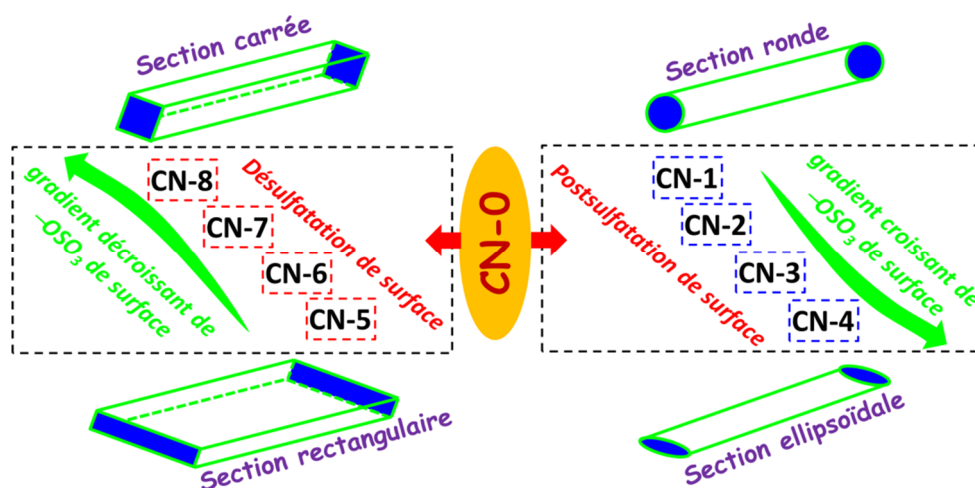
On peut s'attendre à ce que la présence de groupements sulfates à la surface des nanocristaux de cellulose affecte de manière significative différentes propriétés des nanocristaux. L'influence la plus intéressante des groupements sulfates sur les nanocristaux de cellulose est de promouvoir leur dispersion dans l'eau directement liée à la répulsion électrostatique, ce qui induit la formation souhaitable de suspensions colloïdales stables de nanocristaux de cellulose. Par ailleurs, l'introduction d'esters de sulfate chargés permet la formation d'une enveloppe négative autour des nanocristaux, qui peut être utilisée pour l'adsorption électrostatique ou assemblage couche par couche. Il est bien connu que les groupements sulfates provoquent une forte diminution de la température de dégradation des nanocristaux de cellulose, même à faible taux.¹ Cependant, une étude récente a montré une légère augmentation de la température de dégradation pour des niveaux plus élevés de nanocristaux de cellulose sulfatés.⁷ Un autre effet des groupements sulfates est l'altération des propriétés rhéologiques des suspensions de nanocristaux de cellulose, incluant notamment le changement de viscosité,⁸ et les transitions isotrope à cristal liquide et cristal liquide à gel.⁹ Récemment, une étude a révélé en outre un effet intéressant des groupements sulfates de surface des nanocristaux de cellulose en termes d'adhérence. Il a été montré que les nanocristaux de cellulose portant des groupements sulfates

permettent une forte adhérence à des matériaux tels que des gels de PDMA , alors que les nanocristaux de cellulose hydrolysés par HCl portant seulement des groupements hydroxyles se sont avérés inutilisables comme colle.¹⁰

En fait, l'influence directe des groupements sulfates sur les nanocristaux de cellulose est l'altération de la chimie de surface, à savoir la réduction des groupements hydroxyles disponibles. Notamment, pour les études impliquant une modification chimique ultérieure, la question de la teneur exacte en groupements hydroxyles et sulfates (degré de substitution surfacique des groupements hydroxyles totaux ou disponibles par des groupements sulfates) est nécessaire et importante. Il convient de souligner que la détermination du degré de substitution des $-OSO_3^-$ de surface est basée sur la mesure de la dimension et de l'analyse de surface spécifique des nanocristaux de cellulose. Des techniques de caractérisation différentes peuvent conduire à des résultats distincts pour les dimensions des nanocristaux de cellulose (par exemple AFM et TEM). De plus, avec ces différentes méthodes et techniques de calcul, les données de surface spécifique des nanocristaux de cellulose peuvent varier considérablement, et des valeurs telles que 22,9 m²/g,¹¹ 170 m²/g,¹² et 533 m²/g¹³ ont été reportées. Bien que plusieurs études aient tenté de calculer les proportions de groupements sulfates et hydroxyles à la surface des nanocristaux de cellulose après hydrolyse à H₂SO₄, des conclusions contradictoires ont été reportées pour les raisons mentionnées auparavant.^{11,14} L'étude présentée dans ce chapitre est une nouvelle tentative d'analyse de l'influence des groupements sulfates sur la chimie de surface des nanocristaux de cellulose et leurs propriétés physiques selon des calculs théoriques. Comme le montre le "schéma de principe", deux séries d'échantillons de nanocristaux de cellulose (nanocristaux postsulfatés et désulfatés) présentant des gradients de degré de groupements sulfates ont été préparés en régulant les rapports des réactifs et les conditions de réaction. En comparant quatre modèles pour la section (carré, rond, rectangle, ellipse), les différents effets des groupements sulfates sur la chimie de surface et les propriétés physiques

(cristallinité, potentiel zêta, stabilité thermique et biréfringence) des nanocristaux de cellulose sont en outre discutés et validés.

Schéma de principe de la préparation des nanocristaux de cellulose avec un gradient de degré de sulfatation et chimie de surface en fonction des différents modèles de section transversale.



References:

1. Roman, M.; Winter, W. T. Effect of sulfate groups from sulfuric acid hydrolysis on the thermal degradation behavior of bacterial cellulose. *Biomacromolecules* **2004**, *5*, 1671–1677.
2. Beck-Candanedo, S.; Roman, M.; Gray, D. G. Effect of reaction conditions on the properties and behavior of wood cellulose nanocrystal suspensions. *Biomacromolecules* **2005**, *6*, 1048–1054.
3. Jiang, F.; Esker, A. R.; Roman, M. Acid-catalyzed and solvolytic desulfation of H₂SO₄-hydrolyzed cellulose nanocrystals. *Langmuir* **2010**, *26*, 17919–17925.
4. Kalashnikova, I.; Bizot, H.; Cathala, B.; Capron, I. Modulation of cellulose nanocrystals amphiphilic properties to stabilize oil/water interface. *Biomacromolecules* **2012**, *13*, 267–275.
5. Kloser, E.; Gray, D. G. Surface grafting of cellulose nanocrystals with poly(ethylene oxide) in aqueous media. *Langmuir* **2010**, *26*, 13450–13456.

6. Araki, J.; Wada, M.; Kuga, S.; Okano, T. Birefringent glassy phase of a cellulose microcrystal suspension. *Langmuir* **2000**, *16*, 2413–2415.
7. Voronova, M. I.; Surov, O. V.; Zakharov, A. G. Nanocrystalline cellulose with various contents of sulfate groups. *Carbohydr. Polym.* **2013**, *98*, 465–469.
8. Araki, J.; Wada, M.; Kuga, S. Influence of surface charge on viscosity behavior of cellulose microcrystal suspension. *J. Wood. Sci.* **1999**, *45*, 258–261.
9. Shafiei-Sabet, S.; Hamad, W. Y.; Hatzikiriakos, S. G. Influence of degree of sulfation on the rheology of cellulose nanocrystal suspensions. *Rheol. Acta.* **2013**, *52*, 741–751.
10. Rose, S.; PrevotEAU, A.; Elzière, P.; Hourdet, D.; Marcellan, A.; Leibler, L. Nanoparticle solutions as adhesives for gels and biological tissues. *Nature* **2014**, *505*, 382–385.
11. Gu, J.; Catchmark, J. M.; Kaiser, E. Q.; Archibald, D. D. Quantification of cellulose nanowhiskers sulfate esterification levels. *Carbohydr. Polym.* **2013**, *92*, 1809–1816.
12. Dufresne, A. Dynamic mechanical analysis of the interphase in bacterial polyester/cellulose whiskers natural composites. *Compos. Interfaces* **2000**, *7*, 53–67.
13. Siqueira, G.; Bras, J.; Dufresne, A. New process of chemical grafting of cellulose nanoparticles with a long chain isocyanate. *Langmuir* **2010**, *26*, 402–411.
14. Abitbol, T.; Kloser, E.; Gray, D. G. Estimation of the surface sulfur content of cellulose nanocrystals prepared by sulfuric acid hydrolysis. *Cellulose* **2013**, *20*, 785–794.

The work in this chapter is originated from:

Ning Lin and Alain Dufresne, Surface chemistry, morphological analysis and properties of cellulose nanocrystals with graded sulfation degrees. Nanoscale 2014, 6, 5384–5393.

Chapter 2. Surface Chemistry, Morphological Analysis and Properties of Cellulose Nanocrystals with Graded Sulfation Degrees

Ning Lin and Alain Dufresne

Grenoble Institute of Technology (Grenoble INP), The International School of Paper, Print Media and Biomaterials (Pagora), CS10065, 38402 Saint Martin d'Hères Cedex, France

ABSTRACT

The process of sulfuric acid-hydrolysis of cellulose fibers for the preparation of cellulose nanocrystals (CNs) includes an esterification reaction between acid and cellulose molecules, which induce the covalent coupling of sulfate groups on the surface of prepared CNs. Negatively charged sulfate groups play an important role in both surface chemistry and physical properties of CNs. This study explored the strategy of introducing a gradient of sulfate groups on the surface of CNs, and further investigated the effect of the degree of sulfation on surface chemistry, morphology and dimension, and physical properties of different CN samples. Based on the discussion of its surface chemistry, the selection of different cross-section models was reported to significantly affect the calculation of the degree of substitution of sulfate groups on CNs. A new ellipse cross-section model was proposed on the basis of AFM observation. The effect of sulfate groups on crystal properties and thermal stability was discussed and validated, and birefringence behavior of nanocrystal suspensions was observed.

KEYWORDS

Cellulose Nanocrystals, Gradient Sulfation, Surface Chemistry, Morphological Analysis, Physical Property

2.1 Introduction

Despite being the most available natural polymer on earth, it is only quite recently that cellulose has gained prominence as a nanostructured material, in the form of cellulose nanocrystals (CNs) and nanofibrillated cellulose (NFC).¹ Cellulose nanocrystal is being developed for use over a broad range of applications, even if a high number of unknowns remain at date. After intensive studies, it was shown that the potential of CN focused on its mechanical properties as nano-reinforcing phase and advanced functional applications based on its special properties. The sound markets impacted by CNs include composites, electronics (flexible circuits), energy (flexible battery, such as Li-ion battery and solar panels), packaging, coatings, detergents, adhesives, construction, pulp and paper, inks and printing, filtration, medicine and life science (scaffolds in tissue engineering, artificial skin and cartilage, wound healing, and vessel substitutes), optical devices (including reflective properties for security papers and UV or IR reflective barriers), rheological modifiers, and cosmetics.^{1,2} Properties of CNs, related materials, and potential foreshadowed applications have been extensively reviewed, and some recent review articles include preparation technologies,³ properties,⁴ nanocomposites,^{5,6} and functional materials.⁷⁻⁹

Common preparation of CN consists in an acid-induced destructuring process, during which the heterogeneous acid hydrolysis involves the diffusion of acid molecules into cellulose fibers, and following cleavage of glycosidic bonds. Different strong acids have been shown to successfully degrade non-crystalline (amorphous) regions of cellulose fibers to release crystalline cellulosic nanoparticles, such as sulfuric, hydrochloric, phosphoric, hydrobromic, nitric acids, and a mixture composed of hydrochloric and organic acids.¹⁰ Nevertheless, the hydrolysis treatment with sulfuric acid to prepare CNs has been extensively investigated and appears to be the most effective method. One of the main reason for using sulfuric acid as a hydrolyzing agent is that if CNs are prepared using hydrochloric acid, their ability to disperse in solvents is limited and the suspension is unstable tending to flocculate. Indeed, during hydrolysis, sulfuric acid reacts with the surface hydroxyl groups via an esterification

process allowing the grafting of anionic sulfate ester groups ($-OSO_3^-$).¹¹ These sulfate groups are randomly distributed on the surface of the cellulosic nanoparticle. The presence of these negatively charged sulfate ester groups induces the formation of a negative electrostatic layer covering the surface of nanocrystals and promotes their dispersion in solvents. The high stability of sulfuric acid-hydrolyzed CNs results therefore from an electrostatic repulsion between individual nanoparticles.

Besides the promotion of high stability of nanocrystals in solvents, surface $-OSO_3^-$ groups with negative charges also provide CNs the accessibility for diverse functional applications via electrostatic adsorption, such as layer-by-layer (LBL) assembling nanomaterials from anionic nanocrystals and cationic matrix;^{12,13} electrochemical nanocomposites with the process of electrochemical co-deposition;¹⁴ microfiltration membrane with high adsorption capacity against positively charged dye;¹⁵ permselective membranes from exclusion or adsorption for different charged molecules;¹⁶ and electrostatic adsorption of enzymes (cellulase) upon enzymatic hydrolysis of substrates.¹⁷ Recently, it was reported that surface sulfate groups and charge density of CNs even play a significant role in the control of water/oil interface for emulsion stability.¹⁸

The objectives of this study are to discuss the surface chemistry of sulfated cellulose nanocrystals, and further investigate the morphology and properties of nanocrystals with different contents of sulfate groups. Using postsulfation and desulfation treatments, a series of CNs (nine) samples behaving gradient degrees of sulfate groups were prepared through the regulation of reactant ratios and reactive conditions. Chlorosulfonic acid was used as sulfating agent for the postsulfation of CNs, which can provide higher levels of surface sulfation, and avoid the drawbacks of deep degradation of nanocrystals induced by strong sulfuric acid. Figure 2.1 shows the strategy and mechanism of introducing gradient sulfate groups on the surface of CNs. In addition, surface chemistry analysis for sulfated CN is a significant research point because of its crucial influence to subsequent surface modifications, especially the determination of the surface degree of substitution (*DS*) of diverse grafted groups or

molecules on nanocrystals. Several studies reported different DS values ranging from 1/10 to 1/3 or 1/2 of free hydroxyl groups replaced by sulfate groups for 65 wt% H_2SO_4 -hydrolyzed CNs.^{19,20} In this study, based on the comparison of four cross-section models (square, round, rectangle, ellipse), different effects to surface chemistry of CNs were analyzed and discussed. Moreover, surface sulfate groups should significantly affect physical properties of CNs or their suspensions, such as crystal properties, zeta-potential, thermal properties, and birefringence behavior. It should be noted that despite that some studies have reported the influence of the degree of sulfation on the thermal degradation of CNs, inconsistent conclusions were provided. For instance, in an earlier study, it was believed that the sulfate groups borne by CNs caused a significant decrease in degradation temperature, even at low levels.²¹ However, a recent study reported a slight increase of the degradation temperature for higher levels of sulfated groups on CNs.²² In this study, besides the thermal degradation, various effects of sulfate groups to the physical properties of CNs will be further investigated and validated.

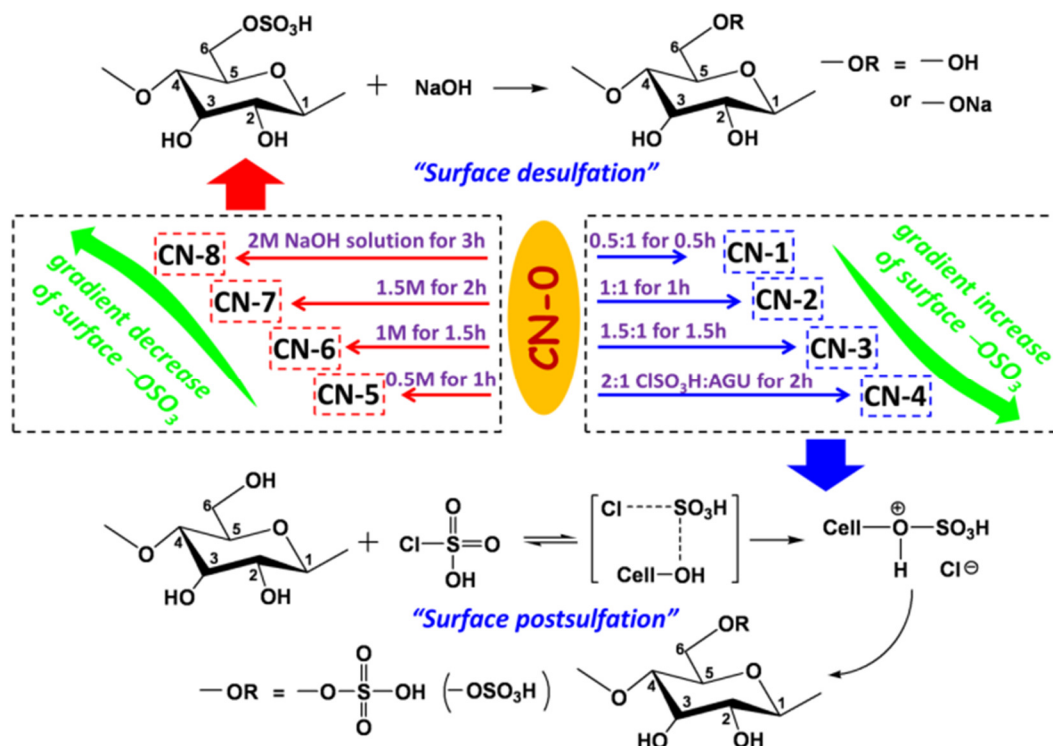


Figure 2.1 Strategy of gradient introducing sulfate groups on the surface of H_2SO_4 -hydrolyzed cellulose nanocrystals.

2.2 Experimental Methodology

2.2.1 Materials

Native cotton fibers were obtained from Whatman filter paper. Sulfuric acid (H_2SO_4 , 98%), chlorosulfonic acid (ClSO_3H), dimethylformamide (DMF), sodium hydroxide (NaOH) and other reagents were purchased from Sigma–Aldrich, and used without further treatment.

2.2.2 Extraction of Cellulose Nanocrystals via Sulfuric Acid Hydrolysis

Cellulose nanocrystals (CNs) were prepared by H_2SO_4 hydrolysis of native cotton fiber, according to our previous protocol.²³ Cotton fiber was milled with a laboratory milling device to obtain a fine particulate substance. Acid hydrolysis was performed at 45 °C with 65 wt% H_2SO_4 (preheated) for 60 min under mechanical stirring (25.0 g fibers for 500 mL solution). The suspension was diluted with ice cubes to stop the reaction and washed until neutrality by successive centrifugations at 10,000 rpm (rotation per minute) for 10 min each step and dialyzed against distilled water for three days. Upon exhaustive dialysis treatment, free acid molecules were removed. CN suspension was dispersed by ultrasonic treatment using a Branson sonifier for three 5-min cycles (with cooling as necessary to prevent overheating). Finally, the released CN powder was obtained by freeze-drying.

2.2.3 Surface Postsulfation of H_2SO_4 -hydrolyzed Cellulose Nanocrystals

Surface postsulfation was realized using chlorosulfonic acid (ClSO_3H) as sulfation agent to obtain sulfated cellulose with different degrees of substitution.^{24,25} About 3.0 g freeze-dried CN, with 18.53 mmol equivalent anhydroglucose unit (AGU), was suspended in 100 mL anhydrous DMF and ultrasonically dispersed with a Branson Sonifier for 5 min. The sulfation agent, a complex mixture of ClSO_3H and DMF, was prepared by slowly adding ClSO_3H into 50 mL anhydrous DMF with constant stirring and cooling in ice bath. (**Caution!** Chlorosulfonic acid is a strong corrosive and volatile chemical; thus, the mixing treatment should be handled in the fume hood with precaution and proper safety protection.) Sulfation of CN was initiated by gradually

adding ClSO_3H into the prepared nanocrystal suspension, with the regulation of reactant ratios between ClSO_3H and AGU ranging from 0.5 to 2.0 mol/mol, keeping vigorous stirring for 0.5–2.0 h at room temperature. The reaction was terminated by adding ethanol. The suspension was washed with anhydrous alcohol and exchanged to water, centrifuged and dialyzed against deionized water for three days. Finally, the products of sulfated CNs were obtained by freeze-drying treatment.

2.2.4 Surface Desulfation of H_2SO_4 -hydrolyzed Cellulose Nanocrystals

It was reported that two different treatments can be performed for the desulfation of CNs, viz. solvolytic desulfation,²⁶ and alkaline desulfation.^{27,28} In order to realize the desulfation gradient, alkaline (NaOH) desulfation approach was used to remove surface sulfate groups on CNs in this work. Different concentrations of alkaline solution (ranging from 0.5 to 2.0 mol/L) were added to the CN aqueous suspension, with the control of maximum alkaline concentration at 2 mol/L. In a typical procedure, 100 mL aqueous CN suspension (resulting CN concentration about 2 wt%) was mixed with 50 mL NaOH solution with given concentration, and the mixture was stirred at 60 °C for 1–3 h. During the reaction, cellulose nanoparticles in suspension gradually aggregated and settled in the bottom because of the removal of surface sulfate groups. With centrifugation and dialysis treatments, the obtained suspension was purified, and finally the desulfated CN powder was prepared by freeze-drying treatment.

On the basis of postsulfation and desulfation experiments, CN samples possessing different contents of surface sulfate groups were named as CN-(0 to 8), as shown in the strategy depicted in Figure 1. In here, CN-0 represents the initial CN product hydrolyzed from 65 wt% sulfuric acid without further modification; CN-(1 to 4) are the further sulfated nanocrystals, and CN-(5 to 8) are desulfated nanocrystals obtained with different reactant ratios and reaction durations.

2.2.5 Characterization and Analyses

Fourier Transform Infrared Spectroscopy (FTIR): Infrared spectra were recorded at room temperature on a FTIR Perkin-Elmer Spectrum One spectrometer to

characterize the surface postsulfation and desulfation of CNs. All freeze-dried samples were prepared as KBr pellets (1 wt% CN powder in anhydrous KBr), and analyzed using a spectral width ranging from 4000 to 400 cm^{-1} with a 2 cm^{-1} resolution and an accumulation of 32 scans.

X-ray Photoelectron Spectroscopy (XPS): Surface postsulfation and desulfation of CNs (samples CN-0; CN-4; CN-8) were further analyzed by XPS following the signal of sulfur element (S) and sodium element (Na). The S/C and Na/C content ratios were calculated according to Eq. (2.1) from the XPS results. The experiments were carried out using an XR3E2 apparatus (Vacuum Generators, U.K.) equipped with an unmonochromated Mg KR X-ray source (1253.6 eV) and operated at 15 kV under a current of 20 mA. Samples were prepared as pastilles (10 mm diameter) and characterized in an ultrahigh vacuum chamber (10^{-8} mbar) with electron collection by a hemispherical analyzer at a 90° angle.

$$S/C = \frac{A_S}{N_S} \times \frac{N_C}{A_C} \quad (2.1)$$

Elemental Analysis: Elemental analysis was used to determine the total content of sulfur element in CN samples, and was performed at Analysis Central Service of the Centre National de la Recherche Scientifique (Vernaison, France). Before analysis, freeze-dried samples were further treated under vacuum at room temperature for 8 h. The sulfur, carbon, and oxygen element contents were measured for postsulfated and desulfated CNs.

Morphology and Dimensions: The morphology of CN samples was observed using atomic force microscopy (AFM). Suspensions of approximately 0.01 wt% nanocrystals were dispersed in water with ultrasonic dispersion for 30 min and then deposited on the mica substrate. The substrate loaded with nanoparticles was imaged in tapping mode with a Nanoscope IIIa microscope from Veeco Instruments. Silicon cantilevers were used to perform the imaging at a frequency of 264–339 kHz and a typical radius of curvature of 10–15 nm. The CN dimensions, including length (L), width (W), and height (H), were measured by Nanoscope software. Over 100 rod-like

nanocrystals were statistically analyzed to determine the average length, width, height and distribution.

Surface Charge: The ζ -potential of CNs in water (0.01 wt%) was determined by a zeta-meter (Zetasizer DTS0230 Malvern Instruments). The instrument measures electrophoretic light scattering of a 35 mW solid state laser beam at a 660 nm wavelength, and all reported values were an average of 5 measurements with confidence intervals of 95%.

Crystal Properties: The crystallinity index and crystalline dimensions in different planes of CNs were measured by X-ray diffraction analysis, in order to investigate the effect of surface sulfate groups to crystalline properties. The X-ray diffraction patterns were recorded on a Philips PW 1720 X-ray generator operated at 45 kV and 40 mA with Cu K α radiation ($\lambda = 0.154$ nm) in the range $2\theta = 5\text{--}50^\circ$ for samples using a fixed time mode with a step interval of 0.066° . The crystallinity index (χ_c) of native cotton and CN was calculated according to Segal equation:

$$\chi_c = \frac{I_{200} - I_{am}}{I_{200}} \times 100\% \quad (2.2)$$

In Eq. (2.2), I_{200} is the overall intensity of the peak at 2θ about 22.7° , and I_{am} represents the intensity of the baseline at 2θ about 18.0° .

Crystalline dimensions of different planes for CNs samples were calculated according to Scherrer equation:

$$B_{hkl} = \frac{0.9\lambda}{\beta_{1/2}\cos\theta} \quad (2.3)$$

In Eq. (2.3), B_{hkl} is the average crystalline width of a specific plane; λ represents the wavelength of incident X-rays ($\lambda = 0.15418$ nm); θ is the center of the peak; and $\beta_{1/2}$ (in radius) represents the full width at half maximum (FWHM) of the reflection peak.

Thermal Degradation: To investigate the effect of sulfate groups with different degrees of substitution on the thermal stability of CNs and native cotton, thermogravimetric analysis (TGA) was performed using a thermal analyzer

Perkin-Elmer TGA-6 under air flow. Samples of ca. 10 mg were heated from 20 to 600 °C at a heating rate of 10 °C/min.

Birefringence Behavior of Suspensions: The suspension of lyophilized CNs was transferred to a 5 mL glass vial, and ultrasonicated for 30 min. The concentration of nanocrystals in suspension was controlled as about 0.5 wt%, which was used to observe the dispersion and birefringence between two crossed polarizers due to macroscopic anisotropy of rod-like nanoparticles. The presence of birefringence was used as the criterion of good dispersability or somewhat aggregation for nanoparticles in aqueous suspensions.²⁹

2.3 Spectroscopy Proofs for Gradient Sulfation of Cellulose Nanocrystals

2.3.1 Fourier Transform Infrared Spectroscopy (FTIR)

The main challenge for the chemical functionalization of cellulose nanocrystals (CNs) is to conduct a reaction taking place on the surface of nanocrystals, while preserving the original morphology and structure to avoid any polymorphic conversion and to maintain the integrity of the crystal.¹⁰ In this study, to realize the further surface sulfation of CNs, the duration and reactant ratio between sulfated agent and CN (ClSO₃H:AGU) are critical conditions. The addition of ClSO₃H was regulated as 0.5, 1.0, 1.5 or maximum 2.0 ratios according to the AGU of cellulose, and the reactions were performed for 0.5, 1.0, 1.5 and 2.0 h, respectively. Under these conditions, the desired achievement of sufficient substitution of hydroxyl groups to sulfated groups and preservation of original crystalline structure and geometrical morphology of nanocrystals can be realized, which will be proved by following characterizations and results. In fact, higher reaction ratios (such as 4:1 for ClSO₃H:AGU) or longer durations (such as 6.0 h) were also attempted in our experiments. However, under these conditions, the turbid suspensions containing nanocrystals was converted to a translucent solution, and a very small amount of gray particles after centrifugation was recovered. It indicated that under high sulfated agent concentrations and

excessive sulfation reactions, the crystalline and chemical structures of CNs may be seriously destroyed and degraded as monosaccharide, and even induced carbonization. On the other hand, for the desulfation reaction the alkaline content should be carefully controlled in order to avoid the transformation of cellulose type I to type II. In our experiments, the surface sulfated moieties are removed under mild alkaline (NaOH) conditions, that is maximum concentration of alkaline was only 2 mol/L (≤ 8 wt%). The yields of postsulfated and desulfated nanocrystals are shown in Table 2.1, which are in the range of 75–87 wt%.

Table 2.1 Yields of modified CN samples after surface postsulfation and desulfation treatments; sulfur content %S (expressed as elemental sulfur by weight content) measured by elemental analysis; surface hydroxyl group ($-\text{OH}$) and sulfate group ($-\text{OSO}_3^-$), contents, and degree of substitution (DS) for various CN samples.

Samples	Yield	Elemental analysis			Surface $-\text{OH}$	Surface $-\text{OSO}_3^-$	$DS_{-\text{OSO}_3^-}$
	%	%S	%C	%O	mmol/g	mmol/g	%
CN-0	—	0.67	42.31	50.75		0.21	13.45
CN-1	86.21	0.77	42.21	50.64		0.24	15.51
CN-2	83.45	0.91	42.25	50.29		0.28	18.28
CN-3	82.76	1.09	42.16	50.40		0.34	21.94
CN-4	79.31	1.31	40.72	50.25	1.55	0.41	26.32
CN-5	87.93	0.53	42.01	51.46		0.17	10.68
CN-6	84.48	0.46	42.17	50.78		0.14	9.27
CN-7	81.03	0.29	42.47	50.97		0.09	5.83
CN-8	75.86	0.18	42.49	51.22		0.06	3.62

To prove the reliability of the postsulfation and desulfation treatments for CNs used in this study, spectroscopic characterization was performed for all samples. From FTIR spectra (as shown in Figure 2.2), the peak located at 1033 cm^{-1} was followed, which was attributed to the stretching vibration of sulfated groups ($-\text{SO}_3$).³⁰ In comparison with pristine nanocrystals (CN-0), the magnitude of the peak gradually increased for postsulfated nanocrystals (solid lines in Figure 2.2), whereas it gradually decreased for desulfated nanocrystals (dot lines in Figure 2.2). These changes indicated the implementation of introducing gradient contents of sulfate groups on the surface of CN samples.

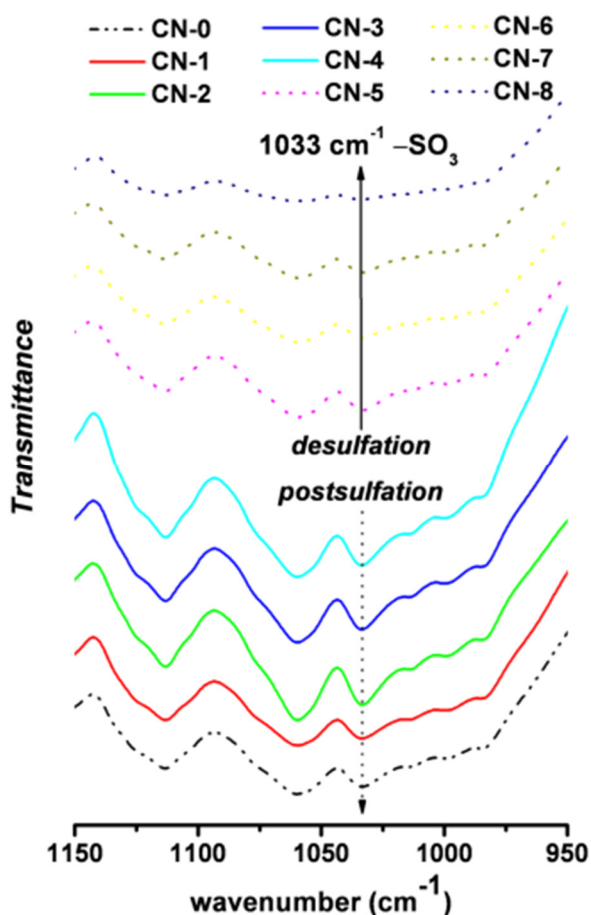


Figure 2.2 FTIR spectra for various CNs samples with postsulfation or desulfation treatment in the wavenumber range 1150 to 950 cm^{-1} .

2.3.2 X-ray photoelectron spectroscopy (XPS)

Surface postsulfation and desulfation of CNs were further analyzed by X-ray photoelectron spectroscopy, which was more accurate and objective. XPS can reveal the elements present in the sample, as well as determine the atomic and mass concentration of the elements. It provides a more quantitative idea for the level of surface modification. Figure 2.3 shows the general XPS spectra for pristine nanocrystals (CN-0), postsulfated nanocrystals (CN-4), and desulfated nanocrystals (CN-8), together with the signal assignments for sulfur (S2p, 165-168 eV) and sodium (Na1s, 1072 eV) elements. The intensity of the sulfur signal peak for the three samples was compared, and content ratio of sulfur to carbon (S/C) elements was calculated. It was shown that postfulfated nanocrystals (CN-4) possessed the maximum S/C ratio value, i.e. 5.4%; whereas desulfated nanocrystals (CN-8) had the

lowest sulfur content, with the S/C ratio of 0.25%. Regarding the sodium element, only CN-8 nanocrystal sample showed the signal of sodium with a Na/C ratio of 4.5%, which was a further proof for the desulfation treatment of CNs.

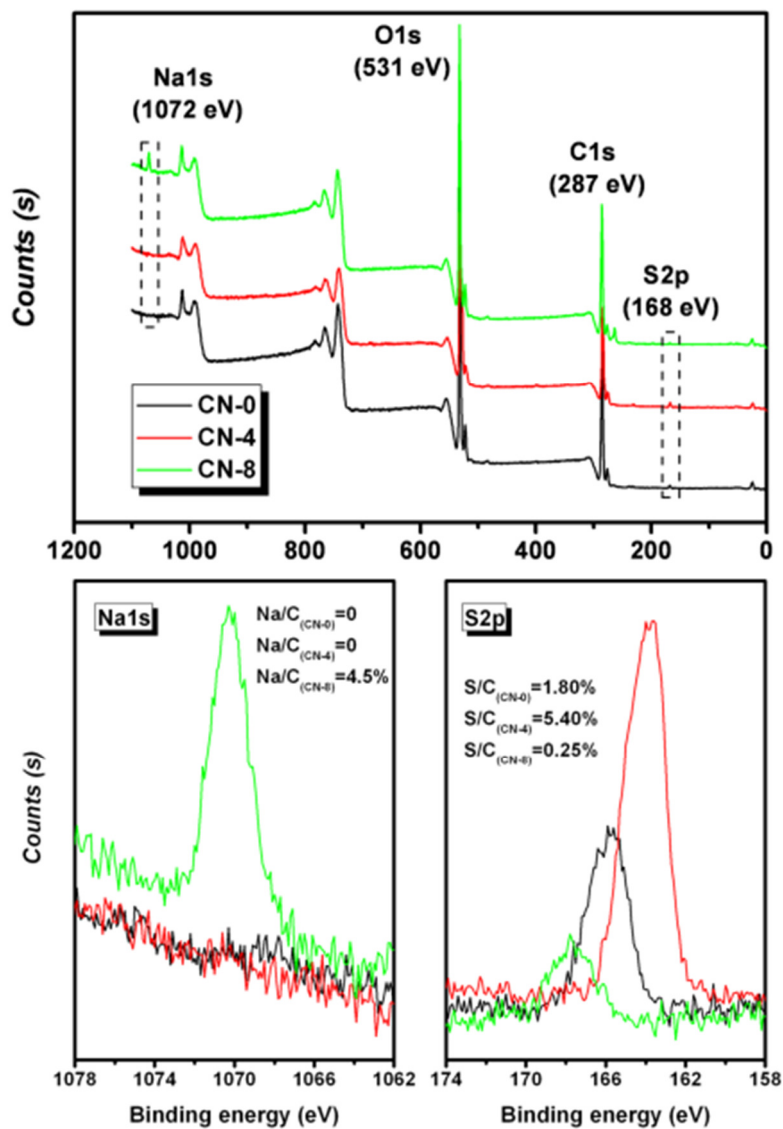


Figure 2.3 General XPS spectra for pristine cellulose nanocrystals (CN-0), postsulfated cellulose nanocrystals (CN-4), and desulfated cellulose nanocrystals (CN-8) with signal assignments (sodium Na1s, sulfur S2p).

The weight contents of sulfur (S), carbon (C), and oxygen (O) elements in the various CNs samples were measured by elemental analysis, and the data are shown in Table 2.1. The sulfur element content in pristine nanocrystals (CN-0) was about 0.67%, which was close to the value reported in the previous report.¹⁹ Regarding the changes

in sulfur content for postsulfated and desulfated nanocrystals, a logical tendency can be observed. In contrast to CN-0, the sulfur content for postsulfated nanocrystals CN-(1 to 4) and desulfated nanocrystals CN-(5 to 8) gradually increased up to a maximum value of 1.31%, and decreased to a minimum value of 0.18%, respectively. In fact, it was reported that during the biosynthesis process, trace amounts of sulfur remained in plant tissues, which can explain the presence of slight sulfur for CN-8 sample.²⁰

2.4 Morphological Observation and Dimensions

Before discussion on CN surface chemistry, the morphology of nanocrystals should be checked, and the geometrical dimensions should be defined. AFM was used to

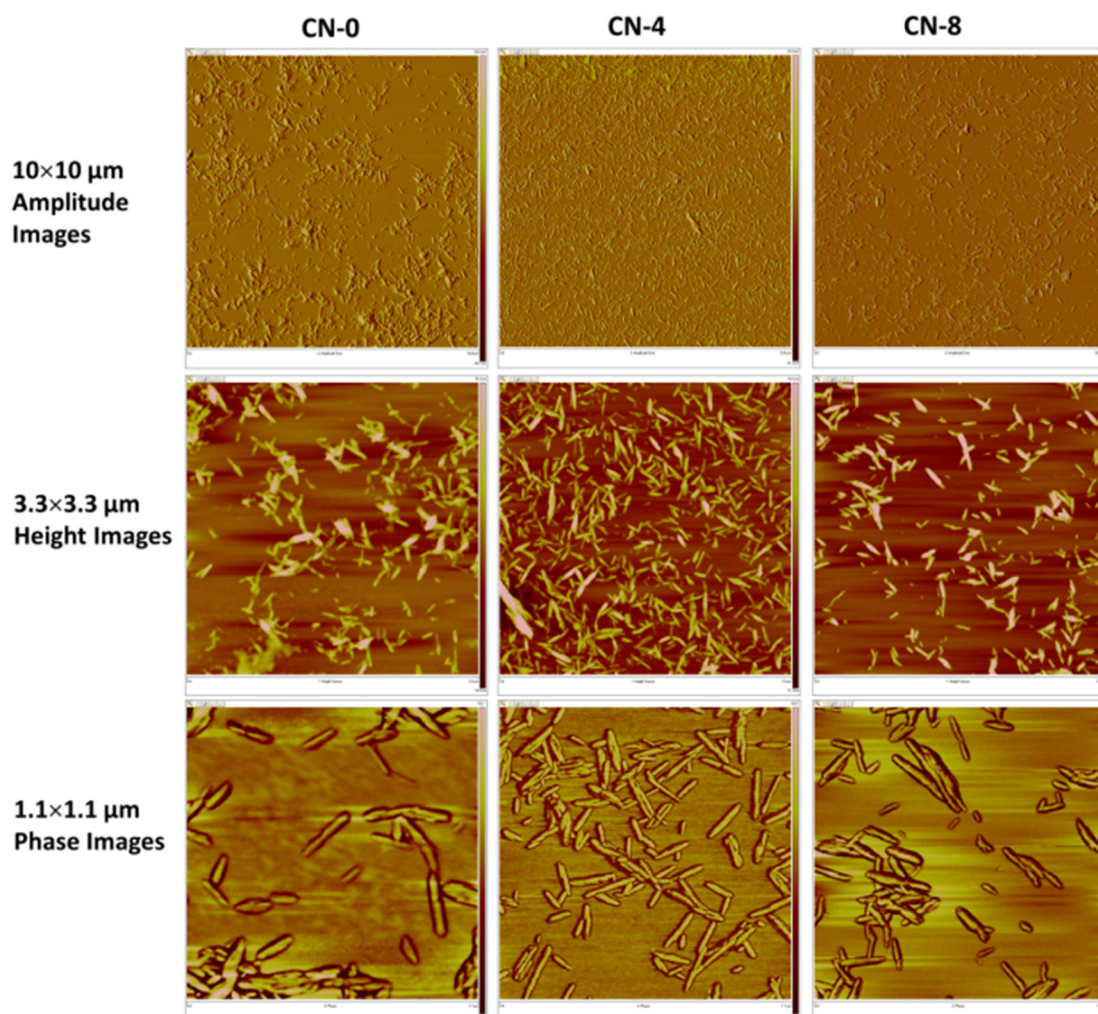


Figure 2.4 AFM images for pristine cellulose nanocrystals (CN-0), postsulfated cellulose nanocrystals (CN-4), and desulfated cellulose nanocrystals (CN-8) at different observation scales.

observe the morphology and measure the dimensions of the nanoparticles. Figure 2.4 shows the amplitude, height and phase images from AFM at different observation scales (10×10 μm; 3.3×3.3 μm; 1.1×1.1 μm). It was shown that all CN samples exhibited the typical and expected rod-like or needle-like morphology, with a length of about 100–300 nm, and width of about 10–30 nm. Interestingly, by comparing the three series images, it seemed that the dimensions of postsulfated nanocrystals CN-4 were more homogeneous, which may be associated to the enhanced electrostatic repulsion among nanoparticles in aqueous suspension.

Further statistical analysis of nanocrystal dimensions was performed by Nanoscope software. As representative samples, statistical analysis for dimensions and distribution determined from AFM images for samples CN-0, CN-4 and CN-8 are shown in Figure 2.5 and Figure 2.6. Through the statistic measurements with over 100 individual nanocrystals from AFM images (mainly focusing on the images with the scale of 3.3×3.3 μm and 1.1×1.1 μm), the average length (*L*), width (*W*) and height (*H*) of CNs were about 150 nm, 22 nm, and 5 nm, respectively. Specifically, pristine nanocrystals CN-0 showed a length of 169.9±86.8 nm, width of 23.0±8.9 nm, and height of 5.2±1.9 nm; whereas postsulfated nanocrystals CN-4 exhibited a length of 152.0±61.6 nm, width of 22.7±8.7 nm, and height of 5.0±1.3 nm; and desulfated nanocrystals CN-8 behaved a length of 148.6±68.1 nm, width of 21.8±8.9 nm, and height of 5.0±1.5 nm. From the dimension changes, it was shown that the average length gradually decreased for modified nanocrystals because of the reduction of large scale nanocrystals. As shown in Figure 2.5, CN-0 nanocrystals with a length higher than 220 nm disappeared in CN-4 and CN-8 samples, which can be attributed to the further removal of amorphous region during the postsulfation and desulfation treatments. Geometrical dimension data for all nine CN samples are summarized in Table 2.2. The nanoscaled dimension and distribution of cotton CNs demonstrate that these nanoparticles have the promising potential to be used as rigid nano-reinforcing filler for composites.

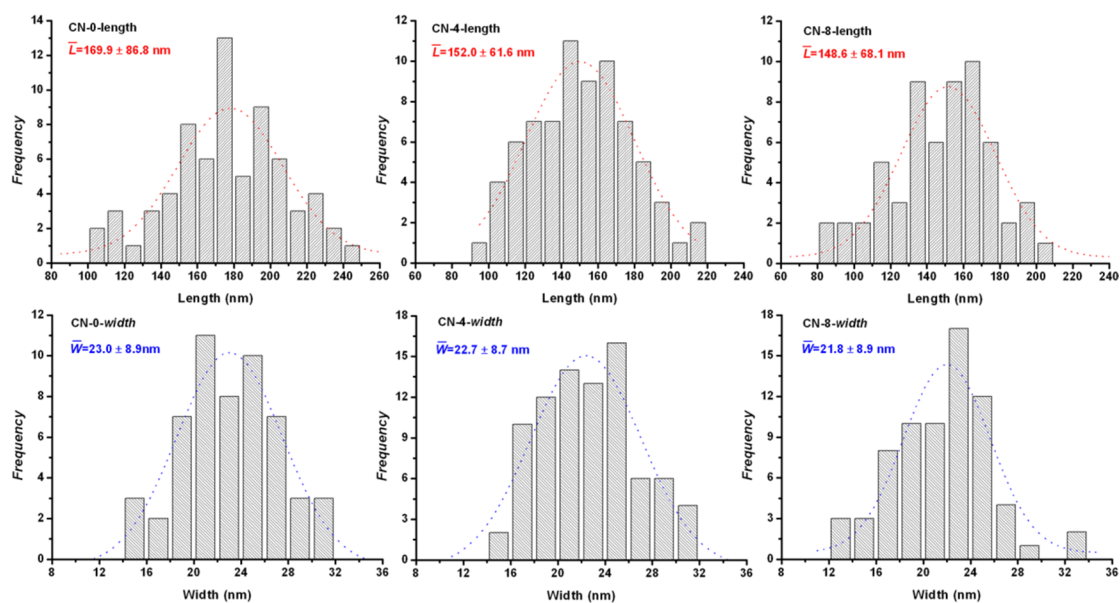


Figure 2.5 Size statistics for length (L) and width (W) from AFM images for cellulose nanocrystal samples (CN-0, CN-4 and CN-8); red dashed lines are Gaussian distribution fitting line according to the statistical data.

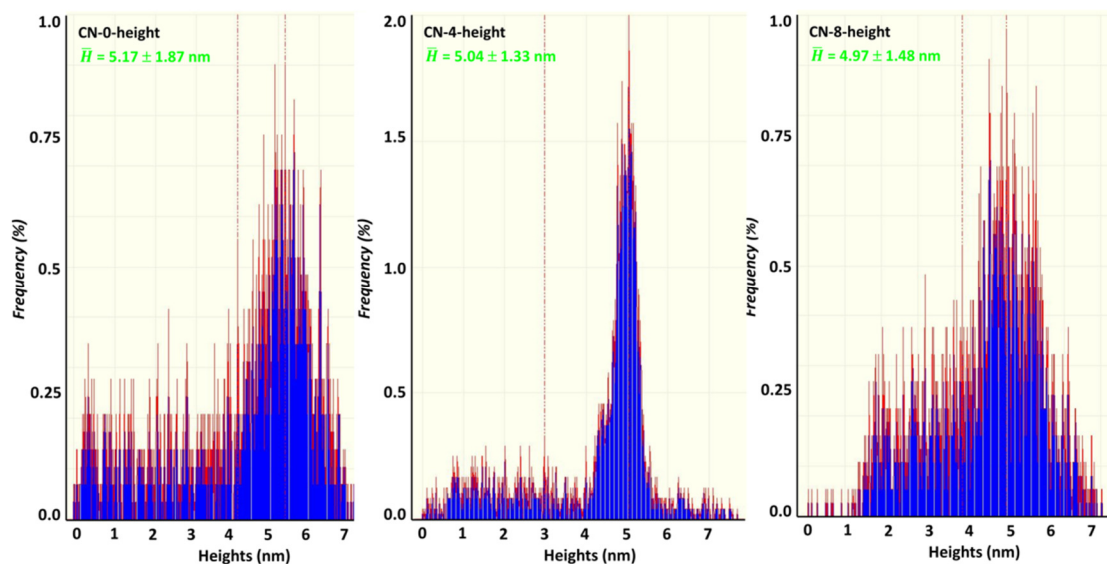


Figure 2.6 Size statistics of height (H) for cellulose nanocrystal samples (CN-0, CN-4 and CN-8) with the analysis of NanoScope software.

Table 2.2 Geometrical dimensions of various CN samples from the results of AFM.

Sample	Geometrical dimension (nm)			Sample	Geometrical dimension (nm)		
	Length	Width	Height		Length	Width	Height
CN-0	169.9±86.8	23.0±8.9	5.2±1.9				
CN-1	159.5±67.4	22.3±10.4	5.3±2.0	CN-5	157.6±71.3	23.6±10.1	5.1±1.7
CN-2	154.1±57.9	21.7±7.9	5.1±1.8	CN-6	150.6±64.8	21.9±8.7	5.1±1.6
CN-3	154.6±69.2	22.3±9.7	5.2±1.5	CN-7	151.6±69.5	22.6±9.4	5.1±1.4
CN-4	152.0±61.6	22.7±8.7	5.0±1.3	CN-8	148.6±68.1	21.8±8.9	5.0±1.5

2.5 Morphological Models and Surface Chemistry of Cellulose Nanocrystals

The degree of substitution (*DS*) of surface hydroxyl groups (–OH) replaced by sulfate groups (–OSO₃[–]) can be calculated according to Eq. (2.4). In this equation, $n_{-OSO_3^-}$ represents the mole fraction of sulfate groups, which can be calculated according to Eq. (2.5) from the results of elemental analysis. The amount of surface (–OH) on CNs [$n_{surface(-OH)}$] can be deduced from some fundamental models (as shown in Figure 2.7 a, b, c), and calculated from Eq. (2.6).

$$DS = \frac{n_{-OSO_3^-}}{n_{surface(-OH)}} \quad (2.4)$$

$$n_{-OSO_3^-} = n_S = \frac{m_S}{M_S} = \frac{m_{CN} S\%}{M_S} \quad (2.5)$$

$$n_{surface(-OH)} = N_0 \cdot A_{total(CN)} \quad (2.6)$$

According to previous reports,^{20,31} the representative elementary crystallite region of cotton CN was proposed (model b), which exhibits a square or parallelogram section with 10 × 10 glucose units based on the *d*-spacing of (110), (1 $\bar{1}$ 0), and (200) planes and its size is roughly 5.3 nm × 6.6 nm. Crystalline dimensions for the three planes can be obtained from XRD experiments. (Further discussion on the effect of sulfate groups on crystalline properties of CNs will be provided in next part.) Taking hydroxyl groups and length of cellobiose unit into consideration (model c), 36 glucan chains are located on the surface of the crystal, which correspond to 120 available

hydroxyl groups. Consequently, the number of hydroxyls per unit surface area (N_0) on cotton cellulose nanocrystal can be calculated as 8.13×10^{-3} mmol/m² according to Eq. (2.7).

$$N_0 = \frac{120 (-OH)}{N_A(2A_{110} + 2A_{1\bar{1}0})} \quad (2.7)$$

In Eq. (2.7),

$$A_{110} = 6.6 \times 1.03 \text{ nm}^2$$

$$A_{1\bar{1}0} = 5.3 \times 1.03 \text{ nm}^2$$

$$N_A = 6.02 \times 10^{23} \text{ (Avogadro's number)}$$

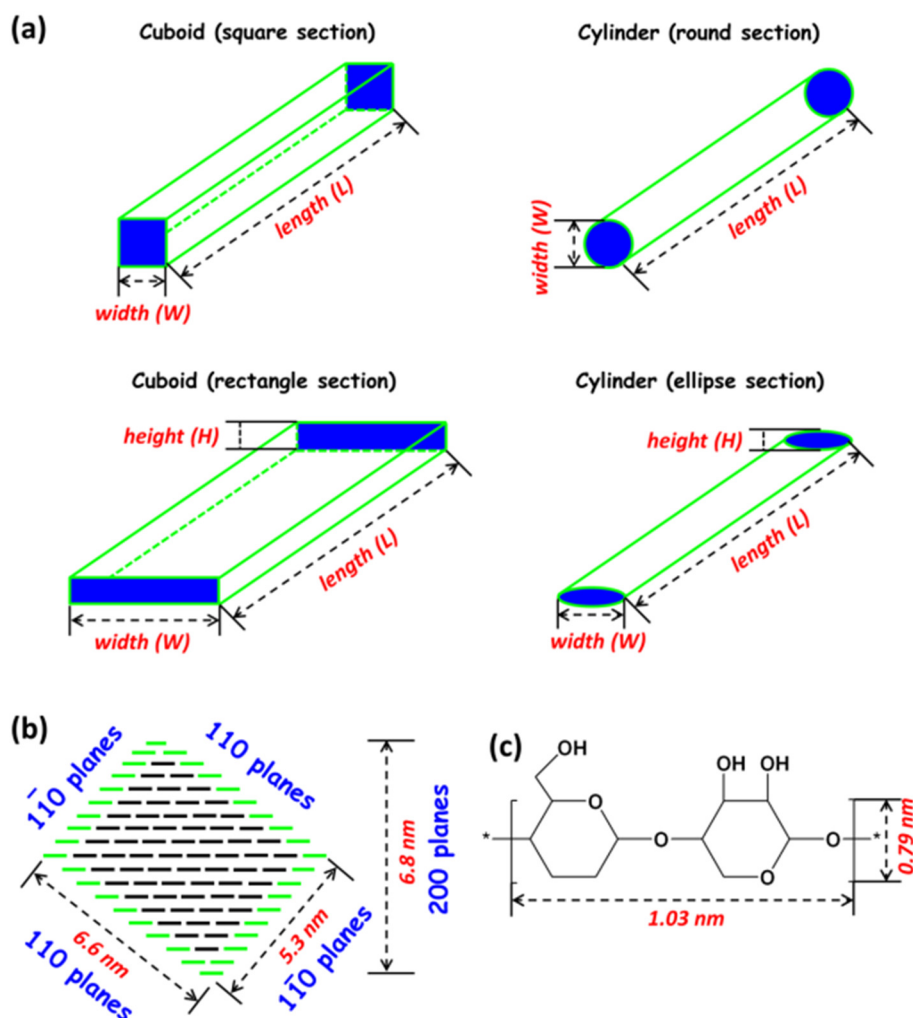


Figure 2.7 Schematic models of (a) an individual rod-like cellulose nanocrystal and dimensions (cuboid shape with square section; cylinder shape with round section; cuboid shape with rectangular section; cylinder shape with ellipsoid section); (b) an idealized elementary crystallite

region for cotton cellulose nanocrystal from the analysis of XRD (one black bar represents a glucan chain, and green bars are surface available glucan chains); (c) chemical conformation and dimensions of one single cellobiose unit.

Consequently, to determine the amount of surface –OH on CNs, the key point is to calculate the value of the total specific surface area [$A_{total(CN)}$], which can be calculated from Eq. (2.8). In this equation, $\rho_{cellulose}$ is the density of cellulose (1.50 g/cm³); $A_{single(CN)}$ and $V_{single(CN)}$ represent the surface area and volume of a single nanocrystal, respectively.

$$A_{total(CN)} = \frac{m_{CN}}{\rho_{cellulose}} \cdot \frac{A_{single(CN)}}{V_{single(CN)}} \quad (2.8)$$

Interestingly, with different cross-section models, the results of $A_{total(CN)}$ will be completely different. Generally, cellulose nanocrystal can be considered as a kind of rod-like or needle-like nanoparticle, so the simplest cross-section model is cuboid or cylinder with the square or round bottom, as shown in model (a). However, in this study, according to AFM observations, the width and height of CNs are different ($W=22$ nm, and $H=5$ nm), which indicates that the cuboid or cylinder model with a rectangular or ellipsoidal cross-section for the nanocrystal may be more reasonable.

If choosing the **cuboid model (square section)** for CN,

$$A_{single(CN)} = 4WL$$

$$V_{single(CN)} = W^2L$$

So, in Eq. (2.8):

$$A_{total(CN)} = \frac{m_{CN}}{\rho_{cellulose}} \cdot \frac{4}{W} \quad (2.8 - 1)$$

If choosing the **cylinder model (round section)** for CN,

$$A_{single(CN)} = \pi WL$$

$$V_{single(CN)} = \pi W^2 L / 4$$

So, in Eq. (2.8):

$$A_{total(CN)} = \frac{m_{CN}}{\rho_{cellulose}} \cdot \frac{4}{W} \quad (2.8 - 2)$$

If choosing the **cuboid model (rectangular section)** for CN,

$$A_{single(CN)} = 2(W + H)L$$

$$V_{single(CN)} = WHL$$

So, in Eq. (2.8):

$$A_{total(CN)} = \frac{m_{CN}}{\rho_{cellulose}} \cdot \frac{2(W + H)}{WH} \quad (2.8 - 3)$$

If choosing the **cylinder model (ellipsoid section)** for CN,

$$A_{single(CN)} = [2\pi H + 4(W - H)]L$$

$$V_{single(CN)} = \pi LHW$$

So, in Eq. (2.8):

$$A_{total(CN)} = \frac{m_{CN}}{\rho_{cellulose}} \cdot \frac{2\pi H + 4(W - H)}{\pi WH} \quad (2.8 - 4)$$

It is observed that the values for $A_{total(CN)}$ using square and round section models show the same results (Eq. 2.8-1 and 2.8-2), depending on the width (W) of the nanocrystal only; whereas the values for $A_{total(CN)}$ using rectangular and ellipsoid section models depend on both the width (W) and height (H) (Eq. 2.8-3 and 2.8-4).

Table 2.3 Total specific surface area [$A_{total(CN)}$], amount of sulfate groups [$n_{-OSO_3^-}$] and surface hydroxyl groups [$n_{surface(-OH)}$], and degree of sulfation substitution (DS) for CN-0 calculated from different cross-section models.

Model	$A_{total(CN)}$ m ²	Surface -OH mmol/g	Surface -OSO ₃ ⁻ mmol/g	$DS_{-OSO_3^-}$ %
Square/Round	117.5	0.96		21.88
Ellipse	191.2	1.55	0.21	13.45
Rectangle	325.4	2.65		7.90

Data for total specific surface area [$A_{total(CN)}$], amount of $n_{-OSO_3^-}$ and $n_{surface(-OH)}$, and degree of substitution (DS) of sulfate groups for CN-0 were calculated based on the different cross-section models, and are summarized in Table 2.3. It is shown that if square or round models are chosen for cotton CNs, more than 20% of surface hydroxyl groups have been substituted by sulfate groups during the H_2SO_4 -esterification hydrolysis, which indicates that most of active hydroxyl groups located on C-6 have been replaced. Therefore, from these two models, desulfation treatment for H_2SO_4 -hydrolyzed CNs is necessary before chemical modification. However, if choosing rectangle model for CNs, only 7.90% (only about 1/3 of the value for square or round models) surface hydroxyl groups is substituted during the H_2SO_4 -hydrolysis, and a large amount of active hydroxyl groups have been remained.

In this study, ellipse model for the CNs cross-section is also proposed, and the DS value of sulfate groups for nine CN samples is shown in Table 2.1. Specifically, if ellipse model is chosen, about 13% of the surface hydroxyl groups are substituted by sulfate groups during hydrolysis of pristine nanocrystal CN-0. The maximum DS value is about 26% for CN-4, which indicates that 1/4 of the hydroxyl groups on the CN surface can be replaced by sulfate groups during the postsulfation treatment.

The proposal of ellipse model for cotton CNs is based on AFM observation and presumption of cross-section shape. Figure 2.8 presents the orthography image of CNs. However, due to the small scale of height dimension (about 5 nm), it was difficult to directly observe and determine the end shape of nanocrystals. With the enlargements of height to ten, thirty, and fifty times ($\times z$ axis), some interesting changes appeared on AFM images. As indicated by the green and blue circles in Figure 2.8, it seems that after enlargement, the shape of CN cross-section transformed to “mountain” with a peak on the top. If the nanocrystal cross-section is rectangular, the size from top to bottom should remain invariable during the height enlargement; whereas ellipsoid cross-section was suitable for this change. Although the ellipse cross-section model should be further validated by other observation techniques,³² it is a new choice to be used for the analysis of CN surface chemistry.

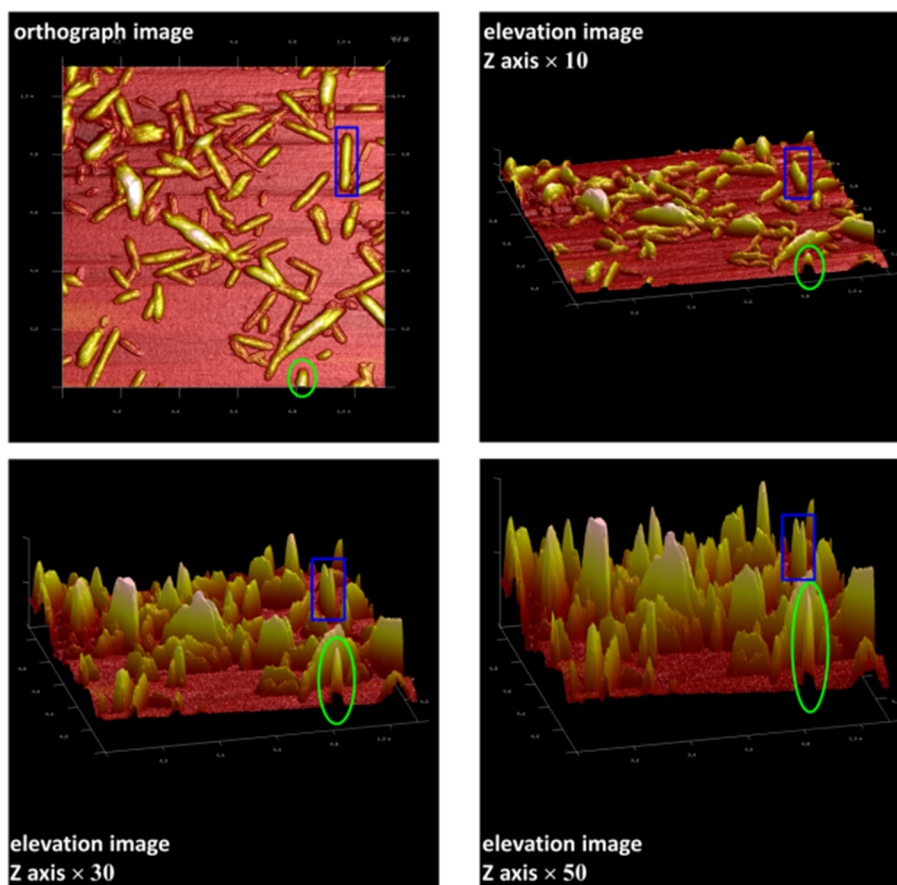


Figure 2.8 AFM image analysis for the observation of the cross-section shape for cellulose nanocrystals (CN-4).

2.6 Effect of Sulfate Groups on the Properties of Cellulose Nanocrystals

Besides the surface chemistry discussed above, different sulfate group contents on the surface of CNs should also significantly affect their physical properties, such as crystalline structure and thermal stability for inherent nanocrystal, and birefringence behavior and rheological behavior for nanocrystal suspensions. Some studies have reported the influence of sulfate groups on the rheological behavior of CN suspensions. For instance, it was reported that the introduction of more sulfate groups on the surface of CNs drastically reduced the viscosity of the suspension and removed the time dependence.³³ Recently, it was found that the degree of sulfation of CNs has a significant effect on the critical concentration at which transitions from isotropic to liquid crystal and liquid crystal to gel occur.³⁴ It is a pity that some inconsistent

conclusions on the effect of sulfate groups were given in different studies, such as thermal stability of sulfated CNs as mentioned in the Introduction Section. In this study, important physical properties of CNs possibly affected by the sulfate group content have been further investigated. Because of the wide range and detailed sulfate group contents (nine samples from minimum to maximum contents), the global trend analysis on properties for sulfated CNs would be more reasonable.

2.6.1 Crystalline Structure and Crystalline Dimensions

Crystal properties are among the most important physical properties of CNs, which can reflect the integrity of the original structure of the nanocrystals. The degree of postsulfation should be carefully controlled to react only on the surface of CNs, in order to maximally introduce sulfate groups and avoid the further structural destruction. On the other hand, due to the use of alkaline solution for desulfation treatment, the polymorphic and chemical transformation of cellulose (such as type I for cotton cellulose in this study) must be prevented. XRD is the common technique for the investigation of crystalline structure of cellulose. The X-ray diffraction patterns for the various CNs with different surface sulfate group contents are shown in Figure 2.9, and the values of the crystallinity index (χ_c) and crystalline dimensions are summarized in Table 2.4. The similar patterns and intensity preservation of diffraction peaks for all samples indicated that the postsulfation and desulfation treatments did not destroy or convert the inherent crystalline structure of nanocrystals. Indeed, the characteristic diffraction peaks at 2θ angles around 14.9° , 16.5° , 20.5° , 22.7° , 34.5° assigned to the typical reflection planes of cellulose I, $1\bar{1}0$, 110, 012, 200, 004, respectively, were preserved.³⁵ The crystallinity index (χ_c) of CNs was calculated according to the Segal method (Eq. 2),³⁶ which exhibited a high crystallinity (about 88% for χ_c) and maintenance of the crystalline structure. From the calculation according to Scherrer equation (Eq. 2.3), the crystalline dimensions of different planes (B_{200} , $B_{1\bar{1}0}$ and B_{110}) for CNs samples can be obtained. As shown in Table 2.4, the sizes of 200, $1\bar{1}0$, and 110 planes for cotton CNs were about 6.8 nm, 5.3 nm, and 6.6 nm, which was consistent with the parallelogram elementary crystallite model proposed in Figure

2.7b. On the basis of XRD results, it can be stated that surface sulfate group content does not obviously affect or has less influence to the crystal properties of CNs.

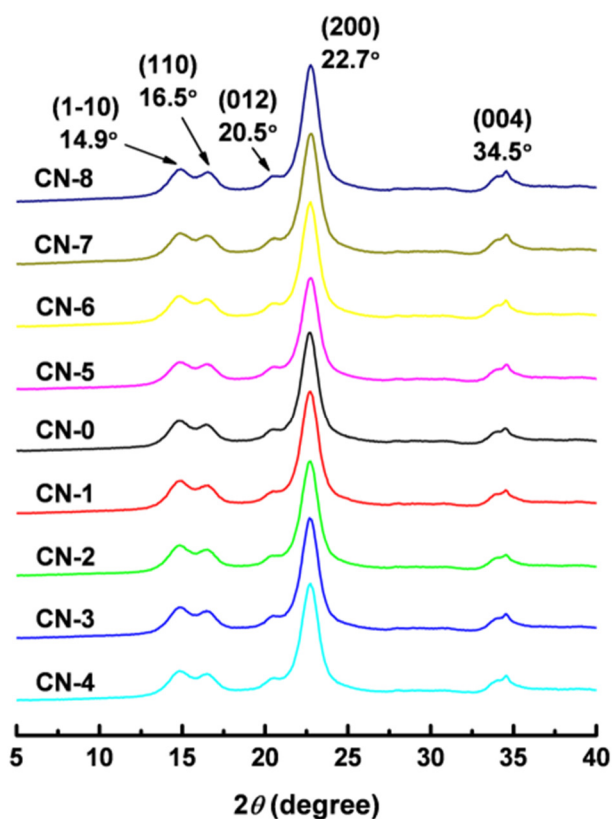


Figure 2.9 X-ray diffraction patterns for various cellulose nanocrystals with different surface sulfate group contents.

Table 2.4 Values of crystallinity index (χ_c), crystalline dimensions (B_{200} , $B_{1\bar{1}0}$ and B_{110}), and ζ -potentials for various CN samples from the results of XRD and zeta-potential analysis.

Sample	χ_c %	Crystalline dimension (nm)			ζ -potential mV
		B_{200}	$B_{1\bar{1}0}$	B_{110}	
CN-0	88.6	6.8	5.3	6.6	-40.4 ± 1.7
CN-1	88.1	6.7	5.3	6.5	-47.8 ± 1.9
CN-2	88.2	6.8	5.3	6.6	-54.8 ± 2.2
CN-3	88.5	6.8	5.3	6.5	-61.7 ± 2.4
CN-4	88.0	6.7	5.3	6.7	-66.1 ± 1.5
CN-5	87.1	6.7	5.2	6.7	-32.8 ± 2.3
CN-6	88.0	6.8	5.2	6.7	-27.6 ± 1.4
CN-7	87.5	6.7	5.3	6.6	-17.9 ± 1.1
CN-8	88.2	6.8	5.3	6.7	-7.4 ± 0.8

2.6.2 ζ -potential of Aqueous Suspensions

Owing to the presence of sulfate groups on their surface, rod-like CNs changed to negatively charged nanoparticles. In the colloidal system of sulfated CNs, the dispersion medium and the stationary layer of fluid attached to the dispersed nanoparticles will provide the potential difference, which is named zeta potential (ζ -potential). The value of zeta potential is related to the stability of the colloidal dispersion, and indicates the degree of repulsion between adjacent, similarly charged particles in a suspension. The effect of sulfate groups on ζ -potential of CNs is presented in Table 2.4. With the increase of sulfate group content, sulfated CNs possessed a more negative surface, and exhibited lower ζ -potential values. Especially for postsulfated nanocrystals sample CN-4, the value of ζ -potential reached -66.1 ± 1.5 mV, which indicated the strong repulsive force between nanoparticles, and therefore the promotion of its dispersion in suspension (as proved by AFM). It is worth noting that desulfation treatment for sulfated nanocrystals was also effective, which can be reflected by the significant increase of ζ -potential for desulfated CN samples.

2.6.3 Thermal Stability

Thermal stability is another important physical property for CNs, which plays a critical role in the preparation of melt processed CN-reinforced composites. As mentioned in the Introduction Section, the effect of sulfate groups on the surface of CNs to thermal stability led to inconsistent conclusions from different reports. Therefore, thermal degradation behavior of sulfated CNs was further investigated by thermogravimetric analysis in this study, which is shown in Figure 2.10. Interestingly, in comparison with all nanocrystal samples, native cotton exhibited the highest thermal stability for the first phase of thermal decomposition (T_{d1}). Because of the hydrolysis and presence of sulfate groups, the values of T_{d1} for all postsulfated nanocrystals sharply decreased to about 150 °C compared with native cotton. By determining T_{d1} for postsulfated CNs themselves (event a in Figure 2.10), it appears that more sulfate groups on nanocrystals induced a lowering of T_{d1} , such as the decrement (Δt_1) of 12.3 °C from CN-1 to CN-4 samples. In contrast to postsulfated

nanocrystals, the values of T_{d1} for desulfated CNs generally enhanced about 100 °C attributed to the removal of sulfate groups and presence of sodium on nanocrystals. From the analysis of T_{d1} for desulfated CNs themselves (event b in Figure 2.10), similar conclusion can be obtained, i.e. less sulfate groups on nanocrystals resulted in higher T_{d1} , such as the increment (Δt_2) of 13.8 °C from CN-5 to CN-8 samples. It should be pointed out that according to our investigation, besides sulfate groups, the introduction of sodium on the surface of CNs may be another factor that significantly affects their thermal property. Furthermore, from the TGA thermograms in Figure 8, thermal degradation behavior of cellulose for the second phase of thermal decomposition (T_{d2}) can also be observed. Differently, all nanocrystal samples possessed higher T_{d2} values than native cotton (about 65 °C), which may be associated to the higher crystallinity for nanocrystal samples.

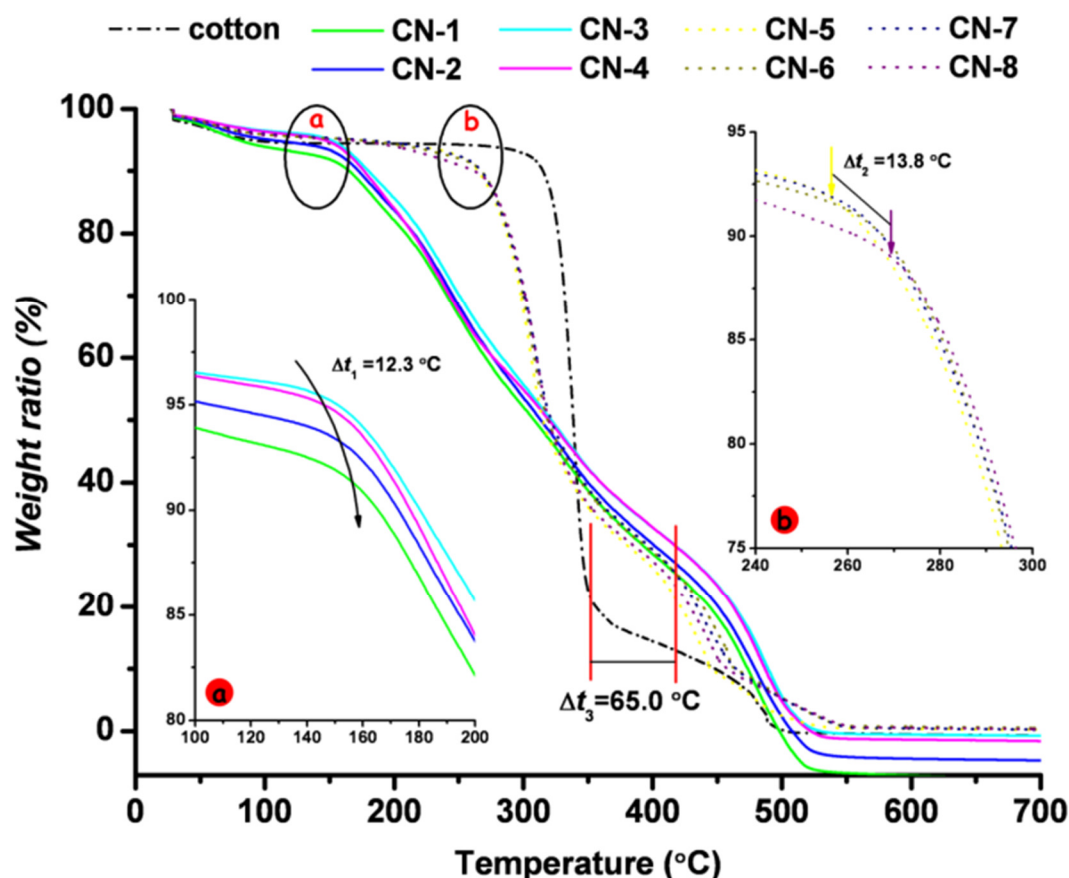


Figure 2.10 Effect of surface sulfate groups on the thermal stability of cellulose nanocrystals (TGA thermograms).

2.6.4 Birefringence of Aqueous Suspensions

In 1959, the birefringence character of acid-treated cellulose and chitin crystallites was first reported,³⁷ which was the behavior through strong adsorption of one of polarized rays to possess two refractive indices. Birefringence of CN suspensions can be observed with two linear polarizers crossed at 90° (cross-nicols or crossed-polars), and gives a quick indication of the successful preparation of well-dispersed CN suspensions. Figure 2.11 shows the photographs of aqueous suspensions of various CNs with postsulfation and desulfation treatments. The presence of negative charges ($-OSO_3^-$) on CN surface induced an electrostatic repulsion between nanoparticles, and the suspensions exhibited the formation of birefringent domains. Because of the stable dispersion and flow anisotropy from alignment of nano-rods under flow state, the birefringence character for postsulfated nanocrystal suspensions was maintained. With the desulfation and progressive removal of sulfate groups, nanoparticles in suspensions tended to aggregate, which induced the reduction and weakening of birefringent domains. Especially for strongly desulfated nanocrystals, samples CN-7 and CN-8, the birefringence behavior of suspensions was difficult to be observed.

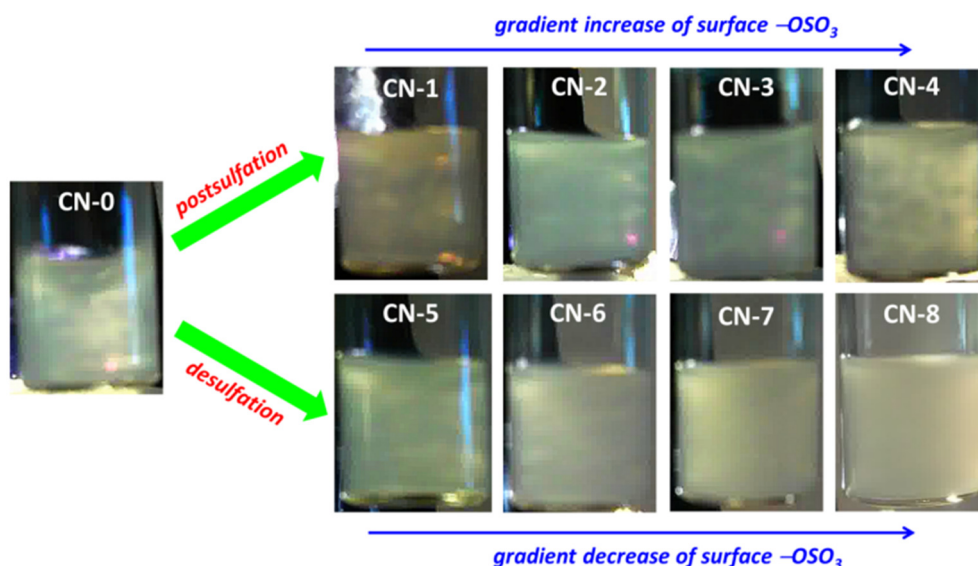


Figure 2.11 Photographs of aqueous suspensions of various cellulose nanocrystals viewed through cross polarizers (0.5 wt%).

2.7 Conclusions

The objective of this study was to investigate how surface sulfate groups affect the surface chemistry and physical properties of cellulose nanocrystals. Through the regulation of reactant ratios and reactive conditions for postsulfation and desulfation, gradient contents of sulfate groups can be introduced on the surface of CNs. Based on the discussion of nanocrystal's surface chemistry, the influence of different cross-section models for the calculation of the degree of substitution of the sulfate groups was investigated, and a new ellipsoid model for cotton CNs was proposed on the basis of AFM observation. Finally, the effects of sulfate groups on diverse properties of CNs and their suspensions have been discussed, and some issues with inconsistent conclusions from previous reports were further validated. Future studies will focus on the electrostatic interactions between negative charges from sulfated CNs and positive charges from cationic polymers or molecules. With the detection and measurement of electrostatic interactions, it is expected to reveal the strength and mechanism of this special interaction from coupling charges and therefore advance the application of CN electrostatic grafting.

2.8 References

1. Dufresne, A. Nanocellulose. From nature to high performance tailored materials; Walter de Gruyter GmbH: Berlin and Boston, MA; **2012**.
2. The global market for nanocellulose to 2017; Futures Markets Inc.: Edinburgh, Lothian EH74NA, United Kingdom, **2012**.
3. Brinchi, L.; Cotana, F.; Fortunati, E.; Kenny, J. M. Production of nanocrystalline cellulose from lignocellulosic biomass: technology and applications. *Carbohydr. Polym.* **2013**, *94*, 154–169.
4. Araki, J. Electrostatic or steric? – preparations and characterizations of well-dispersed systems containing rod-like nanowhiskers of crystalline polysaccharides. *Soft Matter* **2013**, *9*, 4125–4141.
5. Dufresne, A. Nanocellulose: a new ageless bionanomaterial. *Mater. Today* **2013**,

- 16, 220–227.
6. Leung, A. C. W.; Lam, E.; Chong, J.; Hrapovic, S.; Luong, J. H. T. Reinforced plastics and aerogels by nanocrystalline cellulose. *J. Nanopart. Res.* **2013**, *15*, 1636 (24 pages).
 7. Lin, N.; Huang, J.; Dufresne, A. Preparation, properties and applications of polysaccharide nanocrystals in advanced functional nanomaterials: a review. *Nanoscale* **2012**, *4*, 3274–3294.
 8. Tingaut, P.; Zimmermann, T.; Sèbe, G. Cellulose nanocrystals and microfibrillated cellulose as building blocks for the design of hierarchical functional materials. *J. Mater. Chem.* **2012**, *22*, 20105–20111.
 9. Lam, E.; Male, K. B.; Chong, J. H.; Leung, A. C.W.; Luong, J. H. T. Applications of functionalized and nanoparticle-modified nanocrystalline cellulose. *Trends Biotechnol.* **2012**, *30*, 283–290.
 10. Habibi, Y.; Lucia, L. A.; Rojas, O. J. Cellulose nanocrystals: chemistry, self-assembly, and applications. *Chem. Rev.* **2010**, *110*, 3479–3500.
 11. Rånby, B. G. Aqueous colloidal solutions of cellulose micelles. *Acta Chem. Scand.* **1949**, *3*, 649–650.
 12. Cranston, E. D.; Gray, D. G.; Rutland, M. W. Direct surface force measurements of polyelectrolyte multilayer films containing nanocrystalline cellulose. *Langmuir* **2010**, *26*, 17190–17197.
 13. Moreau, C.; Beury, N.; Delorme, N.; Cathala, B. Tuning the architecture of cellulose nanocrystal–poly(allylamine hydrochloride) multilayered thin films: Influence of dipping parameters. *Langmuir* **2012**, *28*, 10425–10436.
 14. Liew, S. Y.; Thielemans, W.; Walsh, D. A. Electrochemical capacitance of nanocomposite polypyrrole/cellulose films. *J. Phys. Chem. C* **2010**, *114*, 17926–17933.
 15. Ma, H.; Burger, C.; Hsiao, B. S.; Chu, B. Nanofibrous microfiltration membrane based on cellulose nanowhiskers. *Biomacromolecules* **2012**, *13*, 180–186.
 16. Thielemans, W.; Warbey, C. R.; Walsh, D. A. Permselective nanostructured membranes based on cellulose nanowhiskers. *Green Chem.* **2009**, *11*, 531–537.

17. Jiang, F.; Kittle, J. D.; Tan, X.; Esker, A. R.; Roman, M. Effects of sulfate groups on the adsorption and activity of cellulases on cellulose substrates. *Langmuir* **2013**, *29*, 3280–3291.
18. Kalashnikova, I.; Bizot, H.; Cathala, B.; Capron, I. Modulation of cellulose nanocrystals amphiphilic properties to stabilize oil/water interface. *Biomacromolecules* **2012**, *13*, 267–275.
19. Abitbol, T.; Kloser, E.; Gray, D. G. Estimation of the surface sulfur content of cellulose nanocrystals prepared by sulfuric acid hydrolysis. *Cellulose* **2013**, *20*, 785–794.
20. Gu, J.; Catchmark, J. M.; Kaiser, E. Q.; Archibald, D. D. Quantification of cellulose nanowhiskers sulfate esterification levels. *Carbohydr. Polym.* **2013**, *92*, 1809–1816.
21. Roman, M.; Winter, W. T. Effect of sulfate groups from sulfuric acid hydrolysis on the thermal degradation behavior of bacterial cellulose. *Biomacromolecules* **2004**, *5*, 1671–1677.
22. Voronova, M. I.; Surov, O. V.; Zakharov, A. G. Nanocrystalline cellulose with various contents of sulfate groups. *Carbohydr. Polym.* **2013**, *98*, 465–469.
23. Lin, N.; Dufresne, A. Physical and/or chemical compatibilization of extruded cellulose nanocrystal reinforced polystyrene nanocomposites. *Macromolecules* **2013**, *46*, 5570–5583.
24. Zhang, K.; Brendler, E.; Geissler, A.; Fischer, S. Synthesis and spectroscopic analysis of cellulose sulfates with regulable total degrees of substitution and sulfation patterns via ^{13}C NMR and FT Raman spectroscopy. *Polymer* **2011**, *52*, 26–32.
25. Wang, Z.-M.; Li, L.; Xiao, K.-J.; Wu, J.-Y. Homogeneous sulfation of bagasse cellulose in an ionic liquid and anticoagulation activity. *Bioresource Technol.* **2009**, *100*, 1687–1690.
26. Jiang, F.; Esker, A. R.; Roman, M. Acid-catalyzed and solvolytic desulfation of H_2SO_4 -hydrolyzed cellulose nanocrystals. *Langmuir* **2010**, *26*, 17919–17925.
27. Kloser, E.; Gray, D. G. Surface grafting of cellulose nanocrystals with

- poly(ethylene oxide) in aqueous media. *Langmuir* **2010**, *26*, 13450–13456.
28. Hasani, M.; Cranston, E. D.; Westman, G.; Gray, D. G. Cationic surface functionalization of cellulose nanocrystals. *Soft Matter* **2008**, *4*, 2238–2244.
29. van den Berg, O.; Capadona, J. R.; Weder, C. Preparation of homogeneous dispersions of tunicate cellulose whiskers in organic solvents. *Biomacromolecules* **2007**, *8*, 1353–1357.
30. Suganuma, S.; Nakajima, K.; Kitano, M.; Yamaguchi, D.; Kato, H.; Hayashi, S.; Hara, M. Hydrolysis of cellulose by amorphous carbon bearing SO₃H, COOH, and OH groups. *J. Am. Chem. Soc.* **2008**, *130*, 12787–12793.
31. Elazzouzi-Hafraoui, S.; Nishiyama, Y.; Putaux, J.-L.; Heux, L.; Dubreuil, F.; Rochas, C. The shape and size distribution of crystalline nanoparticles prepared by acid hydrolysis of native cellulose. *Biomacromolecules* **2008**, *9*, 57–65.
32. Majoinen, J.; Haataja, J. S.; Appelhans, D.; Lederer, A.; Olszewska, A.; Seitsonen, J.; Aseyev, V.; Kontturi, E.; Rosilo, H.; Österberg, M.; Houbenov, N.; Ikkala, O. Supracolloidal multivalent interactions and wrapping of dendronized glycopolymers on native cellulose nanocrystals. *J. Am. Chem. Soc.* **2014**, *136*, 866–869.
33. Araki, J.; Wada, M.; Kuga, S. Influence of surface charge on viscosity behavior of cellulose microcrystal suspension. *J. Wood. Sci.* **1999**, *45*, 258–261.
34. Shafiei-Sabet, S.; Hamad, W. Y.; Hatzikiriakos, S. G. Influence of degree of sulfation on the rheology of cellulose nanocrystal suspensions. *Rheol. Acta.* **2013**, *52*, 741–751.
35. Lin, N.; Bruzzese, C.; Dufresne, A. TEMPO-Oxidized nanocellulose participating as crosslinking aid for alginate-based sponges. *ACS Appl. Mater. Interfaces* **2012**, *4*, 4948–4959.
36. Segal, L.; Creely, J. J.; Martin, A. E.; Conrad, C. M. An empirical method for estimating the degree of crystallinity of native cellulose using the X-ray diffractometer. *Text. Res. J.* **1959**, *29*, 786–794.
37. Marchessault, R. H.; Morehead, F. F.; Walter, N. M. Liquid crystal systems from fibrillar polysaccharides *Nature* **1959**, *184*, 632–633.

CHAPTER 3.

Application of Cellulose Nanocrystals: Extruded Nanocomposites

“Physical and/or Chemical Compatibilization of Extruded Cellulose Nanocrystal Reinforced Polystyrene Nanocomposites”

Chapter 3. Physical and/or Chemical Compatibilization of Extruded Cellulose Nanocrystal Reinforced Polystyrene Nanocomposites

ENGLISH ABSTRACT	156
RESUME FRANÇAIS	159
3.1 Introduction	165
3.2 Experimental Methodology	167
3.2.1 Materials.....	167
3.2.2 Extraction of Cellulose Nanocrystals from Cotton Fiber	168
3.2.3 Carboxylation of Cellulose Nanocrystals	168
3.2.4 Chemical Grafting of PEG5000 on Cellulose Nanocrystals	169
3.2.5 Physical Adsorption of PEO5M on Pristine and Modified Nanocrystals	169
3.2.6 Preparation of Nanocomposites from CN and Polystyrene by Extrusion	170
3.2.7 Characterization and Analyses	171
3.3 Surface Modification and Properties of Cellulose Nanocrystals	175
3.3.1 Surface Grafting of PEG on Cellulose Nanocrystals.....	175
3.3.2 Crystalline Structure	178
3.3.3 Morphology and Surface Adsorption	179
3.3.4 Thermal Stability.....	180
3.3.5 Surface Hydrophilicity.....	181
3.3.6 Rheological Behavior of Modified Cellulose Nanocrystals in Suspension.....	183
3.4 Structure and Properties of Extruded Nanocomposites	184
3.4.1 Appearance Observation and Light Transmittance	184
3.4.2 Dispersion and Microstructure of Nanocrystals in Composites	187
3.4.3 Thermal Properties	190
3.4.4 Mechanical Properties.....	192
3.4.5 Barrier Properties	194
3.5 Conclusions	196
3.6 References	197

ENGLISH ABSTRACT

Since the first report in 1995,¹ cellulose nanocrystals have been widely used as the strength enhancing additive to improve the mechanical performance of a wide range of plastic composites because of their impressive mechanical properties. Commonly, the values of strength and modulus for cellulose nanocrystals are recognized as being in the range of 10 GPa and 100–160 GPa, respectively, which are comparable to Kevlar. Recently, based on the atomic structure model of cellulose in tandem with quantum mechanics, the computed Young's modulus of cellulose nanocrystal was predicted as 206 GPa,² which showed that this special nanoparticle even possess the stiffness of steel and strongly favored its usage in the development of new composite materials. In fact, according to the statistical analysis of Future Markets Inc, about half demand (46%) of nanocellulose (including cellulose nanocrystals and microfibrillated cellulose) by end user market focuses on its composite application.³

For the development of cellulose nanocrystal-based composites, two fundamental issues should be emphasized, which are the composite processing method and the compatibility between the nanoparticles and the matrix. Basically, four main methods are generally employed for the processing of cellulose nanocrystal-based composites, which are casting-evaporation, melt-compounding, electrospinning, and layer-by-layer assembly.⁴ Particularly, the techniques of casting-evaporation and melt-compounding are commonly used for the preparation of cellulose nanocrystal-based composites because of their easy manipulation. Specifically, processing by the casting-evaporation method allows the preservation of individualization state of the nanoparticles resulting from their colloidal dispersion in liquid medium. However, this technique is non-industrial, non-economic, and shows some limitation regarding the choice of the polymeric matrix. In industry, melt-compounding techniques, such as extrusion or injection molding, are commonly used to process thermoplastic polymers because they are “green” (solvent-free), effective and economic processing methods. However, due to the extensive use of sulfuric acid hydrolysis (with high efficiency and promotion of colloidal stability) in

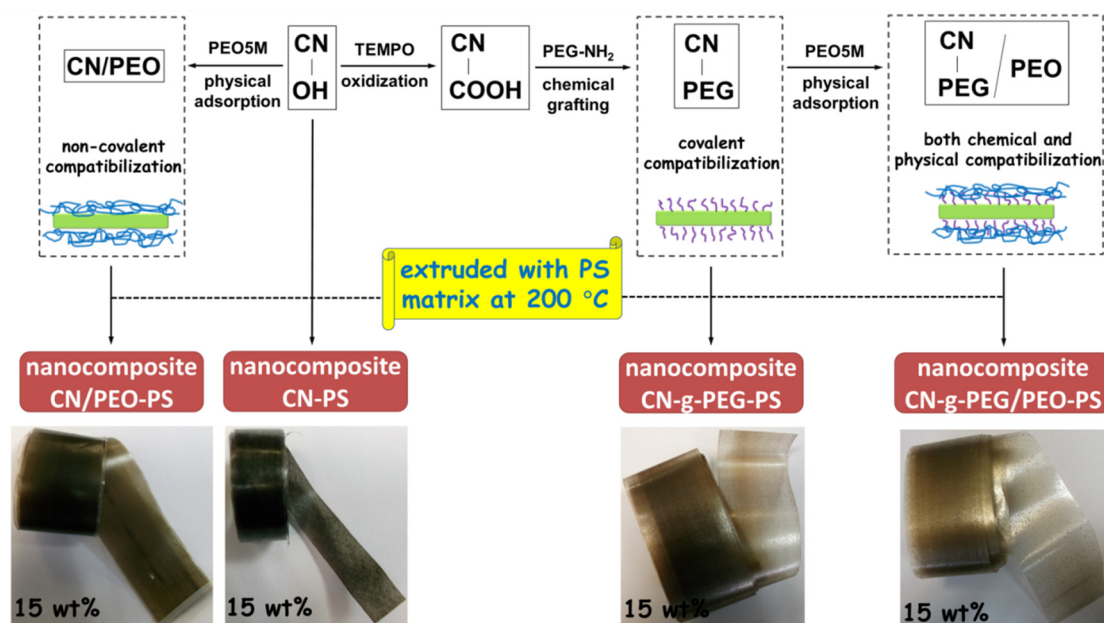
the extraction and production of cellulose nanocrystals, additional surface sulfate groups result in the weakness of their thermal stability (as discussed in the previous work Chapter 2), and limit the thermal processing temperature of cellulose nanocrystal-based composites. Another issue is the inherent incompatibility between cellulose nanoparticles and non-polar molecules (polymeric matrix). During the thermal processing, irreversible self-aggregation of cellulose nanocrystals ascribed to their hydrophilic nature causes weak interfacial adhesion (even microphase separation) between nanoparticles and matrix, and finally induces inferior performances of composites. All of these issues have mainly restricted the practical utilization of melt-compounding to process cellulose nanocrystal-based composites.

In order to improve the thermal stability and promote the compatibility of cellulose nanocrystals with non-polar polymeric matrices during the extrusion process, a novel strategy involving a double-polymer-layer protection and physical and/or chemical compatibilization of cellulose nanocrystals was proposed as shown in the “Schematic diagram”. In this work, cotton cellulose nanocrystals (CNs) were prepared by sulfuric acid hydrolysis. The chemical compatibilization of cellulose nanocrystals (CN-g-PEG) was realized by surface grafting of low molecular weight poly(ethylene glycol) (PEG5000) through chemical carboxylation–amidation reaction. The physical compatibilization of cellulose nanocrystals (CN/PEO) was performed by surface interaction with high molecular weight polyoxyethylene (PEO5M) through physical blending. Meanwhile, because of possible entanglements and interactions between both polymeric chains (PEG and PEO with the same chemical structure), two-layer-modified cellulose nanocrystals (CN-g-PEG/PEO) can be developed, which can induce double-polymer-layer protection and both covalent and non-covalent compatibilization of cellulose nanocrystals in polymer nanocomposites. It was shown that the different surface modification strategies brought cellulose nanocrystals distinct thermal behaviors during extrusion processing. Both CN-g-PEG and CN-g-PEG/PEO nanocrystals showed improved thermal stability, while CN and CN/PEO seriously degraded and carbonized during extrusion. The comparison of

adsorbing PEO capacity between CN and CN-g-PEG was also discussed and it was proved that CN-g-PEG can adsorb about 60 wt% (corresponding to CN-g-PEG weight) PEO chains, but CN can't or can only adsorb a small amount of PEO chains.

Then, four series of extruded nanocomposites were prepared with various loading levels of neat or modified cellulose nanocrystals using polystyrene (PS) as polymeric matrix. Interestingly, only double-polymer-layer modified nanocrystals reinforcing composites (CN-PEG/PEO-PS) were translucent and gave a good appearance. The microstructural analysis of extruded composites indicated that two-layer polymers covering the surface of cellulose nanocrystals can not only protect the nanoparticles from thermal degradation but also facilitate the interactions between nanocrystals and PS matrix. The investigation of mechanical properties, thermal properties, and water vapor barrier performances of extruded composites further proved the different effects of chemical and/or physical compatibilization of modified cellulose nanocrystals.

Schematic diagram of extruded cellulose nanocrystals (CN) reinforced polystyrene (PS) nanocomposites with physical and/or chemical compatibilization



RESUME FRANÇAIS

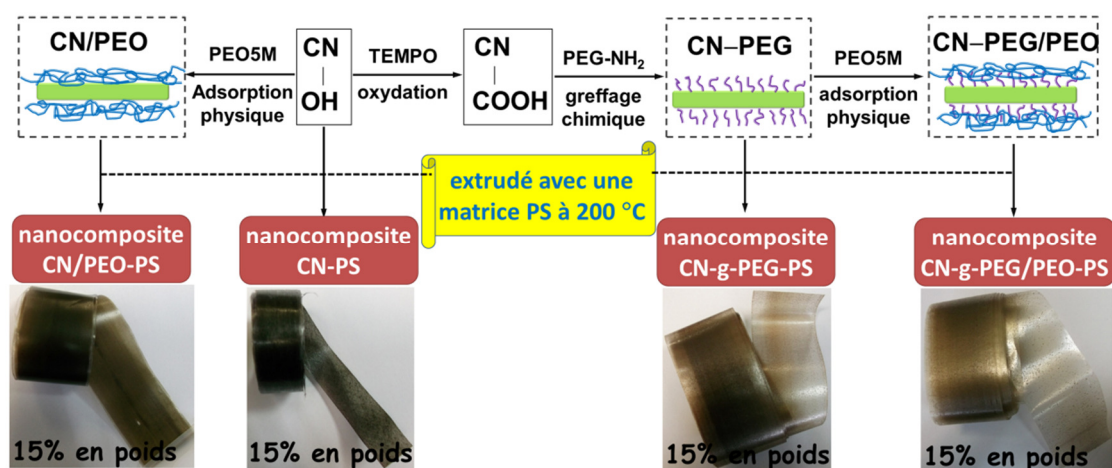
Depuis la première étude en 1995,¹ les nanocristaux de cellulose ont été largement utilisés comme additif de renfort pour améliorer les performances mécaniques d'un large éventail de composites à base de plastique en raison de leurs remarquables propriétés mécaniques. Généralement, les valeurs communément admises pour la résistance et le module des nanocristaux de cellulose sont de l'ordre de 10 GPa et 100-160 GPa, respectivement, valeurs qui sont comparables à celles du Kevlar. Récemment, sur la base du modèle de la structure atomique de la cellulose couplé avec la mécanique quantique, le module d'Young du nanocristal de cellulose a été estimé à 206 GPa,² ce qui montre que cette nanoparticule spéciale présente même une rigidité similaire à celle de l'acier et a fortement favorisé son utilisation dans le développement de nouveaux matériaux composites. De fait, selon l'analyse statistique de Future markets Inc, environ la moitié de la demande (46%) pour la nanocellulose (incluant nanocristaux de cellulose et cellulose microfibrillée) par les utilisateurs finaux se concentre sur son application composite.³

Le développement des composites à base de nanocristaux cellulosiques est cependant tributaire de deux questions fondamentales qui méritent d'être soulignées, à savoir la méthode de mise en forme du composite et la compatibilité entre les nanoparticules et la matrice. Fondamentalement, quatre méthodes principales sont généralement utilisées pour la mise en œuvre des matériaux composites à base de nanocristaux de cellulose, qui sont la coulée-évaporation, le mélange à l'état fondu, l'électrofilage et l'assemblage couche par couche.⁴ En particulier, les techniques de coulée-évaporation et de mélange à l'état fondu sont couramment utilisés pour la préparation de matériaux composites à base de nanocristaux de cellulose en raison de leur manipulation facile. Plus spécifiquement, la mise en forme par le procédé de coulée-évaporation permet de préserver l'état d'individualisation des nanoparticules résultant de leur dispersion colloïdale dans un milieu liquide. Cependant, cette technique est non-industrielle, non économique et montre certaines limitations en ce qui concerne le choix de la matrice polymère. Dans l'industrie, les techniques de

mise en forme à l'état fondu, telles que l'extrusion ou le moulage par injection, sont couramment utilisées pour mettre en œuvre les polymères thermoplastiques parce que ce sont des procédés "verts" (sans solvant), efficaces et économiques. Toutefois, en raison de l'utilisation très répandue de l'hydrolyse à l'acide sulfurique (avec une bonne efficacité et améliorant la stabilité colloïdale) pour l'extraction et la production de nanocristaux de cellulose, des groupes sulfate de surface additionnels se forment ce qui conduit à une réduction de leur stabilité thermique (comme décrit dans l'étude précédente chapitre 2) et limite la température de mise en œuvre thermique des matériaux composites à base de nanocristaux de cellulose. Un autre problème est l'incompatibilité inhérente entre les nanoparticules de cellulose et des molécules non-polaires (matrice polymère). Pendant la transformation thermique, l'auto-agrégation irréversible des nanocristaux de cellulose attribuée à leur nature hydrophile entraîne une faible adhérence interfaciale (et même une micro-séparation de phase) entre les nanoparticules et la matrice, et induit au final de piètres performances aux composites. Tous ces aspects ont essentiellement restreint l'utilisation pratique de la transformation à l'état fondu pour mettre en œuvre les composites à base de nanocristaux cellulosiques. Afin d'améliorer la stabilité thermique et de promouvoir la compatibilité des nanocristaux de cellulose avec des matrices polymères non polaires au cours du processus d'extrusion, une nouvelle stratégie impliquant une double couche polymère physique et/ou chimique protectrice et compatibilisante des nanocristaux de cellulose a été proposée comme illustré dans le "schéma de principe". Dans cette étude, les nanocristaux de cellulose de coton (CNs) ont été préparés par hydrolyse à l'acide sulfurique. La compatibilisation chimique des nanocristaux de cellulose (CN-g-PEG) a été réalisée par greffage en surface de poly (éthylène glycol) (PEG5000) de faible poids moléculaire par réaction chimique de carboxylation-amidation. La compatibilisation physique des nanocristaux de cellulose (CN/PEO) a été réalisée par interaction de surface avec un polyoxyéthylène (PEO5M) de poids moléculaire élevé par mélange physique. Parallèlement, en raison de l'enchevêtrement et des interactions possibles entre les deux chaînes polymères (PEG et PEO avec la même structure chimique), des

nanocristaux de cellulose modifiés avec deux couches (CN-g-PEG/PEO) ont pu être préparés, ce qui peut induire une double-couche polymère de protection et compatibilisation à la fois covalente et non covalente des nanocristaux de cellulose dans les nanocomposites polymères. Nous avons observé que les différentes stratégies de modification de la surface des nanocristaux de cellulose conduisent à des comportements thermiques distincts au cours de la transformation par extrusion. Les nanocristaux CN-g-PEG et CN-g-PEG/PEO ont montré une stabilité thermique améliorée, alors que les nanocristaux CN et CN/PEO sont sérieusement dégradés et carbonisés lors de l'extrusion. La capacité d'adsorption du PEO par les nanocristaux CN et CN -g-PEG a également été discutée et il a été montré que le CN-g-PEG peut adsorber environ 60% (par rapport à la masse de CN-g-PEG) de chaînes de PEO, tandis que les nanocristaux CN ne peuvent pas ou ne peuvent adsorber qu'en faible quantité les chaînes de PEO.

Schéma de principe de la préparation des nanocomposites extrudés à base de polystyrène (PS) renforcé par des nanocristaux de cellulose (CN) compatibilisés physiquement et/ou chimiquement



Par la suite, quatre séries de nanocomposites extrudés ont été préparés avec différents taux de nanocristaux de cellulose vierges ou modifiés en utilisant du polystyrène (PS) comme matrice polymère. Il est intéressant de noter que seuls les composites renforcés avec des nanocristaux de cellulose modifiés avec une double couche polymère (CN-PEG/PEO-PS) étaient translucides et avaient un bon aspect.

L'analyse microstructurale des matériaux composites extrudés a montré que les deux couches polymères en surface des nanocristaux de cellulose permettent non seulement de protéger les nanoparticules de la dégradation thermique, mais également de faciliter les interactions entre les nanocristaux et la matrice PS. L'étude des propriétés mécaniques, des propriétés thermiques et des performances de barrière à la vapeur d'eau des composites extrudés ont souligné les différents effets de la compatibilisation chimique et/ou physique des nanocristaux de cellulose modifiés.

References:

1. Favier, V.; Canova, G. R.; Cavallé, J. Y.; Chanzy, H.; Dufresne, A.; Gauthier, C. Nanocomposite materials from latex and cellulose whiskers. *Polym. Adv. Technol.* **1995**, *6*, 351–355.
2. Dri, F. L.; Hector Jr., L. G.; Moon, R. J.; Zavattieri, P. D. Anisotropy of the elastic properties of crystalline cellulose I_β from first principles density functional theory with Van der Waals interactions. *Cellulose* **2013**, *20*, 2703–2718.
3. The global market for nanocellulose to 2017; Futures Markets Inc., Edinburgh, Lothian EH74NA, United Kingdom, 2012, pp. 1–66.
4. Dufresne, A. "Nanocellulose. From nature to high performance tailored materials". 2012 by Walter de Gruyter GmbH, Berlin/Boston. pp. 235–275.

The work in this chapter is originated from:

Ning Lin and Alain Dufresne, Physical and/or chemical compatibilization of extruded cellulose nanocrystal reinforced polystyrene nanocomposites. *Macromolecules* 2013, 46, 5570–5583.

Chapter 3. Physical and/or Chemical Compatibilization of Extruded Cellulose Nanocrystal Reinforced Polystyrene Nanocomposites

Ning Lin and Alain Dufresne

The International School of Paper, Print Media and Biomaterials (Pagora), Grenoble Institute of Technology (Grenoble INP), CS10065, 38402 Saint Martin d'Hères Cedex, France

ABSTRACT

Impressive mechanical properties and reinforcing capability make cellulose nanocrystal (CN) a promising candidate as biomass nanofiller for the development of polymer-based nanocomposites. With the recent announcement of large-scale CN production, the use of industrial processing techniques for the preparation of CN-reinforced nanocomposites, such as extrusion, is highly required. However, low thermal stability of sulfuric acid-prepared CN limits the processing since most polymeric matrices are processed at temperatures close to 200 °C or above. It has been proved that surface interactions of polymers on CN as compatibilizer, such as hydrophilic polyoxyethylene (PEO), can improve its thermal stability due to the shielding and wrapping of PEO. However, the weak combination between CN and PEO allows the free movement of surface polymer, which can induce the self-aggregation of CN and microphase separation in composites especially during melt processing. Using carboxylation–amidation reaction, short poly(ethylene glycol) (PEG) chains can be first grafted on the surface of the nanocrystals, and immobilize long PEO chains on modified nanocrystals through physical adsorption and entanglement. Two polymeric layers should further improve the thermal stability of CNs, and surface polymeric chains should provide significant dispersibility and compatibilization for extruded nanocomposites. Rheological analysis showed better

PEO adsorption for PEG-grafted nanocrystals than pristine CN. Results from AFM and SEM revealed homogeneous dispersion and good compatibility of modified nanocrystals in PS matrix. Finally, the thermal, mechanical, and barrier properties of ensuing nanocomposites have been investigated to study the effect of physically and/or chemically modified nanocrystals.

KEYWORDS

Cellulose Nanocrystals, Polystyrene, Compatibilization, Extrusion, Nanocomposites

3.1 Introduction

Using controlled strong acid hydrolysis, needle-like or rod-like nanocrystals can be produced by breaking down cellulose fibers and isolating the crystalline domains. With their impressive mechanical properties, such as longitudinal modulus close to 150 GPa, high aspect ratio (10–70) and surface area (few 100 m²/g), cellulose nanocrystals (CNs) have proven to be an ideal candidate as reinforcing bionanofiller for polymeric matrices,^{1–4} since the first demonstration in 1995.⁵ The mass production of CNs, which should increase upward of multiple tons per day in the future, gives a strong boost for their application in composites at industrial scale. According to the forecasting of Future Markets Inc., the production of nanocellulose (including CNs and nanofibrillated cellulose) will increase by 1000% in the next two years, and will likely increase by further 500% at least by 2017.⁶

Apart from their large-scale industrial production, the processing of CN-based nanocomposites is another crucial issue since it determines their usage properties for practical applications. Two challenges deserve more attention during the processing of nanocomposites: (1) the balance between compounding method and dispersion and (2) the compatibility of nanocrystals in polymeric matrices. Wet processing methods such as casting/evaporation, using polymer solution or polymer dispersion (latex) in liquid medium are commonly used in most studies of composites reinforced with CNs.^{7,8} The main advantage of this technique is the preservation of the dispersion state of the nanoparticles in the liquid medium. However, the range of available polymeric matrices is restricted, and this processing technique is both nonindustrial and noneconomic. Melting-compounding techniques, such as extrusion or injection molding, are probably the most convenient processing techniques for the industrial production of CN-based nanocomposites, because of being a green process together with large-scale production and economical availability. Extrusion is a high volume manufacturing process in which polymeric solid material is transported by a screw and progressively melted to form a continuous profile by passing through a die. However, in most scientific studies, this conventional processing technique is

infrequently employed for the preparation of CN-reinforced polymer nanocomposites. This is ascribed to low thermal stability of cellulose and inherent incompatibility between cellulose and most synthetic polymers issues.⁹ The hydrophilic nature of cellulose causes irreversible agglomeration during drying and incompatibility with nonpolar matrices because of the formation of additional hydrogen bonds between nanoparticles. Moreover, because of the introduction of sulfate groups resulting from common acid hydrolysis procedure involving sulfuric acid, CNs present inferior thermal stability with degradation temperature lower than 150 °C. However, most polymeric matrices from petrochemical synthesis are melt and processed at 200 °C or above,¹⁰ which requires higher thermal stability for CNs.

On the basis of previous studies for different nanocomposite systems reinforced with CNs, three strategies are commonly used in the processing of CN based nanocomposites by melt compounding, in order to enhance the compatibility between hydrophilic nanoparticles and hydrophobic matrices.⁹ If a polar polymer is used as matrix, there is no a priori need to compatibilize the filler with the matrix material.^{11,12} For nonpolar polymeric matrices, surface functionalization, such as grafting of hydrophobic moieties or chemical derivatization, can be conducted to tune the compatibility between nanoparticles and matrix.¹³⁻¹⁷ Finally, adsorption of surfactants or macromolecules on the surface of CNs was also attempted to be used as processing aids to compatibilize cellulose nanoparticles and matrix.¹⁸⁻²²

The challenge of melt processing for CN is to find the suitable treatment to both improve the thermal stability and avoid the issues of inherent incompatibility between cellulose and most polymeric matrices. In a previous work, we have demonstrated that physical interaction of polyoxyethylene (PEO) chains on the surface of CNs can improve dispersibility and thermal stability of nanocrystals during the melt processing of low-density polyethylene (LDPE) based nanocomposites.¹⁸ The improved thermal stability of PEO-adsorbed CNs was ascribed to a protection role of wrapped PEO chains that hides the surface sulfate groups of nanocrystals. On the other hand, it has been proved that chemical functionalization on the surface of CNs is a most effective

approach to avoid irreversible agglomeration during drying, and enhance the compatibility between nanoparticles and nonpolar matrices.^{13,23} In this work, surface modification through physical interaction and/or chemical grafting was performed on cellulose nanocrystals, which produces three different types of modified nanocrystals, viz. CN/PEO, CN-g-PEG, and CN-g-PEG/PEO. Together with pristine CN, the reinforcing effect and interfacial mechanisms of four types of nanocrystals extruded with polystyrene were investigated. The PEG-covalent and PEO-noncovalent compatibilization treatments affect the thermal stability of CN and rheological properties in different ways. Moreover, with the combination of strategies of grafting PEG and adsorbing PEO, novel modified nanocrystals, CN-g-PEG/PEO, can be prepared bearing two protective layers for CNs in order to adapt to the conditions of high temperature extrusion. It is supposed that with the common carboxylation–amidation reaction, the short grafted PEG chains (molecular weight 5000 g/mol) will evenly cover the surface of nanocrystals, which provide the first polymeric layer on nanocrystals. Because of the same chemical structure and hydrophilic property, long PEO chains (molecular weight 5×10^6 g/mol) can be tightly coupled on CN-g-PEG nanoparticles through entanglement and physical adsorption. Meanwhile, the immobilization of PEO5M by grafted PEG will restrict the free self-aggregation of the polymer during the processing by extrusion. As the second polymeric layer, PEO5M will play the shielding effect to surface sulfate groups of nanocrystals, and also act as a polymer compatibilizer between rigid nanofiller and polymeric matrix.

3.2 Experimental Methodology

3.2.1 Materials

Native cotton fibers were obtained from Whatman filter paper. Sodium hypochlorite (NaClO) solution was reagent grade and the available chlorine was 10–15%. Methoxypoly(ethylene glycol) amine (MPEG–NH₂) with an average molecular weight (M_w) 5000 g/mol was used in the grafting reaction with an amine loading

content ≥ 0.17 mmol/g. Polyoxyethylene (PEO5M) with $M_w = 5 \times 10^6$ g/mol was used for the physical compatibilization. Polystyrene (PS) with a density 1.047 g/mL and $M_w = 2.8 \times 10^5$ g/mol was chosen as the matrix for the processing of nanocomposites. TEMPO (C₉H₁₈ON, 98%), sodium bromide (NaBr), hydrochloric acid (HCl, 33%), sulfuric acid (H₂SO₄, 98%), *N*-(3-Dimethylaminopropyl)-*N*'-ethylcarbodiimide hydrochloride (EDC), *N*-hydroxysuccinimide (NHS) and other reagents were used without further treatment. All the chemicals and materials were purchased from Sigma–Aldrich.

3.2.2 Extraction of Cellulose Nanocrystals from Cotton Fiber

Cellulose nanocrystals (CNs) were prepared by H₂SO₄ hydrolysis of native cotton fiber, according to our previous literature.²⁴ The fiber was milled with a laboratory milling device to obtain a fine particulate substance and extracted in 2 wt% NaOH solution (50.0 g of fibers for 2 L solution) for 12 h at room temperature and then filtered and rinsed with distilled water. Acid hydrolysis was performed at 45 °C with 65 wt% H₂SO₄ (preheated), for 45 min under mechanical stirring (50.0 g of fibers for 1 L acid solution). Amorphous or paracrystalline regions of cellulose were preferentially hydrolyzed, whereas crystalline regions that have higher resistance to acid attack remained intact. The suspension was diluted with ice cubes to stop the reaction and washed until neutrality by successive centrifugations at 10,000 rpm (rotation per minute) for 10 min each step, and dialyzed against distilled water for five days. After dialysis, the CN dispersion was completed by ultrasonic treatment using a Branson sonifier, and finally the released CN powder was obtained by freeze-drying.

3.2.3 Carboxylation of Cellulose Nanocrystals

TEMPO-mediated oxidation of CN was performed according to the procedure described in the literature.^{25,26} About 20.0 g of CN (123.530 mmol anhydroglucose unit AGU) was suspended in distilled water (1.5 L) and treated by ultrasonic dispersion for 10 min. TEMPO (0.579 g) and NaBr (6.353 g) were dissolved in another 100 mL distilled water and added dropwise to the nanocrystal suspension. A certain amount of 12 wt% NaClO solution was added slowly to the suspension to start the oxidizing

reaction. The pH of the mixture was maintained at 10.0 by adding 0.5 M NaOH, while stirring the suspension for 4 h at room temperature. After oxidation, the reaction was quenched by adding ethanol (ca. 20 mL), and 0.5 M HCl was slowly added to the suspension to adjust the pH to 6.5–7.0. The oxidized cellulose was converted from sodium carboxylate groups (–COONa) to free carboxyl groups (–COOH). The suspension was washed thoroughly with water and then dialyzed for 24 h. Finally, by freeze-drying, the oxidized CN (OCN) powder was obtained.

3.2.4 Chemical Grafting of PEG5000 on Cellulose Nanocrystals

Grafting of PEG5000 onto nanocrystals was performed with the carboxylation–amidation reaction creating a covalent amide bond between a primary amine-terminated polymer and carboxylated CN by COOH–NH₂ coupling.²⁷ It was reported that during this reaction, the addition of NHS to EDC and amidation at neutral pH was critical to avoid the formation of the detrimental stable N-acyl urea instead of the desired amide product.²⁸ The grafting reaction was achieved in aqueous media with the addition of 1.2 mmol –NH₂/1 mmol –COOH. The pH of the suspension was adjusted to 7.5, and maintained throughout the reaction by adding 0.5 M HCl or 0.5 M NaOH solutions. Then, the solution containing EDC and NHS was added in the CN suspension, both 1.5 times equivalent to the carboxyl content. The reaction was carried out for 24 h at 50 °C, and finally coagulated by adding an excess of ethanol. After the reaction, the sample was dialyzed thoroughly against distilled water to remove excess reagents and free MPEG–NH₂.

3.2.5 Physical Adsorption of PEO5M on Pristine and Modified Nanocrystals

The weight ratio of PEO5M and nanocrystals was controlled as 35/65 during the process of physical adsorption. The typical procedure was taken from our previous paper as reference:¹⁸ PEO solutions were prepared by adding 1.25 wt% of the polymer in distilled water. The solution was protected against light by an aluminum foil and weakly stirred at 500 rpm for 4 days at room temperature. The desired amount of pristine (CN) or grafted nanocrystal (CN-g-PEG) aqueous suspension was added to the PEO solution. The proper amount of distilled water was then added to reach a

final PEO concentration in water of 1 wt%, and the mixture was stirred for 5 h. Finally, the suspension was freeze-dried to obtain the solid products.

3.2.6 Preparation of Nanocomposites from Cellulose and Polystyrene by Extrusion

Nanocomposites from unmodified and modified cotton nanocrystals reinforced PS matrix were prepared by twin-screw extrusion. The lyophilizate of nanocrystals and PS pellets were introduced in the mixing chamber of a twin-screw DSM Micro 15 compounder with the following mixing conditions: 200 °C at 150 rpm for 10 min. Extrusion was carried out with a slit die of 0.6 mm in width and 1 cm in length. Four kinds of nanocrystals, namely pristine nanocrystals, PEO5M-physically adsorbed nanocrystals, PEG5000-chemically grafted, and nanocrystals with both chemical PEG5000 grafting and physical PEO5M adsorption, were used to enhance the performance of PS nanocomposites, which were marked as CN–PS, CN/PEO–PS, CN-g-PEG–PS and CN-g-PEG/PEO–PS, respectively. Extruded films prepared from pure polystyrene were coded as PS–F. The compositions and labels for nanocomposites with different nanocrystal contents are shown in Table 3.1.

Table 3.1 Composition of the various extruded nanocomposites.

[PEG-grafting efficiency for CN-g-PEG from elemental analysis: 21.77 wt%; CN (or CN-g-PEG) : PEO5M = 65 : 35 (w/w)]

Nanocomposite	PS	CN	PEO	PEG	Nanocomposite	PS	CN	PEO	PEG
PS-F	100	0	0	0	PS-F	100	0	0	0
CN-PS-2	98.0	2.0	0	0	CN/PEO-PS-2	96.9	2.0	1.1	0
CN-PS-5	95.0	5.0	0	0	CN/PEO-PS-5	92.3	5.0	2.7	0
CN-PS-8	92.0	8.0	0	0	CN/PEO-PS-8	90.7	8.0	4.3	0
CN-PS-12	88.0	12.0	0	0	CN/PEO-PS-12	81.5	12.0	6.5	0
CN-PS-15	85.0	15.0	0	0	CN/PEO-PS-15	76.9	15.0	8.1	0
CN-g-PEG-PS-2	97.4	2.0	0	0.6	CN-g-PEG/PEO-PS-2	96.0	2.0	1.4	0.6
CN-g-PEG-PS-5	93.6	5.0	0	1.4	CN-g-PEG/PEO-PS-5	90.2	5.0	3.4	1.4
CN-g-PEG-PS-8	89.8	8.0	0	2.2	CN-g-PEG/PEO-PS-8	84.3	8.0	5.5	2.2
CN-g-PEG-PS-12	84.7	12.0	0	3.3	CN-g-PEG/PEO-PS-12	76.5	12.0	8.2	3.3
CN-g-PEG-PS-15	80.8	15.0	0	4.2	CN-g-PEG/PEO-PS-15	70.5	15.0	10.3	4.2
CN-g-PEG-PS-20	74.4	20.0	0	5.6	CN-g-PEG/PEO-PS-20	60.6	20.0	13.8	5.6

3.2.7 Characterization and Analyses

Fourier Transform Infrared Spectroscopy (FTIR): Infrared spectra were recorded at room temperature on a FTIR Perkin-Elmer Spectrum One spectrometer to characterize the surface modification of nanocrystals. All freeze-dried samples were prepared as KBr pellets (1 wt% in anhydrous KBr), and analyzed using a spectral width ranging from 4000 to 400 cm^{-1} with a 2 cm^{-1} resolution and an accumulation of 32 scans.

X-ray Photoelectron Spectroscopy (XPS): The chemical modification through PEG chains grafting on the surface of nanocrystals was further analyzed by XPS. The experiments were carried out using an XR3E2 apparatus (Vacuum Generators, U.K.) equipped with an unmonochromated Mg KR X-ray source (1253.6 eV) and operated at 15 kV under a current of 20 mA. Samples were placed in an ultrahigh vacuum chamber (10^{-8} mbar) with electron collection by a hemispherical analyzer at a 90° angle. Signal decomposition was done using Spectrum NT, and the overall spectrum was shifted to ensure that the C–C/C–H contribution to the C 1s signal occurred at 285.0 eV.

Elemental Analysis: Elemental analysis was used to determine the PEG grafting efficiency on nanocrystals, which was performed at Analysis Central Service of the Centre National de la Recherche Scientifique (Vernaison, France). The carbon, oxygen, hydrogen and nitrogen element contents for both CN–COONa and CN-g-PEG samples were measured. PEG-grafting efficiency ($GE\%$) was calculated according to eq. 3.1:

$$GE\% C_{MPEG} + (1 - GE\%) C_{CN} = C_{CN-g-PEG} \quad (3.1)$$

where C is the relative carbon content of the sample. The precision of the measurement is considered to be 0.3% for C and H elements and 0.5% for O element.

X-ray Diffraction (XRD) Analysis: To investigate the effect of PEG grafting and PEO adsorption on cellulose nanocrystals, X-ray measurements were carried out on pristine nanocrystals, pure PEO, and modified nanocrystals. The X-ray diffraction patterns

were recorded on a Philips PW 1720 X-ray generator operated at 30 kV and 20 mA with Cu K α radiation ($\lambda = 0.154$ nm) in the range $2\theta = 5\text{--}50^\circ$ for samples using a fixed time mode with a step interval of 0.02° .

Atomic Force Microscopy (AFM): The morphology of CN, CN-COONa, and CN-g-PEG was observed with AFM. The suspensions of approximately 0.01 wt% were dispersed in water with ultrasonic dispersion for 30 min and then deposited on the mica substrate. The suspension of CN/PEO or CN-g-PEG/PEO complex was magnetically stirred for 1 h, and then deposited on the mica substrate. The substrate loaded with nanoparticles was imaged in tapping mode with a Nanoscope IIIa microscope from Veeco Instruments. Silicon cantilevers, with a typical radius of curvature of 10–15 nm, were used to perform the imaging at a frequency of 264–339 kHz.

The surface morphology of extruded nanocomposite (CN-g-PEG/PEO-PS-20) was investigated by AFM under QNM mode analysis. The film sample was placed on the surface of steel substrate, which was scanned at a frequency < 1 Hz, and changing the rate according to the scan size. In order to observe the morphology of modified nanocrystals in extruded composites, CN-g-PEG/PEO-PS-20 film was dissolved in tetrahydrofuran (THF), and exchanged with acetone to remove most of PS chains. The acetone suspension containing CN-g-PEG/PEO nanoparticles was dropped on the mica substrate, and imaged in tapping mode.

Thermogravimetric Analysis (TGA): The contents of grafted PEG and absorbed PEO on the surface of nanocrystals were determined by thermogravimetric analysis using a thermal analyzer Perkin-Elmer TGA-6 under nitrogen flow. Freeze-dried samples of ca. 10 mg were heated from 30 to 500 °C at a heating rate of 10 °C/min.

Contact Angle Measurements: The surface hydrophilicity of cellulose before and after modification was investigated using contact angle measurement, which was performed at room temperature using a sessile drop contact angle system at Attension Theta contact angle meter. Freeze-dried nanocrystals were compacted under a pressure of 10 MPa with a KBr press to obtain samples with smooth surfaces. A small

drop of water (ca. 5 μL) was deposited on the surface of the sample, while 20 pictures were taken over a period of 10 s. Attension Theta Software was used to calculate the contact angle.

Rheological Behavior of CN or CN-g-PEG and PEO Mixtures: To investigate the capacity of CN-g-PEG and CN to adsorb PEO5M chains, the viscosity of various suspensions containing nanoparticles and PEO5M chains was analyzed with a rotational rheometer, Rheolyst Physica MCR-301. The cone and plate geometry, with a 50 mm diameter plate and an angle of 1° , was used. To prevent solvent evaporation during measurements, the geometry was enclosed in a solvent trap which saturates the atmosphere. The lower pan (sample chamber) was equipped with a Peltier thermoelectric device that insures a controlled temperature, fixed at $20\text{ }^\circ\text{C} \pm 0.1\text{ }^\circ\text{C}$. Viscosity of the suspension was recorded applying a flow cycle consisting in a continuously increasing shear rate ramp from 0.05 to 10 s^{-1} for 4 min. All rheological tests were performed in triplicate.

Transmittance of Visible Light: Transmittance of nanocomposite films was measured with a Shimadzu UV 2401-(PC) UV-vis spectrophotometer. The film samples were cut at $40\text{ mm} \times 35\text{ mm}$, and analyzed with the UV spectrophotometer within a wavelength range 200–800 nm. The transmittance spectra were acquired using air as background. The resolution of the spectrophotometer was 1.5 nm and the photometric accuracy was ± 0.01 in absorption.

Scanning Electron Microscopy (SEM): The microstructure and homogeneity of extruded nanocomposites were observed using SEM on a Quanta 200 FEI device (Everhart–Thornley detector). Before observation, the samples were cryofractured and gold-coated. The cross sections of nanocomposites were observed under an acceleration voltage of 10 kV.

Mechanical Properties: The mechanical properties of nanocomposites were investigated through dynamic mechanical analysis (DMA) measurement using a RSA3 (TA Instruments, USA) equipment working in the tensile mode. The strain amplitude was fixed at 0.05%, well below the limit of the linear viscoelastic regime.

The samples were thin rectangular strips with dimensions of about $10 \times 10 \times 0.1 \text{ mm}^3$. Measurement of the storage tensile modulus (E') was performed in isochronal condition (1 Hz), and the temperature was varied from -60 to $+150 \text{ }^\circ\text{C}$ at a heating rate of $5 \text{ }^\circ\text{C}/\text{min}$.

Thermal Properties: The thermal behavior of nanocomposites was investigated by both differential scanning calorimetry (DSC) and thermogravimetric analysis (TGA). The glass transition temperature of nanocomposites was measured with a Perkin-Elmer DSC instrument using aluminum pans. The samples were scanned from 25 to $250 \text{ }^\circ\text{C}$ at a heating rate of $10 \text{ }^\circ\text{C}/\text{min}$. The thermal degradation of nanocomposites was studied with a thermal analyzer Perkin-Elmer TGA-6 instrument under nitrogen flow in the temperature range from 30 to $600 \text{ }^\circ\text{C}$ at a heating rate of $10 \text{ }^\circ\text{C}/\text{min}$.

Barrier Properties: Direct water vapor permeability (WVP) was determined from the slope of the weight gain versus time curves at $25 \text{ }^\circ\text{C}$. The extruded films were sandwiched between the aluminum top (open O-ring) and bottom parts of a specifically designed permeability cell with screws containing 5.0 g of anhydrous calcium chloride (CaCl_2) to generate 0% relative humidity (RH). A Viton rubber O-ring was placed between the nanocomposite film and the bottom part of the cell to enhance sealability. Then, the cells were placed in the desired environment of 50% RH at $25 \text{ }^\circ\text{C}$, and the water vapor weight gain through the film was monitored as a function of time. Water weight gain was calculated as the total cell weight gain minus the gain through the sealing. All the tests were performed in duplicate, and WVP value for each nanocomposite was calculated as the average according to eq. 3.2:

$$\text{WVP (g/m} \cdot \text{S} \cdot \text{Pa)} = \frac{\Delta m \cdot e}{A \cdot \Delta t \cdot \Delta P} \quad (3.2)$$

where Δm is the mass increase (g) of the CaCl_2 sample, A is the area of the film ($4 \times 10^{-4} \text{ m}^2$), and Δt is the exposure time in the chamber. The thickness of the film is e and ΔP (1425.36 Pa) is the partial water vapor pressure difference across the film specimen corresponding to 50% RH at $25 \text{ }^\circ\text{C}$.

3.3 Surface Modification and Properties of Cellulose Nanocrystals

3.3.1 Surface Grafting of PEG on Cellulose Nanocrystals

Chemical grafting of PEG chains on the surface of cellulose nanocrystals was investigated by FTIR spectroscopy, as shown in Figure 3.1. Although the peaks for CN-g-PEG located at 2889, 1252, and 852 cm^{-1} were overlapped with cellulose component, the increase of intensity for these peaks still can be observed by comparing the spectra for CN-g-PEG and CN, which was ascribed to the coupling of PEG on nanocrystals. More evident changes for modified nanocrystals were presented in the spectrum range 1800–1500 cm^{-1} . Two additional peaks appeared at 1562 and 1705 cm^{-1} on the spectrum for PEG-grafted nanocrystals, corresponding to the stretching vibrations of amide groups and carboxyl groups, respectively.²⁷ These characteristic peaks were not visible on the spectrum for pure MPEG-NH₂. Moreover, it should be pointed out that the appearance of a stretching band at 1612 cm^{-1} on the spectrum for carboxylated (ungrafted) nanocrystals (CN-COONa) was assigned to salt forms of carboxylic acid, as reported in our previous work.²⁴

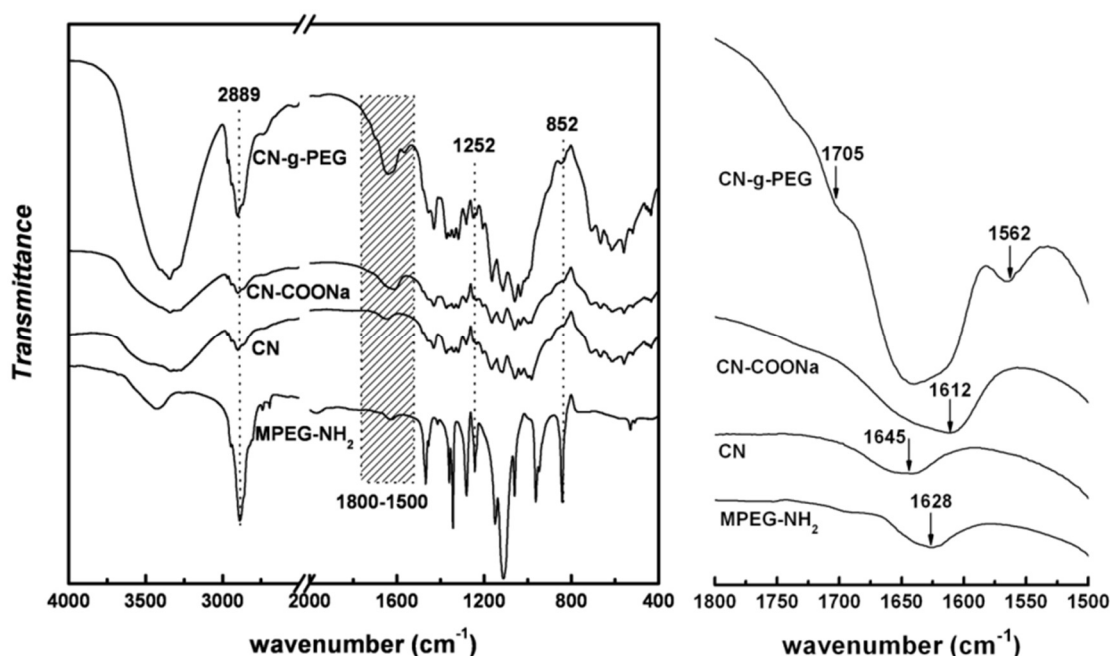


Figure 3.1 FTIR spectra for MPEG-NH₂, CN, CN-COONa, and CN-g-PEG.

Further verification and grafting efficiency for CN surface modification were realized by XPS and elemental analysis. As shown in Figure 3.2, on the general XPS spectra,

there were new signals corresponding to nitrogen (N 1s: 402 eV) and sodium (Na 1s: 1072 eV) assigned to the surface chemistry of CN-g-PEG and CN-COONa samples in comparison with CN. On the other hand, high resolution C 1s spectra were resolved into several components (Table 3.2) which were assigned to C–C/C–H (285 eV, the binding energy scale was changed according to this value as starting position), C–N (286.2 eV), C–O (286.5 eV), O–C–O/C=O (288.05 eV), O–C=O (289.0 eV). It was clear that in comparison with pristine CN and CN-COONa samples, only the spectrum of CN-g-PEG showed evident C–N peak, which corresponded to the covalent coupling from carbodiimide grafting reaction. Furthermore, from the ratio

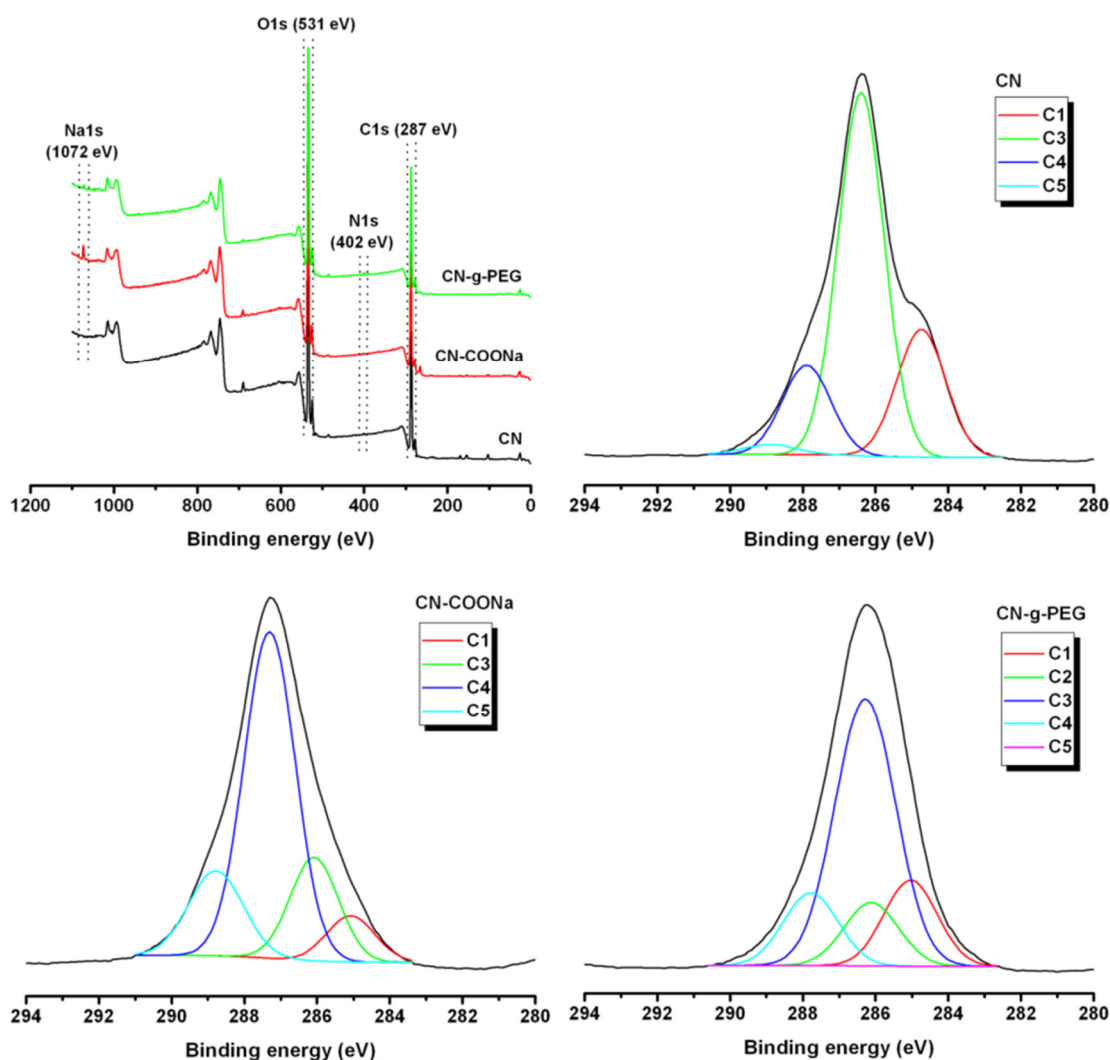


Figure 3.2 General XPS spectra for CN, CN-COONa, and CN-g-PEG with signal assignments; XPS decomposition of the C 1s signal into its constituent contributions for CN, CN-COONa, and CN-g-PEG.

change of different compositions of carbon signal, the proportion of C4 (C=O) and C5 (O-C=O) for CN-COONa sample increased obviously, which indicated the adequate surface modification of nanocrystals from hydroxyl groups to carboxyl groups. The grafting efficiency (GE %) of PEG chains for CN-g-PEG sample was determined from the results of elemental analysis reported in Table 3.2. Because of only surface carboxylation of cellulose nanocrystals, pristine CN and CN-COONa samples have similar chemical compositions, which exhibited small change of element contents (C, O, and H) for carboxyl nanocrystals. However, the significant difference in the elemental composition for pure cellulose and poly(ethylene glycol) provides the possibility to compare the elemental change before and after chemical grafting. The nitrogen content (0.43) for CN-g-PEG samples provided the critical result to prove the successful grafting reaction. Considering instrumental error and adsorption of moisture for hydrophilic materials during the delivery and manipulation, the values of grafting efficiency were confirmed mainly based on the data from carbon element, and calculated according to eq. 3.1 as 21.77 wt%, which was nearly in agreement with previous report (ca. 20–30 wt%).²⁷

Table 3.2 Surface functional group composition as obtained from the decomposition of the C1s signal; carbon, oxygen, hydrogen and nitrogen elements content from elemental analysis.

Samples	C1	C2	C3	C4	C5
	C-C/C-H	C-N	C-O	O-C-O/C=O	O-C=O
BE (eV)	285	286.2	286.5±0.1	288.05±0.05	289.0±0.1
CN	22.4	0.0	60.1	15.6	1.9
CN-COONa	7.9	0.0	17.5	58.4	16.2
CN-g-PEG	15.9	12.2	57.3	13.7	0.9
Samples	Carbon	Oxygen	Hydrogen	Nitrogen	GE ^a
	%	%	%	%	%
MPEG-NH ₂	55.37	36.31	9.29	0.10	—
CN	44.44	49.38	6.17	—	—
CN-COONa	44.13	48.80	6.13	—	—
CN-g-PEG	46.82	45.52	6.57	0.43	21.77

^a GE% is the grafting efficiency of PEG on nanocrystals according to the calculation using Equation (3.1).

3.3.2 Crystalline Structure

The changes in nanocrystal crystallinity induced by chemical grafting and/or physical adsorption were investigated by XRD analysis (Figure 3.3). Pure MPEG–NH₂ and PEO5M showed the same crystalline features at $2\theta = 19.2^\circ$, 22.5° – 23.5° . However, these characteristic peaks cannot be observed on the pattern for CN-g-PEG, which was attributed to the amorphous state of grafted PEG chains, and limited surface crystallization from relatively short chain length.^{27,29} The quite similar patterns for pristine CN, carboxylated CN–COONa, and grafted CN-g-PEG indicated the original integrity of cellulose crystal after chemical modification. In fact, from the calculation according to the Segal method,³⁰ the crystallinity index (I_c) of cellulose was about 90.67% for CN, 89.42% for CN–COONa, and 89.86% for CN-g-PEG. The main peak at $2\theta = 22.5^\circ$ (002) for cellulose shifted to 22.7° , and became broader. Meanwhile, new crystalline peaks at $2\theta = 19.2^\circ$, 26.2° , and 26.9° ascribed to PEG and/or PEO chains appeared on the patterns of these two complexes.

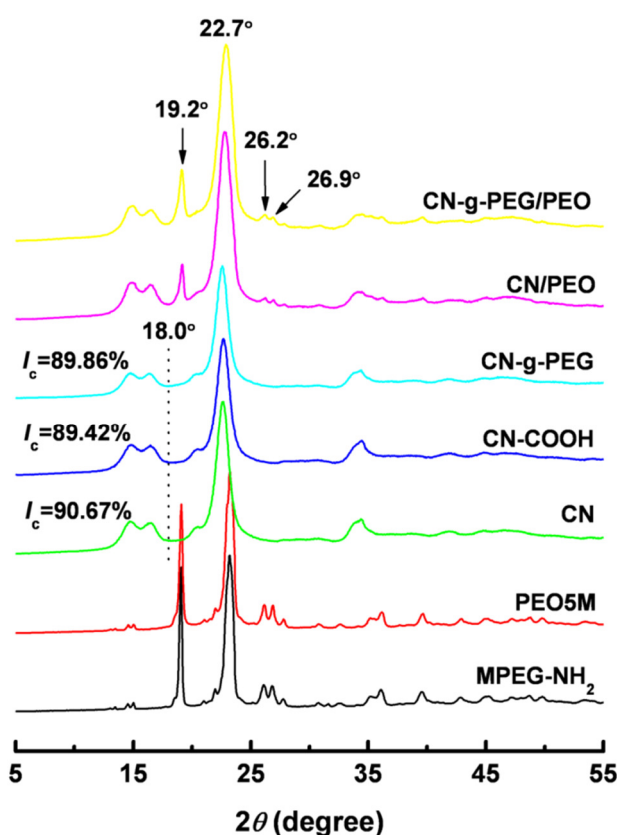


Figure 3.3 X-ray diffraction patterns for pure MPEG–NH₂, PEO5M, CN; CN–COONa, CN-g-PEG; and CN-g-PEG/PEO, CN/PEO complexes.

3.3.3 Morphology and Surface Adsorption

The morphology of pristine CN, chemically modified nanocrystals (CN-COONa and CN-g-PEG), and physically adsorbed complexes (CN/PEO and CN-g-PEG/PEO) were observed using AFM as shown in Figure 3.4. Pristine CN presented a typical rod-like morphology with a length of 100–300 nm and a diameter of 5–20 nm (image A). After carboxylation, CN-COONa also maintained the rod-like shape, and exhibited improved dispersibility in water (image B). Because of the electrostatic repulsion between grafted chains, CN-g-PEG showed much better dispersibility in water than unmodified nanocrystals (image C). By comparing the images for

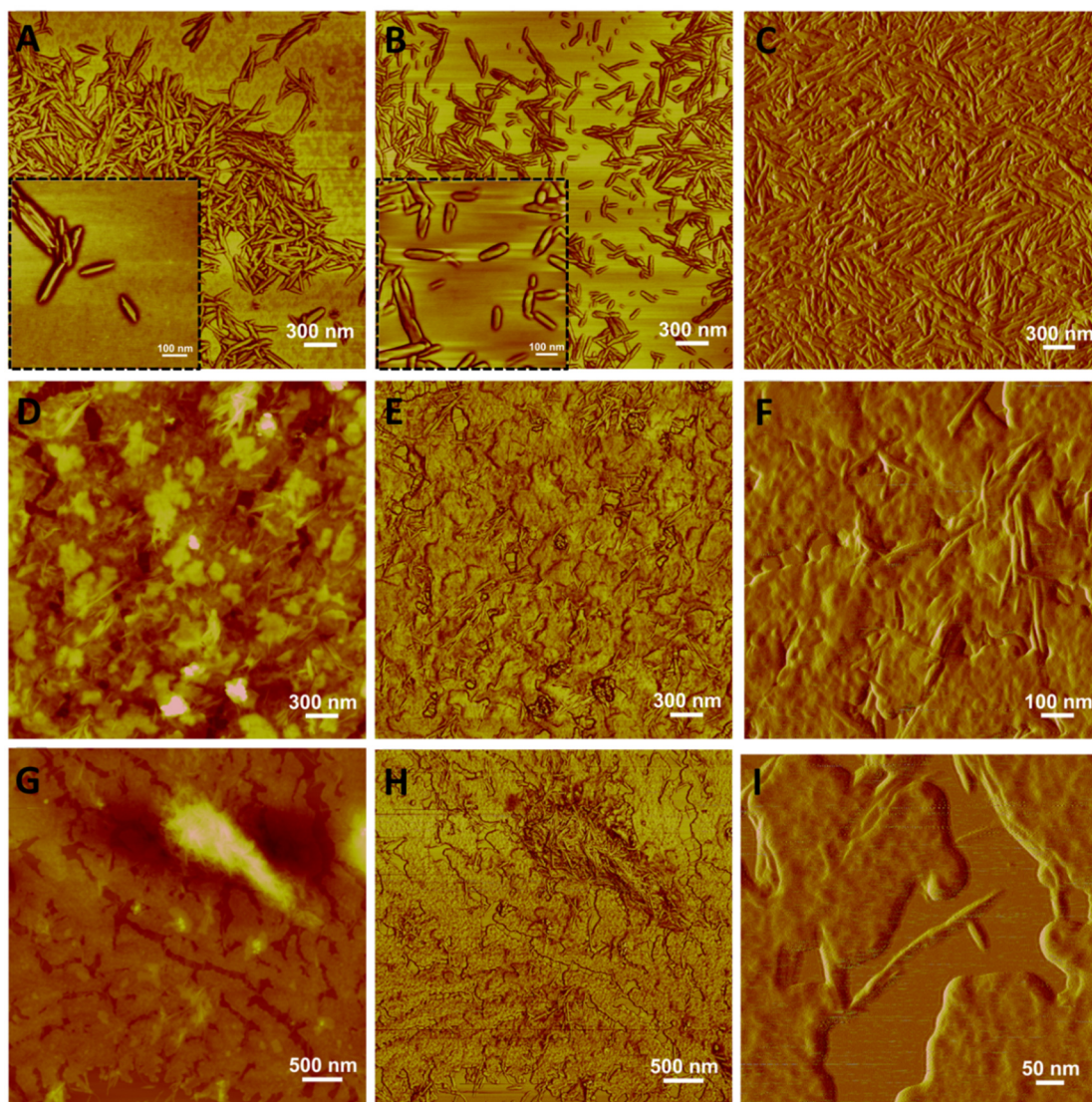


Figure 3.4 AFM images for (A) CN, (B) CN-COONa, (C) CN-g-PEG, (D–F) CN-g-PEG/PEO, and (G–I) CN/PEO.

CN-g-PEG/PEO and CN/PEO, some interesting observations can be found. Because of surface adsorption of high molecular weight polymer (PEO5M), these two samples tended to form a membrane on the substrate. For the complex with homogeneous adsorption and dispersion of nanoparticles, the images for the membrane are regular and ordered, just as CN-g-PEG/PEO in images D and E. Further observation at higher resolution (image F) indicated that nanocrystals embedded in the complex with the surrounding PEG and PEO chains. However, for the CN/PEO complex, a serious aggregation appeared (images G and H), which may include aggregated nanoparticles and/or PEO. In any case, the adsorption of PEO on pristine CN showed irregular arrangement and ineffective organization. With observation at higher resolution, it even appeared some isolated nanocrystals without any immobilization of PEO chain (image I). It was supposed that CN-g-PEG can adsorb PEO more efficiently, and regularly arrange these polymeric chains on the surface of CN-g-PEG; while pristine CN can only immobilize few amount of PEO, and many more polymeric chains should be free and away from nanoparticles. Three additional experiments, TGA for thermal properties, contact angle measurement for surface hydrophilicity, and rheological behavior of the suspensions, were performed to support this supposition.

3.3.4 Thermal Stability

The thermal degradation of nanocrystals before and after chemical and/or physical modification is shown in Figure 3.5. It is known that the presence of sulfate groups on the surface of CN induces the reduction of its thermal stability. This reduction of thermal stability depends on the density of sulfate groups and then hydrolysis conditions. Neat H₂SO₄-prepared CN starts to degrade from 150 °C (Figure 3.5). When PEO is adsorbed on the surface of CN, the degradation temperature of CN/PEO was slightly improved to about 160 °C. Moreover, a two-step degradation process was observed for CN/PEO. The low temperature process starting from 160 °C is most probably ascribed to the degradation of cellulose, and the high temperature process starting at 300 °C is possibly attributed to the degradation of PEO. These results revealed the limited adsorption and weak interaction between pristine nanocrystals

and PEO chains. With the surface grafting of PEG, CN-g-PEG showed a significant enhancement of the degradation temperature, which can be attributed to the uniform shield of sulfate groups induced by the coating with the grafted PEG layer. Regarding the CN-g-PEG/PEO complex, the thermal degradation was further improved, which presented only 5% weight loss at the temperature of 320 °C. This improvement can be explained by the covalent protection provided by the PEG layer, and the close connection and interaction between PEG and PEO chains.

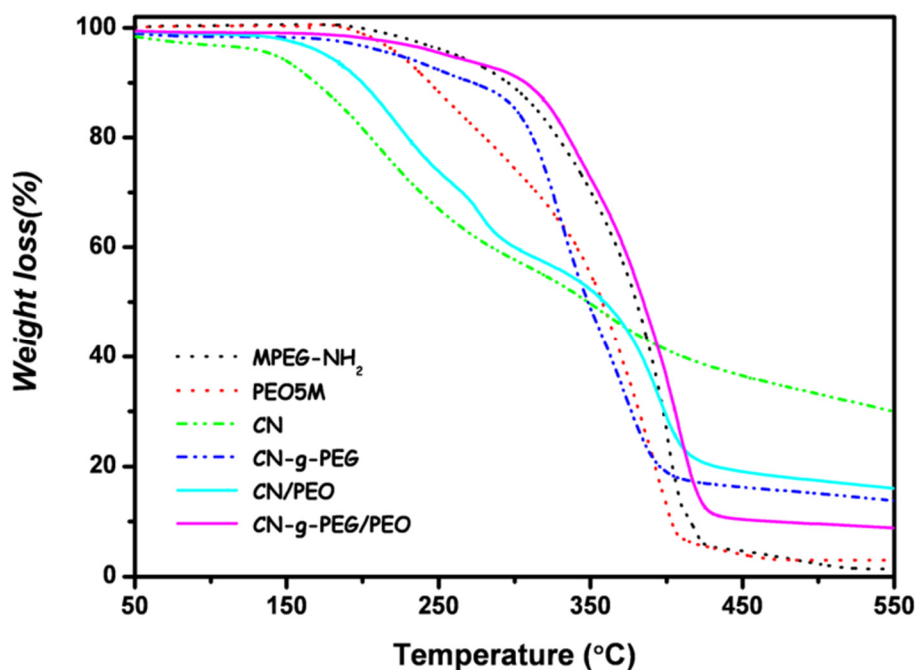


Figure 3.5 TGA thermograms for pure MPEG-NH₂, PEO5M; pristine CN, grafted CN-g-PEG; and CN/PEO and CN-g-PEG/PEO complexes.

3.3.5 Surface Hydrophilicity

The influence of chemical grafting and physical adsorption on the surface hydrophilicity of cellulosic nanoparticles was further investigated by contact angle measurement, as shown in Figure 3.6. The contact angle of the water drop for pristine CN decreased sharply with spreading in 5 s, which resulted from the swelling property of cellulose by water.³¹ For PEG-grafted nanocrystals (CN-g-PEG), the contact angle kept a similar reduction with time as CN due to the gradual spread of the drop on the PEG layer. In spite of similar chemical structure, the dynamic contact angle for pure PEO5M remained roughly constant around 50°, whereas the one for

pure MPEG–NH₂ gradually decreased from 39.6° to 21.8° over 20 s, which indicated the significant effect of the molecular weight of poly(ethylene glycol) polymers to surface hydrophilicity. Interestingly, the value of the contact angle for CN-g-PEG/PEO (67.7°) was even higher than that of pure PEO5M, which reflected the tight combination resulting from entanglements between PEG and PEO chains. On the contrary, because of the weak immobilization and uneven coverage of PEO on pristine nanocrystals (CN/PEO), the water drop was prone to penetrate through the

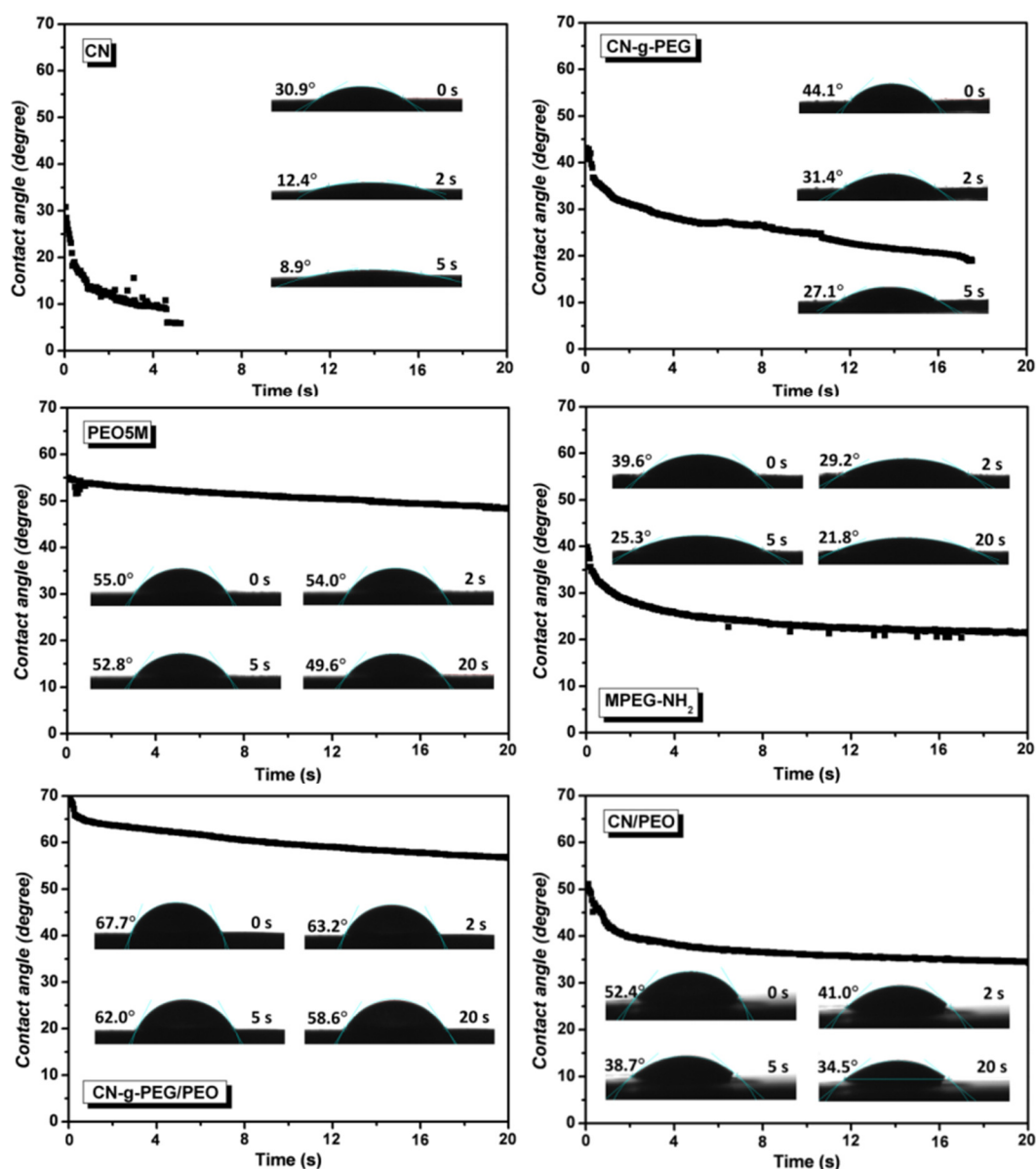


Figure 3.6 Time-dependence of contact angle for one drop of water on sheet samples, and inserted photographs for the water drop on the sheet samples after 0, 2, 5, and 20 s. (Zero time is the moment of drop deposition.)

PEO layer and directly contact the surface of cellulose, which induced the obvious reduction of the contact angle. The difference and change of surface hydrophilicity together with the thermal degradation behavior for CN-g-PEG/PEO and CN/PEO complexes indicated the immobilization of PEO chains from grafted PEG chains.

3.3.6 Rheological Behavior of Modified Cellulose Nanocrystals in Suspension

Direct study of the capability of pristine CN and CN-g-PEG to absorb PEO polymeric chains can be investigated by studying the rheological behavior of nanocrystal suspensions in the presence of PEO. For this study, suspensions with a constant nanocrystal concentration and gradual increase of PEO content as shown in Table 3.3 were prepared and their viscosity vs shear rate was determined.

Table 3.3 Composition, adsorption ratio, and viscosity for CN-g-PEG/PEO (or CN/PEO) suspensions.

CN-g-PEG (or CN)	H ₂ O	PEO5M	PEO%	PEO:CN-g-PEG (or PEO:CN) ^a	Viscosity ^b (CN-g-PEG/PEO)	Viscosity ^b (CN/PEO)
g	g	g	wt%	w/w	Pa·s	Pa·s
0.10	5.38	0	0	0	16.16	0.31
		0.015	0.28	0.15	24.93	0.17
		0.030	0.56	0.30	19.37	0.24
		0.045	0.84	0.45	14.61	1.09
		0.054	1.00	0.54	18.39	5.60
		0.060	1.12	0.60	27.98	7.51
		0.070	1.30	0.70	63.43	25.85
		0.085	1.58	0.85	95.47	198.80

^a The ratio of PEO:CN-g-PEG (or PEO:CN) reflects the capacity of 1.0 g CN-g-PEG (or CN) to adsorb PEO5M chains. ^b Steady shear viscosity of CN-g-PEG/PEO (or CN/PEO) suspension measured for a shear rate of 0.3 s⁻¹.

As shown in Figure 3.7 (A), the suspensions with low PEO content (S-CN/PEO-1 and S-CN/PEO-2) presented a similar behavior as the neat CN suspension, which indicated the capability of surface adsorbing 0.15–0.30 g of PEO for 1.0 g of pristine CN. This result was nearly in accordance with our previous report of optimal ratio for PEO-adsorbed CN (20 wt% PEO/80 wt% CN).¹⁸ The addition of higher PEO contents in the CN suspension releases free polymer chains, and induced the increase of the

viscosity. For PEG-grafted nanocrystals (CN-g-PEG), a maximum of 0.60 g of PEO polymer (S-CN-g-PEG/PEO-5) can be adsorbed. Grafted nanocrystals display roughly a two times higher PEO-adsorbing capability than pristine CN [Figure 3.7 (B)]. The comparison of the rheological behavior between PEO-adsorbed CN-g-PEG and CN suspension proved a more effective adsorption and immobilization of PEO chains on nanocrystals probably because of entanglements between grafted PEG chains and PEO chains. It is worth noting that in this work the ratio of nanocrystals and adsorbed PEO5M was controlled as 65/35 (w/w) to ensure the adsorption of all the PEO on CN-g-PEG, which was close to the capability of surface adsorbing 0.54 g of PEO for 1.0 g of nanocrystals.

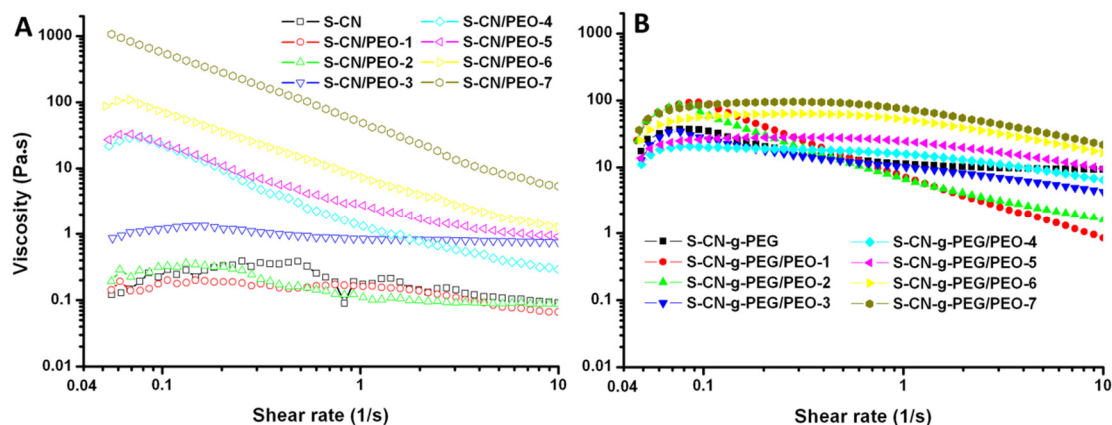


Figure 3.7 Viscosity vs shear rate for suspensions: (A) PEO5M-adsorbed CN; (B) PEO5M-adsorbed CN-g-PEG with a continuously increase of the shear rate from 0.05 to 10 s^{-1} for 4 min at 20 °C. The labels in figure correspond to the gradual increase of PEO5M content in suspensions as shown in Table 3.3.

3.4 Structure and Properties of Extruded Nanocomposites

3.4.1 Appearance Observation and Light Transmittance

Pristine nanocrystals as well as physically and/or chemically modified nanocrystals, viz. CN, CN/PEO, CN-g-PEG, and CN-g-PEG/PEO, were extruded with a PS matrix for the preparation of nanocomposites. The microstructure and interfacial mechanisms were investigated and discussed on the basis of the properties and comparison of the different series of extruded nanocomposites. First, Figure 3.8 shows the appearance of

extruded nanocomposites with the four nanohybrids. The addition of pristine CN progressively darkens the nanocomposites extruded at 200 °C. Despite the homogeneous dispersion of dark dots, the color of nanocomposites gradually darkened with the increase of CN content, which was ascribed to the low thermal degradation temperature of cellulose and further reduction of thermal stability from sulfate groups during the extraction of nanocrystals. Especially, the nanocomposite with 15 wt% pristine CN (CN-PS-15) was completely dark and opaque. Regarding the incorporation of PEO5M-adsorbed nanocrystals (CN/PEO), although the darkness of nanocomposites containing low nanofiller contents was less pronounced, a serious degradation of cellulose still occurred for extruded nanocomposites with higher CN/PEO contents (12 and 15 wt%). It was reported that the adsorbed polymeric PEO layer can play an effect of coating and shielding for surface sulfate groups on nanocrystals.¹⁸ However, it is worth noting that in this previous work extrusion was performed at 160 °C using low density polyethylene as matrix. In the present work, extrusion was carried out at 200 °C. Moreover, when adding higher PEO-adsorbed nanocrystal contents, the physical protection provided by the PEO layer may be lost because of the tendency to aggregation of hydrophilic PEO in hydrophobic PS matrix. The problem of lower thermal stability of CNs can be improved considerably by surface chemical modification. As shown in Figure 3.8, CN-g-PEG-PS based nanocomposites exhibited transparent or translucent appearance, even when introducing high nanofiller contents (20 wt%), which can be attributed to the covalent and close conjunction between PEG chains and nanocrystal. However, due to the shortness of PEG chains, the whole surface of the nanocrystal may not be fully covered by grafted chains, which caused the inhomogeneous appearance of extruded nanocomposites. The most promising materials were nanocomposites reinforced with nanocrystals subjected to both physical and chemical modification, i.e., CN-g-PEG/PEO-PS. All extruded nanocomposites were transparent, and presented homogeneous dispersion of the nanofiller. In comparison with CN/PEO and CN-g-PEG, both a covalently grafted-PEG layer, together with homogeneous PEO-adsorbed layer resulting from tight entanglement and attraction between

compatible PEG and PEO chains were present. The immobilization of long PEO chains on nanocrystals with grafted PEG chains restricted the tendency of PEO self-aggregation, and promoted the protective effects from two polymeric layers.

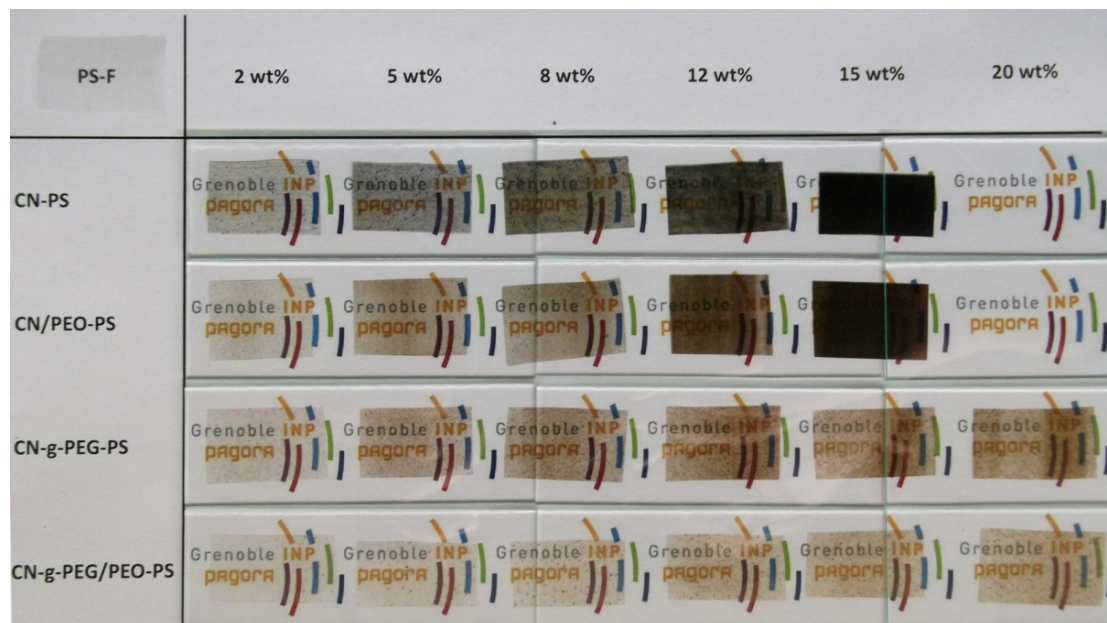


Figure 3.8 Pictures for extruded nanocomposites filled with pristine CN, CN/PEO, CN-g-PEG, and CN-g-PEG/PEO nanohybrids.

The light transmittance ratio of extruded nanocomposites was measured using UV spectrophotometer, as shown in Figure 3.9. It shows that the addition of nanoparticles in PS matrix induced a decrease of light transmittance, especially for composites containing high filler contents. However, this effect was completely different for the four nanohybrids. The introduction of CN or CN/PEO caused a sharp decrease of the light transmittance for PS based nanocomposite films, which presented transmittance ratios as low as 5.75% and 13.9% (maximum visible light at 700 nm) for CN-PS-15 and CN/PEO-15 nanocomposites. For nanocomposites loaded with chemically modified nanocrystals, such as CN-g-PEG-PS-15, the transmittance ratio at light wavelength of 700 nm was improved to 32.5%. However, with the addition of higher CN-g-PEG contents (20 wt%), the transmittance ratio of the nanocomposite decreased sharply. The most interesting result was obtained for CN-g-PEG/PEO-PS nanocomposites. Despite the gradual reduction of the transmittance ratio, when increasing the nanofiller content, all extruded nanocomposites maintained the high

transmittance to some extent, such as all series materials behaving a transmittance ratio of visible light > 40%.

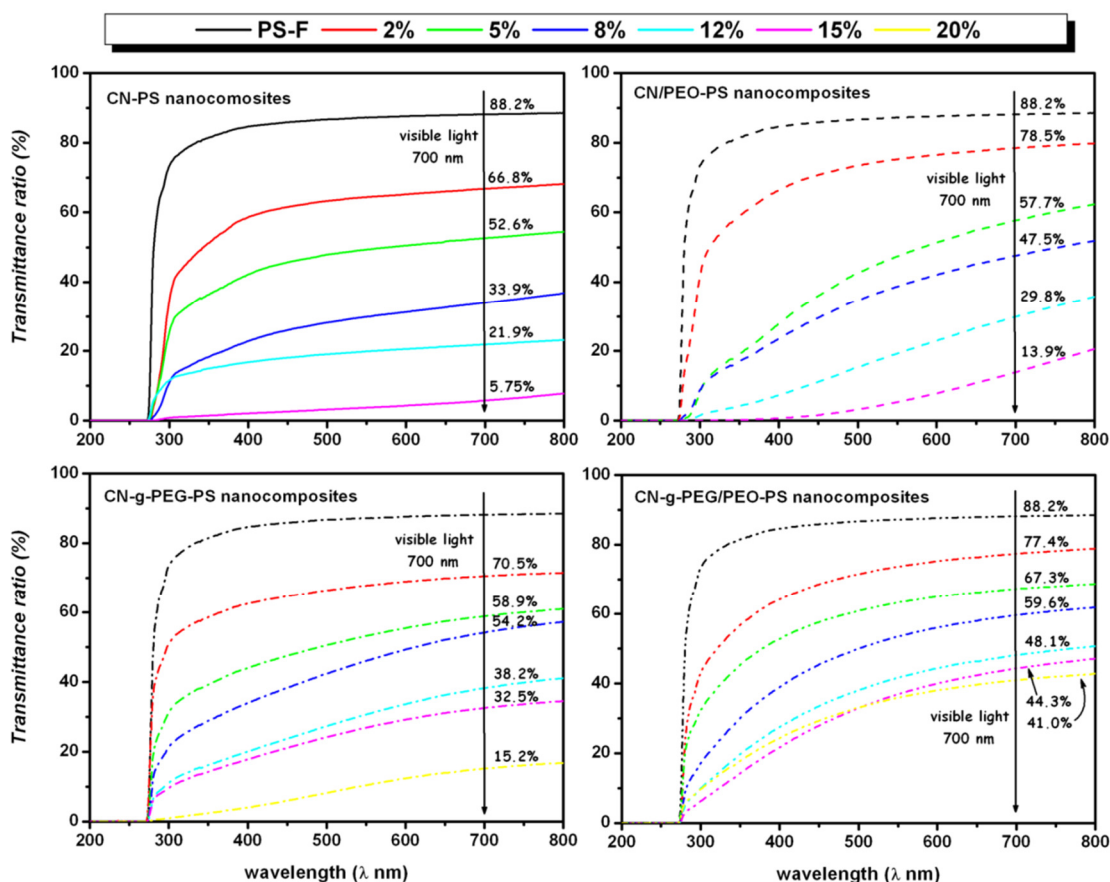


Figure 3.9 UV transmittance spectra for CN-PS, CN/PEO-PS, CN-g-PEG-PS, and CN-g-PEG/PEO-PS nanocomposites.

3.4.2 Dispersion and Microstructure of Nanocrystals in Composites

The surface of CN-g-PEG/PEO-PS-20 nanocomposite and morphology of nanohybrids inside the extruded composite were observed by AFM with QNM and Tapping modes. As shown in Figure 3.10 (A), the surface image of CN-g-PEG/PEO-PS-20 nanocomposite exhibited uniform and regular aspect, which should indicate good compatibility and miscibility of all components in the matrix. The nanoparticles were extracted from the extruded composite by dissolution of the material in THF and exchange to acetone for the removal of the PS matrix. The morphology of the extracted nanoparticles was observed [Figure 3.10 (B)]. It was

observed that hydrophilic CN-g-PEG/PEO complexes aggregated upon drying, but kept their original rod-like shape and dimensions.

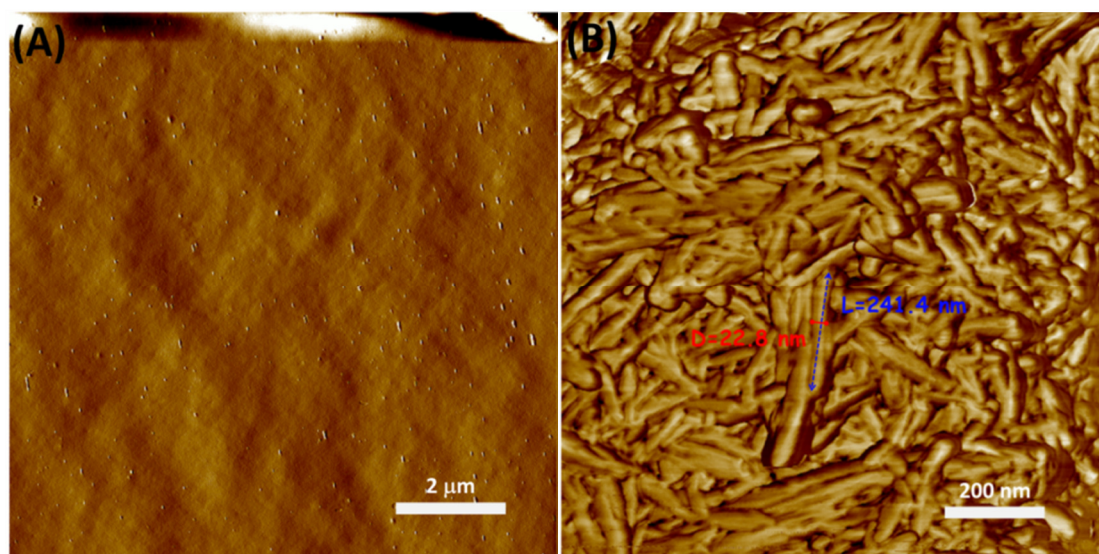


Figure 3.10 AFM images for extruded nanocomposite CN-g-PEG/PEO-PS-20 (A) and suspension of CN-g-PEG/PEO-PS-20 nanocomposite dissolved in THF and exchanged with acetone (B).

Further investigation of the microstructure of extruded nanocomposites was performed by observing their cryofractured cross-section morphology by SEM. As shown in Figure 3.11, compared to neat PS-F (image A), some nanoscaled dark dots were observed for CN-PS-2 nanocomposite (image B). Much more dots appeared in the cross-section morphology of CN-PS-15 nanocomposite (as indicated by yellow arrow and circle in image C), which were attributed to the carbonization and degradation of nanocrystals during extrusion. For PEO-adsorbed nanocrystals, due to the coverage and filling of PEO chains on the surface of nanocrystals, no more dark dots were observed as shown for CN/PEO-PS-2 and CN/PEO-PS-15 (images D and E). However, serious inhomogeneity and microphase separation existed in these nanocomposites, especially for high CN/PEO contents, such as the evident hole in the cross-section of CN/PEO-15 (as indicated by red arrow in image E). Regarding the nanocomposites filled with CN-g-PEG (images F and G) and CN-g-PEG/PEO (images H and I), a similar cross-section morphology as the one observed for PS-F was reported, which indicated the good dispersion level and miscibility of these two nanofillers within the matrix. It is worth noting that although having the same PEO

content, no microphase separation was observed for CN-g-PEG/PEO-PS-15 (image I) contrarily to CN/PEO-PS-15 (image E). It is ascribed to favorable interactions between adsorbed PEO and grafted PS chains in the nanocomposite.

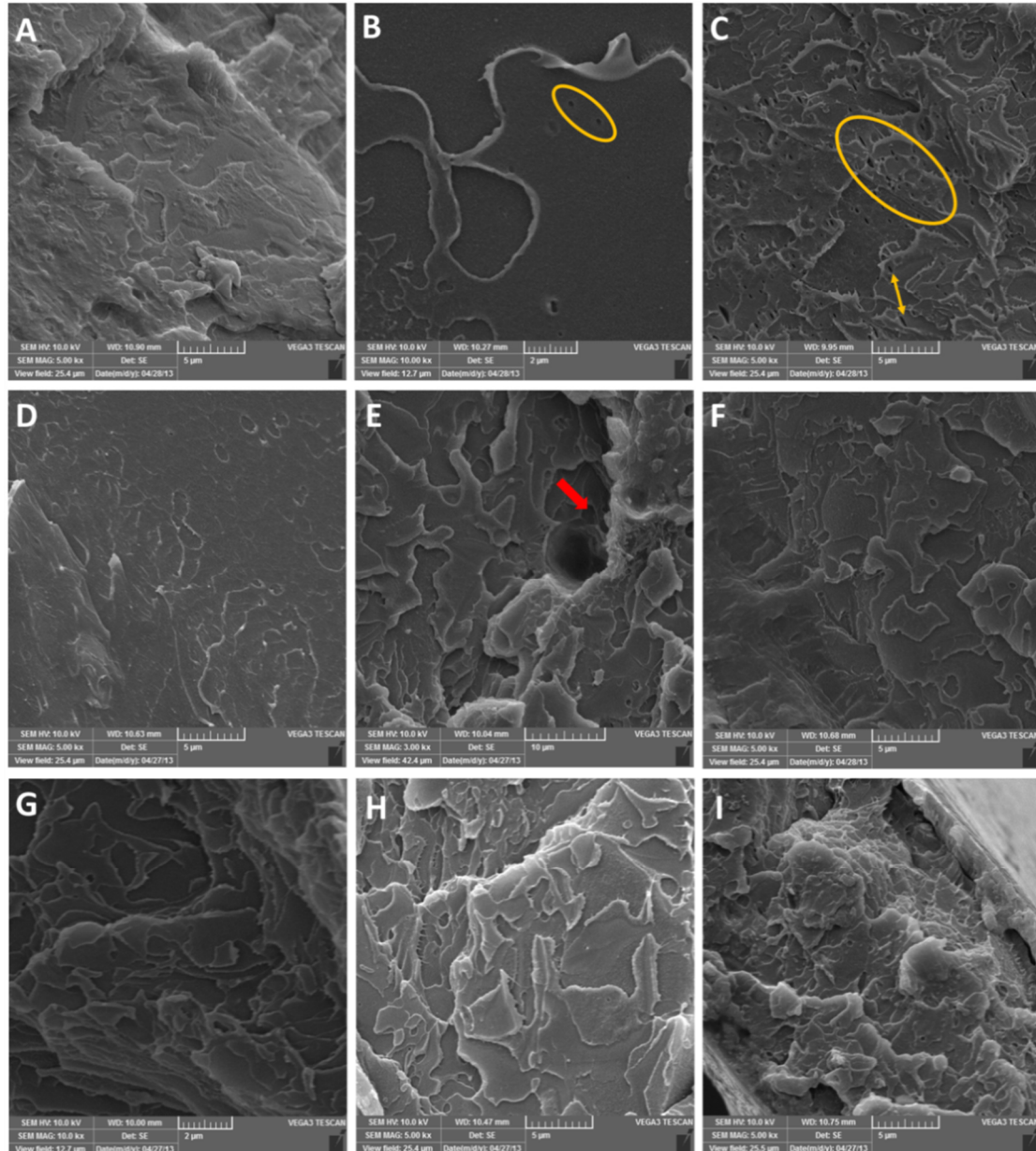


Figure 3.11 SEM images of the cross-section for extruded PS nanocomposites with low (2 wt%) and high nanohybrid content (15 wt%): (A) PS-F; (B) CN-PS-2, (C) CN-PS-15; (D) CN/PEO-PS-2; (E) CN/PEO-PS-15; (F) CN-g-PEG-PS-2; (G) CN-g-PEG-PS-15; (H)CN-g-PEG/PEO-PS-2; (I) CN-g-PEG/PEO-PS-15.

3.4.3 Thermal Properties

The thermal properties of extruded nanocomposites, such as glass transition temperature (T_g) of polystyrene component, melting temperature (T_m) of PEO component, and degradation temperature (T_d), were analyzed using DSC and TGA. As shown in DSC thermograms in Figure 3.12, the introduction of pristine CN or

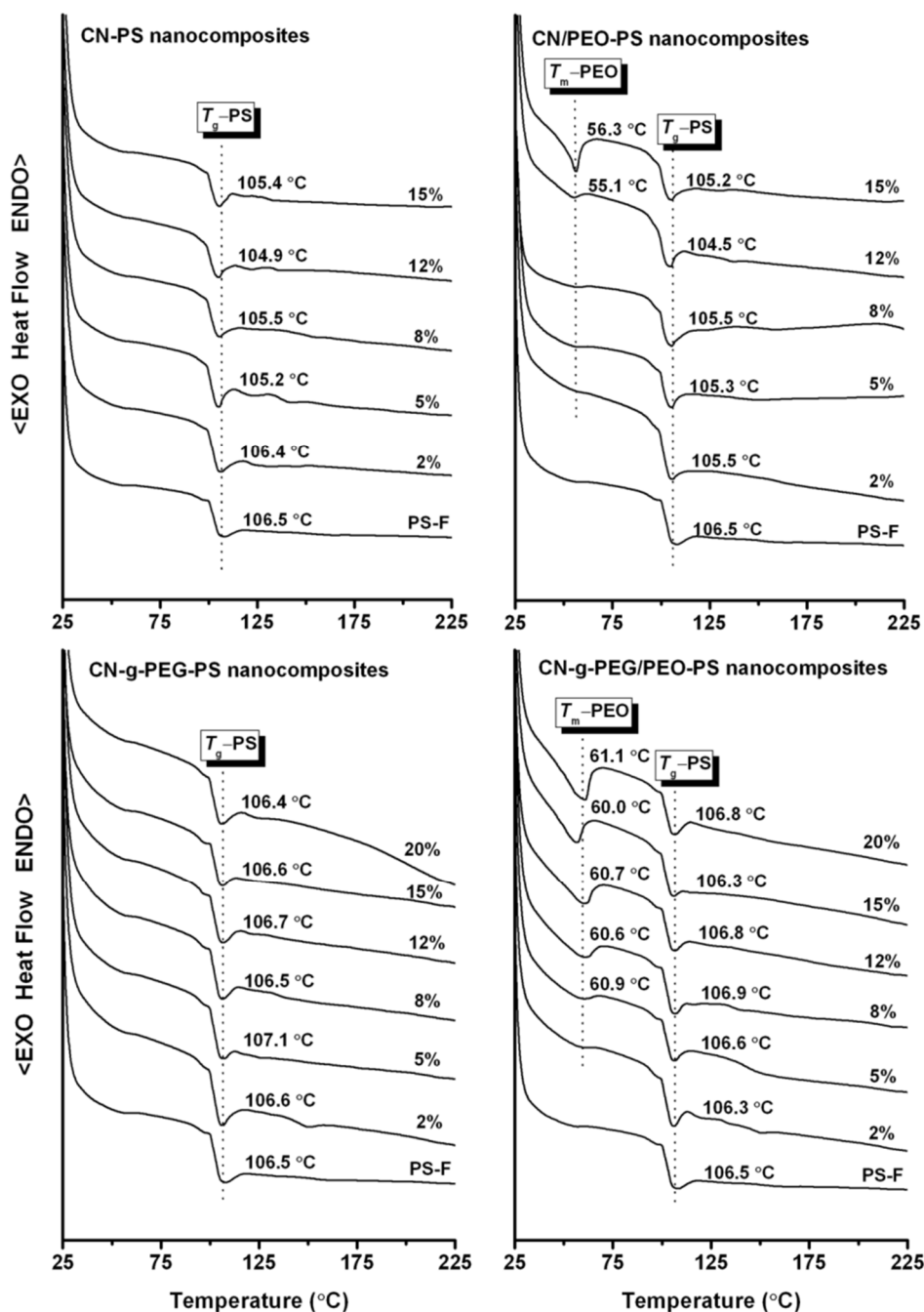


Figure 3.12 DSC thermograms for CN-PS, CN/PEO-PS, CN-g-PEG-PS, and CN-g-PEG/PEO-PS nanocomposites.

CN/PEO in PS matrix caused a slightly gradual decrease of T_g -PS. It is ascribed to inherent incompatibility between cellulose and polystyrene, and ensuing weak interfacial interactions between the nanofiller and the matrix. It indicates that the simple addition of hydrophilic CN and physical PEO adsorption on nanocrystals cannot allow homogeneous dispersion in the hydrophobic PS matrix. On the contrary, for CN-g-PEG and CN-g-PEG/PEO reinforced nanocomposites T_g -PS remains stable or slightly increases upon nanofiller addition. It is an indication that chemical grafting improves the compatibility of the nanoparticles with the PS matrix. Furthermore, a melting endotherm was visible for highly filled PEO-adsorbed CN (CN/PEO and CN-g-PEG/PEO) nanocomposites. It is obviously ascribed to the melting of the PEO phase (T_m -PEO). The same PEO was used for the two series of extruded nanocomposites, but it appears for lower CN contents for PEG-grafted nanoparticles. The chemical grafting improves the ability of adsorbed PEO chains to crystallize possibly because of cocrystallization between grafted and adsorbed polymeric chains. Moreover, T_m -PEO was located around 55–56 °C for CN/PEO–PS and slightly higher than 60 °C for CN-g-PEG/PEO–PS. This significant increase of T_m -PEO for CN-g-PEG/PEO–PS nanocomposites reflects bigger crystal size for PEO.

TGA experiments were performed to evaluate the thermal stability for extruded nanocomposites loaded with low (2 wt%), moderate (8 wt%), and high (15 wt%) nanofiller contents, as shown in Figure 3.13. Compared to neat PS–F material, the initial degradation temperature (T_{d1}) corresponding to 5% weight loss for all extruded nanocomposites was increased; especially for CN/PEO–PS-15 and CN-g-PEG/PEO–PS-15 nanocomposites for which the increment in T_{d1} value was higher than 30 °C. This effect is probably ascribed to favorable interactions between adsorbed PEO chains and PS matrix chains. Complete thermal degradation of polystyrene occurred around 415 °C, as shown in the thermogram for PS–F. However, for extruded nanocomposites this temperature was shifted to about 430 °C. At this temperature the char content was 7%, 5%, 4%, and only 2% for CN–PS-15, CN/PEO–PS-15, CN-g-PEG–PS-15, and CN-g-PEG/PEO–PS-15 nanocomposites,

respectively. The lowest char content for CN-g-PEG/PEO-PS nanocomposites indicates higher compatibility between CN-g-PEG/PEO nanofiller and PS matrix, which promote the integrated architecture of ensuing nanocomposites.

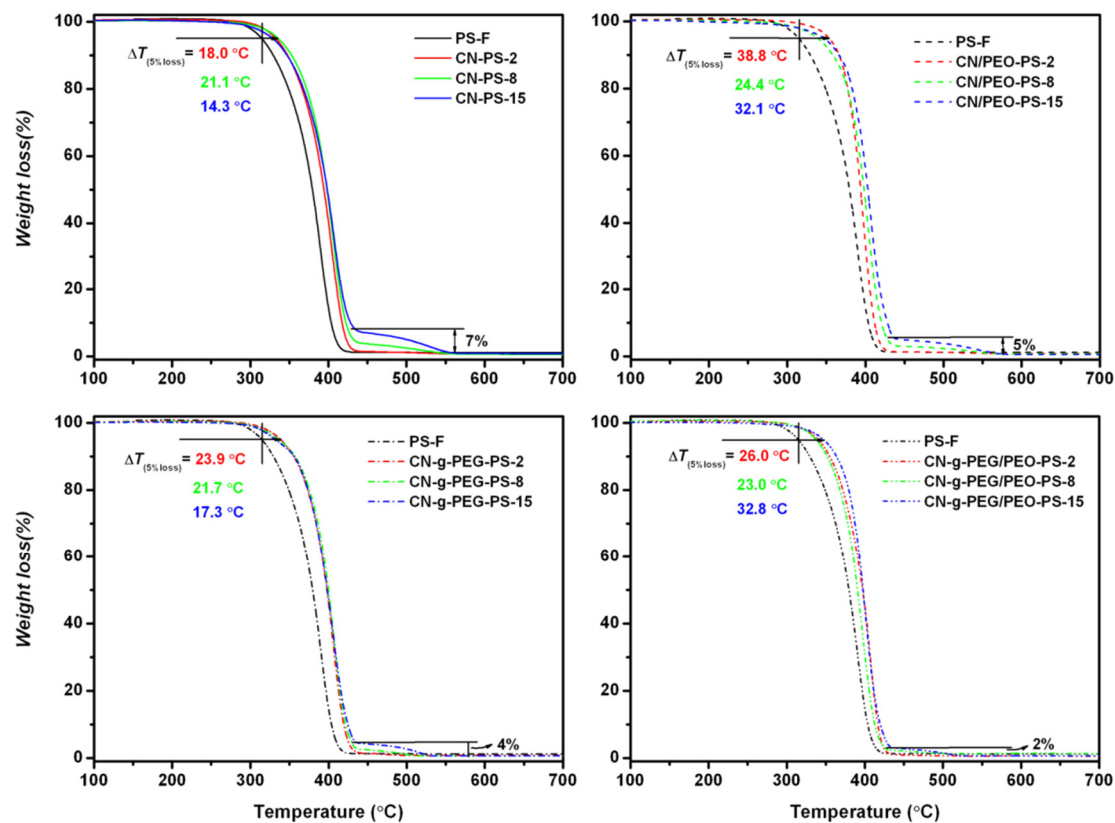


Figure 3.13 TGA for extruded nanocomposites with low (2 wt%), moderate (8 wt%), and high (15 wt%) nanohybrid contents.

3.4.4 Mechanical Properties

The mechanical properties of the four nanocomposite series were investigated by dynamic mechanical analysis (DMA). The evolution of the storage tensile modulus as a function of temperature was determined (results not shown). For the unfilled PS matrix a classical behavior for an amorphous polymer was observed with two plateaus corresponding to the glassy and rubbery state of the polymer and a sharp modulus drop associated with the glass transition temperature (T_g). The glassy modulus of PS was not significantly affected when adding nanocrystals regardless their physical/chemical modification. This is attributed to the fact that in this temperature range the difference between the elastic modulus of CN and that of the glassy PS

matrix was not high enough to easily appreciate a reinforcing effect for such low filler contents.³² However, above T_g , the reinforcing effect of nanocrystals became apparent ($ECN \gg EPS$), and the modulus of nanocomposites was higher than for the neat PS material.

The evolution of the storage tensile modulus at $T_g + 10 \text{ }^\circ\text{C}$ (389 K) as a function of nanocrystal content is plotted in Figure 3.14. For pristine CN (black symbols), a negligible improvement of the stiffness of the material was observed. This could be ascribed to the low thermal stability of this series which resulted in nanocomposites reinforced with degraded CN. However, the maintenance of the storage modulus for CN–PS nanocomposites indicates the possible incomplete thermal degradation of nanocrystals during processing at $200 \text{ }^\circ\text{C}$. For nanocomposites filled with CN/PEO (red symbols), the modulus first slightly increased upon nanofiller addition, and suddenly dropped for CN/PEO contents higher than 10 wt%. Even if the thermal degradation of the nanofiller is limited by adsorbed PEO, this coating restricts the interactions between nanoparticles and then weakens the possible formation of a percolating cellulose network within the polymeric matrix. Moreover, indirect interactions between the nanoparticles are expected to establish through a soft melt PEO interphase. Interestingly, the PEG-grafted CN (CN-g-PEG and CN-g-PEG/PEO nanofillers) provided a higher reinforcing effect to the PS matrix even if it was reported that the chemical modification on polysaccharide nanocrystals induces the partial destruction of the three-dimensional network of nanoparticles, which was unfavorable to the enhancement of mechanical properties.³³ As shown in Figure 3.14, below the percolation threshold ($w_{RC} = 7.49 \text{ wt\%}$, calculated from the critical volume fraction (v_{RC}) of the rigid phase at the percolation threshold),³⁴ the modulus of nanocomposites enhanced gradually. This is obviously ascribed to higher thermal stability and better dispersion within the polymeric matrix of grafted CN. It could also indicate that chemical grafting did not consume all hydroxyl groups on the surface of nanocrystals, which ensured the formation of weak hydrogen bonding between the nanocrystals. However, above the percolation threshold the modulus of

CN-g-PEG-PS nanocomposites continued to gradually increase while it stabilized for CN-g-PEG/PEO-PS nanocomposites. It could be ascribed to adsorbed-PEO chains on the CN surface that may weaken the interactions among remaining free hydroxyl groups, and block the further nanocrystal network architecture.

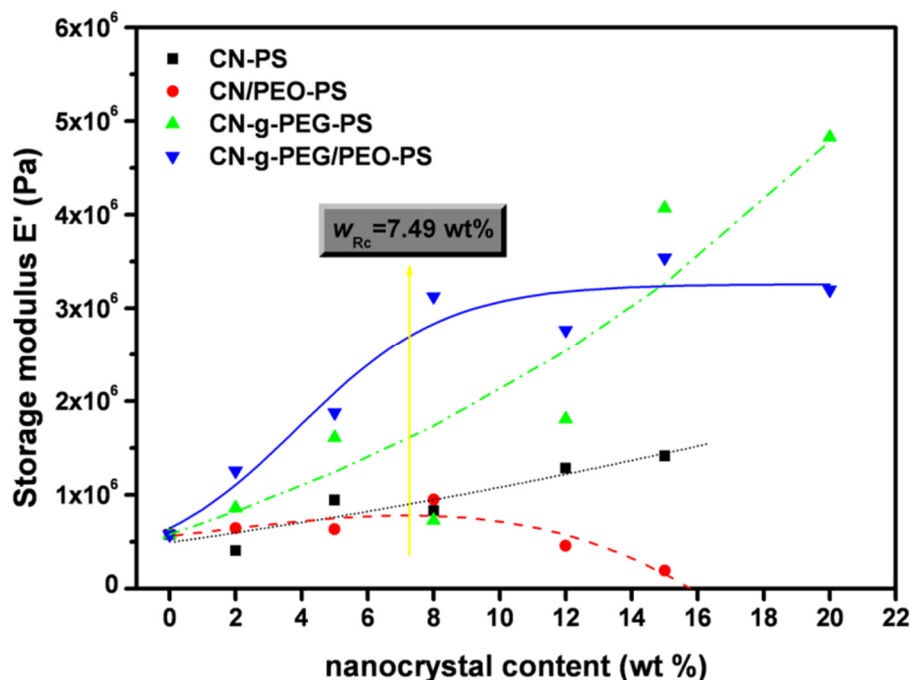


Figure 3.14 Storage modulus at $T_g + 10$ °C (389 K) and fitted curves for extruded nanocomposites vs nanocrystal content.

3.4.5 Barrier Properties

Generally, the introduction of nanocellulose in a polymeric continuous phase improves the barrier performance of nanocomposites, because of the tortuous path induced to the diffusion and permeability of moisture or gas molecules.³⁵ The effect of adding CN, CN/PEO, CN-g-PEG, and CN-g-PEG/PEO nanohybrids on the water vapor permeation (WVP) for extruded nanocomposites is shown in Figure 3.15. With the addition of pristine CN, the WVP value increased remarkably by nearly three to six times compared to neat PS-F material. In fact, during the processing by extrusion at high temperature, pristine CN without any protection inevitably degraded and carbonized, which may leave interstices between nanoparticles and matrix for ensuing nanocomposites (as indicated in Figure 3.11 by SEM observation). These interstices

provided the space and pathway for the travel of moisture, and ultimately deteriorated the water vapor barrier properties of CN–PS nanocomposites. When PEO-adsorbed nanocrystals CN/PEO were used, the possible interstices were filled with PEO chains, and it revived the nanobarrier effect of rigid nanocrystals, which can be proved by the decrease of WVP for nanocomposites containing low CN/PEO contents (< 10 wt%). However, as mentioned before, the incompatibility and microphase separation between superfluous PEO (for 12 and 15 wt% nanofiller contents) and PS in nanocomposites caused the aggregation of hydrophilic PEO chains, which may promote the moisture sorption and increase WVP value again. A similar tendency was obtained for the WVP of CN-g-PEG–PS nanocomposites. As shown in Figure 3.15, the most promising nanocomposites based on their superior water vapor barrier properties were CN-g-PEG/PEO–PS materials, which commonly exhibited a reduction of 35% of WVP in comparison with neat PS–F. For CN-g-PEG/PEO–PS nanocomposites loaded with various nanofiller contents, the chemical grafting and physical adsorption on nanocrystals enhanced the thermal stability and facilitated the homogeneous dispersion and compatibility between modified nanocrystals and matrix. It should be pointed out that entanglements between grafted PEG chains and adsorbed

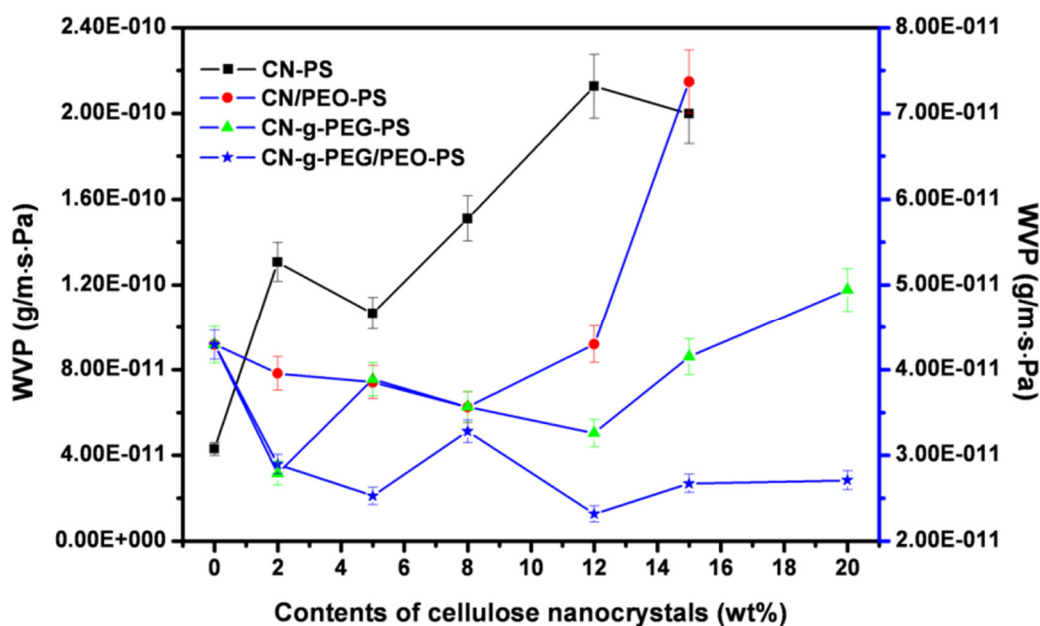


Figure 3.15 Effect of addition of CN, CN/PEO, CN-g-PEG, and CN-g-PEG/PEO nano hybrids on water vapor permeation (WVP) for extruded nanocomposites.

PEO should inhibit the self-aggregation of hydrophilic polymer; and at the same time long PEO chains served as “bridges” promoting the compatibility between modified nanocrystals and matrix. The well dispersed nanoparticles can create a tortuous pathway and block the effective travel for the diffusion of vapor through the composites matrix. Moreover, increased crystallinity of the PEO phase for CN-g-PEG/PEO–PS nanocomposites as shown from DSC analysis probably also facilitates this effect.

3.5 Conclusions

A strategy involving two poly(ethylene glycol)/polyoxyethylene (PEG/PEO) layers on the surface of cellulose nanocrystals using chemical grafting and physical adsorption was investigated. These modifications did not affect the crystallinity of the nanoparticles and improved their thermal stability. Four kinds of nanocrystals, i.e. pristine nanocrystal (CN), PEO-adsorbed nanocrystal (CN/PEO), PEG-grafted nanocrystal (CN-g-PEG), and both PEG-grafted and PEO-adsorbed nanocrystal (CN-g-PEG/PEO), were extruded with a hydrophobic polymeric matrix (PS) to prepare melt processed nanocomposites. The basic idea is consistent with the possibility of entanglements and cocrystallization between short PEG chains and long PEO chains, which can closely wrap and protect the surface of the nanocrystals. Meanwhile, the chemical and physical compatibilization imparted by PEG and PEO layers promoted the interfacial interactions between cellulosic nanoparticles and apolar matrix. Preliminary results showed the possibility of processing modified nanocrystals (CN-g-PEG/PEO) at high temperature (200 °C) avoiding the degradation of the nanoparticle, and providing a good dispersion and compatibility between modified nanocrystals and matrix. Furthermore, the surface modifications of nanocrystals did not block totally the interactions between the nanoparticles, and kept at least partially the three-dimensional network architecture, which is beneficial for the improvement of mechanical properties of extruded nanocomposites. With this strategy, it is expected to overcome an important challenge aimed at melt processing nanocellulose based nanocomposites as industrial products. However, further

investigation is necessary to fully understand the interactions between grafted PEG and adsorbed PEO, such as the chain length ratio (1/10 for PEG/PEO was used in this case), interphase thickness of PEG and PEO layers in extruded nanocomposites. Moreover, a simpler method for the introduction of the first PEG layer on cellulose nanocrystals to replace the chemical grafting reaction, such as electrostatic grafting, is another important issue to drive the practical application of this strategy. All these studies are in progress and will be present in future work.

3.6 References

1. Klemm, D.; Kramer, F.; Moritz, S.; Lindström, T.; Ankerfors, M.; Gray, D.; Dorri, A. Nanocelluloses: A new family of nature-based materials. *Angew. Chem. Int. Edit.* **2011**, *50*, 5438–5466.
2. Habibi, Y.; Lucia, L. A.; Rojas, O. J. Cellulose nanocrystals: Chemistry, self-assembly, and applications. *Chem. Rev.* **2010**, *110*, 3479–3500.
3. Moon, R. J.; Martini, A.; Nairn, J.; Simonsen, J.; Youngblood, J. Cellulose nanomaterials review: structure, properties and nanocomposites. *Chem. Soc. Rev.* **2011**, *40*, 3941–3994.
4. Lin, N.; Huang, J.; Dufresne, A. Preparation, properties and applications of polysaccharide nanocrystals in advanced functional nanomaterials: a review. *Nanoscale* **2012**, *4*, 3274–3294.
5. Favier, V.; Canova, G. R.; Cavailé, J. Y.; Chanzy, H.; Dufresne, A.; Gauthier, C. Nanocomposite materials from latex and cellulose whiskers. *Polym. Adv. Technol.* **1995**, *6*, 351–355.
6. The global market for nanocellulose to 2017; Futures Markets Inc., Edinburgh, Lothian EH74NA, United Kingdom, **2012**.
7. Dagnon, K. L.; Shanmuganathan, K.; Weder, C.; Rowan, S. J. Water-triggered modulus changes of cellulose nanofiber nanocomposites with hydrophobic polymer matrices. *Macromolecules* **2012**, *45*, 4707–4715.
8. Fox, J. D.; Capadona, J. R.; Marasco, P. D.; Rowan, S. J. Bioinspired water-enhanced mechanical gradient nanocomposite films that mimic the

- architecture and properties of the squid beak. *J. Am. Chem. Soc.* **2013**, *135*, 5167–5174.
9. Dufresne, A. “Nanocellulose. From nature to high performance tailored materials”. **2012** by Walter de Gruyter GmbH, Berlin/Boston. pp. 252–260.
 10. Bellayer, S.; Gilman, J. W.; Eidelman, N.; Bourbigot, S.; Flambard, X.; Fox, D. M.; De Long, H. C.; Trulove, P. C. Preparation of homogeneously dispersed multiwalled carbon nanotube/polystyrene nanocomposites via melt extrusion using trialkyl imidazolium compatibilizer. *Adv. Funct. Mater.* **2005**, *5*, 910–916.
 11. Alloin, F.; D’Aprea, A.; Dufresne, A.; El Kissi, N.; Bossard, F. Poly(oxyethylene) and ramie whiskers based nanocomposites: influence of processing: extrusion and casting/evaporation. *Cellulose* **2011**, *18*, 957–973.
 12. Orts, W. J.; Shey, J.; Imam, S. H.; Glenn, G. M.; Guttman, M. E.; Revol, J.-F. Application of cellulose microfibrils in polymer nanocomposites. *J. Polym. Env.* **2005**, *13*, 301–306.
 13. Goffin, A.-L.; Raquez, J.-M.; Duquesne, E.; Siqueira, G.; Habibi, Y.; Dufresne, A.; Dubois, P. From interfacial ring-opening polymerization to melt processing of cellulose nanowhisker-filled polylactide-based nanocomposites. *Biomacromolecules* **2011**, *12*, 2456–2465.
 14. Goffin, A.-L.; Raquez, J.-M.; Duquesne, E.; Siqueira, G.; Habibi, Y.; Dufresne, A.; Dubois, P. Poly(ϵ -caprolactone) based nanocomposites reinforced by surface-grafted cellulose nanowhiskers via extrusion processing: Morphology, rheology, and thermo-mechanical properties. *Polymer* **2011**, *52*, 1532–1538.
 15. de Menezes, A. J.; Siqueira, G.; Curvelo, A. A. S.; Dufresne, A. Extrusion and characterization of functionalized cellulose whiskers reinforced polyethylene nanocomposites. *Polymer* **2009**, *50*, 4552–4563.
 16. Raquez, J.-M.; Murena, Y.; Goffin, A.-L.; Habibi, Y.; Ruelle, B.; DeBuyl, F.; Dubois, P. Surface-modification of cellulose nanowhiskers and their use as nanoreinforcers into polylactide: A sustainably-integrated approach. *Compos. Sci. Technol.* **2012**, *72*, 544–549.
 17. Xu, S. H.; Gu, J.; Luo, Y. F.; Jia, D. M. Effects of partial replacement of silica

- with surface modified nanocrystalline cellulose on properties of natural rubber nanocomposites. *eXPRESS Polym. Lett.* **2012**, *6*, 14–25.
18. Azouz, K. B.; Ramires, E. C.; Van den Fonteyne, W.; El Kissi, N.; Dufresne, A. Simple method for the melt extrusion of a cellulose nanocrystal reinforced hydrophobic polymer. *ACS Macro Lett.* **2012**, *1*, 236–240.
 19. Fortunati, E.; Armentano, I.; Zhou, Q.; Iannoni, A.; Saino, E.; Visai, L.; Berglund, L. A.; Kenny, J. M. Multifunctional bionanocomposite films of poly(lactic acid), cellulose nanocrystals and silver nanoparticles. *Carbohydr. Polym.* **2012**, *87*, 1596–1605.
 20. Zhou, Q.; Brumer, H.; Teeri, T. T. Self-organization of cellulose nanocrystals adsorbed with xyloglucan oligosaccharide–poly(ethylene glycol)–polystyrene triblock copolymer. *Macromolecules* **2009**, *42*, 5430–5432.
 21. Oksman, K.; Mathew, A. P.; Bondeson, D.; Kvien, I. Manufacturing process of cellulose whiskers/poly(lactic acid) nanocomposites. *Compos. Sci. Technol.* **2006**, *66*, 2776–2784.
 22. Bondeson, D.; Oksman, K. Poly(lactic acid)/cellulose whisker nanocomposites modified by poly(vinyl alcohol). *Composites Part A* **2007**, *38*, 2486–2492.
 23. Lin, N.; Chen, G.; Huang, J.; Dufresne, A.; Chang, P. R. Effects of polymer-grafted natural nanocrystals on the structure and mechanical properties of poly(lactic acid): A case of cellulose whisker-graft-polycaprolactone. *J. Appl. Polym. Sci.* **2009**, *113*, 3417–3425.
 24. Lin, N.; Bruzzese, C.; Dufresne, A. TEMPO-Oxidized nanocellulose participating as crosslinking aid for alginate-based sponges. *ACS Appl. Mater. Interfaces* **2012**, *4*, 4948–4959.
 25. Montanari, S.; Roumani, M.; Heux, L.; Vignon, M. R. Topochemistry of carboxylated cellulose nanocrystals resulting from TEMPO-mediated oxidation. *Macromolecules* **2005**, *38*, 1665–1671.
 26. Habibi, Y.; Chanzy, H.; Vignon, M. R. TEMPO-Mediated surface oxidation of cellulose whiskers. *Cellulose* **2006**, *13*, 679–687.
 27. Araki, J.; Wada, M.; Kuga, S. Steric Stabilization of a cellulose microcrystal

- suspension by poly(ethylene glycol) grafting. *Langmuir* **2001**, *17*, 21–27.
28. Follain, N.; Marais, M.-F.; Montanari, S.; Vignon, M. R. Coupling onto surface carboxylated cellulose nanocrystals. *Polymer* **2010**, *51*, 5332–5344.
29. Thielemans, W.; Naceur Belgacem, M.; Dufresne, A. Starch nanocrystals with large chain surface modifications. *Langmuir* **2006**, *22*, 4804–4810.
30. Segal, L.; Creely, J. J.; Martin, A. E. Jr.; Conrad, C. M. An empirical method for estimating the degree of crystallinity of native cellulose using the X-ray diffractometer. *Text. Res. J.* **1959**, *29*, 786–794.
31. Lin, N.; Huang, J.; Chang, P. R.; Feng, J.; Yu J. Surface acetylation of cellulose nanocrystal and its reinforcing function in poly(lactic acid). *Carbohydr. Polym.* **2011**, *83*, 1834–1842.
32. Loos, M.R.; Manas-Zloczower I. Micromechanical models for carbon nanotube and cellulose nanowhisker reinforced composites. *Polym. Eng. Sci.* **2013**, *53*, 882–887.
33. Nair, K.G.; Dufresne, A. Crab shell chitin whiskers reinforced natural rubber nanocomposites. 3. Effect of chemical modification of chitin whiskers. *Biomacromolecules* **2003**, *4*, 1835–1842.
34. Dufresne, A.; Cavaille, J.-Y.; Helbert, W. Thermoplastic nanocomposites filled with wheat straw cellulose whiskers. Part II: Effect of processing and modeling. *Polym. Compos.* **1997**, *18*, 198–210.
35. Lavoine, N.; Desloges, I.; Dufresne, A.; Bras, J. Microfibrillated cellulose—its barrier properties and applications in cellulosic materials: A review. *Carbohydr. Polym.* **2012**, *90*, 735–764.

CHAPTER 4.

Application of Cellulose Nanocrystals: Biocomposite Sponges

“TEMPO-Oxidized Nanocellulose Participating as Crosslinking Aid for Alginate-Based Sponges”

Chapter 4. TEMPO-Oxidized Nanocellulose Participating as Crosslinking Aid for Alginate-Based Sponges

ENGLISH ABSTRACT	204
RESUME FRANÇAIS	207
4.1 Introduction	213
4.2 Experimental Methodology	215
4.2.1 Materials.....	215
4.2.2 Extraction of Cellulose Nanocrystals (CNs).....	215
4.2.3 Preparation of Microfibrillated Cellulose (MFC)	216
4.2.4 TEMPO-Mediated Oxidation of Cellulose Nanocrystals (OCN)	216
4.2.5 TEMPO-Mediated Oxidation of Microfibrillated Cellulose (OMFC)	217
4.2.6 Preparation of Alginate/Nanocellulose Crosslinked Sponges	218
4.2.7 Characterization and Analyses	218
4.3 TEMPO-Mediated Oxidation of Nanocellulose	222
4.3.1 Fourier Transform Infrared Spectroscopy (FTIR).....	222
4.3.2 Determination of the Degree of Oxidation (DO)	224
4.3.3 Morphology and Dimensions of Nanocellulose	224
4.3.4 Crystalline Integrity	226
4.4 Structure and Properties of Crosslinked Sponges	227
4.4.1 Crosslinking and Crystalline Properties	227
4.4.2 Microstructure.....	229
4.4.3 Porosity, Water Absorption, and Structural Stability	230
4.4.4 Mechanical Stability.....	232
4.4.5 Thermal Stability.....	234
4.5 Roles and Mechanisms of Nanocelluloses in Alginate-Based Sponges	236
4.6 Conclusions	238
4.7 References	239

ENGLISH ABSTRACT

As far as compatibility is concerned, the most promising strategy for the construction of nanocomposites is the utilization of filler and matrix bearing similar chemical or physical properties and providing strong interfacial adhesion between both components. For cellulose nanocrystal-based composites, hydrophobic moieties are classically introduced on the surface of nanoparticles through chemical or physical modification, which converts the surface of nanocrystals to a polarity close to the one of the matrix, and hence enhances the filler/matrix interfacial interactions. Further improved interactions can be obtained by chemically or physically introduced polymeric chains on the surface of nanoparticles to promote entanglements between grafted polymer chains and matrix, and possible co-crystallization when using semicrystalline polymers. However, simpler and significant approach for the improvement of the compatibility can also be realized via direct conjunction between the filler and the matrix, such as taking advantage of surface hydroxyl groups of cellulose nanocrystals to graft the waterborne polyurethane prepolymer for the co-construction of nanocomposites¹ or *in situ* crosslinking cellulose nanocrystals with the matrix for the fabrication of hydrogels.^{2,3}

Sodium alginate is a linear and polyanionic copolymer extracted mainly from marine algae, which can be well dissolved in water to form a high-viscosity sol. The most important property of aqueous sodium alginate is the sol–gel transformation with inner sphere ion–alginate complex formation during physical crosslinking with polyvalent cations. Generally, divalent cations can produce a crosslinked “egg-box” assembly resulting from the binding of residing sodium ions in the polyguluronate (G) segments. The chelation at the G-residue of the alginate molecules results in ionic interaction between the guluronic acid groups while the van der Waal forces between alginate segments assist the formation of a three-dimensional gel network.⁴ Sodium alginate can be made into materials with various forms such as sponges, films and microspheres, depending on the crosslinking process and drying techniques. Especially, for alginate-based sponges, it was reported that the porous sponge from

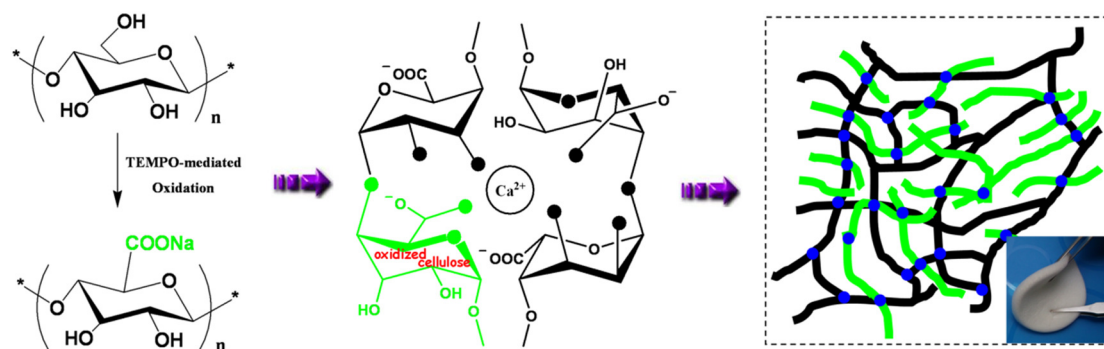
alginate matrix can produce a promising cell delivery system for the cultivation of fibroblast;⁵ silver sulfadiazine-loaded alginate sponges showed good wound healing effect on Wistar rat.⁶ The present interest in alginate for sponge materials involves an understanding of the advantages of alginate and the development of strategies targeted at improving the structural and performance stability of the materials.

Since the first report of TEMPO-mediated oxidation of polysaccharides,⁷ this method opened a new field of efficient and selective conversion chemistry of alcoholic hydroxyl groups to aldehydes, ketones and carboxyl groups under mild conditions. Generally, because of the catalytic oxidation of TEMPO, the C6 primary hydroxyls of cellulose are expected to be oxidized to C6 carboxylate groups by TEMPO/NaBr/NaClO oxidation system in water at pH 10–11.⁸ Different effects of TEMPO-oxidation can be observed depending on the type of nanocellulose, namely cellulose nanocrystals (CN) and microfibrillated cellulose (MFC). Different from highly crystalline and rigid CN, MFC consists of both individual and aggregated nanofibrils made of alternating crystalline and amorphous cellulose domains, which appears as flexible and long cellulose filaments. In the case of TEMPO-oxidized cellulose nanocrystals, carboxyl groups provide negative charges to the nanocrystals (similar effect as sulfate groups), and also promote the individualization of nanoparticles in aqueous suspension. On the other hand, TEMPO-oxidation can be used to extract microfibrillated cellulose with “spontaneous” oxidation and disintegration under mild conditions of overcharged amorphous domain of native cellulose fibers. Interestingly, regardless the type of nanocellulose, after TEMPO-mediated oxidation, the chemical structure of carboxylated cellulose, with the replacement of hydroxyl group to carboxyl group, is quite similar to that of sodium alginate, both possessing pyranoid rings with hydroxyl and carboxyl groups.

Based on our previous study (microspheres obtained from the mixture of cellulose nanocrystals and alginate),⁹ inspired from the similar structure of carboxylated cellulose and sodium alginate, the idea of TEMPO-oxidized nanocellulose participating as crosslinking aid for the construction of alginate-based sponges was

proposed and shown in the “Schematic diagram”. In this study, with the new TEMPO-induced carboxyl groups borne by nanocellulose, oxidized nanocellulose can participate in the construction of crosslinked network and play a fundamental role on the structural and mechanical stability of alginate-based sponges. Two types of oxidized nanocellulose, viz. carboxylated cellulose nanocrystals (OCN) and carboxylated microfibrillated cellulose (OMFC), were introduced in alginate sponges, and unmodified cellulose nanocrystals and microfibrillated cellulose with hydroxyl groups were used as the comparison. The porosity (P), water absorption (WA), water retention (WR), mechanical properties, and thermal properties of sponges were investigated. Sponges reinforced with OMFC display better performance in terms of porosity, water absorption and water retention, with the highest values of P_{\max} ($97.4\pm0.8\%$), WA_{\max} ($1468.4\pm27.1\%$), and WR_{\max} ($846.7\pm19.5\%$) for 50 wt% OMFC loading level. However, sponges reinforced with OCN showed significantly improved mechanical performance. The different performances of sponges indicated the special role and possibility of improvement of the properties for both types of oxidized nanocellulose, in which OCN played more a nano-reinforcing effect to promote the mechanical stability, while OMFC facilitated the structural stability much better. A model of semi-interpenetrating polymer network (SIPN) composed of OMFC and alginate was proposed based on the observation and discussion of the microstructure of crosslinked sponges.

Schematic diagram of TEMPO-induced carboxyl groups on nanocellulose participating in the construction of crosslinked network with “egg-box” multimer for alginate-based sponge.



RESUME FRANÇAIS

En termes de compatibilité, la stratégie la plus prometteuse pour l'élaboration de nanocomposites consiste à utiliser une charge et une matrice présentant des propriétés chimiques ou physiques similaires et offrant ainsi une forte adhésion interfaciale entre les deux composants. Pour les composites à base de nanocristaux de cellulose, la stratégie classique consiste à introduire, par modification chimique ou physique, des segments hydrophobes à la surface des nanocristaux, qui permettent ainsi d'atteindre à la surface des nanocristaux un niveau de polarité proche de celui de la matrice et par conséquent d'améliorer les interactions interfaciales charge/matrice. Des interactions plus importantes peuvent être obtenues en introduisant par voie chimique ou physique des chaînes polymères à la surface des nanoparticules, favorisant ainsi l'enchevêtrement entre les chaînes de polymère greffé et celles de la matrice, et éventuellement la co-cristallisation si des polymères semicristallins sont utilisés. Cependant, une approche plus simple et importante pour l'amélioration de la compatibilité consiste à établir une liaison directe entre la charge et la matrice en profitant des groupements hydroxyles de surface des nanocristaux pour greffer le prépolymère de polyuréthane en phase aqueuse pour la co-construction des nanocomposites¹ ou la réticulation *in situ* des nanocristaux de cellulose avec la matrice pour la fabrication d'hydrogels.^{2,3}

L'alginate de sodium est un copolymère linéaire et polyanionique essentiellement extrait d'algues marines qui se dissout facilement dans l'eau pour former une solution colloïdale de forte viscosité. La propriété la plus importante de l'alginate de sodium aqueux est la transformation sol-gel impliquant la formation d'un complexe ion-alginate lors de la réticulation physique avec des cations polyvalents. En général, les cations divalents peuvent conduire à la formation d'un assemblage réticulé de type "boîte à œufs" résultant de la fixation des ions sodium par les segments polyguluronate (G). La chélation par le résidu G des molécules d'alginate résulte d'une interaction ionique entre les groupements acide guluronique tandis que les forces de van der Waals entre les segments alginate participent à la formation d'un

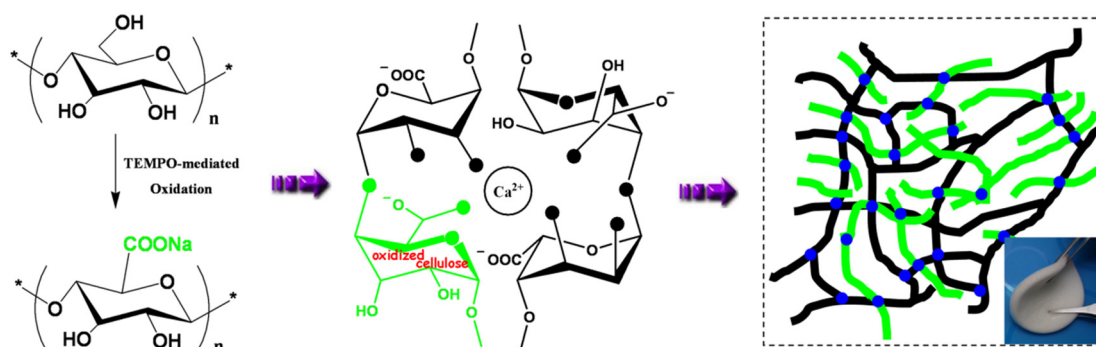
réseau tridimensionnel sous forme de gel.⁴ L'alginate de sodium peut être transformé en matériaux de formes diverses, telles que des éponges, des films et des microsphères, en fonction du procédé de réticulation et des techniques de séchage. Notamment, pour les éponges à base d'alginate, il a été montré que l'éponge poreuse à matrice d'alginate pouvait produire un système prometteur de relargage de cellules pour la culture de fibroblastes;⁵ les éponges d'alginate chargées de sulfadiazine d'argent ont démontré un bon effet cicatrisant sur le rat Wistar.⁶ L'intérêt actuel pour l'alginate sous forme d'éponge nécessite une compréhension des avantages de l'alginate et le développement de stratégies visant à améliorer la stabilité structurelle et la stabilité de la performance de ces matériaux.

Depuis la première étude d'oxydation assistée par TEMPO des polysaccharides,⁷ ce procédé a ouvert un nouveau domaine de chimie de conversion efficace et sélectif des groupements hydroxyles en groupements aldéhydes, cétones et carboxyles en conditions douces. En général, en raison de l'oxydation catalytique de TEMPO, on s'attend à ce que les hydroxyles primaires C6 de la cellulose soient oxydés en groupements carboxylates C6 par le système d'oxydation TEMPO/NaBr/NaClO dans l'eau à pH 10-11.⁸ On observe différents effets de l'oxydation TEMPO selon le type de nanocellulose, à savoir nanocristaux de cellulose (CN) et cellulose microfibrillée (MFC). A la différence des CN très cristallins et rigides, la MFC consiste en nanofibrilles, à la fois individuelles et agrégées, composées d'une alternance de domaines cristallins et amorphes de cellulose. La MFC se présente sous la forme de filaments flexibles et longs. Dans le cas des nanocristaux de cellulose oxydés TEMPO, les groupements carboxyles apportent des charges négatives aux nanocristaux (effet similaire à celui des groupements sulfates) et favorisent également l'individualisation des nanoparticules en suspension aqueuse. Par ailleurs, l'oxydation TEMPO peut être utilisée pour extraire la cellulose microfibrillée par un processus d'oxydation "spontanée" et désintégration dans des conditions douces des domaines amorphes fortement chargés des fibres de cellulose natives. Il est

intéressant de noter que quel que soit le type de nanocellulose, la structure chimique de la cellulose carboxylée après oxydation assistée par TEMPO, impliquant le remplacement du groupe hydroxyle par un groupement carboxyle, est très similaire à celle de l'alginate de sodium, les deux composés possédant des cycles pyranoses avec des groupements hydroxyles et carboxyles. Sur la base de notre étude précédente (microsphères obtenues à partir du mélange de nanocellulose et d'alginate)⁹ et de la similarité de structure de la cellulose carboxylée et de l'alginate de sodium, nous avons proposé l'idée de l'élaboration d'éponges à base d'alginate en utilisant la nanocellulose oxydée TEMPO comme soutien à la réticulation. Cette stratégie est illustrée dans le "schéma de principe". Pour cette étude, grâce aux groupements carboxyles de la nanocellulose résultant du traitement TEMPO, la nanocellulose oxydée peut participer à la construction d'un réseau réticulé et jouer un rôle fondamental sur la stabilité structurelle et mécanique des éponges à base d'alginate. Deux types de nanocellulose oxydée, à savoir nanocristaux de cellulose carboxylés (OCN) et cellulose microfibrillée carboxylée (OMFC), ont été introduits dans les éponges d'alginate. Des nanocristaux de cellulose et de la cellulose microfibrillée non modifiés avec des groupements hydroxyles ont également été utilisés pour comparaison. La porosité (P), l'absorption d'eau (WA), la rétention d'eau (WR), les propriétés mécaniques et les propriétés thermiques des éponges ont été étudiées. Les éponges renforcées avec OMFC présentent les meilleures performances en termes de porosité, d'absorption d'eau et de rétention d'eau avec les plus hautes valeurs de P_{\max} ($97,4 \pm 0,8\%$), WA_{\max} ($1468,4 \pm 27,1\%$), et WR_{\max} ($846,7 \pm 19,5\%$) pour un taux de charge en OMFC de 50% en poids. Cependant, les éponges renforcées avec OCN présentent des performances mécaniques nettement améliorées, avec la valeur la plus élevée de résistance à la compression (126,5 kPa sous une contrainte de compression de 70%) pour un taux de charge en OCN de 10% en poids par rapport à l'éponge d'alginate pure. Les différentes performances des éponges montrent le rôle particulier et la possibilité d'amélioration des propriétés pour les deux types de nanocellulose oxydée, pour lesquelles OCN apporte plutôt un effet de nano-renforcement en favorisant la stabilité mécanique, tandis que

OMFC améliore de manière plus effective la stabilité structurelle. Grâce à une analyse plus approfondie, un modèle de réseau de polymères semi-interpénétrés (SIPN) composé d'OMFC et d'alginate a été proposé sur la base des observations et de la discussion de la microstructure des éponges réticulées.

Schéma de principe de la participation des groupements carboxyles de la nanocellulose résultant du traitement TEMPO à la construction du réseau réticulé avec le multimère "boîte à œufs" pour l'éponge à base d'alginate.



References:

1. Cao, X.; Habibi, Y.; Lucia, L. A. One-pot polymerization, surface grafting, and processing of waterborne polyurethane-cellulose nanocrystal nanocomposites. *J. Mater. Chem.* **2009**, *19*, 7137–7145.
2. Goetz, L.; Foston, M.; Mathew, A. P.; Oksman, K.; Ragauskas, A. J. Poly(methyl vinyl ether-co-maleic acid)-polyethylene glycol nanocomposites cross-linked in situ with cellulose nanowhiskers. *Biomacromolecules* **2010**, *11*, 2660–2666.
3. Dash, R.; Foston, M.; Ragauskas, A. J. Improving the mechanical and thermal properties of gelatin hydrogels cross-linked by cellulose nanowhiskers. *Carbohydr. Polym.* **2013**, *91*, 638–645.
4. Goh, C. H.; Heng, P. S.; Chan, L. Alginates as a useful natural polymer for microencapsulation and therapeutic applications. *Carbohydr. Polym.* **2012**, *88*, 1–12.

5. Shapiro, L.; Cohen, S. Novel alginate sponges for cell culture and transplantation. *Biomaterials* **1997**, *18*, 583–590.
6. Choi, Y. S.; Hong, S. R.; Lee, Y. M.; Song, K.W.; Park, M. H.; Nam, Y. S. Study on gelatin-containing artificial skin: I. Preparation and characteristics of novel gelatin–alginate sponge. *Biomaterials* **1999**, *20*, 409–417.
7. de Nooy, A. E. J.; Besemer, A. C.; van Bekkum, H. Highly selective nitroxyl radical-mediated oxidation of primary alcohol groups in water-soluble glucans. *Carbohydr. Res.* **1995**, *269*, 89–98.
8. Isogai, A.; Saito, T.; Fukuzumi, H. TEMPO-oxidized cellulose nanofibers. *Nanoscale* **2011**, *3*, 71–85.
9. Lin, N.; Huang, J.; Chang, P. R.; Feng, L.; Yu, J. Effect of polysaccharide nanocrystals on structure, properties, and drug release kinetics of alginate-based microspheres. *Colloid. Surface. B* **2011**, *85*, 270–279.

The work in this chapter is originated from:

Ning Lin, Cécile Bruzzese, and Alain Dufresne, TEMPO-Oxidized nanocellulose participating as crosslinking aid for alginate-based sponges. ACS Appl. Mater. Interfaces 2012, 4, 4948–4959.

Chapter 4. TEMPO-Oxidized Nanocellulose Participating as Crosslinking Aid for Alginate-Based Sponges

Ning Lin, Cécile Bruzzese, and Alain Dufresne

Grenoble Institute of Technology (Grenoble INP), The International School of Paper, Print Media, and Biomaterials (Pagora), BP65, 38402 Saint Martin d'Hères Cedex, France

ABSTRACT

Crosslinked polysaccharide sponges have been prepared by freeze-drying of amorphous alginate–oxidized nanocellulose in the presence of a Ca^{2+} ionic crosslinking agent. The new carboxyl groups on the surface of nanocellulose induced by the chemical oxidization provided the possibility of participating in the construction of an alginate-based sponge's structure and played a fundamental role in the structural and mechanical stability of ensuing sponges. Furthermore, enhanced mechanical strength induced by oxidized cellulose nanocrystals and the formation of a semi-interpenetrating polymer network from oxidized microfibrillated cellulose were reported. Together with the facile and ionic crosslinking process, the ultrahigh porosity, promising water absorption and retention, as well as the improved compression strength of the crosslinked sponges should significantly extend the use of this soft material in diverse practical applications.

KEYWORDS

Cellulose Nanocrystals, Microfibrillated Cellulose, Alginate, Crosslinked Sponge

4.1 Introduction

Sponges are attractive soft materials defined as dispersions of gas (usually air) in a solid matrix. They have become the focus of material science due to their applications in the fields of food, pharmaceuticals, agriculture, personal care products, and even electronics. Particularly, as matrices for the construction of diverse biomaterials, sponges are also widely studied as controlled drug delivery systems, wound dressings, and tissue engineering scaffolds. Derived from natural algae, alginate has been proved to be a promising candidate for the fabricating of porous sponges from the gelation-freezing method, which exhibit the desirable advantages of being biocompatible, non-toxic, relatively economical and biodegradable under normal conditions.¹ Alginate is a linear, unbranched polysaccharide composed of α -1,4-linked β -D-mannuronic acid (M-block) and α -L-guluronic acid (G-block), forming stable gels in the presence of divalent cations such as calcium, due to the ionic interaction between cation and the carboxyl functional group through the formation of “egg-box”-calcium linked junctions. However, owing to weak mechanical performance, unstable thermal properties, and uncontrollable structure degradation, the practical application of neat alginate sponge is limited. To solve these problems, intensive research has been performed to prepare composite sponges based on alginate, such as the addition of chitosan,^{2–9} dextran,^{10–12} gelatin,¹³ collagen,^{14,15} keratin,¹⁶ silk fibroin,^{17,18} bacterial cellulose,¹⁹ starch,²⁰ hydroxyapatite,²¹ calcium phosphate,²² and poly(ethylene glycol).²³ It is a pity that most of these works only emphasized on the enhancement of the mechanical performance of sponges, but realized at the expense of biocompatibility (even adding an organic crosslinking agent). The key issue for developing alginate-based sponge is how to closely connect the additive and alginate component and meanwhile preserve the structural coherence of the sponge.

Cellulose is the most abundant natural biopolymer, an almost inexhaustible raw material (extracted from wood, hemp, cotton, etc.) and a useful source of renewable material, which has been used for more than 150 years in a wide variety of

applications. Cellulose nanocrystal (CN) is the rigid crystalline component of natural cellulose obtained from the removal of amorphous regions through hydrolysis with acid, enzyme, or mechanical separation. As a biobased reinforcing nanofiller, CNs have attracted significant interest during the last 20 years because of their numerous advantages, and have been widely used to enhance the properties of various host matrices in the preparation of nanocomposites.^{24–27} Furthermore, the potential of CNs has also been proved for special functional nanomaterials.^{28,29} For example, alginate-based microspheres containing CNs have been designed as a biomedical material to transport drug molecules, which showed improved encapsulation efficiency and promising sustainable drug release profiles.³⁰ More recently, microfibrillated cellulose (MFC), another nanomaterial obtained from natural cellulose (such as wood or plant fibers), has also shown promising improvement on mechanical properties and thermal stability of polymer matrices,^{31,32} such as poly(vinyl alcohol),³³ polypyrrole,³⁴ poly(caprolactone),³⁵ poly(lactic acid),^{36–38} epoxy resin,³⁹ cellulose acetate,⁴⁰ chitosan,^{41,42} and amylopectin.⁴³ In comparison with CN, MFC exhibits both amorphous and crystalline parts and presents a web-like structure with a higher aspect ratio. In a previous work, an attempt to introduce CN and MFC in alginate capsules that were subsequently extruded with a commercial biopolymer for developing thermoplastic nanocomposite materials was reported.⁴⁴

In this study, we attempted a novel approach to design native alginate/cellulose crosslinked sponges by preparing well-dispersed and structure-participating TEMPO-mediated oxidized cellulose nanocrystals (OCN) and TEMPO-oxidized microfibrillated cellulose (OMFC) with divalent calcium ions (Ca^{2+}) crosslinking process. Both cellulose and alginate belong to the polysaccharide family, and their similar chemical structure should provide good compatibility for the ensuing crosslinked sponges. Furthermore, with the new TEMPO-induced carboxyl groups on cellulose, oxidized nanocellulose can participate in the construction of the crosslinked network for alginate-based sponge and play a fundamental role of structural and mechanical stability of the sponges. Particularly, with the ionic

crosslinking of even diffusion-penetration process, as well as the fact that all the components (alginate, cellulose, and water as solvent) originate from nature, biodegradable and nontoxic biosponges can be obtained. Successful TEMPO-oxidized modification of CN and MFC was confirmed by Fourier transform infrared spectroscopy (FTIR) and conductimetric analysis. Based on the analysis of the mechanical and thermal properties, porosity and water absorption, and structure and morphology of the crosslinked sponges, three comparisons have been investigated, namely pristine cellulose and oxidized cellulose, cellulose nanocrystals and microfibrillated cellulose, and neat alginate sponge and sponges containing different cellulose contents. Finally, the roles of different oxidized nanocelluloses and construction mechanism in the three-dimensional network structure of the sponge were discussed.

4.2 Experimental Methodology

4.2.1 Materials

Native cotton fibers were obtained from Whatman filter paper. Sodium hypochlorite (NaClO) solution from Sigma–Aldrich was reagent grade and the available chlorine was 10–15%. 2,2,6,6-tetramethyl-piperidiny-1-oxyl (TEMPO, C₉H₁₈ON, 98%), sodium bromide (NaBr), hydrochloric acid (HCl, 37%), sulfuric acid (H₂SO₄, 98%), and anhydrous ethanol were also obtained from Sigma-Aldrich. Sodium alginate, sodium hydroxide (NaOH), and calcium chloride (CaCl₂) of laboratory grade were purchased from Carl Roth and used without further treatment.

4.2.2 Extraction of Cellulose Nanocrystals (CNs)

Cellulose nanocrystals (CNs) were prepared from cotton fiber, according to previous literature.⁴⁵ The fiber was milled with a laboratory milling device to obtain a fine particulate substance and extracted in 2 wt% aqueous NaOH solution (12.5 g fibers for 500 mL solution) for 12 h at room temperature and then filtered and rinsed with distilled water. Acid hydrolysis was performed at 45 °C with 65 wt % H₂SO₄ (preheated), for 45 min under mechanical stirring (12.5 g fibers for 250 mL solution).

Amorphous or paracrystalline regions of cellulose were preferentially hydrolyzed, whereas crystalline regions that have higher resistance to acid attack remained intact.⁴⁶ The suspension was diluted with ice cubes to stop the reaction and washed until neutrality by successive centrifugations at 10,000 rpm for 10 min each step and dialyzed against distilled water for 5 days. After dialysis, the CN dispersion was completed by ultrasonic treatment using a Branson sonifier, and finally, the released CN powder was obtained by freeze-drying.

4.2.3 Preparation of Microfibrillated Cellulose (MFC)

Microfibrillated cellulose (MFC) was prepared by a high-pressure homogenization process. First, cotton fibers were treated with an alkali aqueous solution (2 wt % NaOH) for 24 h at room temperature under mechanical stirring to remove xylem.⁴⁷ After filtration and rinsing with distilled water several times, the suspension of cotton fibers was pumped through a microfluidizer processor (Model M-110 EH-30). The slurry was passed through the valves that applied high pressure. Size reduction of products occurred into an interaction chamber (IXC) using cells of different sizes. After that, the suspension was sonicated with a Branson sonifier 4 times, each time for 5 min. Finally, the suspension was freeze-dried for the loose MFC sample.

4.2.4 TEMPO-Mediated Oxidation of Cellulose Nanocrystals (OCN)

TEMPO-mediated oxidation of CN was performed according to a procedure described in the literature.^{48,49} About 0.5 g CN was suspended in distilled water (50 mL) and treated by ultrasonic dispersion for 15 min. TEMPO (14.75 mg, 0.094 mmol) and NaBr (162 mg, 1.57 mmol) were dissolved in another 50 mL distilled water and were added dropwise to the CN suspension. A certain amount of 12 wt% NaClO (3.0 g, 4.84 mmol) solution was added slowly to the suspension to start the oxidizing reaction. The pH condition of the mixture was maintained at 10 by adding 0.5 M NaOH, while stirring the suspension for 3 h at room temperature. After oxidation, the reaction was quenched by the addition of ethanol (ca. 1 mL), and the pH was adjusted to 7 with 0.5 M HCl. The suspension of oxidized CN (OCN) was washed thoroughly with water three times and then freeze-dried to obtain a powder.

4.2.5 TEMPO-Mediated Oxidation of Microfibrillated Cellulose (OMFC)

Oxidation of microfibrillated cellulose (OMFC) was performed with the method of TEMPO-mediated oxidation coupled with low speed mechanical treatment.⁵⁰ This method used TEMPO radical as a catalyst with the primary oxidant such as hypochlorite to oxidize the hydroxyl groups on the surface of cellulose. Meanwhile, the oxidation helped to degrade the material such that low speed mechanical treatment fibrillates the cellulose fibers to prepare OMFC.²⁴ Cotton cellulose fiber suspension was homogenized for 30 min, and the pH was regulated at 10 with NaOH solution (0.5 M). Then, the solution of TEMPO and NaBr was added, and the pH of the suspension was maintained at 10. The oxidation process started when the NaClO solution (12 wt%) was added dropwise and stirred continuously at room temperature at 500 rpm for 3 h. After reaction, the OMFC suspension was washed with water 3 times and homogenized again with an Ultra turrax for 30 min. Finally, a solid OMFC sample was obtained by freeze-drying. During the preparation of OMFC, it is worth noting that OMFC suspension should be cooled with an ice bath to avoid thermal degradation resulting from the high-speed shearing during the homogenization treatment.

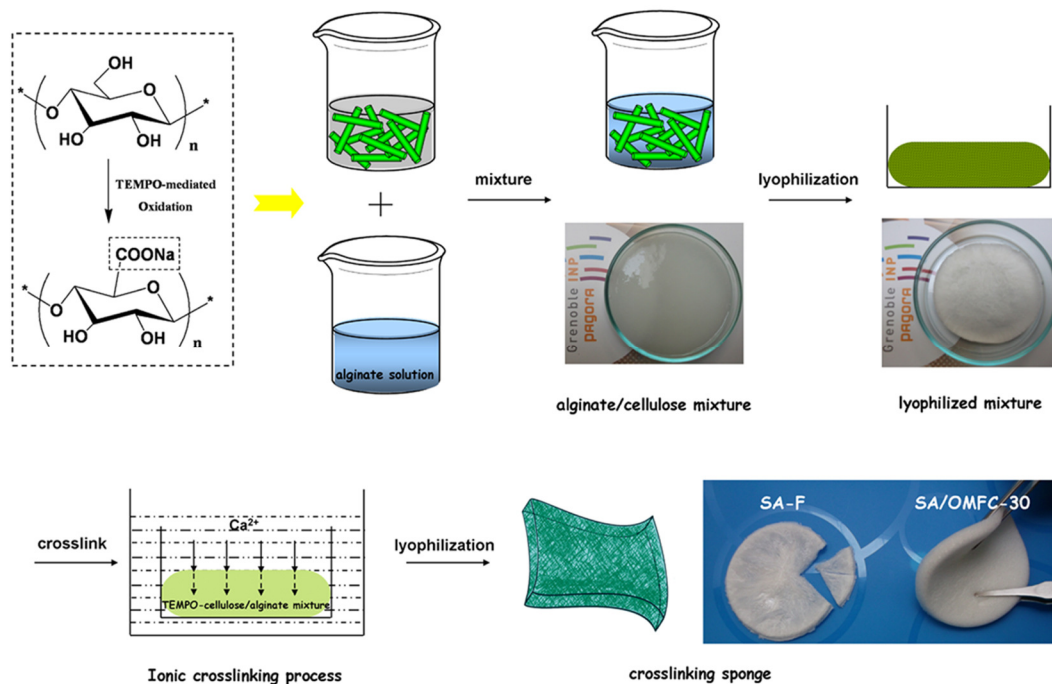


Figure 4.1 Scheme of preparation for alginate-based crosslinked sponge.

4.2.6 Preparation of Alginate/Nanocellulose Crosslinked Sponges

Cellulose (CN, OCN, MFC, OMFC), either oxidized or unmodified, was introduced in the alginate solution for the preparation of bio-crosslinked sponges. The detailed procedure is shown in Figure 4.1. First, homogeneous suspensions (3 wt%) of cellulose were prepared using ultrasonic treatment for 15 min in distilled water. Meanwhile, sodium alginate (SA) was dissolved in water (3 wt%) and mildly stirred for 2 h to obtain a homogeneous solution. Then, nanocellulose suspensions were carefully added in the as-prepared SA solution under mechanical stirring until a homogeneous dispersion was obtained. It should be pointed out that the viscous property of alginate solution facilitated the dispersion and stability of micro/nano-scale cellulose. The alginate/nanocellulose mixture was cast in Petri dish plates and freeze-dried at $-80\text{ }^{\circ}\text{C}$ for 24 h. Whereafter, the freeze-dried mixture was immersed in 5 wt% CaCl_2 aqueous solution and left under quiescent conditions for 12 h to allow the Ca^{2+} -induced crosslinking process with diffusion-penetration reaction. After the process of ionic crosslinking, the mixture was abundantly rinsed with distilled water to remove unbounded Ca^{2+} ions and freeze-dried again to prepare the crosslinked sponge. The weight ratios and compositions of the various alginate/nanocellulose crosslinked sponges are summarized in Table 4.1.

4.2.7 Characterization and Analyses

Fourier Transform Infrared Spectroscopy (FTIR): Infrared spectra were recorded at room temperature on a FTIR Perkin-Elmer Spectrum One spectrometer to characterize nanocellulose powders and alginate/nanocellulose sponges. Freeze-dried unmodified and oxidized nanocellulose powders were analyzed as KBr pellets (1 wt% in anhydrous KBr). Herein, for clear observation, oxidized nanocellulose powders (OCN and OMFC) were converted to their acid forms by ion exchange to displace the carboxyl absorption band toward higher wavelengths. 1 M HCl was slowly added to the oxidized nanocellulose (cellulose-COONa) suspension under magnetic stirring for 30 min. Then, the suspension was washed with 0.01 M HCl and distilled water at least 5 times. The sodium carboxylate groups ($-\text{COONa}$) on oxidized nano-

Table 4.1 Composition, porosity (*P*), water absorption (*WA*) and water retention (*WR*) of various alginate/nanocellulose sponges.

Sample	Cellulose/SA weight ratio		Cellulose suspension		SA solution		<i>P</i>		<i>WA</i>		<i>WR</i>	
	Cellulose (g)	SA (g)	Water (g)	Cellulose (g)	SA (g)	Water (g)	%	%	%	%	%	%
SA-F	0	0.60	0.0	0	0.60	20.0	78.8±0.6	835.3±14.7	221.1±9.6			
SA/CN-10	0.06	0.54	2.0	0.06	0.54	18.0	87.3±0.7	1040.4±21.6	569.0±11.5			
SA/CN-30	0.18	0.42	6.0	0.18	0.42	14.0	82.7±0.4	972.6±16.5	484.5±10.3			
SA/CN-50	0.30	0.30	10.0	0.30	0.30	10.0	81.0±0.5	793.0±11.8	340.9±6.4			
SA/OCN-10	0.06	0.54	2.0	0.06	0.54	18.0	89.3±0.6	1087.1±18.6	532.6±9.2			
SA/OCN-30	0.18	0.42	6.0	0.18	0.42	14.0	85.2±0.6	1021.9±14.3	501.4±11.7			
SA/OCN-50	0.30	0.30	10.0	0.30	0.30	10.0	81.3±0.9	987.2±16.1	442.7±7.9			
SA/MFC-10	0.06	0.54	2.0	0.06	0.54	18.0	88.6±0.7	1132.9±22.4	679.9±10.9			
SA/MFC-30	0.18	0.42	6.0	0.18	0.42	14.0	91.3±0.4	1137.7±27.3	579.4±13.7			
SA/MFC-50	0.30	0.30	10.0	0.30	0.30	10.0	90.0±0.4	1172.8±25.6	543.2±13.2			
SA/OMFC-10	0.06	0.54	2.0	0.06	0.54	18.0	94.2±0.7	1323.8±20.5	734.6±17.1			
SA/OMFC-30	0.18	0.42	6.0	0.18	0.42	14.0	96.5±0.8	1398.5±29.8	808.1±14.3			
SA/OMFC-50	0.30	0.30	10.0	0.30	0.30	10.0	97.4±0.8	1468.4±27.1	846.7±19.5			

cellulose were converted to free carboxyl groups ($-\text{COOH}$).⁵¹ All the powder samples were characterized by FTIR using a spectral width ranging from 4000 to 400 cm^{-1} , and all the sponge samples were recorded in the 4000–600 cm^{-1} range, with a 2 cm^{-1} resolution and an accumulation of 20 scans.

Conductimetry: The carboxyl content of oxidized nanocellulose was determined by conductimetric titration.⁵² Samples (50 mg) were suspended into 15 mL of 0.01 M hydrochloric acid solutions. When a stable suspension was obtained, it was titrated with 0.01 M NaOH. The titration curves presented a remarkable reproducibility and the degree of oxidation (DO) or total amount of carboxyl groups was calculated from:

$$DO = \frac{162 \times C \times (V_2 - V_1)}{w - 36 \times C \times (V_2 - V_1)} \quad (4.1)$$

where C is the NaOH concentration (mol/L), V_1 and V_2 are the amount of NaOH as shown in conductimetric titration curves, and w (g) is the weight of the dried sample.

Atomic Force Microscopy (AFM) and Nanosizer: Four samples of CN, MFC, OCN, and OMFC suspensions of approximately 0.01 wt% in water were sonicated for 15 min and then deposited on the mica substrate. The substrate loaded with the sample was imaged in tapping mode with a Nanoscope IIIa microscope from Veeco Instruments. Silicon cantilevers with a typical radius of curvature of 10–15 nm were used to perform the imaging at a frequency of 264–339 kHz. In addition, the average length and dimension distribution of CN, MFC, OCN, and OMFC were determined with a commercial VASCO particle size analyzer (Zetasizer NanoZS, Malvern, France). The measurement was performed in the range from 10 to 600 nm for CN and OCN and 110 to 3000 nm for MFC and OMFC.

X-ray Diffraction (XRD) Analysis: X-ray measurements were carried out for unmodified and oxidized nanocellulose powders. Sponge samples were cut as square pieces (1.5×1.5 cm) and pressed into a flattened shape. The X-ray diffraction patterns were recorded on a Philips PW 1720 X-ray generator operated at 30 kV and 20 mA with Cu $K\alpha$ radiation ($\lambda = 0.154$ nm) in the range $2\theta = 3\text{--}70^\circ$ for cellulose powders

and $2\theta = 5\text{--}50^\circ$ for sponges using a fixed time mode with a step interval of 0.02° .

Morphological Characterization of Sponges: The microstructure of the sponges was observed using environmental scanning electron microscopy (ESEM) on a Quanta 200 FEI device (Everhart-Thornley Detector) at high voltage (10 kV). Before observation, samples were placed onto the sample holder and coated with gold.

Porosity of Sponges: The average porosity was determined by a fluid replacement method.¹⁴ Ethanol was chosen as the displacement liquid because it penetrates easily into the pores and did not induce shrinkage or swelling. In brief, the geometrical volume (V_s) of the sponge samples was calculated by measuring diameter and height, and the pore volume (V_p) was measured by ethanol displacement method. The pre-weighed sponge (W_o) was immersed in absolute ethanol at room temperature and then placed in a desiccator under a reduced pressure for 5 min to remove air bubbles. After wiping gently with a filter paper to remove surface ethanol, samples were weighed immediately as W_e . The porosity of the sponge was calculated according to the following equation:

$$P = \frac{V_p}{V_s} \times 100 = \frac{W_e - W_o}{\rho_e V_s} \times 100\% \quad (4.2)$$

where ρ_e represents the density of ethanol (0.789 g/cm^3). An average value of five replicates for each sample was taken.

Water Absorption of Sponges: The water sorption of sponges was determined gravimetrically. The freeze-dried sponge sample was cut into a $2.0 \times 1.5 \text{ cm}$ piece and placed in water for 30 min. Subsequently, the wet sponge was removed and weighed immediately after absorbing excess water from the surface with a filter paper. The water absorption rate (WA) was calculated with the following formula:

$$WA = \frac{M_w - M_d}{M_d} \times 100\% \quad (4.3)$$

where M_w (g) and M_d (g) are the weight of the sponge soaked in water and initial dry weight, respectively. An average value of five replicates for each sample was taken.

Water Retention of Sponges: To measure the water retention rate, sponge sample

soaked with water was carefully removed, placed in a centrifuge tube and centrifugated at 3,500 rpm for 3 min. The water retention rate (*WR*) was calculated with the following formula:

$$WR = \frac{M_h - M_d}{M_d} \times 100\% \quad (4.4)$$

where M_h (g) is the weight of the sponge after centrifugation, and M_d (g) is the initial dry weight. An average value of five replicates for each sample was taken.

Reuse Evaluation: Reusable property is defined as the repetitive absorbing ability of sponge sample after drawing off water. The soaked sponge sample was dried to constant weight, and then, the water absorption test was repeated. The values of water absorption rate during the process of absorbing–discharging water for 10 times were measured.

Mechanical Performance: The mechanical properties of all sponge samples (compression test) were investigated using a RSA3 (DMA, TA Instruments) dynamical mechanical analyzer fitted with a 100 N load cell. For compression testing, the sponge samples were prepared as cylinders 1.5 cm in diameter and compressed to 80% of their original thickness with a constant crosshead speed of 0.005 mm/s at room temperature. Mechanical testing results were averaged on five replicates.

Thermal Properties: The thermal behavior of sponge samples was investigated using a Perkin-Elmer DSC 7 differential scanning calorimeter (DSC) instrument using aluminum pans. The samples were scanned from 20 to 250 °C at a heating rate of 10 °C/min. In addition, a thermal analyzer Perkin-Elmer TGA-6 was used for the thermogravimetric analysis under nitrogen flow. Sponge samples of ca. 10 mg were heated from 20 to 600 °C at a heating rate of 10 °C/min.

4.3 TEMPO-Mediated Oxidation of Nanocellulose

4.3.1 Fourier Transform Infrared Spectroscopy (FTIR)

Figure 4.2 presents the FTIR spectra for unmodified CN and MFC,

TEMPO-modified OCN and OMFC, acidic form OCN-COOH and OMFC-COOH obtained by ion exchange, as well as neat sodium alginate powder (SAP). Upon oxidization of the surface hydroxyl groups, some changes in the spectrum of modified nanocellulose can be observed. The most important change is the appearance of the carboxyl groups (C=O) stretching band at 1612 cm^{-1} (OCN) or 1619 cm^{-1} (OMFC) attributed to sodium carboxylate groups ($-\text{COONa}$), similar to the structure of sodium alginate. Meanwhile, to eliminate the interference with the absorbed water band (1640 cm^{-1}) and clearly observe the changes resulting from the modification, HCl treatment of oxidized nanocellulose was performed to largely converted the carboxylate- COONa structure to acid- COOH , as shown in Figure 4.2, with a band characteristic of free carboxyl groups at 1735 cm^{-1} (acidic form

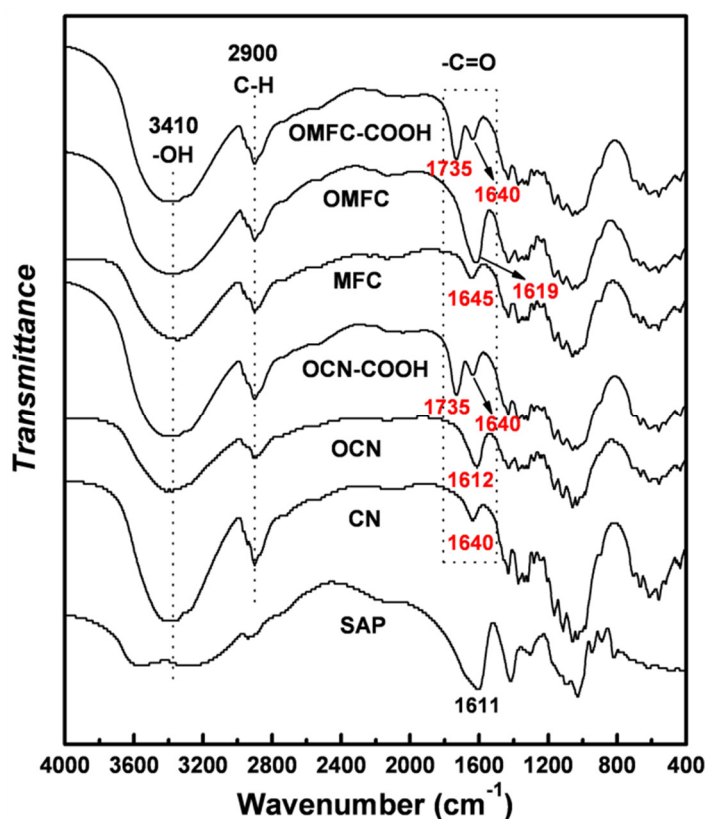


Figure 4.2 FTIR spectra for unmodified cellulose nanocrystals (CN), oxidized cellulose nanocrystals (OCN), acidic form of oxidized cellulose nanocrystals (OCN-COOH); and unmodified microfibrillated cellulose (MFC), oxidized microfibrillated cellulose (OMFC), acidic form of oxidized microfibrillated cellulose (OMFC-COOH) as well as neat sodium alginate powder (SAP).

–COOH). On the other hand, the slight reduction of the bands related to hydrogen bonds stretching vibration of –OH groups around 3400 cm^{-1} and to stretching vibrations of C–H at 2900 cm^{-1} can also be observed. Based on this analysis, the success of the chemical oxidization of cellulose nanocrystals and microfibrillated cellulose was clearly verified by FTIR.

4.3.2 Determination of the Degree of Oxidation (DO)

The degree of oxidation (DO) or total amount of carboxyl groups can be determined by conductimetric titration. Typical titration curves are shown in Figure 4.3. According to the literature,⁴⁸ the maximum degree of TEMPO-oxidation (DO_{max}) of nanocellulose was roughly close to 0.10. Based on the data from titration curves and using eq. 4.1, the values of $\text{DO}_{(\text{OCN})}$ and $\text{DO}_{(\text{OMFC})}$ were 0.092 and 0.095, respectively, which indicated that almost all the surface accessible hydroxyl groups of nanocellulose have been oxidized. These results were consistent with the experimental expectation of slightly excess reaction ratio.

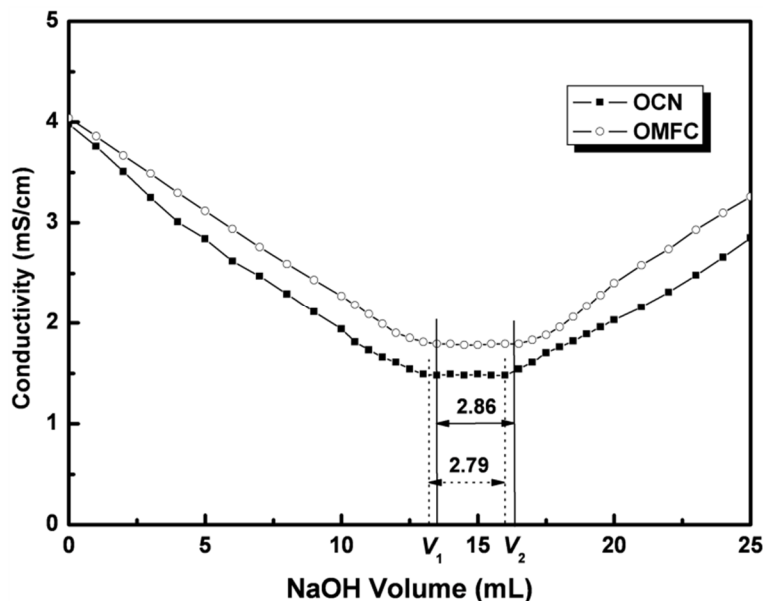


Figure 4.3 Conductimetric titration curves for oxidized cellulose nanocrystals (OCN) and oxidized microfibrillated cellulose (OMFC).

4.3.3 Morphology and Dimensions of Nanocellulose

AFM together with a nanosizer were used to investigate the changes of morphology

and dimensions of nanocellulose before and after oxidation. As shown in Figure 4.4, unmodified CN exhibited a typical rod-like morphology with a length of 100–300 nm and a diameter of 10–30 nm, which was in accordance with our previous report.⁵³ After modification, the average length only slightly decreased from 220 nm (CN) to 204 nm (OCN), and also maintained the rod-like shape. On the other hand, the histogram in Figure 4.4 showed that most MFC presented a relatively uniform size with length of 1.0–1.2 μm and entangled and self-aggregated morphology due to the long chains in AFM image. Similarly to OCN, the TEMPO-mediated oxidation of MFC induced the presence of blurry outline and slight decrease of the dimensions. From the results of the nanosizer and AFM, the preservation of original morphologies and geometrical dimensions of nanocellulose was proved.

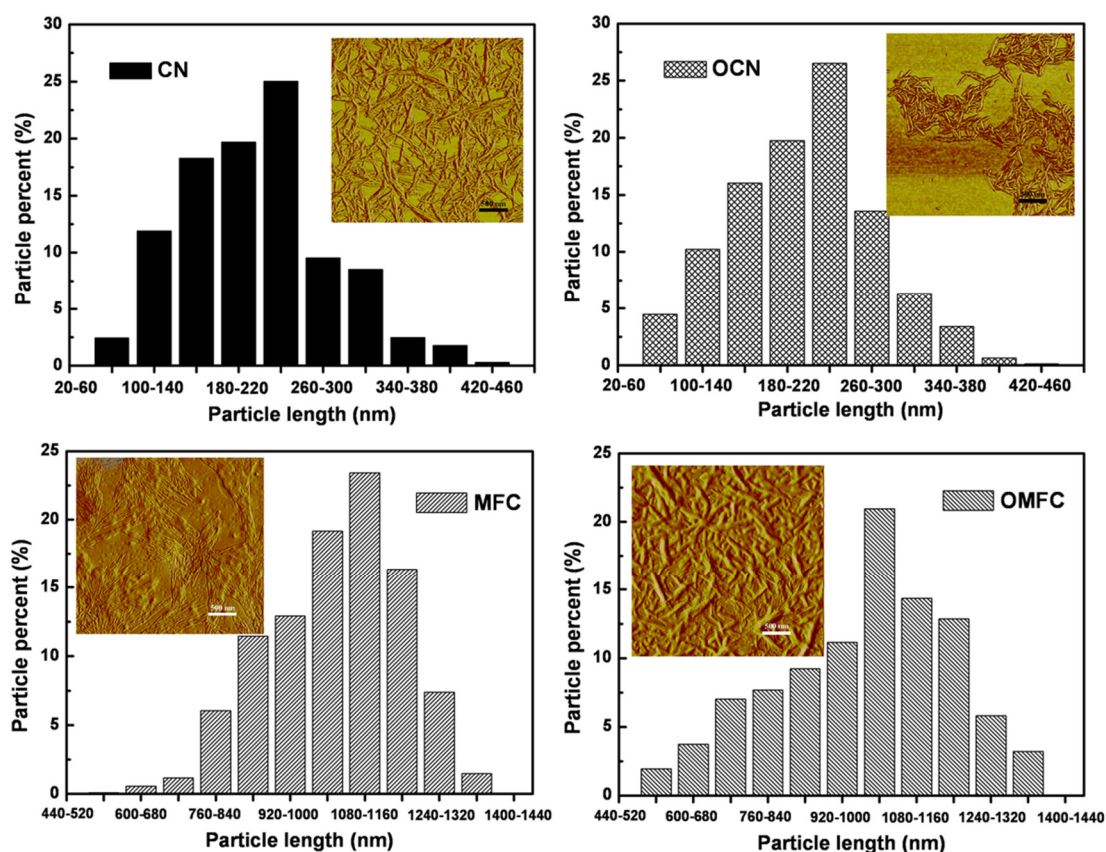


Figure 4.4 Distribution histograms for the length and AFM images (inserted) for CN, OCN, MFC, and OMFC.

4.3.4 Crystalline Integrity

The main challenge when chemically modifying the surface of nanocellulose is to conduct the process in such a way that it only changes the surface, while preserving the original morphology to avoid any polymorphic conversion and to maintain the integrity of the crystal.²⁶ Therefore, the impact of oxidation on the crystalline structure of CN and MFC was further investigated with XRD analysis. As shown in Figure 4.5, in spite of a slight decrease of the intensities, after the modification the main diffraction characteristics of OCN and OMFC from cellulose were still clearly presented, such as the diffraction peaks at 2θ angles around 14.8° (110), 16.4° ($1\bar{1}0$), and 22.6° (200). Meanwhile, the crystallinity index (I_c) of cellulose can be calculated according to the Segal method,⁵⁴ which showed values of 90.3% for CN, 88.5% for OCN, 82.4% for MFC, and 82.6% for OMFC. Based on this analysis, it appears that upon chemical modification the original crystalline structure of CN and MFC was preserved. It is worth noting that in comparison with cellulose, the XRD pattern of alginate powder did not exhibit any distinct crystalline characteristic, which indicated the mainly amorphous structure of alginate.

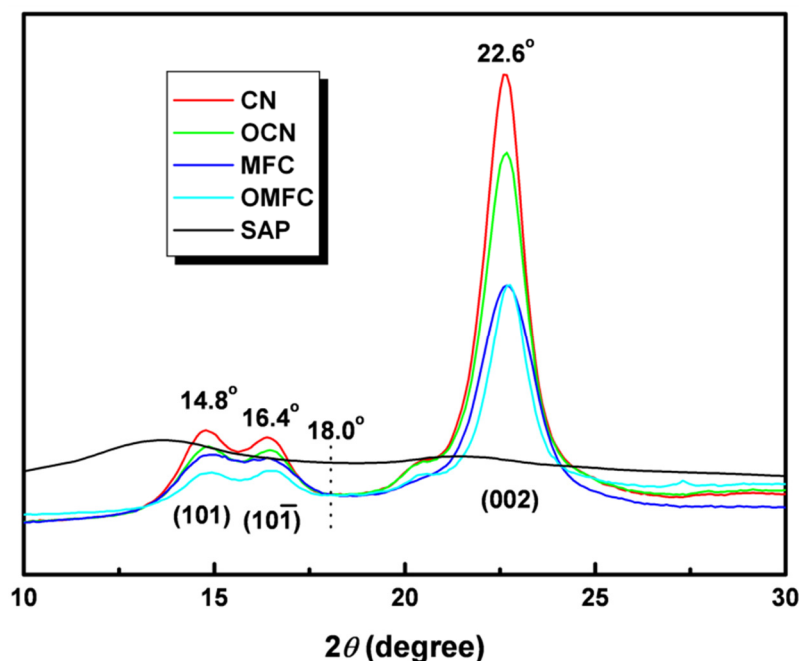


Figure 4.5 X-ray diffraction patterns for CN, OCN, MFC, OMFC, as well as alginate sodium powder (SAP).

4.4 Structure and Properties of Crosslinked Sponges

4.4.1 Crosslinking and Crystalline Properties

The intermolecular interactions between alginate and nanocellulose components in the sponges, especially the ionic interaction after crosslinking, have been confirmed by FTIR analysis, as shown in Figure 4.6. The characteristic peak of alginate is located at 1602 cm^{-1} , corresponding to the carbonyl bond ($-\text{C}=\text{O}$). The peaks at 1426 and 1020 cm^{-1} in both alginate and cellulose were attributed to carboxyl $-\text{COO}-$ and $-\text{C}-\text{O}-\text{C}$ stretching bands, respectively. However, the apparent changes in spectra were observed from the spectrum of SA/OMFC sponge (Figure 4.6B). The typical alginate adsorption bands ($-\text{C}=\text{O}$ and $-\text{COO}-$) shifted toward higher wavelengths, from 1602 to 1612 cm^{-1} and from 1426 to 1435 cm^{-1} , as the OMFC content in sponge increased. These shifts to higher wavelengths could be attributed to the carboxylic groups on oxidized nanocellulose linking adjacent alginate molecules to form the crosslinked network. There was no evident shift of these two bands in the spectra of alginate/unmodified nanocellulose [both SA/CN (Figure 4.6A)

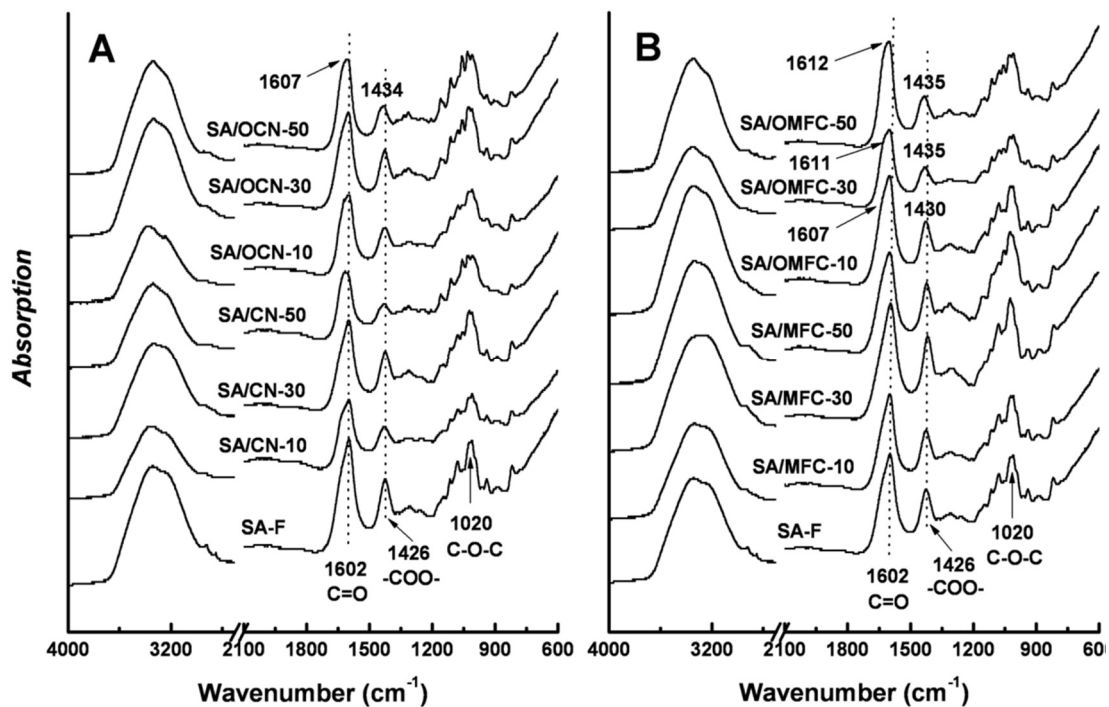


Figure 4.6 FTIR spectra for SA/CN, SA/OCN, SA/MFC, and SA/OMFC sponges with various cellulose contents and neat SA-F sponge.

and SA/MFC] sponges. All these changes suggested the evidence of ionic interactions and molecular compatibility between alginate and oxidized nanocellulose.

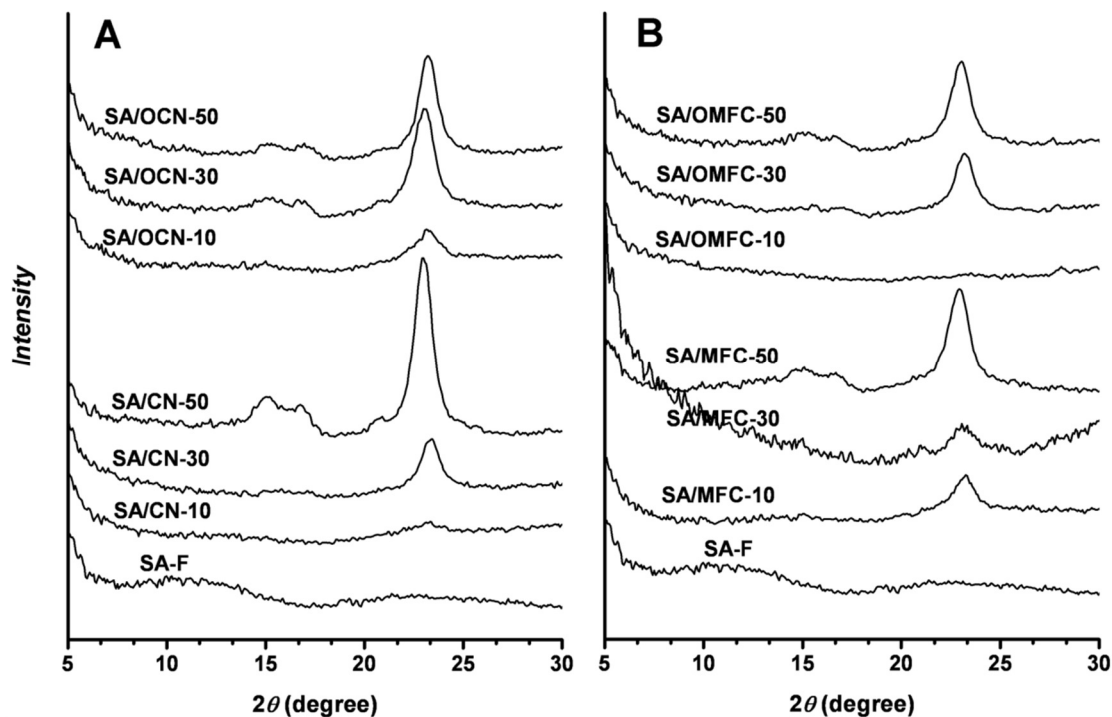


Figure 4.7 XRD patterns for SA/CN, SA/OCN, SA/MFC, and SA/OMFC sponges with various cellulose contents and neat SA-F sponge.

The X-ray diffraction (XRD) patterns of crosslinked sponges can reflect the crystalline structure of these sponges and provide correlations of nanocellulose within alginate component. As shown in Figure 4.7, neat alginate sponge (SA-F) showed an amorphous structure. However, the alginate/nanocellulose sponges gradually presented the crystalline characteristic of cellulose with the increase of cellulose content, such as the diffraction peaks at 14.8° , 16.4° , and particularly 22.6° . This result is consistent with another study on crystalline properties of cellulose nanocrystal–alginate nanocomposite fibers by wide-angle X-ray diffraction (WAXD) analysis.⁵⁵ Moreover, for the sponges with high nanocellulose content (50 wt%), a slightly reduced intensity of characteristic peaks of cellulose was observed upon oxidation. It can be attributed to the effect of ionic crosslinking of oxidized nanocellulose, leading to the close conjunction between oxidized nanocellulose and

amorphous alginate in sponges. In addition, among the patterns of all sponges, SA/CN-50 and SA/MFC-50 showed the strongest diffraction peaks of cellulose, which may indicate some self-aggregation of nanocellulose in alginate sponges and result in the changes of these two sponges.

4.4.2 Microstructure

The cross-section morphologies of the sponges observed by scanning electron microscopy (SEM) are shown in Figure 4.8. The neat alginate sponge (SA-F) exhibited a random stratified structure with a porous morphology [Figure 4.8 (a)], which was in accordance with other reports.^{3,12} When cellulose nanocrystals (CN or OCN) were introduced in alginate, the self-aggregation of nanocrystals appeared in the sponges for high nanocrystal content (50 wt%). Nevertheless, due to the similar chemical structures between cellulose and alginate, CN and OCN still can be compatible with alginate, and no obvious agglomeration or separation at the interface was observed [Figure 4.8 (b) and (c)]. Slightly different from cellulose nanocrystals, sponges containing MFC (SA/MFC-50) showed an irregular network structure with smaller pores [Figure 4.8 (d)] in comparison with neat alginate sponge.

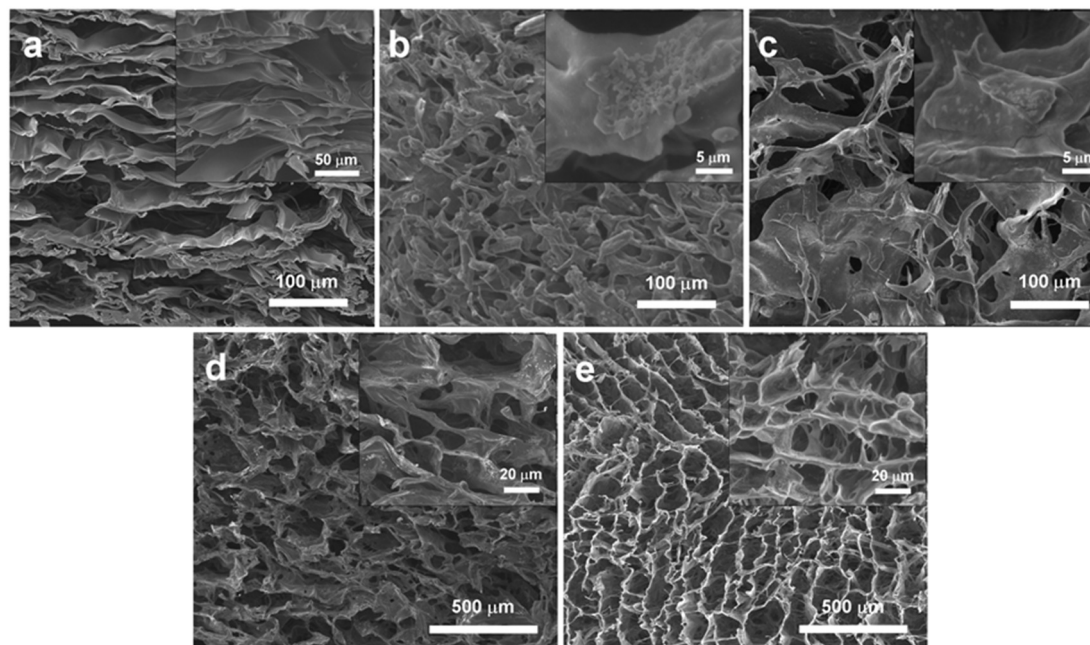


Figure 4.8 SEM images of the cross-section morphology of crosslinked sponges: (a) SA-F, (b) SA/CN-50, (c) SA/OCN-50, (d) SA/MFC-50, and (e) SA/OMFC-50.

The most interesting morphology was obtained for the sponge with 50 wt% OMFC (SA/OMFC-50), which exhibited a highly porous structure from interconnected pores with size in the range of 100–300 μm , as shown in Figure 8e. The high-magnification morphology indicated that a homogeneous combination between oxidized microfibrillated cellulose and alginate component was reached. Meanwhile, there was no apparent or serious self-aggregation or microphase separation in the sponge in spite of the high OMFC content. The introduction of OMFC, as the essential structural component, constituted the regular internal three-dimensional network of crosslinked sponge together with the alginate.

4.4.3 Porosity, Water Absorption, and Structural Stability

Highly porous and interconnected pore structures are required for alginate-based sponges to ensure water absorption and mechanical strength, especially as biomedical materials, such as tissue engineering scaffolds. It is worth noting that the freeze-drying method, which can prevent the destruction of the porous structure during the removal of water, was adopted in the preparation of crosslinked sponges. The porosity (P), water absorption (WA), and water retention (WR) values for the various alginate/cellulose sponges are summarized in Table 4.1. The structural stability was evaluated from the reuse effects of the sponges, as shown in Figure 4.9. In general, compared with the porosity of neat alginate sponge (SA-F, 78.8%), the porosity of all the alginate/nanocellulose sponges was improved above 80%, especially reaching a maximum of 97.4% for the SA/OMFC-50 sponge. For the sponges filled with CNs, for both oxidized and unmodified nanocrystals, the increase in porosity was more remarkable for the sponges with low nanocrystal contents, which may be attributed to the homogeneous dispersion of nanocrystals in alginate-based sponges. On the other hand, with higher length, MFC and OMFC generally presented considerable improvement in the porosity of sponges in comparison with nanocrystals. Especially for SA/OMFC sponges, all of them possessed ultrahigh porosity ($> 94.0\%$). It was presumed that the high porosity of SA/OMFC sponges originated from the internal network microstructure resulting

from the interconnection between alginate and OMFC chains.

Water absorption (*WA*) and water retention (*WR*) are very important properties for sponge materials, which are highly dependent on their inherent structure and morphology. The interconnected pores of sponges will provide indispensable channels and roomage to “reserve” the liquid molecules. As for the sponges composed of regular pore arrangement and “strong” network connection, water molecules will readily pass through and fully permeate the entire sponge. Evidently, in comparison with neat alginate sponge (only 835.3% for SA-F), SA/OMFC crosslinked sponges held more open and ordered pores as well as solid internal structure (from the SEM observation), which exhibited considerable water absorption (> 1300%). At the same time, the uniform and solid porous structure of crosslinked sponge will “lock” the water molecules and prevent the easy runoff of water. Comparing the water retention between neat alginate and SA/OMFC sponges, after the centrifugation treatment, *WR* of SA-F sponge sharply decreased to 321.1%, whereas *WR* of SA/OMFC-50 sponge remained at a level higher than 800%. It should be noted that, similarly to porosity results, no improvement in water absorption and retention for alginate sponges filled with CN was observed. This may be attributed to the simple effect from rigid nanocrystals to the sponges of enhancing the mechanical strength, but not essential to the crosslinked network.

Used as a daily material, the evaluation of reusable effect of sponges is critical for their practical application. Figure 4.9 shows the results, for various alginate/nanocellulose sponges in distilled water, of water absorption during the process of absorbing–discharging water for 10 times. After reusing for only four or five times, the water absorption of neat alginate sponge (SA-F) decreased sharply and was finally reduced by 59% for the tenth time. This can be attributed to the structure disruption of these fragile sponges during the process of repetitive drying and discharging water, and the open pores in the original structure might collapse or conglutinate. In fact, after reusing for 10 times, the shrinkage and collapse of the internal structure were reflected by the change of external shape appearing in neat

alginate sponge, as shown in the inserted image (a) in Figure 4.9. However, the reuse effects of SA/OMFC crosslinked sponges were much better than for the SA-F sponge, which kept water absorption at a fairly high level. For instance, after absorbing–discharging water for 10 times, the water absorption of SA/OMFC-50 sponge only decreased by 18%, and also, its shape integrity was well preserved (inserted image (b) in Figure 4.9).

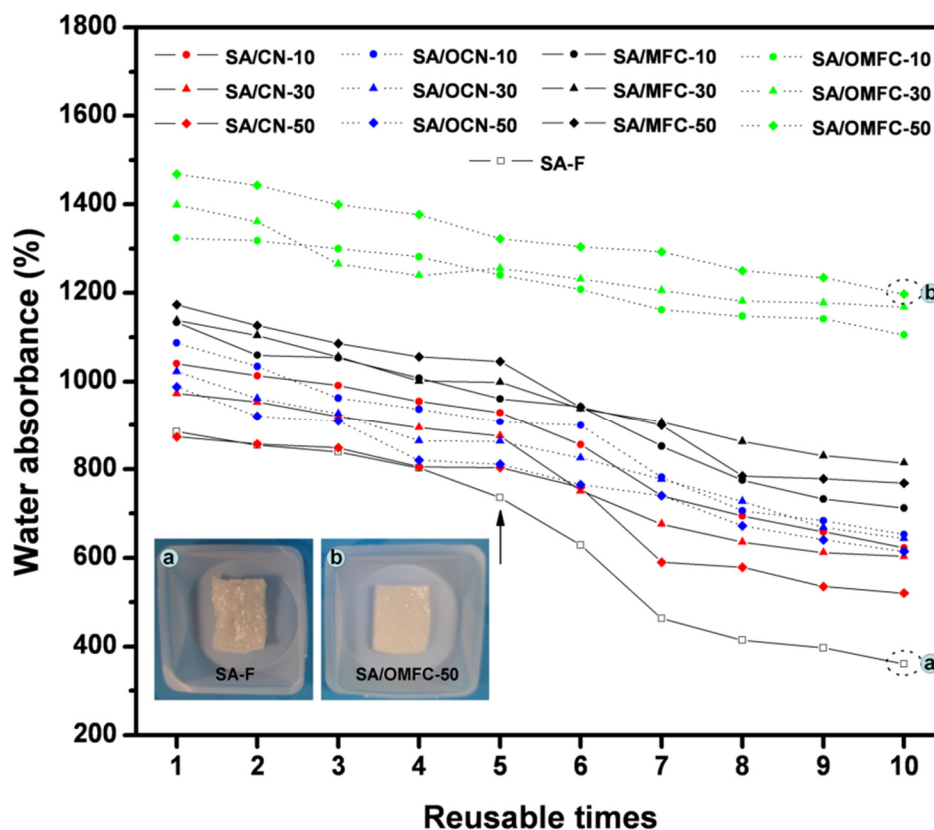


Figure 4.9 Reusable properties for various alginate/nanocellulose crosslinked sponges.

4.4.4 Mechanical Stability

As mentioned, neat alginate sponge is a kind of brittle material with low mechanical performance. On the contrary, sponges containing oxidized microfibrillated cellulose (such as SA/OMFC-30) possessed higher mechanical stability, exhibiting excellent flexibility and strength, as shown in Figure 4.1 and Figure 4.10.

The compressive stress–strain curves for various sponges are shown in Figure 4.10. Mechanical testing of the Ca^{2+} crosslinked sponges under compression indicated that alginate-based sponges filled with (both unmodified and oxidized) cellulose

nanocrystals were generally stronger and more robust than neat alginate. The highest mechanical performance was obtained for SA/OCN-10. For compressive strain of 30%, 50%, and 70%, the compressive strength of SA/OCN-10 increased by factors of 2.78, 2.80, and 2.94, respectively, in comparison with SA-F. It is also worth noting that, compared to pristine nanocrystals, SA/OCN-10 with oxidized nanocrystals exhibited higher mechanical strength than SA/CN-10, which can be attributed to the OCN-participating crosslinking and good conjunction between OCN and alginate during the crosslinking process. However, if superfluous nanocrystals were introduced in sponges, especially for unmodified nanocrystals, this reinforcing effect shaded-off because of the self-aggregation of nanoparticles (such as SA/CN-50). These changes in mechanical properties are consistent with the observed microstructures from SEM and XRD. On the other hand, OMFC also showed considerable improvement of the mechanical properties compared to alginate-based sponges. For compressive strain of 30%, 50%, and 70%, the compressive strength of SA/OMFC-30 increased by factors of 2.03, 1.79, and 1.68, respectively, compared to SA-F. In comparison with the mechanical performance of sponges reinforced with

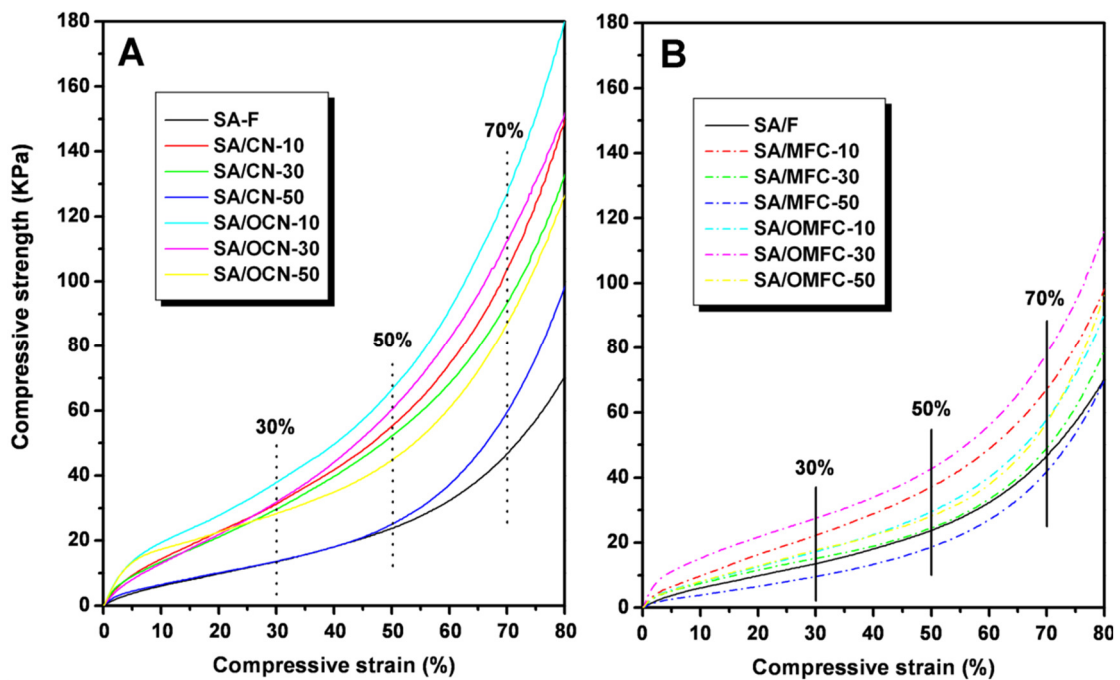


Figure 4.10 Compressive stress–strain curves for various alginate/nanocellulose crosslinked sponges.

both nanocelluloses, it should be pointed out that rigid nanocrystals exhibited a better nano-reinforcing effect, which can be attributed to their capability of effectively enduring and transferring the stress, resulting in higher mechanical strength especially under large compressive strain (such as 70%).

4.4.5 Thermal Stability

As reported in previous studies,⁵⁶ alginate undergoes a two-step thermal degradation process, with a first-step thermal degradation temperature (T_{d1}) in the range 106–190 °C and the second-step (T_{d2}) in the range 219–261 °C. Figure 4.11 shows DSC thermograms for a series of alginate/nanocellulose sponges. As shown in Figure 4.11 (A), the introduction of CN in alginate caused the decrease of the first-stage thermal degradation temperature (T_{d1}) of the sponges, which can be attributed to the influence of rigid nanocrystals. Especially for high CN contents, the T_{d1} of SA/CN-50 sponge was reduced by 15.8 °C in comparison with that of neat alginate sponge (SA-F). Similarly, the addition of OCN induced the decrease of sponges' T_{d1} . Interestingly, as shown in Figure 4.11 (B), sponges filled with OMFC

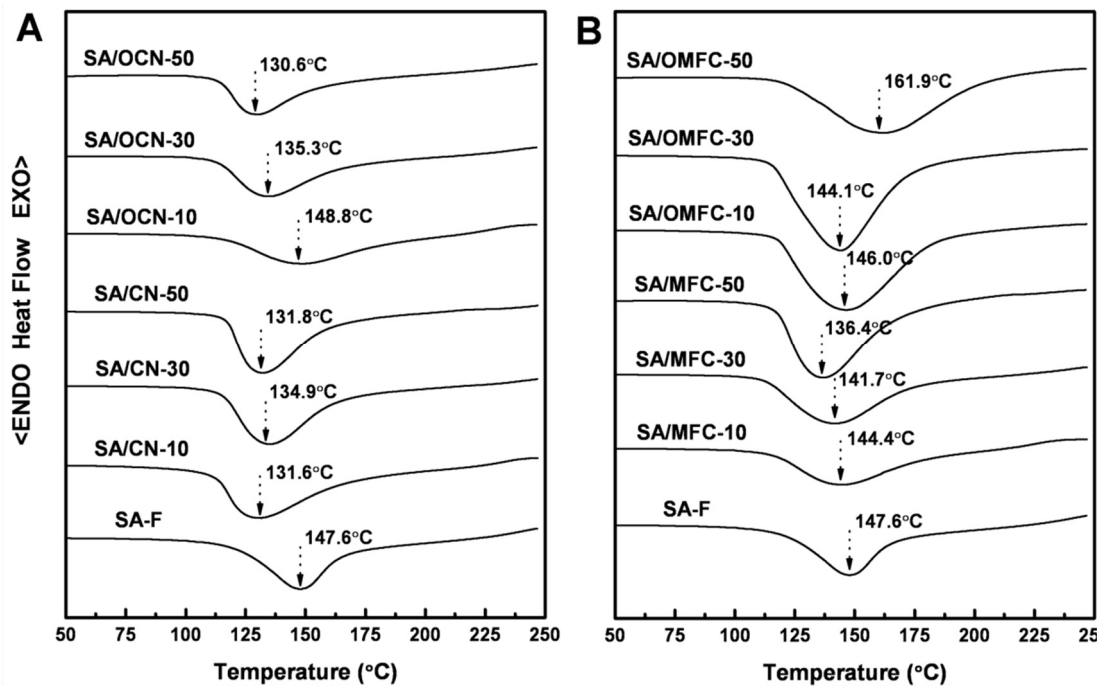


Figure 4.11 DSC thermograms for SA/CN, SA/OCN, SA/MFC, and SA/OMFC sponges with various nanocellulose contents and neat SA-F sponge.

displayed the tendency to gradually increase T_{d1} values. All the first-stage thermal degradation temperatures of sponges were higher than 144 °C, especially for SA/OMFC-50 sponge ($T_{d1} = 161.9$ °C), which was 14.3 °C higher than that for the SA-F sponge.

Thermogravimetric analysis (TGA) was performed to evaluate the presence and evolution of the second-stage (T_{d2}) thermal degradation process in crosslinked alginate-based sponges, as shown in Figure 4.12. The thermograms of neat alginate (SA-F) sponge showed the second-stage degradation at a temperature of 222.0 °C. The degradation temperatures (T_{d2}) of sponges filled with 50 wt% CN and OCN were close to the T_{d2} of SA-F. However, the value of T_{d2} for the sponge filled with OMFC (SA/OMFC-50) shifted toward higher temperatures (237.4 °C), which was 15.4 °C higher than that for SA-F. Moreover, in comparison with the neat alginate sponge, the total weight loss for SA/OMFC-50 was 51.8% (i.e. lower than 58.3% for SA-F). The considerable increase in both the first-stage and second-stage thermal degradation temperatures observed from DSC and TGA experiments indicated a better thermal stability for crosslinked sponges with oxidized nanocellulose (especially for OMFC).

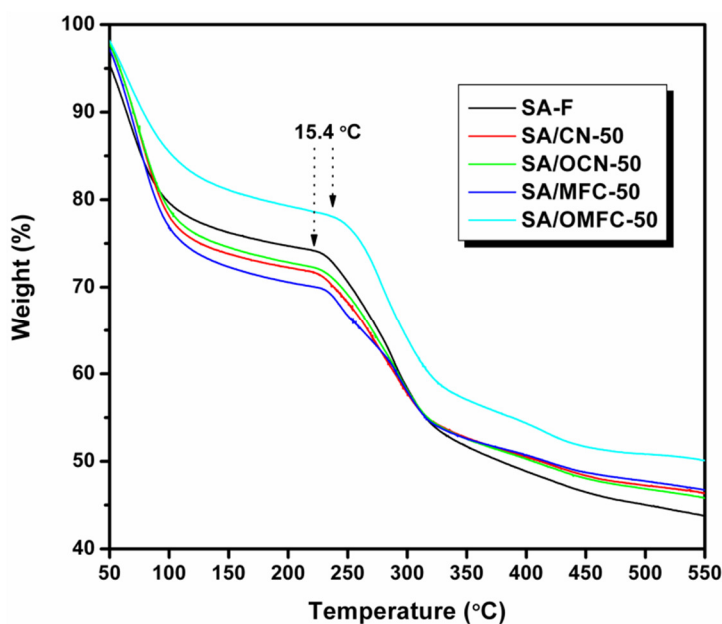


Figure 4.12 TGA thermograms for SA-F, SA/CN-50, SA/OCN-50, SA/MFC-50, and SA/OMFC-50 sponges.

4.5 Roles and Mechanisms of Different Nanocelluloses in Alginate-Based Sponges

The role of nanocellulose in alginate-based sponges can be discussed according to three different effects, namely, (i) by comparing pristine and oxidized nanocellulose, (ii) depending on the nanocellulose content, and (iii) by comparing cellulose nanocrystals and microfibrillated cellulose. First, the surface chemical modification induced by oxidization of nanocellulose is beneficial to enhance the effect of nanocellulose in sponges, as reflected through the higher strength of SA/OCN-10 compared to SA/CN-10 and higher water absorption of SA/OMFC-10 compared to SA/MFC-10. This effect can be attributed to the capability of participating ionic crosslinking of oxidized nanocellulose during the structural formation of alginate-based sponges, as shown in Figure 4.13 (a) and (b). Although it was difficult to observe this physical interaction directly, this effect of oxidized nanocellulose-participating crosslinking was reflected by the results of FTIR, XRD, and the changes of structural, mechanical, and thermal properties.

Despite the fact that oxidized nanocellulose-participating crosslinking should facilitate the close conjunction with alginate component, the content of nanocellulose is another parameter affecting the performance of sponges. From SEM observation and XRD results, it seemed that low nanocellulose contents can be homogeneously dispersed, while superfluous nanocellulose (50 wt%) induced self-aggregation in sponges, which may even cause the microphase separation between nanocellulose and alginate in the system. The influence of nanocellulose content was reflected in the performance of resultant sponges, especially for the sponges with high contents of unmodified nanocellulose, such as the weak water absorption of SA/CN-50 and lower compressive strength of SA/MFC-50 in comparison with neat alginate sponge (SA-F).

It is probably more interesting to compare the role of oxidized nanocrystalline and microfibrillated cellulose. As shown in Figure 4.13 (d), benefiting from the new

carboxyl groups and the advantage of long filaments, OMFC can not only participate to the crosslinking but also can be involved with alginate in the structural construction of the sponge, which can form a semi-interpenetrating polymer network (SIPN) in ensuing alginate-based sponges. Derived from the effect of OMFC-participating network structure, SA/OMFC sponges presented ultrahigh porosity, even pore interconnection, and good structural stability, which is particularly favorable for water absorption and retention. On the other hand,

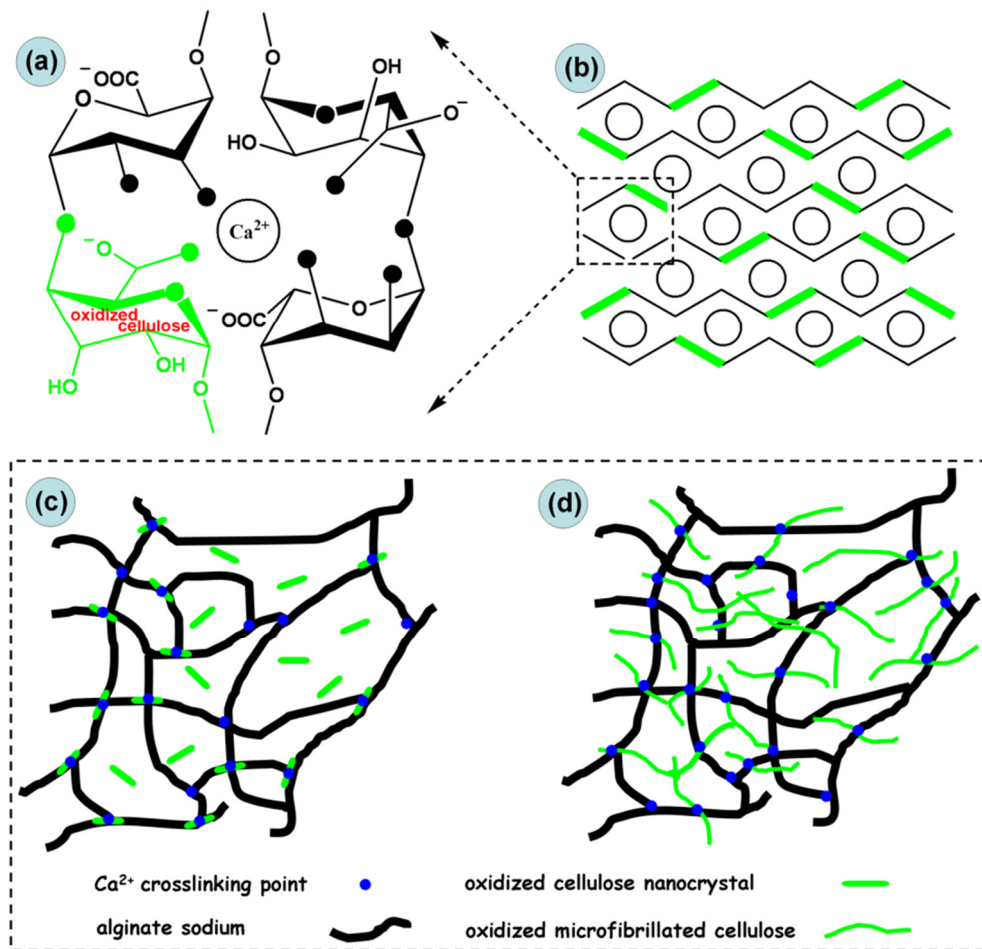


Figure 4.13 Schematic representation of the structure of egg-box junction zones in TEMPO-mediated oxidation of cellulose/alginate/calcium system: (a) coordination of Ca^{2+} in a cavity created by a pair of guluronate sequences along alginate chains; (b) laterally associated egg-box multimer in composite sponge; (c) oxidized cellulose nanocrystals (OCN) in the cross-linking of alginate sponge; (d) construction of the semi-interpenetrating polymer network (SIPN) composed of oxidized microfibrillated cellulose (OMFC) and alginate. The black solid circles in panel a represent the oxygen atoms possibly involved in the coordination with Ca^{2+} .

possessing a rigid and rod-like nanostructure, oxidized nanocrystals are more suitable to enhance the mechanical strength of sponges. As schematized in Figure 4.13 (c), rigid OCN participated in the crosslinking and served as the coupling points with alginate, which is beneficial to the “strong” reinforced framework of sponges. However, compared to OMFC, it is difficult with OCN to build the network structure in sponges, which leads to the weak improvement of porosity and water absorption. The results from FTIR, with the obvious shifts to higher wavelengths for SA/OMFC sponges and only slight shift for SA/OCN sponges despite the high OCN content (50 wt%), also proved the presumption.

4.6 Conclusions

In this work, we designed oxidized nanocellulose-participating crosslinking sponges from two oxidized nanocelluloses and reported remarkable enhanced mechanical strength with oxidized cellulose nanocrystals and promising improved porosity, water absorption, and structural stability with oxidized microfibrillated cellulose. Rigid oxidized cellulose nanocrystals served as the coupling points, and fully played the nanoreinforcement effect for alginate-based sponges, whereas oxidized microfibrillated cellulose can join in the structural construction and form the semi-interpenetrating polymer network for alginate-based sponges. With the improvement of porosity and water absorption as well as high mechanical strength, these sponges have potential applications as kinetic energy absorbers, thermal and acoustic insulating materials, reinforcing platforms, and scaffolds for nanocomposites, etc. Inspired by the different effects of the two oxidized nanocelluloses, we will attempt to incorporate both oxidized nanocrystalline and microfibrillated cellulose in alginate-based materials, and develop application of the ensuing sponges in the field of biomedical materials, such as drug carriers for wound dressing.

4.7 References

1. Augst, A. D.; Kong, H. J.; Mooney, D. J. Alginate hydrogels as biomaterials. *Macromol. Biosci.* **2006**, *6*, 623–633.
2. Hyland, L. L.; Taraban, M. B.; Hammouda, B.; Yu, Y. B. Mutually reinforced multicomponent polysaccharide networks. *Biopolymers* **2011**, *95*, 840–851.
3. Yuan, N.-Y.; Lin, Y.-A.; Ho, M.-H.; Wang, D.-M.; Lai, J.-Y.; Hsieh, H.-J. Effects of the cooling mode on the structure and strength of porous scaffolds made of chitosan, alginate, and carboxymethyl cellulose by the freeze-gelation method. *Carbohydr. Polym.* **2009**, *78*, 349–356.
4. Seo, S.-J.; Kim, I.-Y.; Choi, Y.-J.; Akaike, T.; Cho, C.-S. Enhanced liver functions of hepatocytes cocultured with NIH 3T3 in the alginate/galactosylated chitosan scaffold. *Biomaterials* **2006**, *27*, 1487–1495.
5. Öztürk, E.; Ağalar, C.; Keçeci, K.; Denkbaş, E. B. Preparation and characterization of ciprofloxacin-loaded alginate/chitosan sponge as a wound dressing material. *J. Appl. Polym. Sci.* **2006**, *101*, 1602–1609.
6. Li, Z.; Ramay, H. R.; Hauch, K. D.; Xiao, D.; Zhang, M. Chitosan–alginate hybrid scaffolds for bone tissue engineering. *Biomaterials* **2005**, *26*, 3919–3928.
7. Ho, M.-H.; Kuo, P.-Y.; Hsieh, H.-J.; Hsien, T.-Y.; Hou, L.-T.; Lai, J.-Y.; Wang, D.-M. Preparation of porous scaffolds by using freeze-extraction and freeze-gelation methods. *Biomaterials* **2004**, *25*, 129–138.
8. Lai, H. L.; Abu’Khalil, A.; Craig, D. Q. M. The preparation and characterisation of drug-loaded alginate and chitosan sponges. *Int. J. Pharmaceut.* **2003**, *251*, 175–181.
9. Chung, T. W.; Yang, J.; Akaike, T.; Cho, K. Y.; Nah, J. W.; Kim, S. I.; Cho, C. S. Preparation of alginate/galactosylated chitosan scaffold for hepatocyte attachment. *Biomaterials* **2002**, *23*, 2827–2834.
10. Khan, F.; Khanam, A.; Parihar, M. S.; Bilginya, R.; Rai, K.; Khan, F. Dissipative convective structures and nanoparticles encapsulation in Cu/alginate/dextran composite hydrogels and sponges. *Carbohydr. Polym.* **2011**,

- 83, 586–590.
11. Bilginya, R.; Khan, F.; Mann, S. Spontaneous patterning and nanoparticle encapsulation in carboxymethylcellulose/alginate/dextran hydrogels and sponges. *Mat. Sci. Eng. C-Mater.* **2010**, *30*, 352–356.
 12. Khan, F.; Walsh, D.; Patil, A. J.; Perriman, A. W.; Mann, S. Self-organized structural hierarchy in mixed polysaccharide sponges. *Soft Matter* **2009**, *5*, 3081–3085.
 13. Choi, Y. S.; Hong, S. R.; Lee, Y. M.; Song, K. W.; Park, M. H.; Nam, Y. S. Study on gelatin-containing artificial skin: I. Preparation and characteristics of novel gelatin-alginate sponge. *Biomaterials* **1999**, *20*, 409–417.
 14. Sang, L.; Luo, D.; Xu, S.; Wang, X.; Li, X. Fabrication and evaluation of biomimetic scaffolds by using collagen–alginate fibrillar gels for potential tissue engineering applications. *Mat. Sci. Eng. C-Mater.* **2011**, *31*, 262–271.
 15. Sakai, S.; Masuhara, H.; Yamada, Y.; Ono, T.; Ijima, H.; Kawakami, K. Transition of mechanical property of porous alginate scaffold with cells during culture period. *J. Biosci. Bioeng.* **2005**, *100*, 127–129.
 16. Hamasaki, S.; Tachibana, A.; Tada, D.; Yamauchi, K.; Tanabe, T. Fabrication of highly porous keratin sponges by freeze-drying in the presence of calcium alginate beads. *Mat. Sci. Eng. C-Mater.* **2008**, *28*, 1250–1254.
 17. Roh, D.-H.; Kang, S.-Y.; Kim, J.-Y.; Kwon, Y.-B.; Kweon, H. Y.; Lee, K.-G.; Park, Y.-H.; Baek, R.-M.; Heo, C.-Y.; Choe, J.; Lee, J.-H. Wound healing effect of silk fibroin/alginate-blended sponge in full thickness skin defect of rat. *J. Mater. Sci.-Mater. M.* **2006**, *17*, 547–552.
 18. Lee, K.-G.; Kweon, H. Y.; Yeo, J.-H.; Woo, S.-O.; Lee, J.-H.; Park, Y. H. Structural and physical properties of silk fibroin/alginate blend sponges. *J. Appl. Polym. Sci.* **2004**, *93*, 2174–2179.
 19. Chiaoprakobkij, N.; Sanchavanakit, N.; Subbalekha, K.; Pavasant, P.; Phisalaphong, M. Characterization and biocompatibility of bacterial cellulose/alginate composite sponges with human keratinocytes and gingival fibroblasts. *Carbohydr. Polym.* **2011**, *85*, 548–553.

20. Nussinovitch, A.; Corradini, M. G.; Normand, M. D.; Peleg, M. Effect of starch, sucrose and their combinations on the mechanical and acoustic properties of freeze-dried alginate gels. *Food Res. Int.* **2001**, *34*, 871–878.
21. Lin, H.-R.; Yeh, Y.-J. Porous alginate/hydroxyapatite composite scaffolds for bone tissue engineering: Preparation, characterization, and *in vitro* studies. *J. Biomed. Mater. Res. B* **2004**, *71B*, 52–65.
22. Despang, F.; Börner, A.; Dittrich, R.; Tomandl, G.; Pompe1, W.; Gelinsky, M. Alginate/calcium phosphate scaffolds with oriented, tube-like pores. *Materialwiss. Werkst.* **2005**, *36*, 761–767.
23. Hrynyk, M.; Martins-Green, M.; Barron, A. E.; Neufeld, R. J. Alginate-PEG sponge architecture and role in the design of insulin release dressings. *Biomacromolecules* **2012**, *13*, 1478–1485.
24. Moon, R. J.; Martini, A.; Nairn, J.; Simonsen, J.; Youngblood, J. Cellulose nanomaterials review: structure, properties and nanocomposites. *Chem. Soc. Rev.* **2011**, *40*, 3941–3994.
25. Klemm, D.; Kramer, F.; Moritz, S.; Lindström, T.; Ankerfors, M.; Gray, D.; Dorri, A. Nanocelluloses: A new family of nature-based materials. *Angew. Chem. Int. Edit.* **2011**, *50*, 5438–5466.
26. Habibi, Y.; Lucia, L. A.; Rojas, O. J. Cellulose nanocrystals: Chemistry, self-assembly, and applications. *Chem. Rev.* **2010**, *110*, 3479–3500.
27. Azizi Samir, M. A. S.; Alloin, F.; Dufresne, A. Review of recent research into cellulosic whiskers, their properties and their application in nanocomposite field. *Biomacromolecules* **2005**, *6*, 612–626.
28. Lin, N.; Huang, J.; Dufresne, A. Preparation, properties and applications of polysaccharide nanocrystals in advanced functional nanomaterials: a review. *Nanoscale* **2012**, *4*, 3274–3294.
29. Lam, E.; Male, K. B.; Chong, J. H.; Leung, A. C. W.; Luong J. H. T. Applications of functionalized and nanoparticle-modified nanocrystalline cellulose. *Trends in Biotechnology* **2012**, *30*, 283–290.
30. Lin, N.; Huang, J.; Chang, P. R.; Feng, L.; Yu, J. Effect of polysaccharide

- nanocrystals on structure, properties, and drug release kinetics of alginate-based microspheres. *Colloid. Surface. B* **2011**, *85*, 270–279.
31. Siró, I.; Plackett, D. Microfibrillated cellulose and new nanocomposite materials: A review. *Cellulose* **2010**, *17*, 459–494.
 32. Lavoine, N.; Desloges, I.; Dufresne, A.; Bras, J. Microfibrillated cellulose—its barrier properties and applications in cellulosic materials: A review. *Carbohydr. Polym.* **2012**, *90*, 735–764.
 33. Lu, J.; Wang, T.; Drzal, L. T. Preparation and properties of microfibrillated cellulose polyvinyl alcohol composite materials. *Compos. Part A-Appl. S.* **2008**, *39*, 738–746.
 34. Nyström, G. ; Mihranyan, A.; Razaq, A.; Lindström, T.; Nyholm, L.; Strømme, M. A nanocellulose polypyrrole composite based on microfibrillated cellulose from wood. *J. Phys. Chem. B* **2010**, *114*, 4178–4182.
 35. Lönnberg, H.; Larsson, K.; Lindström, T.; Hult, A.; Malmström, E. Synthesis of polycaprolactone-grafted microfibrillated cellulose for use in novel bionanocomposites—influence of the graft length on the mechanical properties. *ACS Appl. Mater. Inter.* **2011**, *3*, 1426–1433.
 36. Bulota, M.; Tanpichai, S.; Hughes, M.; Eichhorn, S. J. Micromechanics of TEMPO-oxidized fibrillated cellulose composites. *ACS Appl. Mater. Inter.* **2012**, *4*, 331–337.
 37. Tingaut, P.; Zimmermann, T.; Lopez-Suevos, F. Synthesis and characterization of bionanocomposites with tunable properties from poly(lactic acid) and acetylated microfibrillated cellulose. *Biomacromolecules* **2010**, *11*, 454–464.
 38. Suryanegara, L.; Nakagaito, A. N.; Yano, H. The effect of crystallization of PLA on the thermal and mechanical properties of microfibrillated cellulose-reinforced PLA composites. *Compos. Sci. Technol.* **2009**, *69*, 1187–1192.
 39. Lu, J.; Askeland, P.; Drzal, L. T. Surface modification of microfibrillated cellulose for epoxy composite applications. *Polymer* **2008**, *49*, 1285–1296.
 40. Lu, J.; Drzal, L. T. Microfibrillated cellulose/cellulose acetate composites: Effect of surface treatment. *J. Polym. Sci. Pol. Phys.* **2010**, *48*, 153–161.

41. Hassan, M. L.; Hassan, E. A.; Oksman, K. N. Effect of pretreatment of bagasse fibers on the properties of chitosan/microfibrillated cellulose nanocomposites. *J. Mater. Sci.* **2011**, *46*, 1732–1740.
42. Nordqvist, D.; Idermark, J.; Hedenqvist, M. S. Enhancement of the wet properties of transparent chitosan-acetic-acid-salt films using microfibrillated cellulose. *Biomacromolecules* **2007**, *8*, 2398–2403.
43. Plackett, D.; Anturi, H.; Hedenqvist, M.; Ankerfors, M.; Gällstedt, M.; Lindström, T.; Siró, I. Physical properties and morphology of films prepared from microfibrillated cellulose and microfibrillated cellulose in combination with amylopectin. *J. Appl. Polym. Sci.* **2010**, *117*, 3601–3609.
44. Lemahieu, L.; Bras, J.; Tiquet, P.; Augier, S.; Dufresne A. Extrusion of nanocellulose-reinforced nanocomposites using the dispersed nano-objects protective encapsulation (DOPE) process. *Macromol. Mater. Eng.* **2011**, *296*, 984–991.
45. Azouz, K. B.; Ramires, E. C.; Van den Fonteyne, W.; Kissi, N. E.; Dufresne, A. Simple method for the melt extrusion of a cellulose nanocrystal reinforced hydrophobic polymer. *ACS Macro Lett.* **2012**, *1*, 236–240.
46. Ruiz, M. M.; Cavallé, J. Y.; Dufresne, A.; Gérard, J. F.; Graillat, C. Processing and characterization of new thermoset nanocomposites based on cellulose whiskers. *Compos. Interface.* **2000**, *7*, 117–131.
47. Okubo, K.; Fujii, T.; Thostenson, E. T. Multi-scale hybrid biocomposite: Processing and mechanical characterization of bamboo fiber reinforced PLA with microfibrillated cellulose. *Compos. Part A-Appl. S.* **2009**, *40*, 469–475.
48. Habibi, Y.; Chanzy, H.; Vignon, M. R. TEMPO-mediated surface oxidation of cellulose whiskers. *Cellulose* **2006**, *13*, 679–687.
49. Isogai, A.; Saito, T.; Fujisawa, S. *Nanoscale* **2011**, *3*, 71–85.
50. Saito, T.; Nishiyama, Y.; Putaux, J. L.; Vignon M.; Isogai, A. Homogeneous suspensions of individualized microfibrils from TEMPO-catalyzed oxidation of native cellulose. *Biomacromolecules* **2006**, *7*, 1687–1691.
51. Okita, Y.; Fujisawa, S.; Saito, T.; Isogai, A. TEMPO-Oxidized cellulose

- nanofibrils dispersed in organic solvents. *Biomacromolecules* **2011**, *12*, 518–522.
52. da Silva Perez, D.; Montanari, S.; Vignon M. R. TEMPO-Mediated oxidation of cellulose III. *Biomacromolecules* **2003**, *4*, 1417–1425.
53. Lin, N.; Huang, J.; Chang, P. R.; Feng, J.; Yu, J. Surface acetylation of cellulose nanocrystal and its reinforcing function in poly(lactic acid). *Carbohydr. Polym.* **2011**, *83*, 1834–1842.
54. Segal, L.; Creely, J. J.; Martin, A. E. Jr.; Conrad, C. M. An empirical method for estimating the degree of crystallinity of native cellulose using the X-ray diffractometer. *Text. Res. J.* **1959**, *29*, 786–794.
55. Ureña-Benavides, E. E.; Kitchens, C. L. Wide-angle X-ray diffraction of cellulose nanocrystal–alginate nanocomposite fibers. *Macromolecules* **2011**, *44*, 3478–3484.
56. Siddaramaiah; Mruthyunjaya Swamy, T. M.; Ramaraj, B.; Lee, J. H. Sodium alginate and its blends with starch: Thermal and morphological properties. *J. Appl. Polym. Sci.* **2008**, *109*, 4075–4081.

CHAPTER 5.

Application of Cellulose Nanocrystals: Supramolecular Hydrogels

“Supramolecular Hydrogels from *In Situ* Host–Guest Inclusion between Chemically Modified Cellulose Nanocrystals and Cyclodextrin”

Chapter 5. Supramolecular Hydrogels from *In Situ* Host–Guest Inclusion between Chemically Modified Cellulose Nanocrystals and Cyclodextrin

ENGLISH ABSTRACT.....	248
RESUME FRANÇAIS	251
5.1 Introduction.....	257
5.2 Experimental Methodology	259
5.2.1 Materials.....	259
5.2.2 Extraction of Cellulose Nanocrystals (CN)	260
5.2.3 Synthesis of β -Cyclodextrin-Grafted Cellulose Nanocrystals [β CD-g-CN (1)].....	260
5.2.4 Inclusion Complex of β CD-g-CN/Pluronic Polymers (2)	261
5.2.5 Supramolecular Hydrogels via <i>In Situ</i> Inclusion [β CD-g-CN/Pluronic] -[α CD]/Pluronic] (3)	262
5.2.6 Characterization and Analyses	263
5.3 Chemical Modification of Cellulose Nanocrystals.....	267
5.3.1 Chemical Grafting of β -CD on the Surface.....	267
5.3.2 Inclusion of Pluronic Polymers in Grafted β -CD	269
5.4 Structure and Properties of Supramolecular Hydrogels.....	271
5.4.1 Crystalline Structure of Inclusive Complexes	271
5.4.2 Morphology and Dimensions of CN and Hydrogels.....	274
5.4.3 Rheological Behavior of Hydrogels.....	275
5.4.4 pH-Sensitivity of Hydrogels	278
5.5 Drug Release and Mechanism Study.....	279
5.6 Conclusions	281
5.7 References	282

ENGLISH ABSTRACT

Hydrogels are defined as three-dimensional polymer network materials able to entrap large amounts of solvent (usually water), and widely used in the fields of food, cosmetics, biomaterials, agriculture etc. On the one hand, rod-like cellulose nanocrystals (CN) can form hydrogels by themselves under some conditions resulting from the strong hydrogen bonding interactions between nanoparticles. It was reported that aqueous suspensions with 0.4 wt% CN extracted from softwood flour can form a transparent hydrogel with unique rigid and uniform morphology.¹ Surface modified tunicate CN with either carboxylic acid (–COOH) or amine (–NH₂) in water can also form hydrogels, and exhibit pH-sensitivity.² Moreover, by involving a solvent exchange process, stable organogels based on CN can be prepared by dispersing the nanoparticles in glycerol,³ ethanol,⁴ or acetone.⁵ On the other hand, composite hydrogels based on CN can be developed by physical blending or chemical crosslinking. Physical hydrogels based on CN are fabricated by direct introduction of the nanoparticles in the hydrogel matrix with ionic or hydrogen bonding interactions, while chemical hydrogels based on CN are formed by the crosslinking of the nanoparticles and hydrogel matrix therefore involving additional covalent bonding interactions. Generally, by adding rigid CN in appropriate concentrations, the structural stability and elastic modulus of composite hydrogels can be improved and enhanced.⁶ Although diverse materials (from synthetic polymeric matrices, e.g. poly(NIPAM-co-BMA)⁷ to natural polymeric matrices, e.g. agarose⁸) have been used as matrix for the preparation of CN-based hydrogels, the development of novel hydrogel systems based on CN and its further applications still attract much more attention, especially for chemically crosslinked hydrogels.

Cyclodextrin (CD), a family of macrocyclic oligosaccharides linked by α -1, 4 glycosidic bonds, has been extensively studied in diverse fields since its discovery by Villiers in 1891.⁹ Among them, α -, β -, and γ -cyclodextrins are the most common members, which are composed of 6, 7, and 8 glucose units with different scales, respectively. The hydrophobic cavity of CD gives it inclusion capacity with a variety of compounds

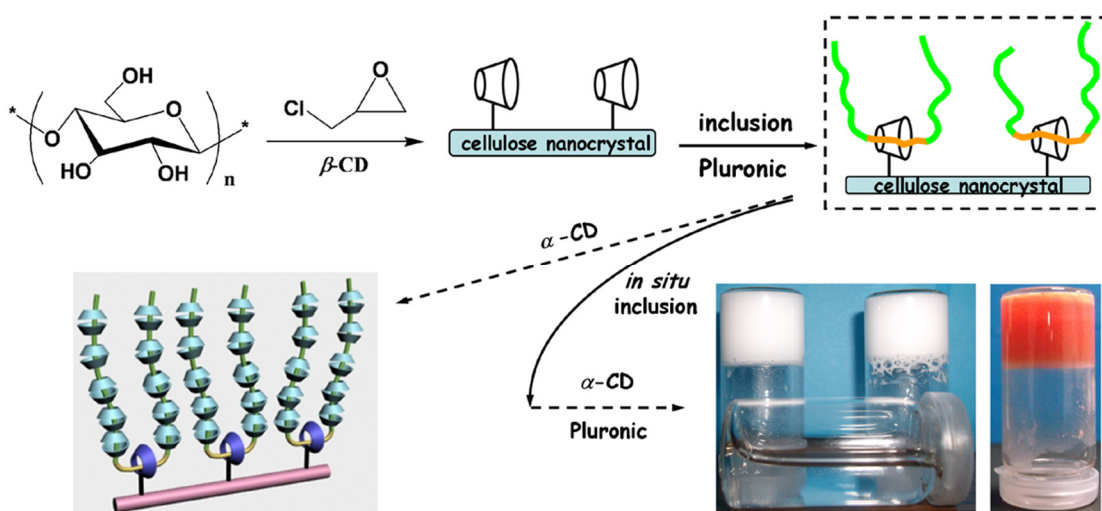
ranging from small molecule, ions, proteins, oligonucleotides, and selected polymers. Since the first report on the formation of hydrogels through the complexes inclusion with high molecular weight PEG and α -CD,¹⁰ threading CD units onto polymer chains to form polypseudorotaxanes as physical crosslinkers has become the most extensively studied approach for engineering supramolecular hydrogels based on CD.¹¹ The physicochemical properties, biocompatibility, biodegradability, and sensitivity of CD-based supramolecular hydrogels can be elegantly tailored by carefully selecting appropriate guest polymers for assembling, and further regulate various functions for the hydrogels, such as temperature-, photon-, chemical-, redox-, or pH-sensitivities. It should be pointed out that since CD-based hydrogels are formed by supramolecular self-assembly in an aqueous solution without the use of chemical crosslinkers, *in situ* loading of drug payload can be achieved at room temperature, which is especially beneficial to biomacromolecular drugs. Therefore, CD-based hydrogels derived from complexes inclusion have been extensively investigated and used as injectable drug delivery systems.¹²

The combination of cellulose nanocrystals and cyclodextrin-based hydrogels can be realized through simple doping and blending for the formation of physical hydrogels, which has been reported previously.¹³ In this study, based on the inclusion of high molecular weight triblock copolymer and α -CD, composite hydrogels were fabricated by the introduction of pristine CN. However, it was reported that the concentration of CN in all composite hydrogels must be lower than 2.5 wt%, and only the hydrogel with loading level of 0.5 wt% CN gave the highest storage modulus. In spite of no further explanation on this issue in this study, it can be presumed that pristine CN seriously self-aggregated during hydrogel preparation due to the hydrophilicity of cellulose, which restricted the loading levels to low values and limited the effect of CN in hydrogels.

The present work is an attempt to design a novel chemical hydrogel with the construction of participating cellulose nanocrystals and cyclodextrin via the “host-guest” inclusion method from selective grafted chains and different types of

cyclodextrins. The key factor of this strategy emphasized on the utilization of a block copolymer (polymeric segments with distinct properties) and CD (with different sizes and recognition) for the selective inclusions, as shown in the “Schematic diagram”. By means of grafted β -CD as target sites, Pluronic polymers have been introduced on the surface of modified CN with the first inclusion between β -CD and hydrophobic segment of Pluronic polymer [poly(propylene glycol), PPG]. Pluronic polymers were semi-chemically immobilized on the surface of CN, which provided the possibility of the second inclusion through uncovered poly(ethylene glycol) segments on CN and α -CD. Attributed to the effect of *in situ* crosslinking, modified cellulose nanocrystals can strongly interact with CD, which will restrict their aggregation and induce the construction of supramolecular hydrogels. The highest concentration of CN in this hydrogel system can reach more than 10 wt%, and with the introduction of high loading levels of modified nanocrystals (>5 wt%), a significant enhancement of the structural and thermal stability of *in situ* hydrogels can be achieved. Further *in vitro* drug release study indicated that these supramolecular hydrogels can be promising drug carrier, which exhibited prolonged drug release behavior for doxorubicin with special release kinetics.

Schematic diagram of the synthesis pathway for the preparation of supramolecular hydrogels from *in situ* inclusion between cellulose nanocrystals (CN) and cyclodextrin (CD).



RESUME FRANÇAIS

Les hydrogels sont par définition des matériaux constitués d'un réseau polymère tridimensionnel capable de piéger de grandes quantités de solvant (habituellement de l'eau), et largement utilisés dans les domaines de l'alimentaire, de la cosmétique, des biomatériaux, de l'agriculture, etc. D'une part les nanocristaux de cellulose (CN) sous forme de bâtonnets peuvent former des hydrogels par eux-mêmes sous certaines conditions grâce aux fortes interactions de type liaison hydrogène entre nanoparticules. Il a été montré que des suspensions aqueuses contenant 0,4% en poids de CN extraits de farine de résineux pouvaient former un hydrogel transparent avec une morphologie rigide et uniforme unique.¹ Des CN de tunicier modifiés en surface avec de l'acide carboxylique (-COOH) ou une amine (-NH₂) dans l'eau peuvent également former des hydrogels et présenter une sensibilité au pH.² En outre, par un processus d'échange de solvants, des organogels stables à base de CN peuvent être préparés en dispersant les nanoparticules dans du glycérol,³ de l'éthanol⁴ ou de l'acétone.⁵ D'autre part, les hydrogels composites à base de CN peuvent être préparés par mélange physique ou réticulation chimique. Les hydrogels physiques à base de CN sont obtenus par introduction directe des nanoparticules dans la matrice d'hydrogel par des interactions ioniques ou liaison hydrogène, tandis que les hydrogels chimiques à base de CN sont formés par la réticulation des nanoparticules et de la matrice d'hydrogel impliquant donc des interactions supplémentaires de type liaison covalente. En général, en ajoutant des nanocristaux de cellulose rigides en concentrations appropriées, la stabilité structurelle et le module élastique des hydrogels composites peuvent être améliorés et renforcés.⁶ Bien que divers matériaux (à partir de matrices polymères synthétiques, par exemple le poly(NIPAM-co-BMA)⁷ ou de matrices polymères naturels, par exemple l'agarose⁸) ont été utilisés comme matrice pour la préparation d'hydrogels à base de CN, le développement de nouveaux systèmes hydrogel à base de CN et leurs applications ultérieures attirent toujours l'attention des chercheurs, en particulier pour les hydrogels réticulés chimiquement.

Les cyclodextrines (CD), une famille d'oligosaccharides macrocycliques liés par des liaisons glycosidiques de type α -1, 4, ont été largement étudiées dans divers domaines depuis leur découverte par Villiers en 1891.⁹ Dans cette famille de composés, les cyclodextrines α , β et γ sont les membres les plus courants, qui sont composées de 6, 7 et 8 unités glucose, respectivement, avec des échelles différentes. La cavité hydrophobe de la CD lui confère une capacité d'inclusion de divers composés, comme des petites molécules, des ions, des protéines, des oligonucléotides et certains polymères. Depuis la première étude sur la formation d'hydrogels à partir de complexes d'inclusion avec des PEG de poids moléculaire élevé et de α -CD,¹⁰ l'inclusion d'unités CD sur des chaînes polymères pour former des polypseudorotaxanes comme agent de réticulation physique est devenu l'approche la plus largement étudiée pour les hydrogels supramoléculaires industriels à base de CD ou de ses dérivés.¹¹ Les propriétés physico-chimiques, la biocompatibilité, la biodégradabilité, et la sensibilité des hydrogels supramoléculaires à base de CD peuvent être élégamment adaptées en sélectionnant soigneusement les polymères hôtes appropriés pour l'assemblage et ajuster davantage les différentes fonctions des hydrogels, telles que la sensibilité à la température, aux photons, aux produits chimiques, au potentiel redox ou au pH. Il convient de souligner que puisque les hydrogels à base de CD sont formés par auto-assemblage supramoléculaire en solution aqueuse sans l'utilisation d'agents de réticulation chimiques, le chargement *in situ* de principes actifs peut être réalisé à température ambiante, ce qui est particulièrement bénéfique pour les médicaments biomacromoléculaires. Par conséquent, les hydrogels à base de CD provenant de complexes d'inclusion ont été largement étudiés et utilisés comme systèmes de relargage de médicaments injectables.¹²

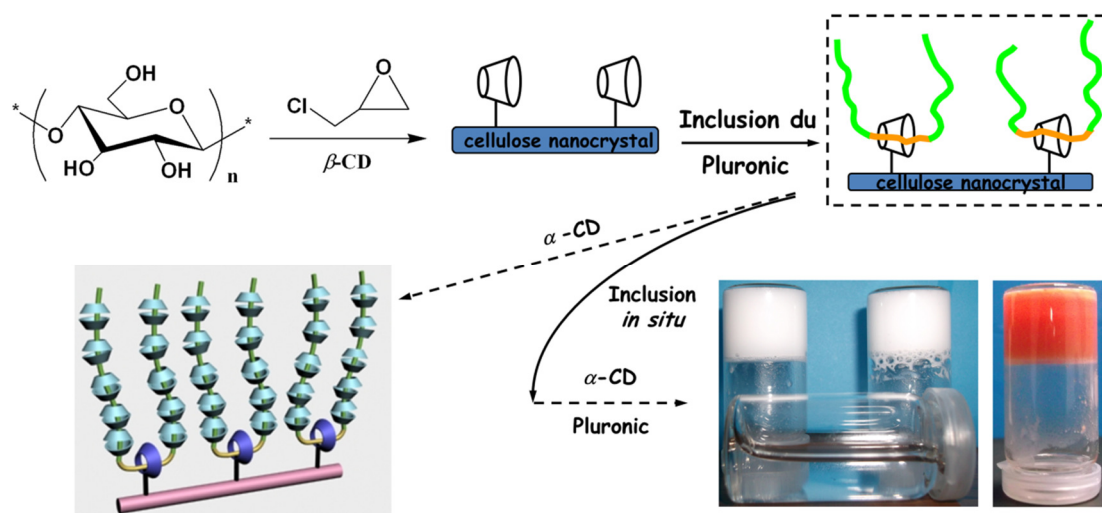
L'association de nanocristaux de cellulose et d'hydrogels à base de cyclodextrine peut être réalisée par simple dopage et mélange conduisant à la formation d'hydrogels physiques, comme reporté précédemment.¹³ Dans cette étude, des hydrogels composites ont été fabriqués par inclusion de copolymères séquencés triblocs de

poids moléculaire élevé et de α -CD et par introduction de CN vierges. Cependant, cette étude souligne que la concentration en CN dans tous les hydrogels composites doit être inférieure à 2,5% en poids et que l'hydrogel avec un taux de charge en CN de 0,5% en poids donnait le module de conservation le plus élevé. Malgré l'absence d'explication sur ce sujet dans cette étude, on peut supposer que les CN vierges s'auto-agrègent fortement lors de la préparation de l'hydrogel en raison de l'hydrophilie de la cellulose, ce qui limite le taux de charge à des valeurs faibles et limite l'effet des CN dans les hydrogels.

Dans notre étude, nous avons tenté de concevoir un nouvel hydrogel chimique à partir d'une stratégie visant à associer dans l'élaboration de l'hydrogel les nanocristaux de cellulose et la cyclodextrine, eux-mêmes associés par la méthode "hôte-invité" à partir de chaînes greffées sélectivement et différents types de cyclodextrines. Le facteur clé de cette stratégie a consisté en l'utilisation d'un copolymère séquencé (segments polymères avec des propriétés distinctes) et de CD (avec différentes tailles et reconnaissance) pour des inclusions sélectives comme indiqué dans le "Schéma de principe". En utilisant des β -CD comme sites cibles, les polymères Pluronic ont été introduits à la surface du CN modifié par une première inclusion entre la β -CD et le segment hydrophobe du polymère Pluronic [poly(propylène glycol), PPG]. Les polymères Pluronic ont été ainsi chimiquement semi-immobilisés à la surface des CN, ce qui a permis la seconde inclusion entre les segments libres du poly (éthylène glycol) à la surface des CN et la α -CD. Par un effet de réticulation *in situ*, les nanocristaux de cellulose modifiés ont pu interagir fortement avec la CD, ce qui a permis de limiter leur agrégation et conduire à la formation d'hydrogels supramoléculaires. La concentration en CN dans cet hydrogel peut être supérieure à 10% en poids, et grâce à l'ajout de taux élevés de nanocristaux modifiés (> 5% en poids), une amélioration significative de la stabilité structurelle et thermique des hydrogels *in situ* a pu être obtenue. En outre, une étude de relargage de médicament *in vitro* a montré que ces hydrogels supramoléculaires peuvent être des vecteurs de médicaments prometteurs, présentant un comportement de

libération de médicament prolongée pour la doxorubicine avec une cinétique de relargage spéciale.

Schéma de principe de la voie de synthèse pour la préparation d'hydrogels supramoléculaires par inclusion *in situ* entre des nanocristaux de cellulose (CN) et la cyclodextrine (CD).



References:

1. Gong, G.; Mathew, A. P.; Oksman, K. Strong aqueous gels of cellulose nanofibers and nanowhiskers isolated from softwood floor. *Tappi J.* **2011**, *2*, 7–14.
2. Way, A. E.; Hsu, L.; Shanmuganathan, K.; Weder, C.; Rowan, S. J. pH-responsive cellulose nanocrystal gels and nanocomposites. *ACS Macro Lett.* **2012**, *1*, 1001–1006.
3. Dorris, A.; Gray, D. G. Gelation of cellulose nanocrystal suspensions in glycerol. *Cellulose* **2012**, *19*, 687–694.
4. Siqueira, G.; Mathew, A. P.; Oksman, K. Processing of cellulose nanowhiskers/cellulose acetate butyrate nanocomposites using sol–gel process to facilitate dispersion. *Compos. Sci. Technol.* **2011**, *71*, 1886–1892.
5. Capadona, J. R.; Shanmuganathan, K.; Triftschuh, S.; Seidel, S.; Rowan, S. J.; Weder, C. Polymer nanocomposites with nanowhiskers isolated from microcrystalline cellulose. *Biomacromolecules* **2009**, *10*, 712–716.

6. Lin, N.; Huang, J.; Dufresne, A. Preparation, properties and applications of polysaccharide nanocrystals in advanced functional nanomaterials: a review. *Nanoscale* **2012**, *4*, 3274–3294.
7. Wu, L.; Zhou, H.; Sun, H.-J.; Zhao, Y.; Yang, X.; Cheng, S. Z. D.; Yang, G. Thermoresponsive bacterial cellulose whisker/poly(NIPAM-co-BMA) nanogel complexes: synthesis, characterization, and biological evaluation. *Biomacromolecules* **2013**, *14*, 1078–1084.
8. Osorio-Madrado, A.; Eder, M.; Rueggeberg, M.; Pandey, J. K.; Harrington, M. J.; Nishiyama, Y.; Putaux, J.-L.; Rochas, C.; Burgert, I. Reorientation of cellulose nanowhiskers in agarose hydrogels under tensile loading. *Biomacromolecules* **2012**, *13*, 850–856.
9. Villiers, A. Sur la fermentation de la féculé par l'action du ferment butyrique. *C. R. Acad. Sci.* **1891**, *112*, 536–538.
10. Li, J.; Harada, A.; Kamachi, M. Sol–gel transition during inclusion complex formation between α -cyclodextrin and high molecular weight poly(ethylene glycol)s in aqueous solution. *Polym. J.* **1994**, *26*, 1019–1026.
11. Zhang, J.; Ma, P. X. Cyclodextrin-based supramolecular systems for drug delivery: Recent progress and future perspective. *Adv. Drug Deliv. Rev.* **2013**, *65*, 1215–1233.
12. Concheiro, A.; Alvarez-Lorenzo, C. Chemically cross-linked and grafted cyclodextrin hydrogels: From nanostructures to drug-eluting medical devices. *Adv. Drug Deliv. Rev.* **2013**, *65*, 1188–1203.
13. Zhang, X.; Huang, J.; Chang, P. R.; Li, J.; Chen, Y.; Wang, D.; Yu, J.; Chen, J. Structure and properties of polysaccharide nanocrystal-doped supramolecular hydrogels based on cyclodextrin inclusion. *Polymer* **2010**, *51*, 4398–4407.

The work in this chapter is originated from:

Ning Lin and Alain Dufresne, Supramolecular hydrogels from in situ host–guest inclusion between chemically modified cellulose nanocrystals and cyclodextrin. Biomacromolecules 2013, 14, 871–880.

Chapter 5. Supramolecular Hydrogels from *In Situ* Host–Guest Inclusion between Chemically Modified Cellulose Nanocrystals and Cyclodextrin

Ning Lin and Alain Dufresne

Grenoble Institute of Technology (Grenoble INP), The International School of Paper, Print Media and Biomaterials (Pagora), CS10065, 38402 Saint Martin d'Hères Cedex, France

ABSTRACT

When grafted β -cyclodextrin is used as targeting sites, Pluronic polymers have been introduced on the surface of cellulose nanocrystals by means of inclusion interaction between β -cyclodextrin and hydrophobic segment of the polymer. Because of the steric stabilization effect, surface poly(ethylene glycol) chains facilitate the dispersion and compatibility of nanocrystals, which also enhance the loading levels of nanocrystals in the hydrogel system. Meanwhile, uncovered poly(ethylene glycol) segments render the participating inclusion of α -cyclodextrin for the architecture of *in situ* hydrogels. Surface grafting and inclusion reactions were proved by solid ^{13}C NMR and FTIR. Grafting efficiency of β -cyclodextrin and inclusion efficiency of Pluronic on the surface of nanocrystals were confirmed by UV spectroscopy and elemental analysis. A significant enhancement of the structural and thermal stability of *in situ* hydrogels with high loading levels of modified nanocrystals (> 5.77 wt%) was observed by rheological analysis. Further study reveals the performance and behavior of hydrogels under a different pH environment. Finally, *in situ* hydrogels were used as drug carrier for *in vitro* release of doxorubicin and exhibit the behavior of prolonged drug release with special release kinetics.

KEYWORDS

Cellulose Nanocrystals, Cyclodextrin, Host–Guest Inclusion, Hydrogels

5.1 Introduction

Cellulose nanocrystal (CN) has attracted a great deal of interest in material science due to its appealing intrinsic properties including nanodimensions, high surface area, unique morphology, low density, and mechanical strength, as well as availability, renewability, and biodegradability.¹ Abundant hydroxyl groups on the surface of CN are suitable for physical adsorption or diverse chemical modifications including esterification, etherification, oxidation, silylation, and polymer grafting.^{2–4} Modified nanocrystals with alternative surface properties were not only widely used as nanofiller to enhance various matrices through the development of composites,^{5,6} but also for the exploration of advanced functional nanomaterials.^{7,8} Recently, much more attention focused on the application of CN in the field of biomaterials, such as fluorescent labels for bioimaging,^{9,10} labeled carriers for DNA detection¹¹ and photodynamic therapy,¹² enzyme immobilization,^{13,14} photobactericidal material,^{15,16} biomedical scaffold,^{17,18} and hydrogels.^{19,20} Hydrogel materials have shown wide potential applications in the biomaterial field, such as drug delivery, because of their safety, biocompatibility and biodegradability. Among hydrogel systems, hydrogels based on supramolecular self-assembly between cyclodextrin (CD) and polymeric chains are most widely studied, and have promising application prospects. Particularly, supramolecular hydrogels formed with the host–guest inclusion between polymer and CD molecules, exhibit reversible thixotropism, making them suitable for syringeable drug delivery application.²¹ Although CN has attracted wide attention in the utilization as physical reinforcing filler in various hydrogel matrices, such as cyclodextrin,²² agarose,^{23,24} poly(vinyl alcohol),²⁵ poly(*N*-isopropyl acrylamide),²⁶ and poly(2-hydroxyethylmethacrylate),²⁷ to the best of our knowledge, only one example of pristine CN in cyclodextrin-based hydrogel has been reported.²² However, in this study, due to the strong hydrophilicity and easy self-assembling property of this highly crystalline nanoparticle, the loading level of CN in cyclodextrin hydrogel was quite low (< 2.5 wt%).²² Recently, it was shown that a weak reinforcing percolating network from surface-modified CN can be formed in aqueous gels.²⁸ If

only introducing CN with extremely low contents, it is believed that the rigid network formed by the linkage of these nanoparticles cannot be obtained, and even weaken the promising nanoreinforcing effect for ensuing materials.

Herein, with the strategy of surface chemical modification of CN with Pluronic polymers (poloxamer), the loading level of CN was elevated, and the dispersion of the nanoparticles was improved. As shown in Figure 5.1 (A), β -cyclodextrin (β -CD) was first covalently grafted on the surface of CN using epichlorohydrin (EPI) as coupling agent, which is a typical strategy for the synthesis of cyclodextrin derivatives. Afterward, Pluronic polymer was immobilized on modified CN by inclusion of the hydrophobic polymeric segments in grafted β -CD [Figure 5.1 (B)]. This process was performed with the assistant of ultrasonic treatment to induce the inclusion. Pluronic polymers used here were triblock copolymers with different molecular weights (Pluronic F68 or F108), both bearing hydrophobic poly(propylene glycol) (PPG) and hydrophilic poly(ethylene glycol) (PEG) segments (PEG-*b*-PPG-*b*-PEG). The inclusion of the hydrophobic PPG chain segments in the inner cavity of β -CD allows closely connecting the polymer and the nanoparticle, contrary to surface physical adsorption of polymers on CN. Finally, with the in situ “host–guest” inclusion of uncovered PEG chain segments in smaller size α -cyclodextrin (α -CD) molecules, the architecture of supramolecular hydrogel based on modified CN can be formed [Figure 5.1 (C)]. This work is an attempt to design a novel hydrogel with the construction of participating CN in hydrogels via the interactions between compatible grafted chains and polymeric matrix. The key factor of this strategy emphasized on the use of block copolymer and cyclodextrin with different sizes and selected inclusive interactions. Pluronic polymers were semichemically immobilized on the surface of CN, which provided the possibility of good dispersion, and in situ inclusion of nanocrystals in the hydrogel system. Moreover, the similar structure of CN and CD, both from polysaccharide, preserved the biocompatibility and biodegradability of ensuing materials, which endowed a “green” note to the hydrogel with promising mechanical property, thermal stability, and sustained drug release behavior. These supramolecular

hydrogels formed with rigid nanocrystals can promote the potential application of nanocellulose in the field of biomedical technology and nanoscience.

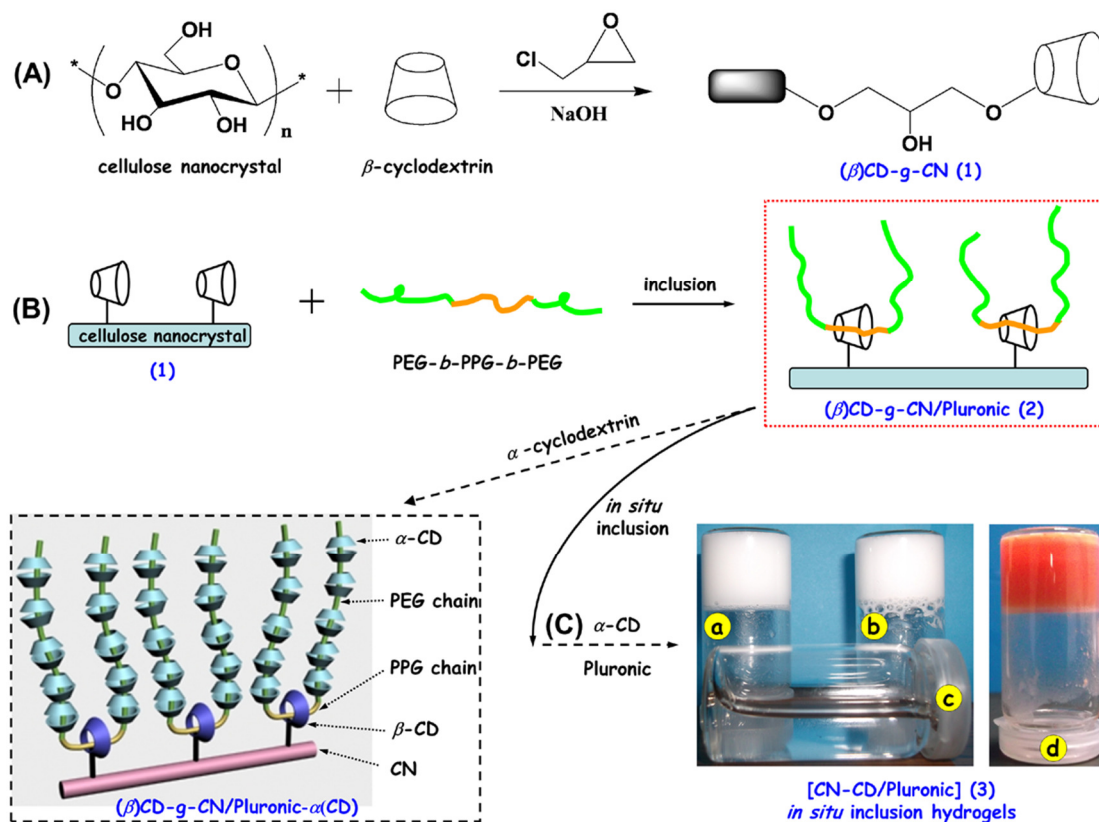


Figure 5.1 Synthesis pathway for (A) β -cyclodextrin grafting on cellulose nanocrystal (β) CD-g-CN; (B) inclusion complex of (β) CD-g-CN and Pluronic polymers; (C) supramolecular hydrogels from *in situ* inclusion between (β) CD-g-CN/Pluronic and α -CD: (a) hydrogel CN-CD/F68-2, (b) hydrogel CN-CD/F108-2, (c) water, (d) drug-loaded hydrogel CN-CD/F108-2-Dox.

5.2 Experimental Methodology

5.2.1 Materials

Native cotton fibers were obtained from Whatman filter paper. α -Cyclodextrin (α -CD), β -Cyclodextrin (β -CD), Pluronic polymer F68 (PEG₇₆-*b*-PPG₃₀-*b*-PEG₇₆, $M_n = 8400$), phenolphthalein, sodium carbonate (Na₂CO₃), and Pluronic polymer F108 (PEG₁₃₃-*b*-PPG₅₀-*b*-PEG₁₃₃, $M_n = 14600$) were reagent grade from Sigma–Aldrich. Epichlorohydrin (99%) was obtained from Acros Organics. Sodium hydroxide (NaOH) and sulfuric acid (H₂SO₄, 98%) of laboratory grade were purchased from Carl-Roth

and used without further treatment. Doxorubicin hydrochloride (Dox·HCl) was chosen as the model drug and purchased from Sigma–Aldrich.

5.2.2 Extraction of Cellulose Nanocrystals (CN)

Cellulose nanocrystals (CN) were prepared by H₂SO₄ hydrolysis of native cotton fiber, according to our previous literature.²⁹ The fiber was milled with a laboratory milling device to obtain a fine particulate substance and extracted in 2 wt% aqueous NaOH solution (12.5 g fibers for 500 mL solution) for 12 h at room temperature and then filtered and rinsed with distilled water. Acid hydrolysis was performed at 45 °C with 65 wt% H₂SO₄ (preheated) for 45 min under mechanical stirring (12.5 g fibers for 250 mL solution). Amorphous or paracrystalline regions of cellulose were preferentially hydrolyzed, whereas crystalline regions that have higher resistance to acid attack remained intact. The suspension was diluted with ice cubes to stop the reaction and washed until neutrality by successive centrifugations at 10,000 rpm (rotation per minute) for 10 min each step and dialyzed against distilled water for five days. After dialysis, the CN dispersion was completed by ultrasonic treatment using a Branson sonifier, and finally, the released CN powder was obtained by freeze-drying.

5.2.3 Synthesis of β -Cyclodextrin-Grafted Cellulose Nanocrystals [(β)CD-g-CN (1)]

The grafting reaction of β -cyclodextrin on the surface of cellulose nanocrystals was accomplished using epichlorohydrin (EPI) as coupling agent through a one-step procedure [Figure 5.1 (A)].³⁰ First, 4.0 g NaOH was dissolved in 20 mL of distilled water as the aqueous NaOH solution. β -CD (10.351 g, 9.12 mmol) was dissolved in the prepared NaOH solution. At the same time, 1.0 g CN was dispersed in another 20 mL of distilled water as homogeneous suspension, added in the β -CD alkaline solution, and stabilized for 30 min. The desired amount of EPI (5.96 mL, 76 mmol) was thus added into the reaction medium, and the reaction was allowed to proceed at 40 °C for 6 h. It should be pointed out that the EPI/CD molar ratio was controlled at about 8.3 (below 10) to avoid self-crosslinking of β -CD. Meanwhile, the effective NaOH solution concentration was controlled at about 16 wt% to facilitate the grafting

reaction.³⁰ After modification, the suspension was centrifuged at 10,000 rpm for 15 min and washed with distilled water repeatedly until neutrality to remove both ungrafted β -CD and residual NaOH. Finally, the grafted product [(β) CD-g-CN (1)] was obtained as powder by freeze-drying for 2 days.

The grafting efficiency of β -CD on the surface of CN was confirmed with the methods of weight measurement and photometric titration. Three grafting experiments were repeated for weight measurement. After grafting β -CD, the weights of products (β)CD-g-CN were 1.1579, 1.1684, and 1.1368 g, corresponding to a grafting efficiency of 15.79, 16.84, and 13.68 wt%, respectively. According to the results of weight measurement, the average β -CD grafting efficiency was 15.44 wt%. Further accurate measurement from photometric titration was also used to investigate the β -CD grafting efficiency (GE%) for (β)CD-g-CN.

5.2.4 Inclusion Complex of (β)CD-g-CN/Pluronic Polymers (2)

Theoretically, due to the dimensions as well as hydrophilic and hydrophobic property of β -CD and Pluronic polymers, one grafted β -CD should host one guest Pluronic chain for the inclusion. In this work, expecting for complete inclusion, the molar ratio between grafted β -CD and Pluronic polymer was regulated as 1:2. The protocol for the preparation of inclusion complex [(β) CD-g-CN/Pluronic (2)] was as follow: 500 mg powdered (β)CD-g-CN (74.4 μ mol grafted β -CD according to the 16.89 wt% grafting efficiency from photometric titration analysis) was dispersed in 10 mL of distilled water under mechanical stirring for 12 h and then ultrasonicated for 30 min. Meanwhile, 1.25 g (148.8 μ mol) Pluronic F68 (PEG₇₆-*b*-PPG₃₀-*b*-PEG₇₆) was dissolved in another 40 mL of distilled water. It should be pointed out that because of the hydrophobic interactions among PPG chains, Pluronic polymers may self-associate in water to form micelles.³¹ To avoid it, a dilute aqueous solution of Pluronic polymer (45.7 mg/mL) was used for the inclusion between (β)CD-g-CN and Pluronic polymers. The Pluronic solution was protected against light by an aluminum foil and weakly stirred for 12 h at room temperature. Then, the aqueous suspension containing (β)CD-g-CN was added dropwise into the Pluronic solution and the

mixture was submitted to mild ultrasonic assistant treatment for 20 min and mechanical stirring for 72 h at room temperature. During the reaction, the hydrophobic PPG chains can insert into the hydrophobic cavity of β -CD and form the stable inclusion complex resulting from the physical crosslinking interaction.³² As for Pluronic F108 (PEG₁₃₃-*b*-PPG₅₀-*b*-PEG₁₃₃), due to different molecular weight, 2.173 g F108 polymer was mixed with 500 mg (β)CD-*g*-CN suspension.

The suspension of inclusion complex was centrifugated at 10,000 rpm for 10 min to collect the precipitate and the supernatant. The powdered (β)CD-*g*-CN/Pluronic precipitate was washed with distilled water and the supernatant was analyzed with FTIR tracing method. Because of the hydrophilic property of PEG chains, free Pluronic polymer dissolves in water, but inclusive Pluronic polymer forms stable suspensions. This process of successive solubilization-centrifugation was performed repeatedly until the disappearance of the characteristics bands of Pluronic from the result of FTIR. The content of inclusive Pluronic was confirmed by elemental analysis.

5.2.5 Supramolecular Hydrogels via *In Situ* Inclusion [(β)CD-*g*-CN/Pluronic] -[α (CD)/ Pluronic] (3)

The architecture of in situ supramolecular hydrogel was realized with the “host–guest” inclusion between α -CD, Pluronic polymer, and modified CN. The preparation method of in situ hydrogels CN-CD/F68 (3) was adapted from previous literature.^{33,34} The powdered (β)CD-*g*-CN/F68 was dispersed in 3.5 mL of water, with specific F68 polymer content according to the inclusion efficiency from the result of elemental analysis. Another controlled weight of pure F68 was added in the suspension of modified CN under mild stirring at 4 °C until a stable suspension was obtained. It was reported that the viscosity of Pluronic aqueous solution remains unchanged under such temperature conditions.³³ Another saturated solution of α -CD (1.5 mL water) was added in the mixture of modified CN and pure F68, in which the concentrations of Pluronic F68 and α -CD were 13 and 9.7 w/v, respectively. The mixture was ultrasonicated for 10 min and then conditioned overnight at room temperature for

gelation. A similar method was used for the preparation of supramolecular hydrogels CN-CD/F108. Neat hydrogels of F68/ α -CD and F108/ α -CD were also prepared with the same approach and concentration as the reference. The composition, concentration, and codification of the various hydrogels are summarized in Table 5.1.

To prove the capability of inclusion between (β)CD-*g*-CN/Pluronic and α -CD, the complex of (β)CD-*g*-CN/Pluronic- α (CD) was prepared independently, isolated by centrifugation, and washed with a limited amount of water to remove free α -CD.³⁵

Table 5.1 Composition, solid content, and weight ratio of the various hydrogels.

Hydrogels	CN- <i>g</i> -(β)CD /Pluronic	Nanocrystals		Pluronic polymers		α -cyclodextrin		H ₂ O mL
		Weight	CN% ^a	Added Pluronic ^b	Pluronic%	Weight	α -CD%	
		mg	w/w	mg	w/v	mg	w/v	
F68/ α -CD	0	0	0	650.0				
F108/ α -CD	0	0	0	650.0				
CN-CD/F68-1	50	36.5	3.09	643.9				
CN-CD/F68-2	100	72.9	5.96	637.8	13.00	485	9.70	5
CN- CD/F68-3	200	145.9	11.13	625.5				
CN-CD/F108-1	50	35.1	2.98	642.2				
CN-CD/F108-2	100	70.2	5.77	634.4				
CN-CD/F108-3	200	140.3	10.76	618.9				

^a CN% is the weight ratio of nanocrystals in solid components, which was calculated according to the following equation:

$$CN\% = \frac{m_{CN-g-(\beta)CD/Pluronic} \times (1 - IE\%) \times (1 - GE\%)}{m_{CN-g-(\beta)CD/Pluronic} + m_{added Pluronic} + m_{\alpha-CD}} \quad (5.1)$$

^b The “added Pluronic” is the addition of pure Pluronic polymer to reach the controlled ratio of Pluronic in hydrogels, which was calculated:

$$m_{added Pluronic} = 650 - m_{CN-g-(\beta)CD/Pluronic} \times IE\% \quad (5.2)$$

5.2.6 Characterization and Analyses

Solid State ¹³C Cross-Polarization–Magic Angle Spinning Spectroscopy: ¹³C CP-MAS NMR experiment for the proof of grafting of β -CD on the surface of CN was performed on a AVANCE400 solid instrument spectrometer with a MAS rate of 6 kHz, at 75.5 MHz carbon frequency and at room temperature. The contact time for CP

was 1 ms with a proton 90 pulse of 5.5 μ s and decoupling power of 45 kHz. The delay time after the acquisition of the FID signal was 2 s. The chemical shifts were calibrated with the hexamethylbenzene standard methyl resonance at 17.3 ppm.

UV–vis Spectroscopy: The content of grafted β -CD in (β)CD-g-CN (I) was analyzed with a Shimadzu UV 2401-(PC) UV–vis spectrophotometer. Phenolphthalein (phe) was used as indicator to detect the change of absorbency. First, together with sodium carbonate solution, pure phe solution, phe solution containing 50 mg unmodified CN, and phe solution containing 50 mg (β)CD-g-CN were well dispersed and stabilized for 20 h. The phe absorption experiment was performed on the UV spectrophotometer using 1 cm thick quartz cuvette with wavelengths ranging from 450 to 650 nm to confirm the characteristic absorbed wavelength (λ_{\max}) of phe solution.

The standard curve for the weight of β -CD and absorbency of phe solution was quantified with the photometric titration method. Two mL phe solution and 2 mL sodium carbonate solution were added in #1 volumetric flask (25 mL), and set the volume to the mark with distilled water. β -CD solutions of 1, 2, 3, 4, and 5 mL were added in #2, #3, #4, #5, and #6 volumetric flask (25 mL), respectively, and then 10 mL of distilled water was added in each flask. After that, both 2 mL of phe solution and 2 mL of sodium carbonate solution were added in each flask (except #1), and finally the volume was set to the mark with distilled water. All solutions were submitted to absorption analysis at the wavelength of 552 nm (λ_{\max}), and the standard curve and equation from the weight of β -CD (W , mg) and absorbency of phe (A) was determined.

Similar experiments were carried out for the measurement of grafted β -CD content. Five samples of 5, 10, 20, 30, and 40 mg (β)CD-g-CN in 10 mL of distilled water were added in another #7, #8, #9, #10, and #11 volumetric flask (25 mL), respectively, and then both 2 mL of phe solution and 2 mL of sodium carbonate solution were added. All mixtures were set the volume to the mark of volumetric flask with distilled water and stabilized for 20 h. The absorbency at the wavelength of 552 nm was recorded and corresponded to the weight content of grafted β -CD according to the

standard equation. Finally, the β -CD grafting efficiency of CN-g-(β)CD (I) can be calculated.

Fourier Transform Infrared Spectroscopy (FTIR): Infrared spectra were recorded at room temperature on a FTIR Perkin-Elmer Spectrum One spectrometer to characterize CN, (β)CD-g-CN, (β)CD-g-CN/Pluronic, and β -CD. Freeze-dried powders were analyzed as KBr pellets (1 wt % in anhydrous KBr) using a spectral width ranging from 4000 to 400 cm^{-1} with a 2 cm^{-1} resolution and an accumulation of 20 scans. On the other hand, during the preparation of inclusion complex (β)CD-g-CN/Pluronic, the supernatants containing free Pluronic polymers were collected from the process of successive solubilization-centrifugation. The supernatant was carefully dropped on the surface of neat KBr compressing tablet, and water was vaporized at room temperature for 12 h. The KBr tablet together with Pluronic polymers on the surface were also characterized by FTIR.

Elemental Analysis: Elemental analysis was performed at Analysis Central Service of the Centre National de la Recherche Scientifique (Vernaison, France). The carbon, oxygen, and hydrogen element contents for both (β)CD-g-CN/F68 and (β)CD-g-CN/F108 samples were measured. The results from elemental analysis were used to determine the content of inclusive Pluronic polymers for (β)CD-g-CN/Pluronic ($IE\%$) according to eq. 5.3:

$$IE\%C_{Pluronic} + (1 - IE\%)C_{CN-g-(\beta)CD} = C_{CN-g-(\beta)CD/Pluronic} \quad (5.3)$$

where C is the relative carbon content in the sample; $IE\%$ is the inclusion efficiency for inclusive Pluronic polymers for grafted β -CD. The precision of the measurement is considered to be 0.3% for C and H elements and 0.5% for O element.

X-ray Diffraction Analysis (XRD): XRD was used to prove the possibility of inclusion interactions between (β)CD-g-CN/Pluronic and α -CD, which was recorded on a Philips PW 1720 X-ray generator operated at 30 kV and 20 mA with Cu $K\alpha$ radiation ($\lambda = 0.154$ nm) in a range of $2\theta = 3\text{--}50^\circ$ using a fixed time mode with a step interval of 0.02° .

Transmission Electron (TEM) and Optical Microscopy: The dimensions and morphology of pristine CN were observed by TEM. Drops of 0.001 wt% cellulose suspensions were deposited on glow discharged carbon-coated TEM grids. The specimens were then negatively stained with 2% uranyl acetate. After complete drying under room conditions, specimens were observed using a Philips CM200 electron microscope operating at 80 kV.

The morphology of hydrogel crystals was directly observed by optical microscopy. The hydrogel was dropped on the glass slide, and formed after standing a period of time in aqueous solution. Excess water was removed carefully with the absorption by the edge of filter paper, and the morphology was observed after the complete dryness.

Rheological Analysis: Viscoelastic behavior of hydrogels was evaluated on a Rheolyst Physica MCR-301 rheometer. Viscosity of the hydrogel was recorded applying a flow cycle consisting in a continuously increasing shear rate ramp at 20 °C from 0.05 to 10 s⁻¹ for 4 min. The storage (G') and the loss (G'') moduli were recorded under the shear stress of 100 Pa in the range of 0.5–100 rad/s angular frequency interval using a cone–plate geometry (diameter 20 mm, angle 1°). The dependence of G' and G'' on temperature was evaluated at 20 rad/s and 50 Pa in the range of 20–70 °C.

The influence of pH conditions on the property of hydrogel was investigated to determine the loss (G'') and storage (G') moduli with different pH ranging from 1 to 11. The adjustment of pH conditions was achieved by the addition of HCl and NH₄OH, which was a negligible amount. Tests were conducted in triplicate at a fixed frequency of 1 Hz with 50 Pa shear stress at 20 °C.

In Vitro Release of Doxorubicin·HCl from Hydrogels: Doxorubicin·HCl (1.0 mg) was dissolved in 2 mL of distilled water and then (β)CD-*g*-CN/Pluronic and controlled amount of Pluronic was added. The mixture was kept at 4 °C overnight in order to obtain a homogeneous suspension. Afterward, α -CD was added to induce *in situ* host–guest inclusion and form stable hydrogel. The study of in vitro drug release was performed in water at 37 °C. The hydrogel was placed in a test tube with 20 mL

of water and then incubated in a shaking water bath. Solution of 3 mL aliquots containing released drug was withdrawn from the testing tube periodically. The volume of solution in the tube was kept constant by adding another 3 mL of water after each sampling. The cumulative release ratio of doxorubicin·HCl from hydrogels was measured by UV/vis spectrophotometer (Shimadzu UV 2401-(PC)) at the absorbency of 481 nm. The experiment for *in vitro* drug release was performed in triplicate.

5.3 Chemical Modification of Cellulose Nanocrystals

5.3.1 Chemical Grafting of β -CD on the Surface

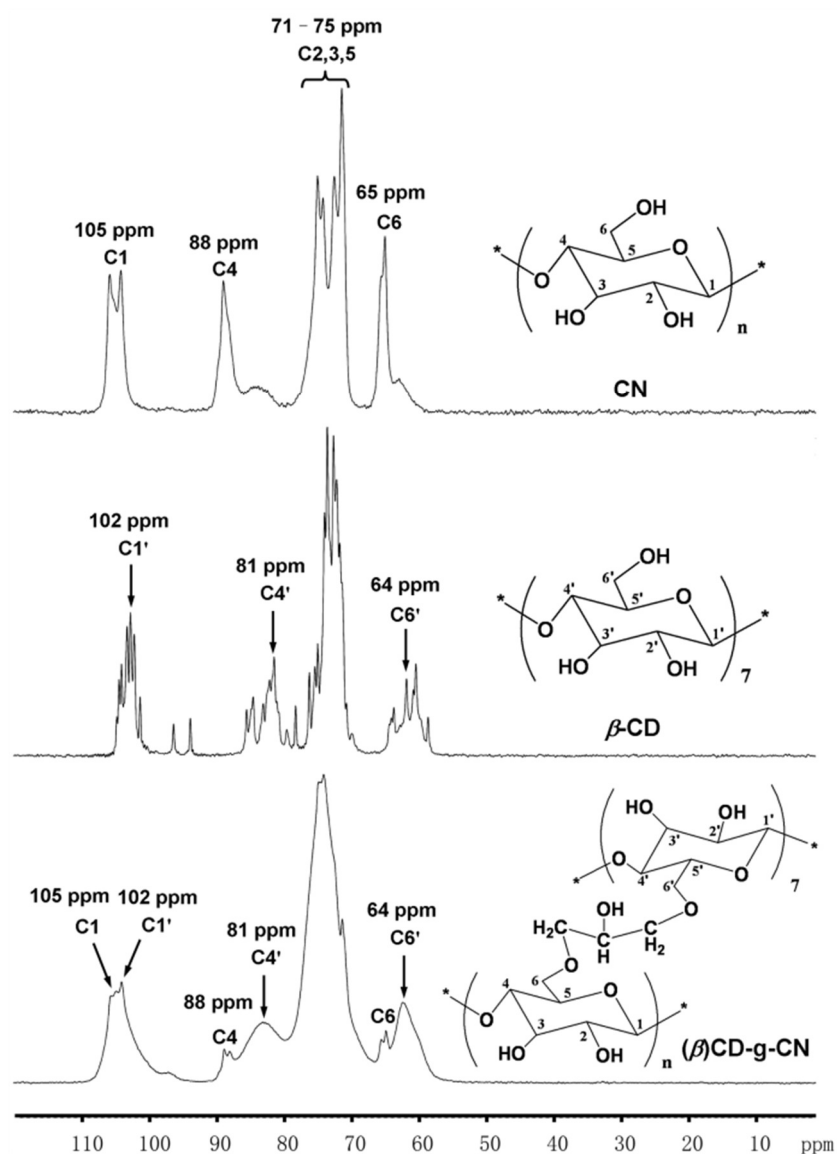


Figure 5.2 ^{13}C (CP/MAS) solid-state NMR spectra of CN, β -CD, and (β) CD-g-CN.

The ^{13}C CP-MAS spectra of CN, $\beta\text{-CD}$, and $(\beta)\text{CD-g-CN}$ are shown in Figure 5.2. The chemical shifts of carbon atoms from original CN were assigned to C1 (105 ppm), C4 (88 ppm), C2, 3, 5 (71–75 ppm), and C6 (65 ppm). Possessing the same glucose structure units, the characteristic chemical shifts related to C2', 3', 5' for $\beta\text{-CD}$ superimpose with cellulose. However, because of different monomer unit quantity and molecular conformations, the presence of $\beta\text{-CD}$ can be determined by the position shifts of C1' (102 ppm), C4' (81 ppm), and C6' (64 ppm). As shown in the spectrum of $(\beta)\text{CD-g-CN}$, all carbon characteristics from both CN and $\beta\text{-CD}$ can be identified, which indicates the surface grafting of $\beta\text{-CD}$ and integrity of CN.

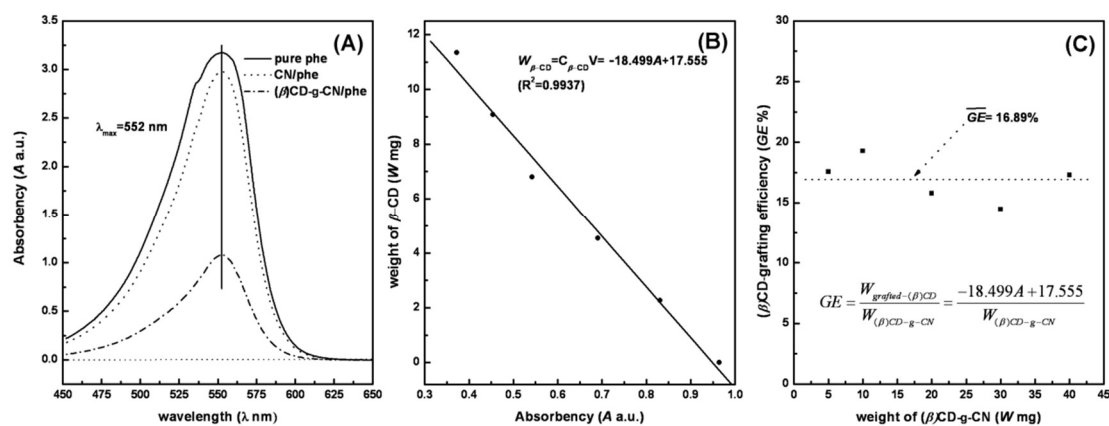


Figure 5.3 (A) UV absorption spectra for pure phenolphthalein solution (phe), phe solution treated with pristine CN (CN/phe), and phe solution treated with $\beta\text{-CD}$ grafted CN ($(\beta)\text{CD-g-CN/phe}$); (B) standard curve and equation from $\beta\text{-CD}$ content and phe absorbency; (C) $\beta\text{-CD}$ grafting efficiency from $(\beta)\text{CD-g-CN}$ samples with different quantities.

Under $\text{pH} > 10$ conditions, phenolphthalein (phe) aqueous solution shows red color, which darkens when increasing phe concentration. It was reported that the hydrophobic group of phe molecule can insert into the hydrophobic cavity of $\beta\text{-CD}$, which reduce the free phe concentration in solution, and finally cause the decline of absorbency from light color solution. As shown in the UV–vis spectra of Figure 5.3 (A), the impact of pristine CN was negligible on the phe molecule, which showed tiny absorption and a slight decrease of absorbency in comparison with neat phe solution. However, the introduction of $(\beta)\text{CD-g-CN}$ caused a sharp reduction of absorbency, which indicates that the hydrophobic cavity of $\beta\text{-CD}$ includes plentiful phe molecules.

Based on Beer–Lambert law, within a range of controlled concentration, the content of grafted β -CD on the surface of CN can be detected according to the absorbency of alkaline phe solution. The absorbency of phenolphthalein (A) showed a negative correlation with the concentration of grafted β -CD ($C_{\beta\text{-CD}}$, mg/mL), which was in agreement with the weight of grafted β -CD ($W_{\beta\text{-CD}}$, mg) because of the same volume of solution (25 mL) used in the experiment. The standard curve and equation between A and $W_{\beta\text{-CD}}$ are shown in Figure 5.3 (B). Different quantities of (β)CD-g-CN (5, 10, 20, 30, 40 mg) were added in the phe solution, and the content of grafted β -CD was calculated from absorbency according to the equation reported in Figure 5.3 (B). As shown in Figure 5.3 (C), the average value of β -CD grafting efficiency (GE%) was determined as 16.89 wt% using this photometric titration method, which is almost in agreement with the result of weight measurement (15.44 wt%).

5.3.2 Inclusion of Pluronic Polymers in Grafted β -CD

Although possessing similar glucose unit structure, the grafting and inclusion reaction between CN, β -CD and Pluronic polymers can be investigated by the change of peak intensity for specific bond stretching bands. Figure 5.4 (A, B) shows the FTIR spectra of CN before and after grafting or inclusion reaction. With the surface grafting of β -CD on CN, the intensity of three peaks located at 1163, 1113, and 1059 cm^{-1} decreased, which are ascribed to antisymmetric bridge oxygen stretching, antisymmetric in-phase ring stretching and C–O stretching for cellulose, respectively. Furthermore, another C–O stretching band at 1031 cm^{-1} broadened after surface grafting. These results are in agreement with other reports for cyclodextrin-EPI cellulose.³⁰ By comparing the spectra for (β)CD-g-CN and (β)CD-g-CN/Pluronic, it is interesting to note that the intensity of the peaks located at 1031 and 898 cm^{-1} slightly increased, which can be attributed to the emerging C–O groups and antisymmetric out-of-phase stretching carbon from the inclusive PEG-PPG-PEG polymer. However, it was very important to confirm the inclusion reaction between grafted β -CD and Pluronic polymers and prove the complete removal of free and surface physically adsorbed Pluronic polymers on nanocrystals. An experiment of FTIR tracing was

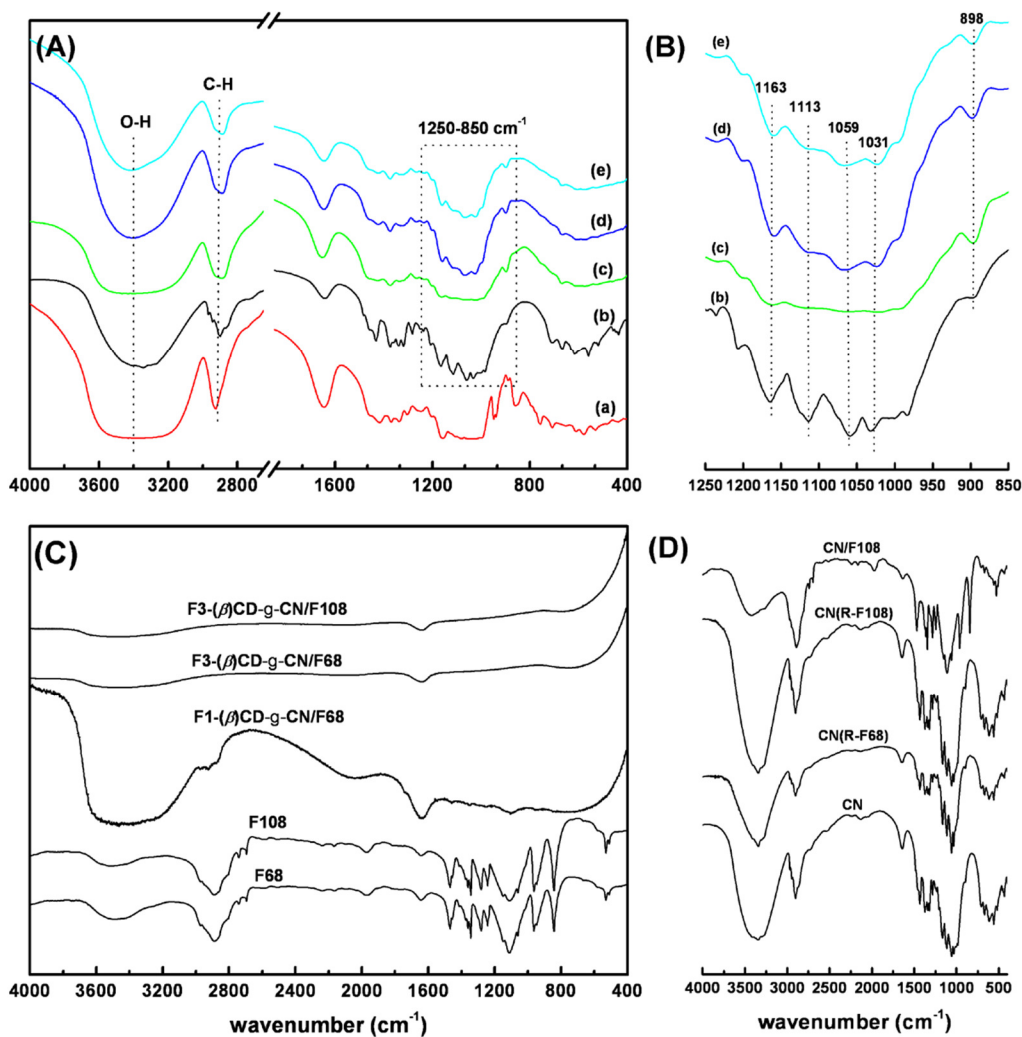


Figure 5.4 FTIR spectra for (A, B) CN before and after chemical modifications: (a) β -CD, (b) CN, (c) (β) CD-*g*-CN, (d) (β) CD-*g*-CN/F68, (e) (β) CD-*g*-CN/F108; (C) pure Pluronic polymers and supernatants from the preparation of (β) CD-*g*-CN/Pluronic complexes with the treatment of successive solubilization-centrifugation (F1 and F3 represent the supernatant after the treatment for one and three times); (D) comparisons between pristine CN, CN/F108 with physically adsorbed Pluronic F108, and CN(R-Pluronic) from the purification of CN/Pluronic with the removal of adsorbed Pluronic using successive solubilization-centrifugation method.

designed to investigate the effect of the process of successive solubilization-centrifugation during the preparation of inclusion complex ((β) CD-*g*-CN/Pluronic). As shown in Figure 5.4 (C), after the post-treatment of purification for three times, the spectra for the supernatant (F3) from washed (β) CD-*g*-CN/Pluronic did not exhibit any characteristics of Pluronic polymers, which proved the availability of free Pluronic removal using this method. On the other hand, the physical mixture of

CN/Pluronic was also prepared using the same concentration and treated with the same purification treatment. By comparing the spectra of CN(R-Pluronic) and pure CN, it was observed that they were nearly similar [as shown in Figure 5.4 (D)], which indicates that the purification treatment can also effectively remove the polymer physically adsorbed on the surface of nanocrystals. It should be pointed out that, because the main body of (β)CD-*g*-CN is cellulose (only 16.89 wt% grafted β -CD), the possible physical adsorption of Pluronic was supposed to mainly occur on the surface of CN. Consequently, the above comparative experiments were carried out on CN to prove the effect of purification.

The content or inclusion efficiency (*IE%*) of Pluronic polymer on the surface of (β)CD-*g*-CN/Pluronic complexes was determined by elemental analysis. As shown in Table 5.2, with the similar glucose unit structure ($C_6H_{10}O_5$), CN and β -CD have the same theoretical values for the three element contents (C, O, and H), resulting in small change of element contents for the grafted nanocrystals [(β)CD-*g*-CN]. On the other hand, although presenting different molecular weights and polymer segments, there is a little difference in theoretical values for element contents between the two Pluronic polymers. Regarding experimental values of these original materials, because of the instrumental error and influence of hydrophilicity of cellulose and β -CD, some variance of the experimental values was inevitable for CN and β -CD, which was mainly attributed to the adsorption of moisture (H_2O) during the delivery and experiment. Therefore, the values of inclusion efficiency were confirmed mainly based on the data from carbon element, and calculated according to eq. 5.3 As shown in Table 5.2, the inclusion efficiency (*IE%*) of Pluronic polymers for (β)CD-*g*-CN/F68 and (β)CD-*g*-CN/F108 complexes were 12.25 and 15.57 wt%, respectively.

5.4 Structure and Properties of Supramolecular Hydrogels

5.4.1 Crystalline Structure of Inclusive Complexes

The inclusion of polymeric chains in cyclodextrin can also be investigated with XRD analysis. The crystalline diffraction patterns of original materials and various

inclusive complexes are presented in Figure 5.5. As shown in Figure 5.5 (A), the characteristic diffraction peaks of cellulose, β -CD and α -CD, on one hand, and Pluronic polymers on the other hand were assigned to the 2θ angles at 22.6, 12.9, 14.3, 19.1, and 23.2°, respectively. The sharp diffraction peak for inclusive complexes located at about 20.0° strongly supports the channel-type crystalline structure of the obtained polyrotaxanes [Figure 5.5 (B)], which indicated that cyclodextrin underwent a solid-state phase transformation as it formed an inclusion compound with polymeric chains.³⁶ Pluronic F108 with longer polymeric chains can include more α -CD molecules than short Pluronic F68, which is reflected through the higher intensity for (β)CD-g-CN/F108- α (CD) complex at 20.0°. On the other hand, by comparing the diffraction patterns of (β)CD-g-CN/Pluronic and (β)CD-g-CN/Pluronic- α (CD) complexes, the crystalline feature of α -CD appeared with the emergence of a weak peak at 14.3°. In general, the inclusive complexes or hydrogels of cyclodextrin and polymers do not present the obvious crystalline features of cyclodextrin. However, in this case, the inclusion between α -CD and PEG chains occurred at the surface of CN,

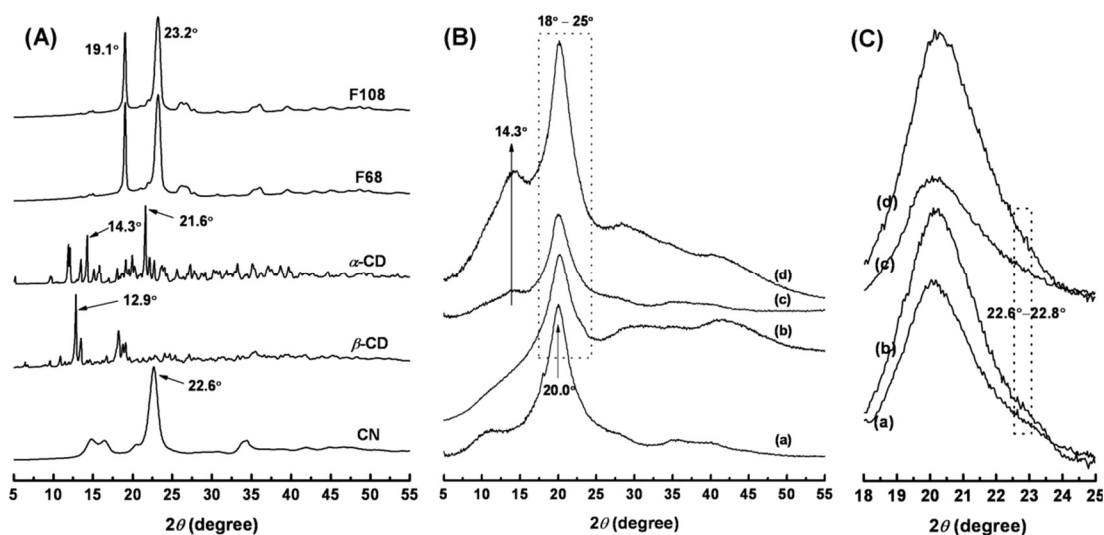


Figure 5.5 X-ray diffraction patterns of (A) original materials: CN, β -CD, α -CD, Pluronic F68, and F108; (B, C) inclusive complexes of (a) (β)CD-g-CN/F68, (b) (β)CD-g-CN/F108, (c) (β)CD-g-CN/F68- α (CD), (d) (β)CD-g-CN/F108- α (CD).

Table 5.2 Chemical composition, element content and inclusion efficiency of Pluronic polymers obtained from elemental analysis.

Sample	Chemical formula	Theoretical values			Experimental values		
		Carbon%	Oxygen%	Hydrogen%	Carbon%	Oxygen%	Hydrogen%
CN	(C ₆ H ₁₀ O ₅) _n	—	—	—	42.92	49.38	6.67
β -CD	C ₄₂ H ₇₀ O ₃₅	44.44	49.38	6.17	42.32	51.29	6.78
CN-g-(β)CD	—	—	—	—	42.96	49.11	6.86
Pluronic F68	C ₃₉₄ H ₇₉₀ O ₁₈₃	55.98	34.67	9.35	55.94	34.73	9.55
Pluronic F108	C ₆₈₂ H _{1,366} O ₃₁₇	55.97	34.69	9.34	56.13	34.75	9.49
CN-g-(β)CD/Pluronic F68	—	—	—	—	44.55	48.75	6.94
CN-g-(β)CD/Pluronic F108	—	—	—	—	45.01	48.51	6.77
<i>IE</i> -F68(%) ^a	—	—	—	—	12.25	—	—
<i>IE</i> -F108(%) ^a	—	—	—	—	15.57	—	—

^a *IE*-Pluronic (*IE*%) represents the inclusion efficiency of Pluronic polymers inclusive with β -CD, which was calculated according to eq. 5.3.

which may induce the arrangement of inclusive chains (PEG/ α -CD), and cause the slight exhibition of α -CD crystalline feature. This phenomenon also indicates the capability of inclusion between (β)CD-*g*-CN/Pluronic and α -CD, which ensured the future *in situ* formation of hydrogels. In addition, the crystalline character of cellulose was covered in these patterns, which induced the broadening of the peak observed between 18 and 25°. By magnifying the patterns, the traces of crystalline cellulose can be observed with a ill-defined peak located at about 22.6°, as shown in Figure 5.5 (C).

5.4.2 Morphology and Dimensions of CN and Hydrogels

TEM was used to observe the morphology and dimensions of cellulose nanocrystals, as shown in Figure 5.6. Nanocrystals exhibited a typical rod-like morphology with a length of 200–400 nm and a diameter of 10–20 nm with an aspect ratio (L/d) of about 18. This result was in accordance with our previous report for the morphological observation of cellulose nanocrystals using atomic force microscopy (AFM).²⁹ Generally, during the process of observation, the inclusion complex of α -CD/PEG hydrogel recrystallizes in water and forms crystals of regular shapes with facets on microscope grid at room temperature.³⁵ As shown in Figure 5.7, both in situ hydrogels derived from Pluronic F68 and F108 exhibited the regular appearance with rectangular morphology in the size range of about 10–20 μm long and 2–4 μm wide.

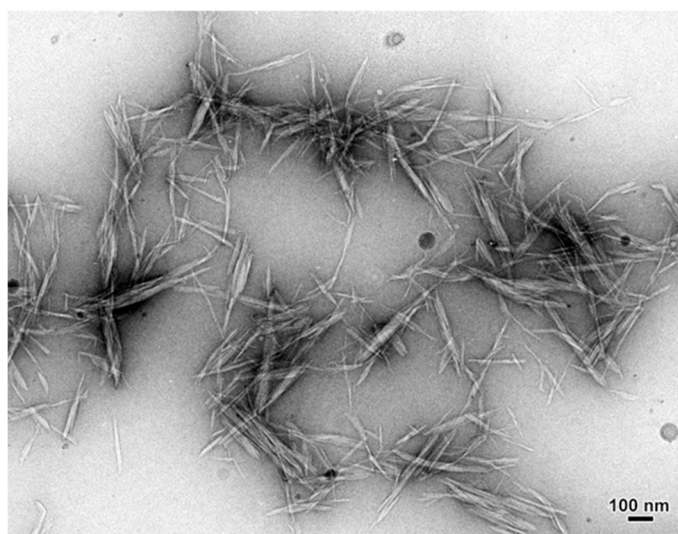


Figure 5.6 TEM micrographs of cellulose nanocrystals.

In comparison with the F68-hydrogels [Figure 5.7 (A, B)], F108-hydrogels [Figure 7 (C, D)] show higher length ($> 15 \mu\text{m}$) and much coarser surface, which may be attributed to the longer PEG chains of Pluronic F108 in the hydrogel system.

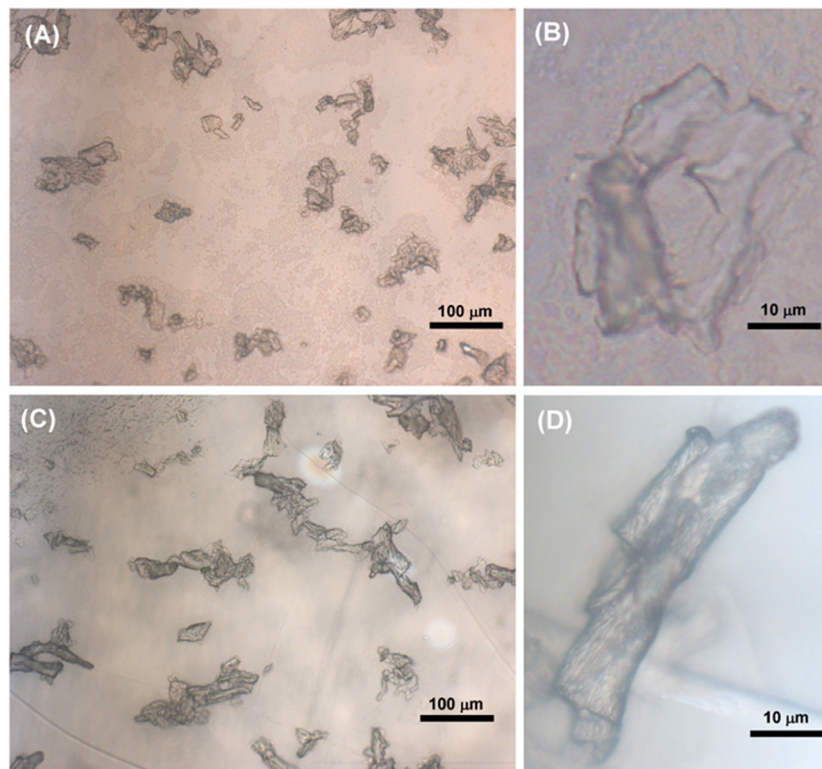


Figure 5.7 Optical microscopy images of *in situ* supramolecular hydrogels of (A, B) CN-CD/F68-2 and (C, D) CN-CD/F108-2.

5.4.3 Rheological Behavior of Hydrogels

When modified CN were introduced into the architecture of hydrogels, these nanoparticles can participate to the *in situ* inclusion between polymers and cyclodextrin via the surface grafted polymeric chains, which endowed strong coupling between nanocrystals and hydrogel. On the other hand, if the loading level of added nanoparticles reaches a critical content, such as the percolation threshold (v_{RC}), the strong interactions (such as hydrogen bonding) among nanoparticles should force them to associate/interact with each other for supporting the tridimensional percolating network.³⁷ It is believed that both interactions are beneficial for the performance of the hydrogel, and should strengthen and improve the structural stability and rheological behavior of ensuing hydrogels. Before the discussion of

rheological properties of *in situ* hydrogels, the value of v_{Rc} can be calculated with the dependence upon the aspect ratio (L/d) of rod-like CN according to eq. 5.2:

$$v_{Rc} = \frac{0.7}{L/d} \quad (5.4)$$

The v_{Rc} value is therefore inversely proportional to the aspect ratio of CN. According to the observations from TEM, the value of v_{Rc} in this case was close to 3.89 vol% (6.09 wt% with the density of cotton cellulose 1.565 g/mg).

The rheological behavior of hydrogels was investigated on the basis of three aspects, including change of viscosity as a function of the shear rate, dependence of storage moduli (G') and loss moduli (G'') as a function of angular frequency and temperature. When subjected to flow experiments, all hydrogels exhibited the physical nature of gelation and were found to be thixotropic and reversible, as shown in Figure 5.8 (A, A'). Even for *in situ* hydrogel with the highest initial viscosity (CN-CD/F108-3), the viscosity of the hydrogel greatly reduced when increasing the shear rate. This property makes the hydrogels syringeable, which is useful and important for drug delivery systems. Two different effects on the rheological behavior of *in situ* hydrogels as a function of angular frequency were observed depending on the CN content, as shown in Figure 5.8 (B, B'). With the addition of only 50 mg modified CN, the improvement of the mechanical properties of the hydrogel was unobvious (CN-CD/Pluronic-1) in comparison with the neat hydrogel (Pluronic/ α -CD). However, when the loading level increased above 100 mg, the moduli of both F68- and F108-hydrogels were enhanced significantly. Meanwhile, with the introduction of enough modified CN, the *in situ* hydrogels can maintain better structural stability in contrast to the sharp decrease of moduli observed for neat hydrogels under high angular frequency. The dependence of the hydrogel moduli as a function of temperature is shown in Figure 5.8 (C, C'). The effect of introducing modified CN in hydrogels was more evident and induced the promising thermal stability for *in situ* hydrogels contrary to the strong variation induced by sol–gel transition for neat hydrogels. It should be pointed out that the F108-hydrogels commonly presented

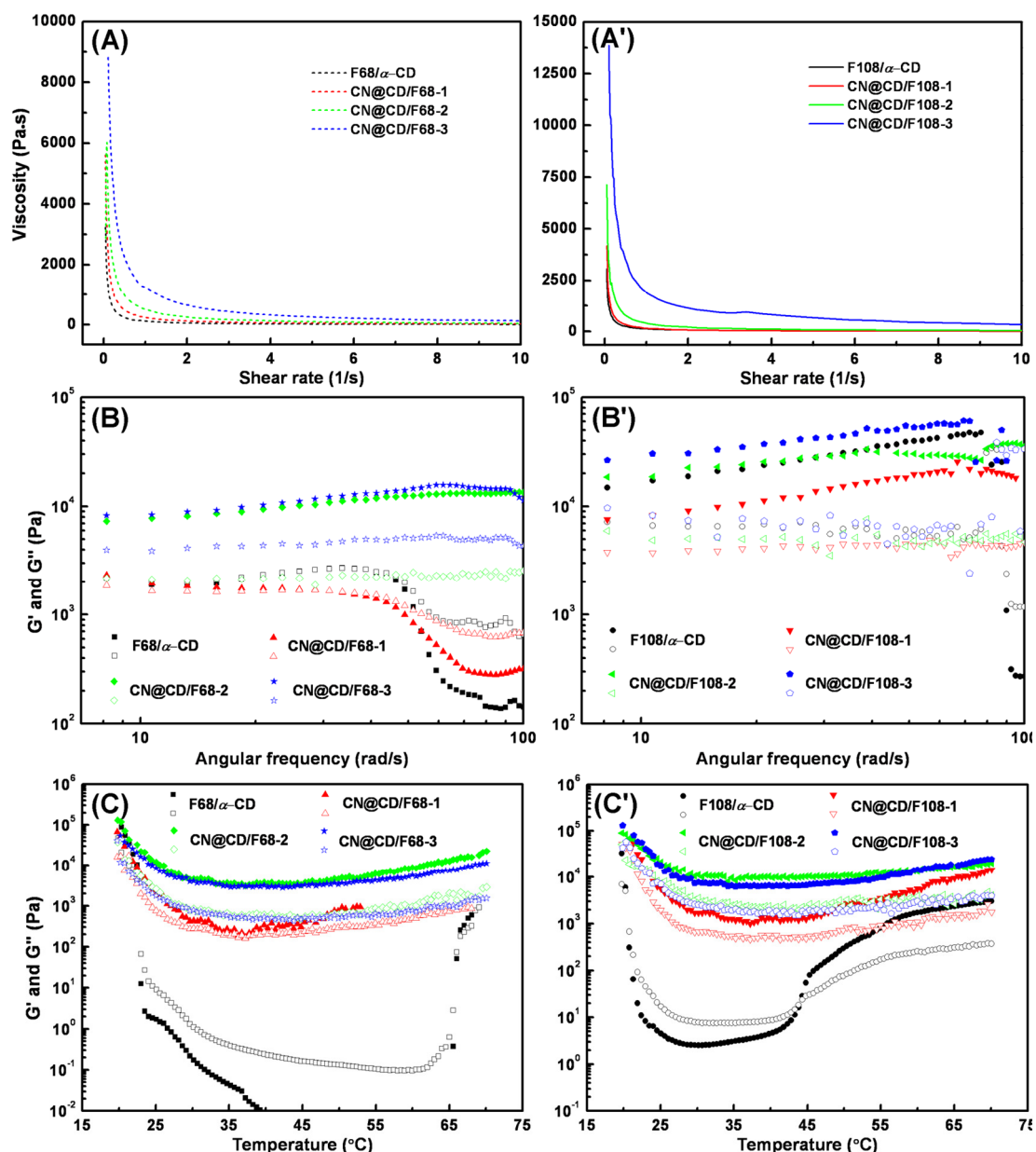


Figure 5.8 Rheological behavior of hydrogels: (A, A') viscosity vs shear rate; (B, B') storage modulus (G' , filled symbols) and loss modulus (G'' , open symbols) vs angular frequency; (C, C') G' (filled symbols) and G'' (open symbols) vs temperature at a fixed frequency of 20 rad/s and 50 Pa shear stress in the range of 20–70 °C.

better mechanical properties and thermal stability than F68-hydrogels, which may be attributed to the longer polymeric chains with more inclusive cyclodextrin molecules for Pluronic F108. In addition, based on the rheological behavior of in situ hydrogels, it was interesting that the mechanical properties of CN-CD/Pluronic-2 were similar to that of CN-CD/Pluronic-3, which indicates that the introduction of CN in the hydrogel

CN-CD/Pluronic-2 may be a critical point for the support of some special structure. According to the results of elemental analysis reported in Table 5.1, the true contents of CN in hydrogels CN-CD/F68-2 and CN-CD/F108-2 were 5.96 and 5.77 wt%, respectively, which were very close to the previously calculated percolation threshold (v_{RC} , 6.09 wt%). It was believed that cellulose nanoparticles with adequate loading level could form the percolating network in the architecture of hydrogels and properly improved the performance of *in situ* hydrogels.

5.4.4 pH-Sensitivity of Hydrogels

The influence of different pH values on the properties (G' and G'') of hydrogels was investigated under acidic, neutral, and alkaline conditions. As shown in Figure 5.9 (A), under acidic conditions, in situ hydrogels CN-CD/F68-2 and CN-CD/F68-3 kept high moduli and stability, which was about 5 times higher than for neat hydrogels. The maximum values of G' for all hydrogels appeared in neutral condition (pH = 7). However, when increasing the pH value to alkaline environment, the moduli for all hydrogels dropped sharply, which may be attributed to the higher solubility and

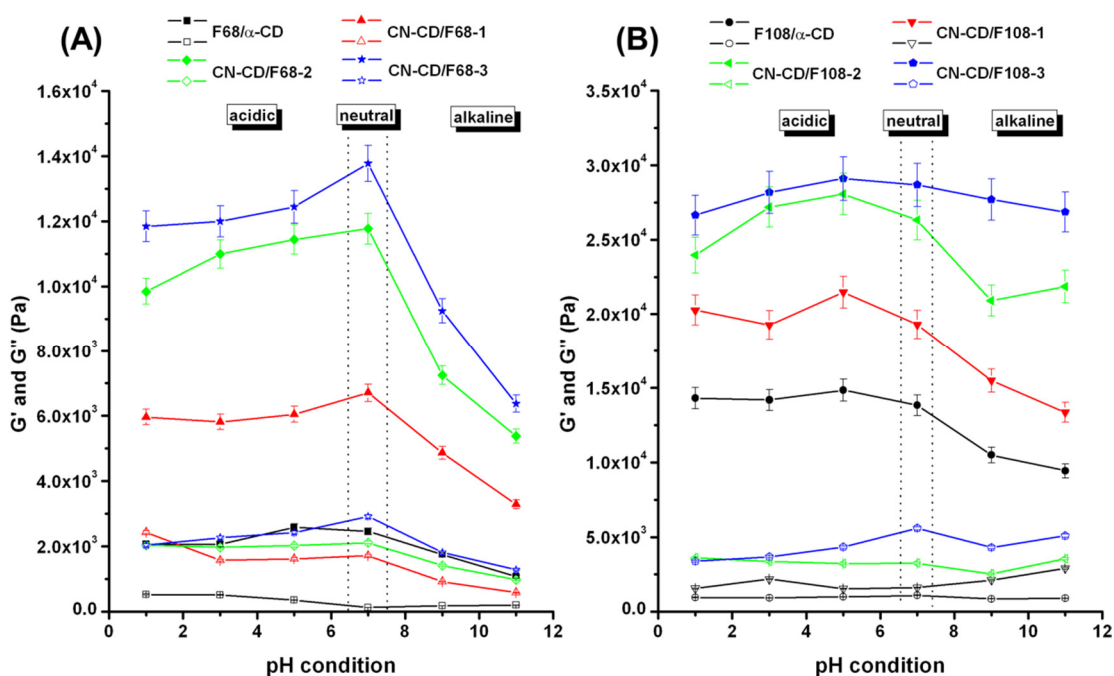


Figure 5.9 Evolution of G' (filled symbols) and G'' (open symbols) for various hydrogels under different pH conditions at a fixed frequency of 1 Hz with 50 Pa shear stress at 20 °C.

dissolution of cyclodextrin in alkaline condition. Similar results can also be observed for the CN-CD/F108 hydrogel system [Figure 5.9 (B)]. However, it was interesting that, different from other hydrogels, hydrogel CN-CD/F108-3 preserved a storage moduli (G') at high levels and seemed to possess the ability of alkaline resistance. A further study will focus on this interesting phenomenon.

5.5 Drug Release and Mechanism Study

Doxorubicin is an anticancer drug, which is widely used in the resistant of solid tumors, including breast cancer, ovarian carcinoma, transitional cell bladder carcinoma, and thyroid carcinoma. However, the non-negligible side effect, primarily the cardiotoxicity resulting from high concentration of drug in blood, demands ideal carrier for this drug for effective drug controlled release.³⁸ As shown in Figure 5.10 (A), in situ hydrogels formed with participating modified CN (CN-CD/F68-2-Dox and CN-CD/F108-2-Dox) exhibited promising controlled release behavior with sustained release for about one week, whereas neat hydrogels (F68/ α -CD and F108/ α -CD) displayed an initial burst release and shortened release period (only 2.5 days). The prolonged drug release for in situ hydrogels upon modified CN introduction was supposed to result from two factors. As reported in our previous literature,³⁹ rigid CN has been proven to induce physical “obstruction effect” in an alginate-based microsphere for controlled drug release property. On the other hand, in this study, if the loading level of nanocrystals reaches the percolation threshold, inducing a network structure with linkage among nanoparticles, it may provide another “locking effect” to delay the diffusion of doxorubicin molecules (as shown in Figure 10B). Both effects from modified nanocrystals led to the sustained drug release of in situ hydrogels. It is worth noting that when comparing the hydrogels formed with different Pluronic chains, there was no significant relation between the length of chains used in the hydrogel and the drug release behavior. However, the final cumulative release ratio depended on the length of used Pluronic for hydrogels, which indicates the lower final cumulative release for hydrogels with longer Pluronic chains.

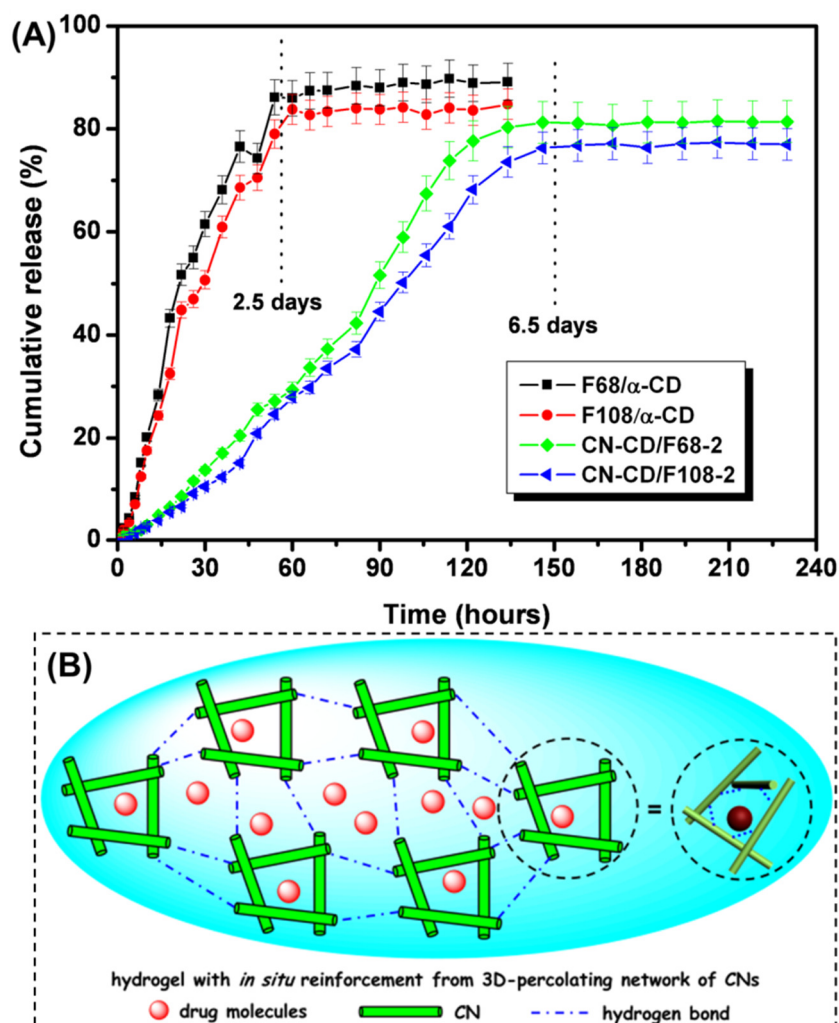


Figure 5.10 (A) In vitro release profiles of doxorubicin·HCl for hydrogels with different compositions; (B) possible “locking effect” from the linkage between nanoparticles.

To prove the different release mechanisms for hydrogels, Ritger-Peppas equation was used to analyze the results of drug release:

$$Q = kt^n \quad (\ln Q = k' + n \ln t) \quad (5.5)$$

where Q is the amount of drug released at time t ; k is a constant associated with the structural and geometrical characteristics of dosage form; and n is the release (diffusion) exponent, which depends on the release mechanism. It was reported that n values approximating to 0.50 indicate a Fickian diffusion release, whereas the n value in the range of 0.50 to 0.85 represents both diffusion-controlled release and non-Fickian diffusion release (anomalous transport).⁴⁰ Estimated parameters and fitted equations for the various hydrogels with different compositions are shown in Table

5.3. It was shown that neat hydrogels (Pluronic/ α -CD-Dox) underwent the common Fickian diffusion, but in situ hydrogels (CN/CD-Pluronic-Dox) exhibited an anomalous transport release mechanism. These results revealed the different effects and changes of in situ hydrogels with the introduction of modified nanocrystals compared to neat hydrogels.

Table 5.3 Estimated parameters and drug release mechanism for drug release of hydrogels according to Ritger-Peppas equation.

Sample	Equation	k	n	R^a	Mechanism
F68/ α -CD-Dox	$\ln Q = 2.387 + 0.465 \ln t$	10.885	0.465	0.890	Fickian diffusion
F108/ α -CD-Dox	$\ln Q = 2.170 + 0.498 \ln t$	8.760	0.498	0.897	Fickian diffusion
CN-CD/F68-2-Dox	$\ln Q = 0.393 + 0.771 \ln t$	1.482	0.771	0.931	anomalous transport
CN-CD/F108-2-Dox	$\ln Q = 0.003 + 0.832 \ln t$	1.003	0.832	0.945	anomalous transport

^a R is the regression coefficient for the fitted curves according to Ritger-Peppas equation.

5.6 Conclusions

This work was an attempt to use chemical modification methods to promote the compatibility and enhance the loading levels of cellulose nanocrystals in hydrogel materials. Meanwhile, uncovered polymeric chains render the participating inclusion of α -cyclodextrin for the architecture of in situ hydrogels. Grafting efficiency of β -cyclodextrin on the surface of nanocrystals was confirmed by UV spectroscopy as 16.89 wt%, and inclusion efficiency of Pluronic F68 and F108 polymers were measured by elemental analysis as 12.25 and 15.57 wt%, respectively. With the introduction of high loading levels of modified nanocrystals (> 5 wt%), a significant enhancement of structural and thermal stability of in situ hydrogels was observed from rheological analysis. A further study revealed the performance of hydrogels as drug carrier for in vitro release of doxorubicin and exhibited the behavior of prolonged drug release with special release kinetics, which was attributed to the “obstruction effect” and “locking effect”. Based on their performances and properties, these in situ hydrogels as syringeable drug delivery provide a scientific example for the application of biomass nanocrystals in the field of biomedical materials.

5.7 References

1. Azizi Samir, M. A. S.; Alloin, F.; Dufresne, A. Review of recent research into cellulosic whiskers, their properties and their application in nanocomposite field. *Biomacromolecules* **2005**, *6*, 612–626.
2. Habibi, Y.; Lucia, A. L.; Rojas, O. J. Cellulose nanocrystals: Chemistry, self-assembly, and applications. *Chem. Rev.* **2010**, *110*, 3479–3500.
3. Klemm, D.; Kramer, F.; Moritz, S.; Lindström, T.; Ankerfors, M.; Gray, D.; Dorris, A. Nanocelluloses: A new family of nature-based materials. *Angew. Chem. Int. Ed.* **2011**, *50*, 5438–5466.
4. Moon, R. J.; Martini, A.; Nairn, J.; Simonsen, J.; Youngblood, J. Cellulose nanomaterials review: structure, properties and nanocomposites. *Chem. Soc. Rev.* **2011**, *40*, 3941–3994.
5. Dufresne, A. Processing of polymer nanocomposites reinforced with polysaccharide nanocrystals. *Molecules* **2010**, *15*, 4111–4128.
6. Eichhorn, S. J.; Dufresne, A.; Aranguren, M.; Marcovich, N. E.; Capadona, J. R.; Rowan, S. J.; Weder, C.; Thielemans, W.; Roman, M.; Renneckar, S.; Gindl, W.; Veigel, S.; Keckes, J.; Yano, H.; Abe, K.; Nogi, M.; Nakagaito, A. N.; Mangalam, A.; Simonsen, J.; Benight, A. S.; Bismarck, A.; Berglund, L. A.; Peijs, T. Review: current international research into cellulose nanofibres and nanocomposites. *J. Mater. Sci.* **2010**, *45*, 1–33.
7. Lin, N.; Huang, J.; Dufresne, A. Preparation, properties and applications of polysaccharide nanocrystals in advanced functional nanomaterials: a review. *Nanoscale* **2012**, *4*, 3274–3294.
8. Lam, E.; Male, K. B.; Chong, J. H.; Leung, A. C. W.; Luong, J. H. T. Applications of functionalized and nanoparticle-modified nanocrystalline cellulose. *Trends Biotechnol.* **2012**, *30*, 283–290.
9. Dong, S.; Roman, M. Fluorescently labeled cellulose nanocrystals for bioimaging applications. *J. Am. Chem. Soc.* **2007**, *129*, 13810–13811.
10. Mahmoud, K. A.; Mena, J. A.; Male, K. B.; Hrapovic, S.; Kamen A.; Luong, J. H.

- T. Effect of surface charge on the cellular uptake and cytotoxicity of fluorescent labeled cellulose nanocrystals. *ACS Appl. Mater. Interfaces* **2010**, *2*, 2924–2932.
11. Liu, H.; Wang, D.; Song, Z.; Shang, S. Preparation of silver nanoparticles on cellulose nanocrystals and the application in electrochemical detection of DNA hybridization. *Cellulose* **2011**, *18*, 67–74.
 12. Drogat, N.; Granet, R.; Le Morvan, C.; Bégau-Grimaud, G.; Krausz, P.; Sol, V. Chlorin-PEI-labeled cellulose nanocrystals: Synthesis, characterization and potential application in PDT. *Bioorg. Med. Chem. Lett.* **2012**, *22*, 3648–3652.
 13. Mahmoud, K. A.; Male, K. B.; Hrapovic, S.; Luong, J. H. T. Cellulose nanocrystal/gold nanoparticle composite as a matrix for enzyme immobilization. *ACS Appl. Mater. Interfaces* **2009**, *1*, 1383–1386.
 14. Edwards, J. V.; Prevost, N. T.; Condon, B.; French, A.; Wu, Q. Immobilization of lysozyme-cellulose amide-linked conjugates on cellulose I and II cotton nanocrystalline preparations. *Cellulose* **2012**, *19*, 495–506.
 15. Feese, E.; Sadeghifar, H.; Gracz, H. S.; Argyropoulos, D. S.; Ghiladi, R. A. Photobactericidal porphyrin-cellulose nanocrystals: Synthesis, characterization, and antimicrobial properties. *Biomacromolecules* **2011**, *12*, 3528–3539.
 16. Carpenter, B. L.; Feese, E.; Sadeghifar, H.; Argyropoulos, D. S.; Ghiladi, R. A. Porphyrin-cellulose nanocrystals: A photobactericidal material that exhibits broad spectrum antimicrobial activity. *Photochem. Photobiol.* **2012**, *88*, 527–536.
 17. Wang, Y.; Chang, C.; Zhang, L. Effects of freezing/thawing cycles and cellulose nanowhiskers on structure and properties of biocompatible starch/PVA sponges. *Macromol. Mater. Eng.* **2010**, *295*, 137–145.
 18. Gatenholm, P.; Klemm, D. Bacterial nanocellulose as a renewable material for biomedical applications. *MRS Bulletin* **2010**, *35*, 208–213.
 19. Chang, C.; Zhang, L. Cellulose-based hydrogels: Present status and application prospects. *Carbohydr. Polym.* **2011**, *84*, 40–53.
 20. Sannino, A.; Demitri, C.; Madaghiele, M. Biodegradable cellulose-based hydrogels: design and applications. *Materials* **2009**, *2*, 353–373.
 21. Li, J. Self-assembled supramolecular hydrogels based on polymer–cyclodextrin

- inclusion complexes for drug delivery. *NPG Asia Mater.* **2010**, *2*, 112–118.
22. Zhang, X.; Huang, J.; Chang, P. R.; Li, J.; Chen, Y.; Wang, D.; Yu, J.; Chen, J. Structure and properties of polysaccharide nanocrystal-doped supramolecular hydrogels based on cyclodextrin inclusion. *Polymer* **2010**, *51*, 4398–4407.
23. Osorio-Madrado, A.; Eder, M.; Rueggeberg, M.; Pandey, J. K.; Harrington, M. J.; Nishiyama, Y.; Putaux, J.-L.; Rochas, C.; Burgert, I. Reorientation of cellulose nanowhiskers in agarose hydrogels under tensile loading. *Biomacromolecules* **2012**, *13*, 850–856.
24. Bica, C. I. D.; Borsali, R.; Rochas, C.; Geissler, E. Dynamics of cellulose whiskers spatially trapped in agarose hydrogels. *Macromolecules* **2006**, *39*, 3622–3627.
25. Abitbol, T.; Johnstone, T.; Quinn, T. M.; Gray, D. G. Reinforcement with cellulose nanocrystals of poly(vinyl alcohol) hydrogels prepared by cyclic freezing and thawing. *Soft Matter* **2011**, *7*, 2373–2379.
26. Cha, R.; He, Z.; Ni, Y. Preparation and characterization of thermal/pH-sensitive hydrogel from carboxylated nanocrystalline cellulose. *Carbohydr. Polym.* **2012**, *88*, 713–718.
27. Karaaslan, M. A.; Tshabalala, M. A.; Yelle, D. J.; Buschle-Diller, G. Nanoreinforced biocompatible hydrogels from wood hemicelluloses and cellulose whiskers. *Carbohydr. Polym.* **2011**, *86*, 192–201.
28. Way, A. E.; Hsu, L.; Shanmuganathan, K.; Weder, C.; Rowan, S. J. pH-Responsive cellulose nanocrystal gels and nanocomposites. *ACS Macro Lett.* **2012**, *1*, 1001–1006.
29. Lin, N.; Bruzzese, C.; Dufresne, A. TEMPO-Oxidized nanocellulose participating as crosslinking aid for alginate-based sponges. *ACS Appl. Mater. Interfaces* **2012**, *4*, 4948–4959.
30. Zhao, Q.; Wang, S.; Cheng, X.; Yam, R. C. M.; Kong, D.; Li, R. K. Y. Surface Modification of cellulose fiber via supramolecular assembly of biodegradable polyesters by the aid of host–guest inclusion complexation. *Biomacromolecules* **2010**, *11*, 1364–1369.

31. Mortensen, K.; Pedersen, J. S. Structural study on the micelle formation of poly(ethylene oxide)-poly(propylene oxide)-poly(ethylene oxide) triblock copolymer in aqueous solution. *Macromolecules* **1993**, *26*, 805–812.
32. Tsai, C.-C.; Leng, S.; Jeong, K.-U.; Van Horn, R. M.; Wang, C.-L.; Zhang, W.-B.; Graham, M. J.; Huang, J.; Ho, R.-M.; Chen, Y.; Lotz, B.; Cheng, S. Z. D. Supramolecular structure of β -cyclodextrin and poly(ethylene oxide)-*block*-poly(propylene oxide)-*block*-poly(ethylene oxide) inclusion complexes *Macromolecules* **2010**, *43*, 9454–9461.
33. Li, J.; Li, X.; Zhou, Z.; Ni, X.; Leong, K. W. Formation of supramolecular hydrogels induced by inclusion complexation between Pluronics and α -cyclodextrin. *Macromolecules* **2001**, *34*, 7236–7237.
34. Simões, S. M. N.; Veiga, F.; Torres-Labandeira, J. J.; Ribeiro, A. C. F.; Sandez-Macho, M. I.; Concheiro, A.; Alvarez-Lorenzo, C. Syringeable Pluronic– α -cyclodextrin supramolecular gels for sustained delivery of vancomycin. *Eur. J. Pharm. Biopharm.* **2012**, *80*, 103–112.
35. He, L.; Huang, J.; Chen, Y.; Xu, X.; Liu, L. Inclusion interaction of highly densely PEO grafted polymer brush and α -cyclodextrin. *Macromolecules* **2005**, *38*, 3845–3851.
36. Peet, J.; Rusa, C. C.; Hunt, M. A.; Tonelli, A. E.; Balik, C. M. Solid-state complexation of poly(ethylene glycol) with α -cyclodextrin. *Macromolecules* **2005**, *38*, 537–541.
37. Dufresne, A. Polysaccharide nanocrystal reinforced nanocomposites. *Can. J. Chem.* **2008**, *86*, 484–494.
38. Xun, W.; Wu, D.-Q.; Li, Z.-Y.; Wang, H.-Y.; Huang, F.-W.; Cheng, S.-X.; Zhang, X.-Z.; Zhuo R.-X. Peptide-functionalized thermo-sensitive hydrogels for sustained drug delivery. *Macromol. Biosci.* **2009**, *9*, 1219–1226.
39. Lin, N.; Huang, J.; Chang, P. R.; Feng L.; Yu, J. Effect of polysaccharide nanocrystals on structure, properties, and drug release kinetics of alginate-based microspheres. *Colloid. Surface. B* **2011**, *85*, 270–279.

40. Ritger, P. L.; Peppas, N. A. A simple equation for description of solute release II. Fickian and anomalous release from swellable devices. *J. Control. Release* **1987**, *5*, 37–42.

CHAPTER 6.

General Conclusions and Perspectives for Future Research

Chapter 6. General Conclusions and Perspectives for Future Research

Research

6.1 General Conclusions

The main objective of this thesis was to investigate the properties of cellulose nanocrystals and to develop their applications as building blocks for nanocomposites and functional materials. The main innovations of the studies introduced in the thesis include: i) the preparation of cellulose nanocrystals with gradient sulfation degrees and analysis of surface chemistry affected by different cross-section models; ii) extrusion of cellulose nanocrystals reinforced polystyrene nanocomposites with physical and/or chemical modification and compatibilization; iii) use of TEMPO-induced carboxyl groups on nanocellulose participating in the construction of crosslinked network with “egg-box” multimer for the preparation of alginate-based sponge; and iv) development of supramolecular hydrogels from in situ inclusion between modified cellulose nanocrystals and cyclodextrin for drug delivery application.

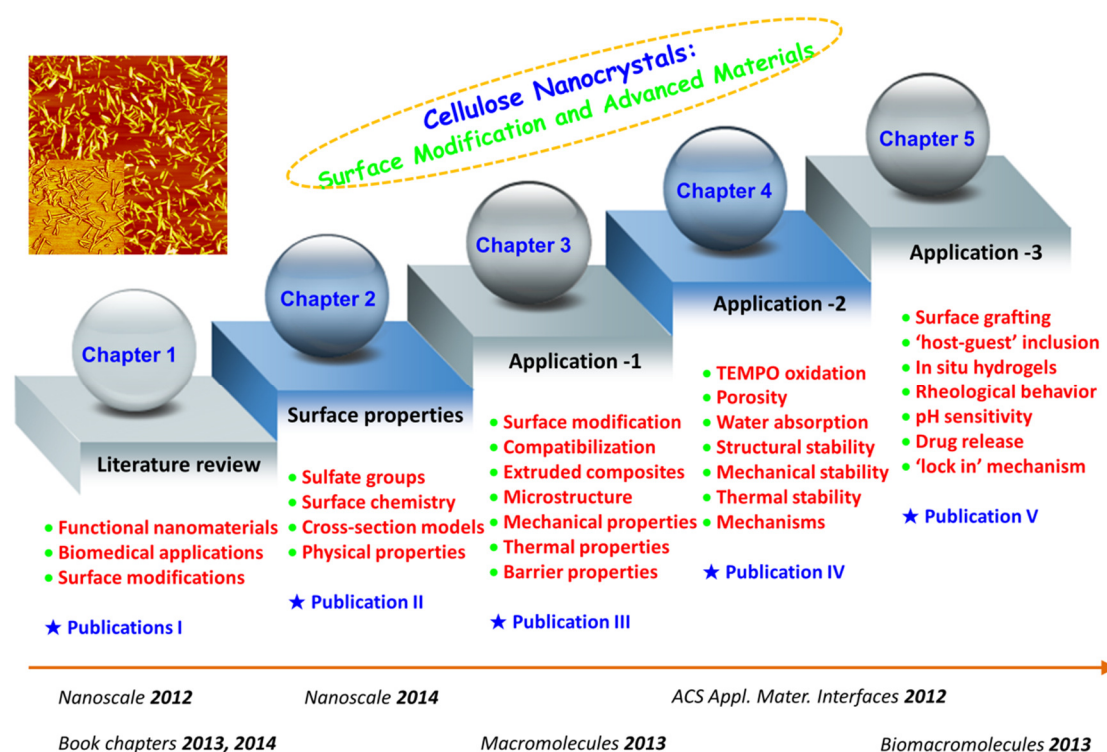


Figure 6.1 Schematic illustration of the research topics and results presented in this thesis.

Revolving around the properties and applications of cellulose nanocrystals, diverse modifications have been performed on cellulose nanocrystals in order to further investigate their surface properties and tailor their applicability for various advanced materials. General research topics for each study are summarized in Figure 6.1.

In chapter 1, the state of the art on research on the topic of cellulose nanocrystals (also including cellulose whiskers and nanocrystalline cellulose) was reviewed, and significant studies were specially introduced on the basis of four parts, viz. preparation and production; physical, chemical and biological properties; surface modification; as well as traditional and advanced applications. In view of my PhD studies, the emphasis of literature review in this chapter was put on the physical and chemical properties, surface modification, and functional nanomaterials.

The research work introduced in chapter 2 originated from the following questions: “how many active hydroxyl groups have been replaced by sulfate groups during H_2SO_4 hydrolysis; and how surface sulfate groups affect the surface chemistry and physical properties of cellulose nanocrystals?” To answer these questions, gradient contents of sulfate groups were introduced on the surface of cellulose nanocrystals through the regulation of reactant ratios and reactive conditions for postsulfation and desulfation. Based on the analysis of surface chemistry for gradient modified nanocrystals, it was proved that the choice of different cross-section models will significantly affect the calculation of the degree of substitution of sulfate groups on cellulose nanocrystals. Taking cotton cellulose nanocrystals as example, if square or round model was chosen for nanocrystals, more than 20% of surface hydroxyl groups have been substituted by sulfate groups during the H_2SO_4 -esterification hydrolysis (65 wt% acid concentration, 45 °C), which indicated that most of the active hydroxyl groups located on C-6 have been replaced during the extraction. If ellipse model was chosen, about 13% of the surface hydroxyl groups were replaced by sulfate groups during hydrolysis. However, if choosing rectangle model for cellulose nanocrystals, only 7.9% of the surface hydroxyl groups was substituted during the H_2SO_4 -hydrolysis (only about 1/3 of the value for square or round model), and a large

amount of active hydroxyl groups have been remained. Moreover, the effect of sulfate groups on various physical properties of cellulose nanocrystals and their suspensions have been discussed. The parallelogram elementary crystallite model for cotton cellulose nanocrystals was further validated by XRD analysis, and determination of negative charges induced by the presence of sulfate groups on cellulose nanocrystals by ζ -potential measurement. The influence of sulfate groups on the thermal stability of cellulose nanocrystals was investigated, which indicated that more sulfate groups on nanocrystals induced a lowering of the temperature corresponding to the first phase of thermal decomposition (T_{d1}), and higher crystallinity for nanocrystals resulting in higher second phase thermal decomposition temperature (T_{d2}). From the observation of birefringence of aqueous suspensions, it was concluded that the dispersion and formation of birefringent domains can be affected by the content of surface sulfate groups on nanocrystals.

Chapter 3 was a study on the preparation of extruded composites in order to settle the thermal stability issue of cellulose nanocrystals during melting-coumpounding of polymer nanocomposites. A strategy involving two poly(ethylene glycol)/polyoxyethylene (PEG/PEO) layers on the surface of cellulose nanocrystals using chemical grafting and physical interactions was proposed. Four kinds of nanocrystals, i.e. pristine nanocrystal, PEO-adsorbed nanocrystal, PEG-grafted nanocrystal, and both PEG-grafted and PEO-adsorbed nanocrystal, were extruded with a hydrophobic polymeric matrix (PS) to prepare nanocomposites. The basic idea was consistent with the possibility of entanglements and co-crystallization between short PEG chains and long PEO chains, which can closely wrap and protect the surface of the nanocrystals. Meanwhile, the chemical and physical compatibilization imparted by PEG and PEO layers promoted the interfacial interactions between cellulosic nanoparticles and apolar matrix. The possibility of processing modified nanocrystals (CN-g-PEG/PEO) at high temperature (200 °C) avoiding the degradation of the nanoparticle, and providing a good dispersion and compatibility between modified nanocrystals and matrix was shown. Furthermore, the nanocrystal surface

modifications did not block totally the interactions between the nanoparticles, and kept at least partially the three-dimensional network architecture, which was beneficial for the improvement of mechanical properties of extruded nanocomposites. Indeed, from the results of TGA, double-layer modified cellulose nanocrystals showed a significant enhancement of degradation temperature (about 120 °C increase in comparison with pristine cellulose nanocrystals), which can be attributed to the uniform shield of sulfate groups induced by the coating with the grafted PEG chains and protection of adsorbed PEO layer. Extruded nanocomposites filled with double-layer modified cellulose nanocrystals exhibited transparent appearance and high transmittance ratios. Meanwhile, improved mechanical and water vapor barrier performances were observed on these extruded nanocomposites. With the strategy proposed in this study, it is expected to overcome an important challenge aimed at melt processing cellulose nanocrystal-based composites for industrial production.

With the purpose of improving weak performance (mechanical and structural stability) of neat alginate sponges, oxidized nanocellulose-participating crosslinked sponges were designed and investigated. This topic was discussed in chapter 4. Two types of nanocellulose extracted from cotton were used in this study, viz. cellulose nanocrystals with 'rigid' rod-like morphology and microfibrillated cellulose with 'soft' filament morphology. After TEMPO-selective oxidation treatment, modified nanocellulose possessed the capability of participating to ionic crosslinking during the structural formation of alginate-based sponges. Interestingly, different types of oxidized nanocellulose provided distinct enhancing effects for sponges. Remarkable reinforced mechanical strength was reported with oxidized cellulose nanocrystals whereas promising improved porosity, water absorption, and structural stability were observed for oxidized microfibrillated cellulose. More specifically, compared with the porosity (78.8%), water absorption (835.3%) and water retention (221.1%) of neat alginate sponge, crosslinked sponge filled with 50 wt% oxidized microfibrillated cellulose possessed ultrahigh porosity (97.4%), water absorption (1468.4%) and water retention (846.7%). Even after reusing for 10 times, this kind of crosslinked sponges

filled with oxidized microfibrillated cellulose can maintain high levels of water absorption. However, oxidized cellulose nanocrystals have a better impact on the reinforcement of mechanical properties of sponges. For compressive strains of 30%, 50%, and 70%, the compressive strength of crosslinked sponges containing 10 wt% oxidized cellulose nanocrystals increased by factors of 2.78, 2.80, and 2.94, in comparison with neat alginate sponge, respectively. It was supposed that rigid oxidized cellulose nanocrystals served as the coupling points, and fully played the nano-reinforcement effect for alginate-based sponges, whereas oxidized microfibrillated cellulose can join in the structural construction and form the semi-interpenetrating polymer network for alginate-based sponges.

Inspired from the study of physical blending of pristine polysaccharide nanocrystals and cyclodextrin, an attempt of using chemical modification methods to promote the compatibility and enhance the cellulose nanocrystal loading levels in cyclodextrin-based hydrogel materials was performed and reported in chapter 5. β -cyclodextrin was first covalently grafted on the surface of cellulose nanocrystals using epichlorohydrin as coupling agent. Then, Pluronic polymer was immobilized on modified cellulose nanocrystals by inclusion of the hydrophobic polymeric segments in grafted β -cyclodextrin. Pluronic polymers used in this study were tri-block copolymers with different molecular weights (Pluronic F68 or F108), both bearing hydrophobic PPG and hydrophilic PEG segments (PEG-*b*-PPG-*b*-PEG). The inclusion of the hydrophobic PPG chain segments in the inner cavity of β -CD allowed the close connection of chains and nanoparticles. Finally, through the ‘host-guest’ inclusion interactions between modified cellulose nanocrystals, Pluronic polymers, and different size of cyclodextrins, in situ hydrogels were prepared and developed as novel drug carrier. With the introduction of high loading levels of modified nanocrystals (> 5 wt%), a significant enhancement of the structural and thermal stability for in situ hydrogels was observed from rheological analysis. Meanwhile, these in situ hydrogels bearing modified cellulose nanocrystals showed special pH-sensitivity. A further study revealed the performance of in situ hydrogels as drug

carrier for in vitro release of doxorubicin, which showed promising controlled release behavior with sustained release for about one week whereas neat hydrogels displayed an initial burst release and shortened release period (only 2.5 days). The prolonged drug release behavior for in situ hydrogels was analyzed by release kinetics, and was supposed to be attributed to the “obstruction effect” and “locking effect” from modified cellulose nanocrystals. Based on their performances and properties, these in situ hydrogels as syringeable drug delivery provide a scientific example for the application of biomass nanocrystals in the field of biomedical materials.

6.2 Possible Research Points for Further Study

Table 6.1 Future research points for the studies presented in this thesis.

Studies in this thesis	Future research points
Surface chemistry and properties of CN with gradient sulfation degrees	<ul style="list-style-type: none"> • Investigation of electrostatic interactions between negative charges from sulfated CN and positive charges from cationic polymers or molecules • Measurement of strength and mechanism of electrostatic interactions from coupling charges • Strategy for surface electrostatic grafting on CN
Physical and/or chemical compatibilization of extruded CN reinforced PS nanocomposites	<ul style="list-style-type: none"> • Further investigation on interactions between grafted PEG and adsorbed PEO • Effect of PEG/PEO chain lengths ratio to compatibility • Measurement of interphase thickness of PEG and PEO layers in extruded nanocomposites • Simpler method for the replacement of PEG chemical grafting on the surface of CN • Investigation of other polymers or copolymers
TEMPO-Oxidized nanocellulose participating as crosslinking aid for alginate-based sponges	<ul style="list-style-type: none"> • Direct proofs for participating crosslinking of oxidized nanocellulose, alginate and Ca^{2+} • Attempt of incorporating both oxidized CN and oxidized MFC in sponges for synergistic enhancements • Development of ensuing sponges in biomedical applications, such as drug-loaded wound dressing
Supramolecular hydrogels from in situ host–guest inclusion between modified CN and cyclodextrin	<ul style="list-style-type: none"> • Characterization of ‘obstruction effect’ and ‘locking effect’ of CN-based drug delivery systems • Presence of CNs (with surface hydroxyl groups and/or sulfate groups) to structure and activity of drug molecules • Development of multi-membrane hydrogel systems for novel drug release behavior

Following the studies introduced in this thesis, some research topics can be carried out in future works. Table 6.1 shows some points originated from the studies developed in each chapter. Specifically, for the study on “gradient sulfate groups on cellulose nanocrystals” reported in chapter 2, future research can focus on the electrostatic interactions between negative charges from sulfated nanocrystals and positive charges from cationic polymers or molecules. With the detection and measurement of electrostatic interactions, it is expected to reveal the strength and mechanism of this special interaction from coupling charges and therefore advance the application of cellulose nanocrystal electrostatic grafting. Figure 6.2 provides the research strategy of polymer electrostatic grafting onto cellulose nanocrystals and proposes the original questions of “Is it true for more sulfate groups, more adsorbed polymeric chains and stronger electrostatic interactions?”

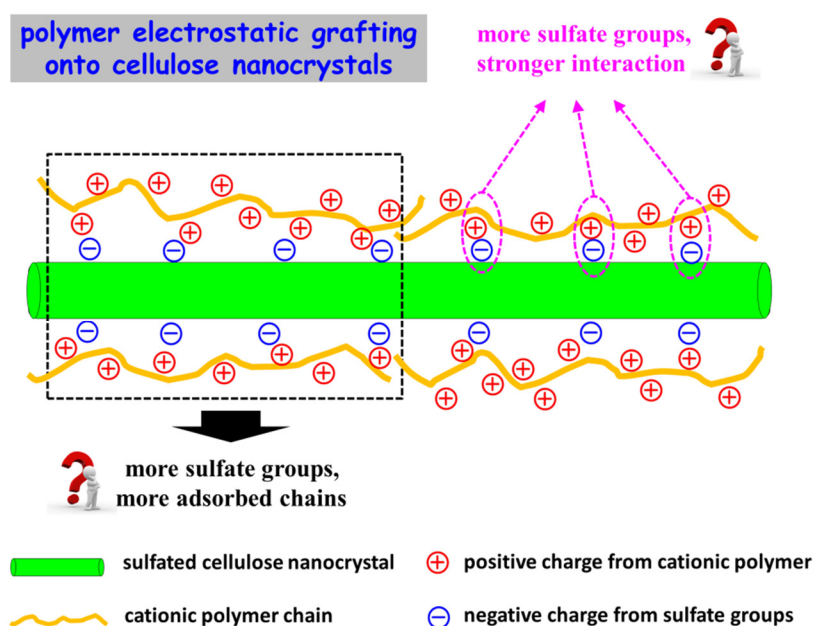


Figure 6.2 Strategy of polymer electrostatic grafting onto cellulose nanocrystals.

Regarding the study on “extruded cellulose nanocrystal-based composites” reported in chapter 3, further investigation is necessary to fully understand the interactions between grafted PEG and adsorbed PEO, such as the effect of chain length ratio (1/10 for PEG/PEO was used in this case), and interphase thickness of PEG and PEO layers in extruded nanocomposites. A careful control of the amount of decorating PEG/PEO chains is also desirable to monitor the possibility of hydrogen bonding between

nanoparticles. Moreover, a simpler method for the introduction of the first PEG layer on cellulose nanocrystals would be to use electrostatic grafting instead of the chemical grafting reaction. It is another important issue to drive the practical application of this strategy.

With respect to the study on “crosslinked alginate sponges” reported in chapter 4 and inspired from the different effects of two oxidized nanocelluloses, it will be interesting to attempt the idea of incorporating both oxidized nanocrystalline and microfibrillated cellulose in alginate-based materials, and develop applications of the ensuing sponges in the field of biomedical materials, such as drug carriers for wound dressing or bio scaffolds.

Regarding the study on “supramolecular hydrogels from cellulose nanocrystals and cyclodextrin” reported in chapter 5, further investigation on the effect of surface properties of cellulose nanocrystals to the structure and bioactivity of drug molecules can significantly promote their application in novel biomedical nanomaterials. In addition, taking advantage of the ‘obstruction effect’ and ‘locking effect’ from cellulose nanocrystals, it is promising to develop complexing drug delivery systems for novel drug release behaviors, such as multi-membrane hydrogel systems. In the following one year, some ideas will be carried out during my post-doctoral research.

6.3 Perspectives and Challenges in Future

It can be evidenced that cellulose nanocrystal is a unique and magic material. Cellulose nanocrystal can be used in all kinds of fields, but it is still a rather new material to us. There are still many unknown properties or undiscovered applications for cellulose nanocrystals. Despite being the most available and common natural polymer on earth, it is only recently that the prominence of this nanostructured material was recognized. Now we stand on the edge of breakthrough of cellulose nanocrystal research, and maybe it is the right corner for future materials science.

It is impossible to predict which fields will become the practical market for cellulose nanocrystals in future. Now, more and more researchers are attracted by this material,

and in the near future cellulose nanocrystals may be possibly used for the development of ultimate body armor, super-flexible screens, high-efficiency filters, bendable batteries, ultra-absorbent aerogels, cars and computers, bounteous biofuel, cosmetics, money currency etc. And now they are not just illusion. As few examples, IBM is reported to use cellulose nanocrystals to create components for computers, and the US army is considering cellulose nanocrystals to make lightweight body armor and ballistic glass.

Generally, the exploration of suitable approaches for cellulose nanocrystal in diverse types of materials is everlasting challenge for its future study. On the topic of production, the issues of cost reduction, properties control, and sustainability of supply are the challenges for cellulose nanocrystals. Promising commercial cellulose nanocrystals should be the products with both low cost and controllable properties (such as controlled dimensions, surface properties etc.). Regarding the application of cellulose nanocrystals in composites and functional materials, how to regulate or balance the compatibility and the formation of rigid network, and how to characterize the interactions between cellulose nanocrystals and diverse molecules, are the future challenges. In order to improve the compatibility between nanoparticles and polymeric matrices, surface modifications are commonly performed on cellulose nanocrystals. However, these surface treatments always limit the interactions among nanoparticles, which induce the weak formation of rigid network and inferior nano-reinforcing effects from cellulose nanocrystals. On the other hand, derived from intramolecules or surface groups, it is very difficult to directly observe or detect the physical interactions between cellulose nanocrystals and diverse molecules in various functional materials (such as interactions between cellulose nanocrystals and drug molecules, calcium crosslinking in this dissertation). Finally, the preservation of nano-reinforcing effect of cellulose nanocrystals in different conditions is another challenge, such as keeping high mechanical or barrier properties in wet atmosphere for prepared nanomaterials.

Cellulose nanocrystal is a precious gift from Nature, which deserves future study!

Résumé en Français

Introduction générale

Le nanocristal de cellulose est l'élément constitutif structurel primaire des plantes et peut être extrait de manière économique du bois et des fibres végétales, ou de la tunicine et de la cellulose bactérienne. L'hydrolyse des régions amorphes de la cellulose native permet de libérer les nanocristaux de cellulose – domaines cellulosiques cristallins, sous forme de bâtonnets rigides de 5–20 nm de diamètre et quelques dizaines à quelques centaines de nanomètres de longueur. Le développement des technologies d'extraction et de l'application des nanocristaux de cellulose a été activement poursuivi par divers groupes, notamment aux USA, au Canada et en Europe.¹ En tant que nanomatériau abondant et renouvelable, le nanocristal de cellulose pourrait être utilisé pour fabriquer et développer une large gamme de produits à haute valeur ajoutée, comme (i) des matériaux biomédicaux pour les produits pharmaceutiques et l'administration de médicaments, le remplacement de l'os et la réparation des dents, etc., (ii) des matériaux composites avancés (fibres filées et textiles à haute résistance, polymères renforcés et bioplastiques novateurs; emballages "intelligents", etc., (iii) des additifs pour l'alimentation, les cosmétiques, les revêtements, les peintures, les adhésifs, les pigments et encres; (iv) des composants structurels pour la fabrication du papier, la construction, l'aérospatiale et les transports, (v) des matériaux optiquement commutables et irisés.²

Depuis la première étude sur l'utilisation des nanocristaux de cellulose comme phase de renfort dans des nanocomposites il y a environ 20 ans, une quantité importante de littérature a été consacrée à la recherche sur les nanocristaux de cellulose. Différentes terminologies ont été utilisées dans la littérature pour désigner ces nanoparticules cellulosiques hautement cristallines, comme "nanocristaux de cellulose", "cellulose nanocristalline", "nanotrichites de cellulose" (ou simplement

"trichites"), "microcristaux de cellulose en bâtonnet", "cristallites de cellulose" et "micelles de cellulose" (dans la littérature la plus ancienne).

En 2011, certaines normes internationales sur la nanocellulose ont été proposées par la Division Nanotechnologie Internationale de TAPPI, et la nomenclature "nanocristaux de cellulose" a été recommandée comme désignation générale.³ Notamment, au cours des dix dernières années, l'étude des nanocristaux de cellulose est devenu un sujet chaud et d'actualité partout dans le monde. De plus en plus de chercheurs se consacrent à l'étude de ce merveilleux nanomatériau, et chaque année de nombreuses conférences académiques sont proposées pour stimuler le développement des nanocristaux de cellulose, comme par exemple au cours de l'année 2013, "TAPPI International Conference on Nanotechnology for Renewable Materials", "245th ACS National Meeting-Divisions of Composites from Natural Resources", "EPNOE 2013 International Polysaccharide Conference", etc.

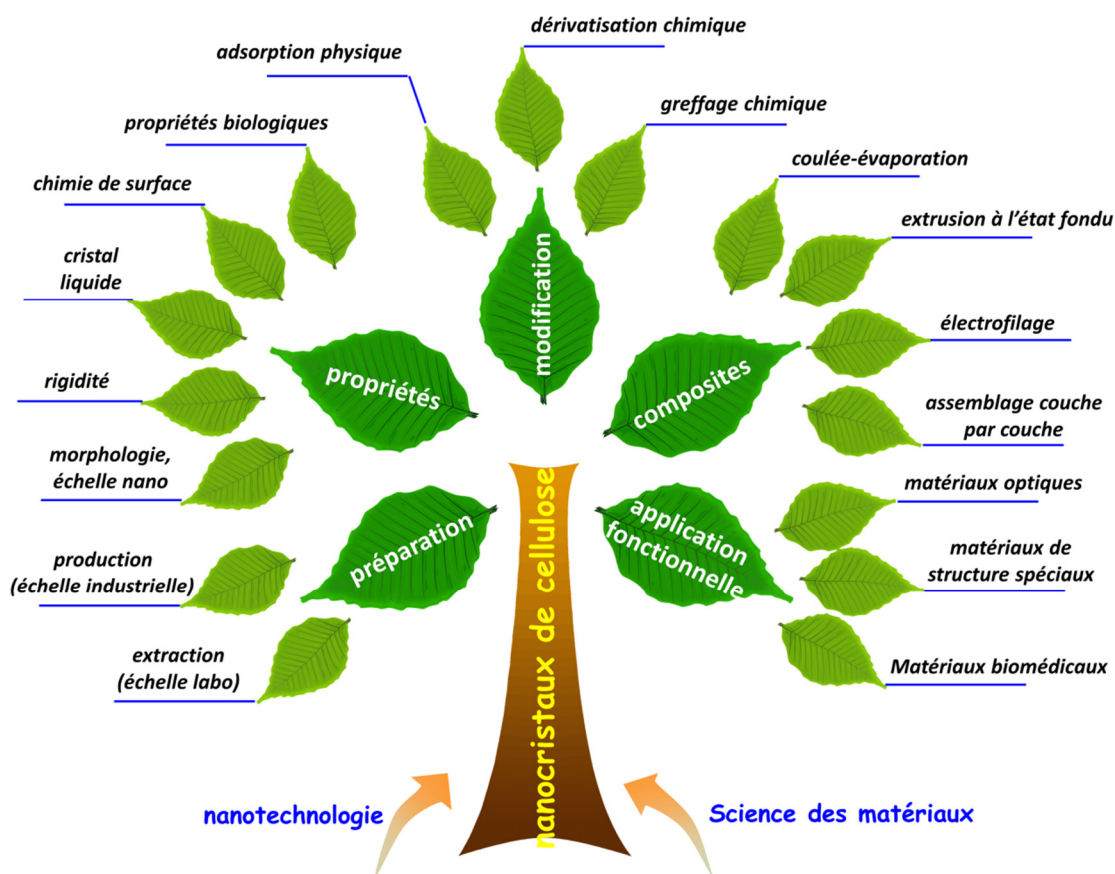


Figure 1. Dendrogramme de la classification et des sujets de recherche sur les nanocristaux de cellulose.

Du point de vue de la nanotechnologie et de la science des matériaux, les sujets de recherche sur les nanocristaux de cellulose peuvent être divisés en quatre domaines, à savoir la préparation, les propriétés, la modification, et les applications (incluant les composites et les matériaux fonctionnels) comme le montre la figure 1. En ce qui concerne la préparation des nanocristaux de cellulose, différentes approches pour l'extraction des nanocristaux de cellulose à l'échelle du laboratoire sont fréquemment reportées. Cependant, la technique idéale d'un procédé "vert", "simple" et à "bas cout" pour la production à grande échelle de nanocristaux de cellulose est toujours en cours de recherche. L'étude des propriétés des nanocristaux de cellulose inclue leur propriétés physiques, de chimie de surface et biologiques. L'objectif de la modification de surface des nanocristaux de cellulose est la régulation des propriétés de surface ou l'apport de nouvelles molécules fonctionnelles pour diverses applications. Pour l'application traditionnelle comme nano-renfort des nanocristaux de cellulose, quatre approches de mise en œuvre sont principalement appliquées pour préparer des composites à base de nanocristaux cellulosiques, viz. Evaporation, fusion-mélange, électrofilage, et assemblage couche à couche. L'émergence des matériaux fonctionnels liée à certaines propriétés uniques des nanocristaux de cellulose attire de plus en plus l'attention des chercheurs, en particulier au cours des cinq dernières années, comme les matériaux optiquement ajustables, les matériaux mécaniquement adaptatifs et divers matériaux biomédicaux à base de nanocristaux de cellulose .

La Figure 2 (A) indique le nombre d'articles de recherche publiés sur les nanocristaux de cellulose au cours des dix dernières années selon le système ISI Web of Knowledge. De manière générale, l'augmentation du nombre de publications sur les nanocristaux de cellulose est plus marquée sur la période 2004-2013, ce qui induit le changement brusque de quelques articles en 2004 à plus de 180 articles en 2013. Plus précisément, au cours de ces années, un saut dans l'augmentation continue du nombre d'articles sur l'étude des nanocristaux de cellulose est apparu depuis 2008. L'analyse des thèmes de recherche des études sur les nanocristaux de cellulose en

2013 est plus intéressante et indique les points les plus ciblés dans cette recherche. Comme le montre la Figure 2 (B), en 2013, l'étude sur l'application des nanocristaux de cellulose (incluant les composites et les matériaux fonctionnels) est sans doute le principal intérêt de recherche et représente environ 60% des publications. On constate qu'il y est moins d'études sur l'extraction seule des nanocristaux de cellulose, mais plus d'études sur le développement de procédés différents pour l'obtention des nanocristaux de cellulose ayant des propriétés de surface contrôlées, telles que l'extraction de nanocristaux de cellulose thermostables par hydrolyse à l'acide phosphorique,⁴ la synthèse de nanocristaux de cellulose carboxylés guidée par la spectroscopie Raman avec du persulfate d'ammonium,⁵ les nanocristaux de cellulose de taille contrôlée par hydrolyse acide composée⁶ etc. On observe également une diminution du nombre d'études sur la modification de surface seule des nanocristaux de cellulose. Dans les études sur les nouvelles modifications de surface, le but spécifique de la modification est toujours impliqué, en particulier la modification fonctionnelle pour contribuer à un rôle additionnel ou l'effet des nanocristaux de cellulose. Ces changements reflètent le retour rationnel des études

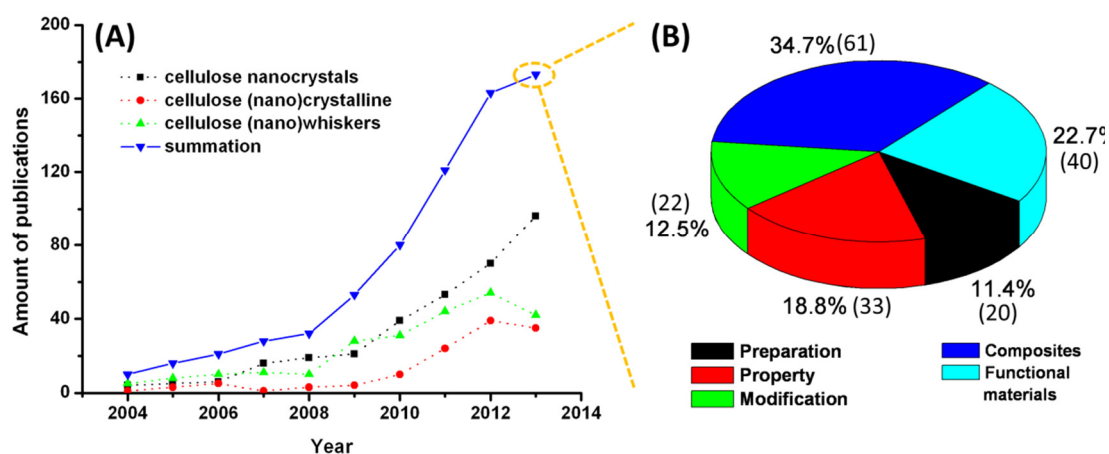


Figure 2. (A) Evolution du nombre d'articles de recherche sur les nanocristaux de cellulose au cours des dix dernières années (2004-2013) selon le système ISI Web of Knowledge; (B) Proportions des différents thèmes de recherche abordés dans les publications de l'année 2013. (Dans les statistiques sur les proportions des différents sujets pour les publications en 2013, les articles de synthèse sont exclus, et certaines publications peuvent impliquer deux thèmes de recherche.)

sur le sujet, qui exigent des modifications plus raisonnées et utiles des nanocristaux de cellulose, comme l'intégration de nanoparticules d'or/magnétiques à la surface du nanocristal de cellulose pour une immobilisation efficace,⁷ la conjugaison d'aminotrisulfonate tétraphénylporphyrine sur les nanocristaux de cellulose pour des propriétés de liaison particulières et la production de singulets oxygène⁸ etc. Il est intéressant de voir qu'au cours de la dernière année, de nombreuses publications mettent l'accent sur l'étude ou la discussion des propriétés des nanocristaux de cellulose, comme la distribution d'orientation des nanocristaux de cellulose par anisotropie diamagnétique,⁹ l'effet des groupements sulfates sur l'adsorption d'enzyme type cellulases,¹⁰ la prédiction de la rigidité des nanocristaux de cellulose avec des modèles de mécanique quantique,¹¹ les comportements d'auto-assemblage de nanocristaux de cellulose bactérienne et de tunicier¹² etc. Bien que les mécanismes de certaines études doivent être vérifiés, l'exploration fondamentale des propriétés du nanocristal de cellulose est si importante qu'elle favorise considérablement son application. En ce qui concerne les applications des nanocristaux de cellulose, l'étude de ceux-ci comme phase de nano-renfort pour préparer divers composites est encore l'un des sujets de recherche commun. Toutefois, pour répondre aux exigences des produits industriels, de nombreuses études mettent en œuvre les composites à base de nanocristaux de cellulose avec une approche de mélange à l'état fondu. Les matériaux fonctionnels à base de nanocristaux de cellulose ont été un sujet attractif en 2013 (40% des études d'application), en raison de l'innovation engendrée par divers matériaux à haute valeur ajoutée avec des propriétés nouvelles ou améliorées, telles que les nanocomposites à gradient mécanique avec des nanocristaux de cellulose réticulés,¹³ les cellules solaires organiques recyclables sur substrats de nanocristaux de cellulose,¹⁴ les hydrogels sensibles photoniques à base de nanocristaux de cellulose,¹⁵ la culture de myogénèse de squelette musculaire sur des nanocristaux de cellulose¹⁶ etc. Bien que certaines recherches ne soient basées que sur des études préliminaires, il y a un grand potentiel sur ce sujet pour l'application des nanocristaux de cellulose.

Le nanocrystal de cellulose est à la fois un ancien et un nouveau matériau. Il s'agit d'un matériau si ancien depuis sa première extraction en 1947, et il est également si nouveau en raison de son importance récente au cours seulement des 20 dernières années. Cette thèse est le résumé de mes recherches au cours des trois dernières années sur ce bionanomatérial sans âge et la structure de la thèse est illustrée sur la Figure 3. Le chapitre 1 est une revue de la littérature sur les nanocristaux de cellulose. Dans ce chapitre, quatre domaines de la recherche sur les nanocristaux de cellulose (préparation, propriétés, modification, et applications) sont introduits en détail à travers l'analyse et la comparaison de publications sélectionnées. Le chapitre 2 est un travail de recherche sur les propriétés des nanocristaux de cellulose. Dans ce chapitre, l'effet d'un gradient de groupements sulfates portés par les nanocristaux de cellulose sur la chimie de surface, la morphologie et les propriétés physiques est étudié et discuté. Les chapitres 3, 4 et 5 sont des travaux de recherche sur certaines applications des nanocristaux de cellulose, à savoir la préparation de nanocomposites par extrusion, d'éponges biocomposites et d'hydrogels supramoléculaires. Dans le chapitre 3, une nouvelle stratégie impliquant une protection polymère double-couche et une compatibilisation physique et/ou chimique des nanocristaux de cellulose est proposée pour à la fois améliorer la stabilité thermique et promouvoir la compatibilité des nanocristaux de cellulose avec des matrices polymères non polaires au cours du processus d'extrusion. Dans le chapitre 4, avec l'idée de la participation en tant qu'aide à la réticulation de nanocellulose oxydée TEMPO pour la construction des matériaux (deux types de nanocellulose sont utilisés, nanocristaux de cellulose et cellulose microfibrillée), des éponges à base d'alginate sont développées avec une meilleure stabilité mécanique ou stabilité structurelle. Des hydrogels supramoléculaires résultant d'une inclusion hôte-invité in situ entre nanocristaux de cellulose chimiquement modifiés et cyclodextrine sont étudiés dans le chapitre 5. Dans cette étude, la combinaison de nanocristaux de cellulose et de cyclodextrine dans les hydrogels est réalisée à partir d'une conception intelligente et l'application des hydrogels préparés pour le relargage de médicaments est en outre analysée et discutée. Le dernier chapitre

(chapitre 6) regroupe les conclusions de cette thèse et les perspectives pour des recherches futures sur les nanocristaux de cellulose.



Figure 3. Structure et organisation de cette thèse.

Conclusions générales

L'objectif principal de cette thèse était d'étudier les propriétés des nanocristaux de cellulose et de développer leurs applications comme blocs de construction pour des nanocomposites et des matériaux fonctionnels. Les principales innovations des études présentées dans la thèse comprennent: i) la préparation de nanocristaux de cellulose avec des gradients de degré de sulfatation et l'analyse de la chimie de surface pour différents modèles de section; ii) l'extrusion de nanocomposites à base de polystyrène renforcé par des nanocristaux de cellulose en utilisant une méthode de modification physique et/ou chimique et de compatibilisation, iii) l'utilisation de groupements carboxyles induits par TEMPO sur la nanocellulose participant à la construction du réseau réticulé type "boite à œufs" avec un multimère pour la préparation d'une éponge à base d'alginate, et iv) le développement d'hydrogels

supramoléculaires par inclusion in situ de nanocristaux de cellulose modifiés et de cyclodextrine pour une application d'administration de médicament.

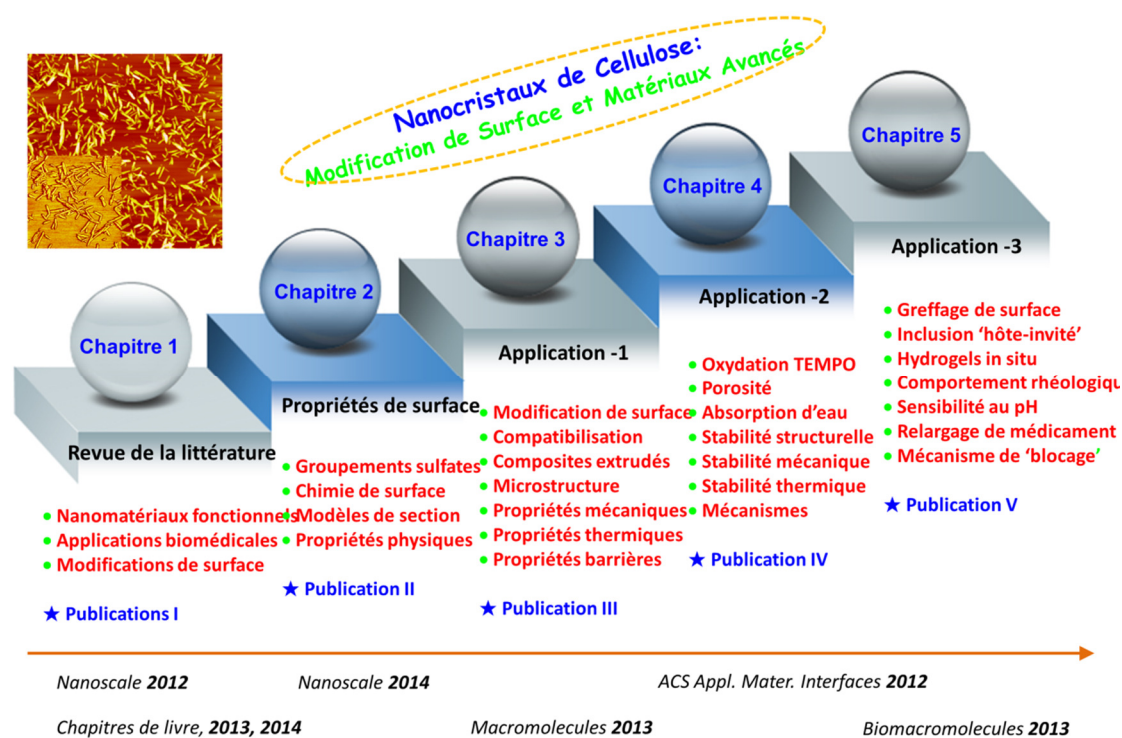


Figure 4 Représentation schématique des sujets de recherche et des résultats présentés dans cette thèse.

Centrées autour des propriétés et applications des nanocristaux de cellulose, diverses modifications ont été effectuées sur des nanocristaux de cellulose de coton afin d'approfondir leurs propriétés de surface et d'adapter leur applicabilité à différents matériaux avancés. Les thèmes généraux de recherche pour chaque étude sont résumés dans la figure 6.1.

Dans le chapitre 1, l'état de l'art de la recherche sur le thème des nanocristaux de cellulose (incluant également les whiskers de cellulose et la cellulose nanocristalline) a été examiné, et des études importantes ont été spécialement introduites sur la base de quatre parties, à savoir la préparation et la production; les propriétés physiques, chimiques et biologiques; la modification de surface; ainsi que des applications traditionnelles et plus avancées. Compte tenu de mes études de doctorat, au cours de la revue de la littérature présentée dans ce chapitre, l'accent a

été mis sur les propriétés physiques et chimiques, la modification de surface et les nanomatériaux fonctionnels.

Le travail de recherche présenté dans le chapitre 2 repose sur les questions suivantes: "combien de groupements hydroxyles actifs ont été remplacés par des groupements sulfates pendant l'hydrolyse avec H_2SO_4 , et comment les groupements sulfate de surface affectent la chimie de surface et les propriétés physiques des nanocristaux de cellulose?" Pour répondre à ces questions, des gradients de groupements sulfates ont été introduits à la surface des nanocristaux de cellulose en régulant les rapports des réactifs et les conditions de réaction pour la postsulfation et la désulfatation. Sur la base de l'analyse de la chimie de surface des nanocristaux modifiés, il a été prouvé que le choix de différents modèles de section transversale affecte de manière significative le calcul du degré de substitution des groupements sulfates des nanocristaux de cellulose. En considérant des nanocristaux de cellulose de coton comme exemple, si le modèle carré ou rond est choisi pour les nanocristaux, plus de 20% des groupements hydroxyles de surface sont substitués par des groupements sulfates au cours de l'hydrolyse-estérification par H_2SO_4 (concentration en acide de 65% en poids, 45°C), ce qui indique que la plupart des groupements hydroxyle actifs situés en C6 ont été remplacés au cours de l'extraction. Si le modèle d'ellipse est choisi, environ 13 % des groupements hydroxyles de surface sont remplacés par des groupements sulfates au cours de l'hydrolyse. Toutefois, en choisissant le modèle rectangle pour les nanocristaux de cellulose, seulement 7,9 % des groupements hydroxyles de surface sont substitué au cours de l'hydrolyse avec H_2SO_4 (seulement environ 1/3 de la valeur correspondant au modèle carré ou rond), et une grande quantité de groupements hydroxyles actifs subsistent. En outre, l'effet des groupements sulfates sur les différentes propriétés physiques des nanocristaux de cellulose et de leurs suspensions a été discuté. De plus, le modèle parallélogramme de la cristallite élémentaire des nanocristaux de cellulose de coton a été validé par analyse de diffraction des rayons X et par la détermination des charges négatives induites par la présence des groupements sulfates sur les nanocristaux de cellulose

par mesure du potentiel ζ . L'influence des groupements sulfates sur la stabilité thermique des nanocristaux de cellulose a été étudiée, et cette étude a révélé qu'une quantité croissante de groupements sulfates sur les nanocristaux induit un abaissement de la température correspondant à la première phase de décomposition thermique (Td_1), et une cristallinité plus élevée pour les nanocristaux se traduisant par une température plus élevée de la deuxième phase de décomposition thermique (Td_2). A partir de l'observation de la biréfringence des suspensions aqueuses, il a été conclu que la dispersion et la formation de domaines biréfringents peuvent être affectées par la teneur en groupements sulfates de la surface des nanocristaux.

Le chapitre 3 est une étude sur la préparation de composites extrudés visant à résoudre les problèmes de stabilité thermique des nanocristaux de cellulose au cours de la mise en forme à l'état fondu des nanocomposites polymères. Une stratégie impliquant deux couches de poly(éthylène glycol)/polyoxyéthylène (PEG/PEO) à la surface des nanocristaux de cellulose grâce à un greffage chimique et des interactions physiques a été proposée. Quatre types de nanocristaux, à savoir des nanocristaux vierges, des nanocristaux adsorbés avec du PEO, des nanocristaux greffés avec du PEG, et des nanocristaux à la fois greffés avec du PEG et adsorbés avec du PEO, ont été extrudés avec une matrice polymère hydrophobe (PS) pour préparer des nanocomposites. L'idée de base s'appuyait sur la possibilité d'enchevêtrements et de co-cristallisation entre les chaînes de PEG courtes et les longues chaînes de PEO, pouvant étroitement envelopper et protéger la surface des nanocristaux. Parallèlement, la compatibilisation chimique et physique conférée par les couches de PEG et de PEO a favorisé les interactions interfaciales entre les nanoparticules de cellulose et la matrice apolaire. La possibilité de mettre en forme les nanocristaux modifiés (CN-g-PEG/PEO) à haute température (200°C) en évitant la dégradation de la nanoparticule et en offrant une bonne dispersion et une bonne compatibilité entre les nanocristaux modifiés et la matrice a été montrée. En outre, les modifications de surface des nanocristaux n'ont pas bloqué totalement les

interactions entre les nanoparticules et ont maintenu au moins partiellement l'architecture de réseau en trois dimensions, qui a été bénéfique pour l'amélioration des propriétés mécaniques des nanocomposites extrudés. En effet, les résultats d'ATG ont montré que les nanocristaux de cellulose modifiés par une double couche présentent une amélioration significative de la température de dégradation (environ 120°C d'augmentation par rapport aux nanocristaux de cellulose vierges), qui peut être attribuée à la protection uniforme des groupements sulfates induite par l'enrobage avec les chaînes de PEG greffées et par la protection de la couche de PEO adsorbé. Les nanocomposites extrudés et chargés avec des nanocristaux de cellulose modifiés avec une double couche présentaient un aspect transparent et des taux de transmittance élevés. Parallèlement, des performances mécaniques et barrières à la vapeur d'eau améliorées ont été observées pour ces nanocomposites extrudés. La stratégie proposée dans cette étude devrait permettre de surmonter un défi important visant à mettre en forme à l'état fondu des composites à base de nanocristaux de cellulose pour une production industrielle.

Dans l'optique d'améliorer la faible performance (stabilité mécanique et structurelle) des éponges d'alginate pur, des éponges réticulées avec le soutien de nanocellulose oxydée ont été élaborées et étudiées. Ce sujet a été abordé dans le chapitre 4. Deux types de nanocellulose extraite de coton ont été utilisés dans cette étude, à savoir des nanocristaux de cellulose avec une morphologie en bâtonnet "rigide" et de la cellulose microfibrillée avec une morphologie en longs filaments "souples". Après le traitement d'oxydation sélectif TEMPO, la nanocellulose modifiée présentait la capacité de participer à une réticulation ionique lors de la formation structurale des éponges à base d'alginate. Il est intéressant de noter que les différents types de nanocellulose oxydée apportent des améliorations distinctes aux éponges. Une résistance mécanique remarquablement renforcée a été rapportée pour les nanocristaux de cellulose oxydés tandis que des améliorations prometteuses de la porosité, de l'absorption d'eau, et de la stabilité structurelle ont été observées pour la cellulose microfibrillée oxydée. Plus spécifiquement, par rapport à la porosité

(78,8 %), l'absorption d'eau (835,3 %) et la rétention d'eau (221,1 %) de l'éponge d'alginate pur, une éponge réticulée et chargée avec 50% en poids de cellulose microfibrillée oxydée possédait une porosité (97,4 %), une absorption d'eau (1468,4 %) et une rétention d'eau (846,7 %) très importantes. Même après 10 utilisations, ce type d'éponges réticulées et chargées avec la cellulose microfibrillée oxydée peuvent maintenir des niveaux élevés d'absorption d'eau. Cependant, les nanocristaux de cellulose oxydés ont un meilleur impact sur le renforcement des propriétés mécaniques des éponges. Pour des contraintes de compression de 30 %, 50% et 70 %, la résistance à la compression des éponges réticulées contenant 10 % en poids de nanocristaux de cellulose oxydés ont augmenté d'un facteur 2,78, 2,80 et 2,94, en comparaison avec l'éponge d'alginate pur, respectivement. Il a été supposé que les nanocristaux de cellulose oxydés rigides servaient de points de couplage et remplissaient totalement l'effet de nano-renfort pour les éponges à base d'alginate, tandis que la cellulose microfibrillée oxydée pouvait se joindre à la construction structurale et former le réseau polymère semi-interpénétré des éponges à base d'alginate.

Inspiré par l'étude du mélange physique de nanocristaux polysaccharides vierges et de cyclodextrine, une tentative d'utiliser des méthodes de modification chimique pour promouvoir la compatibilité et améliorer les taux de charge en nanocristaux de cellulose dans des matériaux hydrogels à base de cyclodextrine a été réalisée et rapportée dans le chapitre 5. La β -cyclodextrine a tout d'abord été greffée de manière covalente à la surface des nanocristaux de cellulose à l'aide de l'épichlorhydrine comme agent de couplage. Ensuite, le polymère Pluronic a été immobilisé sur les nanocristaux de cellulose modifiés par inclusion des segments polymères hydrophobes dans la β -cyclodextrine greffée. Les polymères Pluronic utilisés dans cette étude étaient des copolymères triblocs avec des masses moléculaires différentes (Pluronic F68 ou F108), portant à la fois des segments PPG hydrophobes et des segments PEG hydrophiles (PEG-*b*-PPG-*b*-PEG). L'inclusion des segments hydrophobes de la chaîne de PPG dans la cavité interne de la β -CD a

permis une connexion intime des chaînes et des nanoparticules. Enfin, par des interactions d'inclusion de type "hôte-invité" entre les nanocristaux de cellulose modifiés, les polymères Pluronic et des cyclodextrines de différentes tailles, des hydrogels ont été préparés *in situ* et utilisés comme nouveau vecteur de médicaments. Grâce à l'introduction de taux de charge élevés de nanocristaux modifiés (> à 5% en poids), une amélioration notable de la stabilité structurelle et thermique des hydrogels *in situ* a été observée à partir de l'analyse rhéologique. Parallèlement, ces hydrogels formés *in situ* et incluant des nanocristaux de cellulose modifiés ont montré une sensibilité au pH particulière. Une étude ultérieure a révélé la performance des hydrogels formés *in situ* comme vecteur de médicament pour la libération *in vitro* de la doxorubicine, avec un comportement prometteur de libération contrôlée montrant une libération prolongée pendant environ une semaine alors que les hydrogels purs affichent une libération initiale rapide et une période de libération courte (seulement 2,5 jours). Le comportement de libération prolongée de médicament des hydrogels formés *in situ* a été analysé grâce à une cinétique de libération et a été attribué à "l'effet d'obstruction" et "l'effet de blocage" des nanocristaux de cellulose modifiés. À partir de leurs performances et de leurs propriétés, ces hydrogels injectables formés *in situ* fournissent un exemple scientifique pour l'application des nanocristaux issus de la biomasse dans le domaine des matériaux biomédicaux.

Perspectives pour la recherche future

Nous constatons que le nanocristal de cellulose est un matériau unique et magique. Le nanocristal de cellulose peut être utilisé dans toutes sortes de domaines, mais il reste un matériau relativement nouveau pour nous. Il subsiste encore beaucoup de propriétés ou d'applications inconnues des nanocristaux de cellulose. En dépit d'être le polymère naturel le plus disponible et répandu sur terre, ce n'est que récemment que l'importance de ce matériau nanostructuré a été reconnue. Nous sommes maintenant à l'orée de la percée de la recherche sur le nanocristal de cellulose et c'est peut-être une opportunité pour la science des matériaux du futur.

Tableau 1 Activités de recherche future pour les études présentées dans cette thèse.

Etudes de cette thèse	Activités de recherche future
Chimie de surface et propriétés des NC avec des gradients de degré de sulfatation	<ul style="list-style-type: none"> • Etude des interactions électrostatiques entre les charges négatives des NC sulfatés et les charges positives de polymères ou molécules cationiques • Mesure de la force et du mécanisme des interactions électrostatiques des charges de couplage • Stratégie de greffage électrostatique de surface des
Compatibilisation physique et/ou chimique de nanocomposites extrudés PS renforcé par des NC	<ul style="list-style-type: none"> • Etude approfondie des interactions entre le PEG greffé et le PEO adsorbé • Effet du rapport des longueurs de chaîne PEG/PEO sur la compatibilité • Mesure de l'épaisseur de l'interphase des couches de PEG et PEO dans les composites extrudés • Méthode plus simple pour remplacer le greffage chimique du PEG à la surface des NC • Etude d'autres polymères ou copolymères
Nanocellulose oxydée TEMPO assistant la réticulation des éponges à base d'alginate	<ul style="list-style-type: none"> • Preuves directes de l'assistance à la réticulation de la nanocellulose oxydée, de l'alginate et de Ca²⁺ • Tentative d'incorporation simultanée de NC oxydé et de MFC oxydée dans les éponges pour des améliorations synergiques • Développement de ces éponges dans des applications biomédicales, comme des pansements médicamenteux actifs
Hydrogels supramoléculaires pour inclusion hôte-invité in situ entre NC modifié et cyclodextrine	<ul style="list-style-type: none"> • Caractérisation de "l'effet d'obstruction" et de "l'effet de blocage" des systèmes de relargage de médicament à base de NC • Présence des NCs (avec des groupements hydroxyles et/ou sulfates de surface) sur la structure et l'activité des médicaments • Développement de systèmes hydrogels multi-membranes pour de nouveaux comportements de libération de médicaments

A partir des études présentées dans cette thèse, certains sujets de recherche peuvent être traités dans des travaux futurs. Le tableau 6.1 présente quelques points issus des études développées dans chaque chapitre. Plus précisément, pour l'étude sur les "gradients de groupements sulfates sur les nanocristaux de cellulose" présentée dans le chapitre 2, la recherche future peut se concentrer sur les interactions électrostatiques entre les charges négatives des nanocristaux sulfatés et

les charges positives de polymères ou molécules cationiques. En détectant et mesurant les interactions électrostatiques, on pourrait accéder à la force et au mécanisme de cette interaction particulière à partir des charges de couplage et donc favoriser l'application du greffage électrostatique du nanocrystal de cellulose. La Figure 6.2 montre la stratégie de recherche du greffage électrostatique de polymère sur des nanocristaux de cellulose et propose les questions initiales de l'étude: "Est-il possible que la multiplication des groupements sulfates entraîne un nombre plus important de chaînes polymères adsorbées et des interactions électrostatiques plus fortes?"

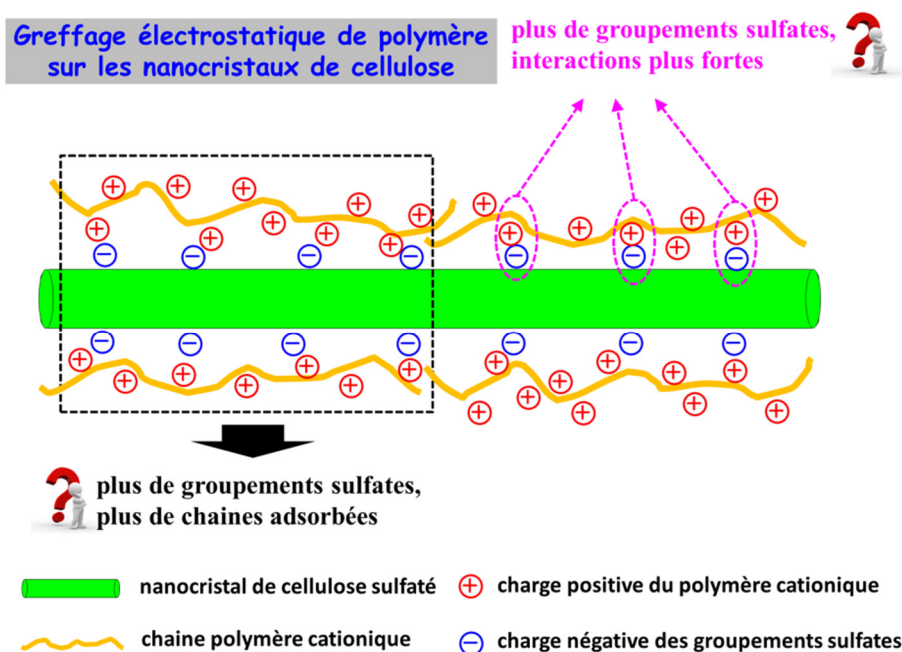


Figure 5 Stratégie du greffage électrostatique de polymère sur les nanocristaux de cellulose.

En ce qui concerne l'étude sur les "composites extrudés à base de nanocristaux de cellulose" présentée dans le chapitre 3, un examen plus approfondi est nécessaire pour bien comprendre les interactions entre PEG greffé et PEO adsorbé, comme le rapport des longueurs de chaîne (un rapport PEG/PEO de 1/10 a été utilisé dans ce cas) et l'épaisseur de l'interphase des couches de PEG et PEO dans les nanocomposites extrudés. Un contrôle minutieux de la quantité de chaînes PEG/PEO en surface est également souhaitable pour pouvoir contrôler la possibilité de liaison hydrogène entre les nanoparticules. De plus, un procédé plus simple pour l'introduction de la première couche de PEG sur les nanocristaux de cellulose serait

d'utiliser le greffage électrostatique au lieu de la réaction de greffage chimique. C'est un point important pour promouvoir l'application pratique de cette stratégie.

Pour l'étude sur les "éponges réticulées d'alginate" présentée dans le chapitre 4 et inspirée des différences d'effet de deux nanocelluloses oxydées, il sera intéressant d'essayer d'intégrer à la fois la cellulose nanocristalline et la cellulose microfibrillée oxydées dans les matériaux à base d'alginate et de développer des applications de ces éponges dans le domaine des matériaux biomédicaux comme vecteurs de médicaments pour les pansements ou des bio supports.

Pour ce qui est de l'étude sur les "hydrogels supramoléculaires de nanocristaux de cellulose et cyclodextrine" reportée dans le chapitre 5, un examen plus approfondi de l'effet des propriétés de surface des nanocristaux de cellulose sur la structure et l'activité biologique des molécules actives pourrait promouvoir leur application pour de nouveaux nanomatériaux biomédicaux. En outre, en profitant de l'effet "d'obstruction" et de "l'effet de verrouillage" des nanocristaux de cellulose, il serait intéressant de développer des systèmes de relargage complexant de médicaments pour de nouveaux comportements de libération de médicament, tels que des systèmes hydrogel multi-membranes. Dans l'année à venir, quelques idées seront développées au cours de ma recherche post-doctorale.

Il est impossible de prédire quel domaine va devenir le marché pratique pour les nanocristaux de cellulose dans l'avenir. Actuellement, de plus en plus de chercheurs de tous les types de domaines sont attirés par ce produit et dans le proche futur les nanocristaux de cellulose pourraient être utilisés pour le développement de blindages corporels, d'écrans ultra-flexibles, de filtres à haute efficacité, de batteries flexibles, d'ultra-aérogels absorbants, de voitures et d'ordinateurs, de biocarburants, etc. Il ne s'agit pas seulement d'illusions. A titre d'exemple, IBM prévoit d'utiliser des nanocristaux de cellulose pour créer des composants d'ordinateurs et l'armée américaine envisage l'utilisation des nanocristaux de cellulose pour des protections légères et des gilets pare-balles. Le nanocristal de cellulose est un don précieux de la nature!

Références:

1. Leung, A. C. W.; Lam, E.; Chong, J.; Hrapovic, S.; Luong, J. H. T. Reinforced plastics and aerogels by nanocrystalline cellulose. *J. Nanopart. Res.* **2013**, *15*, 1636 (24 pages).
2. From the introduction of the product of nanocrystalline cellulose in the company of CelluForce. http://celluforce.com/en/product_applications.php
3. TAPPI People Resources Solutions, "Roadmap for the development of international standards for nanocellulose". Published at October 24th, **2011**. <http://www.tappinano.org/pdf/RoadmapforNanocelluloseStandards.pdf>
4. Espinosa, S. C.; Kuhnt, T.; Foster, E. J.; Weder, C. Isolation of thermally stable cellulose nanocrystals by phosphoric acid hydrolysis. *Biomacromolecules* **2013**, *14*, 1223–1230.
5. Lam, E.; Leung, A. C. W.; Liu, Y.; Majid, E.; Hrapovic, S.; Male, K. B.; Luong, J. H. T. Green strategy guided by raman spectroscopy for the synthesis of ammonium carboxylated nanocrystalline cellulose and the recovery of byproducts. *ACS Sustainable Chem. Eng.* **2013**, *1*, 278–283.
6. Baek, C.; Hanif, Z.; Cho, S.-W.; Kim, D.-I.; Um, S. H. Shape control of cellulose nanocrystals via compositional acid hydrolysis. *J. Biomed. Nanotechnol.* **2013**, *9*, 1293–1298.
7. Mahmoud, K. A.; Lam, E.; Hrapovic, S.; Luong, J. H. T. Preparation of well-dispersed gold/magnetite nanoparticles embedded on cellulose nanocrystals for efficient immobilization of papain enzyme. *ACS Appl. Mater. Interfaces* **2013**, *5*, 4978–4985.
8. Chauhan, P.; Hadad, C.; Sartorelli, A.; Zarattini, M.; Herreros-López, A.; Mba, M.; Maggini, M.; Prato, M.; Carofiglio, T. Nanocrystalline cellulose–porphyrin hybrids: synthesis, supramolecular properties, and singlet-oxygen production. *Chem. Commun.* **2013**, *49*, 8525–8527.

9. Song, G.; Kimura, F.; Kimura, T.; Piao, G. Orientational distribution of cellulose nanocrystals in a cellulose whisker as studied by diamagnetic anisotropy. *Macromolecules* **2013**, *46*, 8957–8963.
10. Jiang, F.; Kittle, J. D.; Tan, X.; Esker, A. R.; Roman, M. Effects of sulfate groups on the adsorption and activity of cellulases on cellulose substrates. *Langmuir* **2013**, *29*, 3280–3291.
11. Dri, F. L.; Hector Jr., L. G.; Moon, R. J.; Zavattieri, P. D. Anisotropy of the elastic properties of crystalline cellulose I_β from first principles density functional theory with Van der Waals interactions. *Cellulose* **2013**, *20*, 2703–2718.
12. Khandelwal, M.; Windle, A. H. Self-assembly of bacterial and tunicate cellulose nanowhiskers. *Polymer* **2013**, *54*, 5199–5206.
13. Fox, J. D.; Capadona, J. R.; Marasco, P. D.; Rowan, S. J. Bioinspired water-enhanced mechanical gradient nanocomposite films that mimic the architecture and properties of the squid beak. *J. Am. Chem. Soc.* **2013**, *135*, 5167–5174.
14. Zhou, Y.; Fuentes-Hernandez, C.; Khan, T. M.; Liu, J.-C.; Hsu, J.; Shim, J. W.; Dindar, A.; Youngblood, J. P.; Moon, R. J.; Kippelen, B. Recyclable organic solar cells on cellulose nanocrystal substrates. *Sci. Rep.* **2013**, *3*, 1536 (5 pages).
15. Kelly, J. A.; Shukaliak, A. M.; Cheung, C. C. Y.; Shopsowitz, K. E.; Hamad, W. Y.; MacLachlan, M. J. Responsive photonic hydrogels based on nanocrystalline cellulose. *Angew. Chem. Int. Ed.* **2013**, *52*, 8912–8916.
16. Dugan, J. M.; Collins, R. F.; Gough, J. E.; Eichhorn, S. J. Oriented surfaces of adsorbed cellulose nanowhiskers promote skeletal muscle myogenesis. *Acta Biomaterialia* **2013**, *9*, 4707–4715.

Appendix and Abbreviations

A-174	γ -Methacryloxypropyl trimethoxy silane
AFM	Atomic force microscope
BDMSiCl	<i>n</i> -Butyldimethylchlorosilane
BMA	Butylmetacrylate
BSA	Bovine serum albumin
CAB	Cellulose acetate butyrate
CGTase	Cyclodextrin glycosyl transferase
CN	Cellulose nanocrystal
CTAB	Cetyl trimethylammonium bromide
DDMSiCl	<i>n</i> -Dodecyldimethylchlorosilane
DMAP	4-Dimethylaminopyridine
DMF	<i>N,N'</i> -Dimethylformamide
DODA	Diocadecyldimethylammonium
DOX	Doxorubicin hydrochloride
EA	Ethyl acrylate
EDC·HCl	<i>N</i> -(3-Dimethylaminopropyl)- <i>N'</i> -ethylcarbodiimide hydrochloride
EPTMAC	2,3-Epoxypropyltrimethylammonium chloride
FAM-SE	Fluorophores 5-(and-6)-carboxyfluorescein succinimidyl ester
FEG-SEM	Field-emission gun scanning electron microscope
FITC	Fluorescein isothiocyanate
GTMAC	Glycidyltrimethylammonium chloride
IPDMSiCl	Isopropyldimethylchlorosilane
LDH	Lactate dehydrogenase
MAH	Maleic anhydride
MCC	Microcrystalline Cellulose
MFC	Microfibrillated cellulose

MMA	methylmethacrylate
MPS	Methacryloxypropyltrimethoxysilane
MTT	3-(4,5-Dimethylthiazol-2-yl)-2,5-diphenyltetrazolium bromide
NMR	Nuclear magnetic resonance
ODMSiCl	<i>n</i> -Octyldimethylchlorosilane
OG-SE	Oregon Green 488 carboxylic acid, succinimidyl ester
PA	Polyamide
PAA	Poly(acrylic acid)
PAM	Polyacrylamide
PBMA	Poly(butylmethacrylate)
PANI–PPE	Polyaniline–Poly(<i>p</i> -phenylene ethynylene)
PDDA	Poly(diallyldimethylammonium chloride)
PDMA	Poly(dimethylacrylamide)
PDMAEMA	Poly [2-(<i>N,N</i> -dimethyl amino) ethyl methacrylate]
PEDOT/PSS	Poly(3,4-ethylenedioxythiophene)/Poly(styrene sulfonate)
PEG	Poly(ethylene glycol)
PEI	Poly(ethylene imine)
PHA	Poly(allylamine hydrochloride)
PHBV	Poly(3-hydroxybutyrate- <i>co</i> -3-hydroxyvalerate)
PHEMA	Poly(2-hydroxyethylmethacrylate)
PI	Phenyl isocyanate
PLA	Poly(lactic acid)
PMMAZO	Poly{6-[4-(4-methoxyphenylazo) phenoxy] hexyl methacrylate }
PMVEMA	Poly(methyl vinyl ether comaleic acid)
Poly(EO–EPI)	Poly(ethyleneoxide–epichlorohydrin)
Poly(MVE- <i>co</i> -MA) –PEG	Poly(methyl vinyl ether- <i>co</i> -maleic acid)–polyethylene glycol

PNiPAAm	Poly(<i>N</i> -isopropylacrylamide)
Poly(NIPAM- <i>co</i> -BMA)	Poly(2-hydroxyethylmethacrylate)
PS	Polystyrene
PSE	1-Pyrenebutyric acid N-hydroxy succinimide ester
PVA	Poly(vinyl alcohol)
RBITC	Rotary Bangalore IT Corridor
TAMRA-SE	Fluorophore 5-(and-6)-carboxytetramethylrhodamine succinimidyl ester
TEM	Transmission electron microscope
TEMPO	2,2,6,6-Tetramethyl-piperidiny-1-oxyl
TET	Tetracycline hydrochloride
TDI	Toluene diisocyanate
TMI	Isopropenyl- α,α' -dimethylbenzyl isocyanate
UPy	Ureidopyrimidone

Résumé

Ce travail porte sur les propriétés des nanocristaux de cellulose, leur modification de surface et le développement de matériaux avancés. Diverses approches sont utilisées sur ces substrats nanométriques visant à modifier leurs propriétés de surface et étendre leur utilisation dans des applications très sophistiquées, telles que la postsulfation et la désulfatation, le greffage et l'adsorption de polymères, l'oxydation sélective, le greffage moléculaire et l'inclusion "hôte-invité". Sur la base de modifications de surface, l'analyse des propriétés (pour différents taux de groupements sulfates) et divers nanomatériaux dérivés des nanocristaux de cellulose sont étudiés et préparés, notamment des nanocristaux sulfatés à différents taux, des nanocomposites extrudés, des éponges biocomposites et des hydrogels supramoléculaires. L'effet d'un gradient de groupements sulfates sur la chimie de surface, la morphologie et les propriétés physiques des nanocristaux de cellulose est discuté et notamment quatre modèles de section transversale sont comparés pour la détermination de la mesure du degré de substitution surfacique des nanocristaux de cellulose. Une stratégie nouvelle de protection impliquant une double couche polymère et la compatibilisation physique et/ou chimique des nanocristaux de cellulose est proposée afin de promouvoir à la fois la stabilité thermique des nanoparticules et la compatibilité des nanocristaux avec des matrices polymères non polaires au cours de la mise en forme par extrusion. En participant à la réticulation pour la construction de matériaux avancés, des nanocristaux de cellulose sélectivement oxydés (et de la cellulose microfibrillée oxydée pour comparaison) sont introduits dans de l'alginate pour développer des éponges biocomposites présentant une meilleure stabilité mécanique et une meilleure stabilité structurelle. Grâce à la conception intelligente par inclusion 'hôte-invité' in situ entre des nanocristaux de cellulose chimiquement modifiés et la cyclodextrine, deux polysaccharides hydrophiles sont combinés dans des hydrogels supramoléculaires pour l'administration de médicaments. En un mot, cette thèse contribue à l'avancée des nanocristaux de cellulose dans les domaines de l'analyse des propriétés et le développement des applications.

Mots-clés: *nanocristaux de cellulose, modification de surface, nanocomposites, éponges, hydrogels, gradient de sulfatation, compatibilisation, inclusion hôte-invité*

Abstract

The present work focuses on the properties of cellulose nanocrystals, their surface modification and development of advanced materials. Diverse approaches are employed on these nanoscaled substrates aiming to modify their surface properties and extend their use in highly sophisticated applications, such as postsulfation and desulfation, polymer grafting and adsorption, selective oxidation, molecular grafting, and 'host-guest' inclusion. On the basis of surface modifications, properties analysis (for different sulfate group contents) and various nanomaterials derived from cellulose nanocrystals are investigated and prepared, including gradient sulfated nanocrystals, extruded nanocomposites, biocomposite sponges, and supramolecular hydrogels. The effect of gradient degrees of sulfate groups on cellulose nanocrystals to surface chemistry, morphology and physical properties are discussed, particularly four cross-section models are compared for the determination of the surface degree of substitution on cellulose nanocrystals. A novel strategy involving a double-polymer-layer shield and physical and/or chemical compatibilization of cellulose nanocrystals is proposed, in order to realize both improvement of thermal stability and promotion of compatibility for nanocrystals with non-polar polymeric matrices during processing by melt-extrusion. With the idea of participating as crosslinking aid for the construction of advanced materials, selectively oxidized cellulose nanocrystals (with oxidized microfibrillated cellulose as comparison) are introduced in alginate for the development of biocomposite sponges with improved mechanical stability or structural stability. Through the smart design of in situ 'host-guest' inclusion between chemically modified cellulose nanocrystals and cyclodextrin, two hydrophilic polysaccharides are combined in supramolecular hydrogels for use as drug delivery. In a word, this dissertation contributes to the advances of cellulose nanocrystals in the topics of property analysis and application development.

Keywords: *cellulose nanocrystals, surface modification, nanocomposites, sponges, hydrogels, gradient sulfation, compatibilization, host-guest inclusion, extrusion*